eman ta zabal zazu
Universidad del País Vasco
Euskal Herriko Unibertsitatea
MEDIKUNTZA ETA ERIZAINTZA FAKULTATEA
FACULTAD DE MEDICINA Y ENFERMERÍA

Exploring the role of Myelin Regulatory Factor in oligodendrocyte dysfunction in models of Alzheimer's disease

Uxue Balantzategi Fernandez de Arroiabe

2024

Director:
Dr. Elena Alberdi Alfonso

This work was supported by:

- Ayuda Predoctoral de Formación de Personal Investigador no Doctor, Departamento de Educación del Gobierno Vasco, convocatoria 2019 **PRE_2019_1_0317**

- Ministerio de Ciencia, Innovación y Universidades (MICIU) **PID2019-108465RB-I00**, **PID2022-140236OB-I00**

- Gobierno Vasco **PIBA_2020_1_0012**, **IT1203-19**, **IT1551-22**

- Centro de Investigación Biomédica en Red Enfermedades Neurodegenerativas (CIBERNED) **CB06/05/0076**

TABLE OF CONTENTS

MATERIAL & METHODS

ABSTRACT

Oligodendrocyte dysfunction, myelin degeneration and alterations in white matter structures are early events in Alzheimer's disease that contribute to cognitive deficits. Amyloid β oligomers (Aβo) have been proposed to induce changes in oligodendrocytes and myelin, although the underlying molecular mechanisms remain incompletely understood. The differentiation program that oligodendrocyte progenitor cells undergo to become mature myelinating oligodendrocytes is intricately regulated by transcription factors, among which myelin regulatory factor (MYRF) plays an essential role. The self-cleaved N-terminal of MYRF (N-MYRF) translocates from the endoplasmic reticulum into the nucleus to induce the expression of myelin-related genes such as myelin basic protein (MBP); subsequently, N-MYRF is phosphorylated by GSK3 and degraded via the ubiquitin-proteasome system. Despite the significance of MYRF in oligodendrocyte differentiation and myelination, little is known about its involvement in Alzheimer's disease.

With the aim of uncovering alterations in oligodendroglial lineage cells in the context of Alzheimer's disease, through immunohistochemistry and EdU labelling we observed that the oligodendroglial population dynamics was disturbed within both the corpus callosum and the dentate gyrus of 3xTg-AD mice. Specifically, oligodendrocyte maturation was promoted, alongside region-specific oligodendrocyte loss in the dentate gyrus. Similarly, intracerebral injection of Aβo in WT mice also enhanced oligodendrocyte differentiation and maturation, suggesting that the observed oligodendrocyte alterations in 3xTg-AD mice were, at least in part, triggered by the presence of Aβo. Furthermore, bulk RNA sequencing analysis of oligodendrocytes isolated from adult 3xTg-AD mice revealed differential expression of multiple genes, primarily involved in critical biological processes such as ubiquitination, autophagy, and lipid metabolism. Additionally, upregulation of genes associated with pathways including oxidative stress and DNA damage indicated potential disruptions in oligodendrocytes at early stages of AD. Moreover, we found that Aβo increase MYRF protein levels both *in vivo* and *in vitro*, and, consistently, 3xTg-AD mice also exhibited more $MYRF^{+}$ oligodendrocytes than WT mice. Interestingly, sustained MYRF overexpression was found to be toxic for oligodendrocytes *in vitro*, suggesting a potential role for MYRF in Aβo-induced oligodendrocyte impairments. Mechanistically, we observed that Aβo slow down nuclear

MYRF degradation by altering both the PKC/GSK3 signaling pathway and Fbxw7-mediated ubiquitination. This leads to ineffective clearance of MYRF in the nucleus, potentially resulting in an aberrant transcriptional activity that affects oligodendrocytes and myelin-related gene expression. Finally, we evaluated and validated PKC inhibition as a potential pharmacological strategy to reverse the observed Aβo-induced alterations in MYRF, oligodendrocytes, and myelin *in vivo*. Administration of the pan-PKC inhibitor Gö6983 successfully rescued the Aβo-triggered precocious oligodendrocyte maturation and the increased myelination in the spinal cord of zebrafish larvae. Similarly, continuous intracerebroventricular infusion of Gö6983 in 3xTg-AD mice resulted in reduced MYRF levels within the hippocampus, and reversed both the oligodendrocyte loss and the promoted differentiation in the dentate gyrus.

In summary, our findings elucidate an Aβo-induced aberrant signaling pathway for MYRF degradation, with functional implications for oligodendrocytes in Alzheimer's disease models. Additionally, we propose PKC inhibition as a potential pharmacological strategy to mitigate these disruptions that may be contributing to the onset and progression of AD pathology.

ABBREVIATIONS

3xTg-AD	Triple transgenic mouse model of AD
5XFAD	Transgenic mouse model with five familial AD
a.u.	Arbitrary units
Aβ	Amyloid β peptide
Aβo	Amyloid β oligomers
Ac-CoA	Acetilcoenzima A
AD	Alzheimer's disease
Adamts4	ADAM metallopeptidase with thrombospondin type 1 motif 4
AICD	APP intracytoplasmic domain
Akt	Serine/threonine protein kinase
ANOVA	Analysis of variance
AP	Antero-posterior
Apbb1	Amyloid beta precursor protein binding family B member 1
APC	Adenomatous Polyposis Coli
ApoE	Apolipoprotein E
APP	Amyloid precursor protein
APP/PS1	Double transgenic mouse model of AD
Arf1	ADP-ribosylation factor 1
Aspa	Aspartoacylase gene
ATP	Adenosine triphosphate
BACE	β-site amyloid precursor protein cleaving enzyme
BDNF	Brain-derived neurotrophic factor
bHLH	Basic helix-loop-helix
BP	Biological processes
BSA	Bovine serum albumin
C-MYRF	C-terminal fragment of MYRF
Ca^{2+}	Calcium
CaMKII	Ca^{2+}/calmodulin-dependent protein kinase II
Caspr	Contactin associated protein 1
CC	Corpus Callosum
Cdc42	Cell Division Cycle 42
cDNA	Complementary DNA
ChIP-seq	Chromatin immunoprecipitation-sequencing
CHX	Cycloheximide
CNP/CNPase	2´, 3´-Cyclic nucleotide-3´-phosphodiesterase
CNS	Central nervous system
CNTF	Cilliary neurotrophic factor
Cntn1/2	Contactin-1/-2
Cox20	Cytochrome c oxidase assembly factor
CSF	Cerebrospinal fluid
Ctrl	Control

Cul1	Cullin 1
DAG	Diacylglicerol
DAPI	4’-6-diamidino-2-phenylindale
DBD	DNA-binding domain
DEG	Differentially expressed gene
DG	Dentate gyrus
dH_2O	Distilled water
DIV	Days *in vitro*
DMEM	Dulbecco’s modified Eagle´s medium
DMSO	Dimethyl sulfoxide
DNA	Deoxyribonucleic acid
DNAse	Deoxyribonuclease
Dpf	Days post fertilization
DTT	Dithiothreitol
DV	Dorso-ventral
E1	Ubiquitin-activating enzyme
E2	Ubiquitin-conjugating enzyme
E3	Ubiquitin ligase
EDTA	Ethylenediamine tetraacetic acid
EdU	5’-ethynyl-2’-deoxyuridine
EGFP	Enhanced Green Fluorescent Protein
Eif4e	Eukaryotic translation initiation factor 4E
EM	Electron microscopy
ER	Endoplasmic reticulum
Eri1	Exoribonuclease 1
ERK	Extracellular signal-regulated kinase
EtOH	Ethanol
EV(s)	Extracellular vesicle(s)
F-actin	Filamentous actin
FBS	Fetal bovine serum
Fbxw7	F-box and WD repeat domain-containing 7
FDA	Food and Drug Administration
FGF	Fibroblast growth factor
Fgfr2	Fibroblast growth factor receptor 2
FISH	Fluorescence *in situ* Hybridization
FL-MYRF	Full-length MYRF
Flna	Filamin A
FTH1	Ferritin heavy chain
GAPDH	Glyceraldehyde-3-phosphate dehydrogenase
GFP	Green Fluorescent Protien
GM	Grey matter
GO	Gene ontology
Gpd1	Glycerol-3-phosphate dehydrogenase 1
Gpr37	G Protein-Coupled Receptor 37

GSK3	Glycogen synthase kinase-3
GTPase	GTP hydrolase
h	Hour
Hapln2	Hyaluronan and Proteoglycan Link Protein 2
HBSS	Hank's balanced salt solution
HEK293T	Human Embryonic Kidney 293T
Hes1/5	Basic helix-loop-helix transcription factor 1/5
Hnrnpu	Heterogeneous Nuclear Ribonucleoprotein U
Hpf	Hours post fertilization
HRP	Horseradish peroxidase
Iba1	Ionized calcium-binding adaptor molecule 1
ICA	Intramolecular Chaperone Auto-cleavage
ICC	Immunocytochemistry
ICV	Intracerebroventricular
Id2/4	Inhibitor of DNA binding 2/4
IDT	Integrated DNA Technologies
IGF-1	Insulin-like growth factor 1
IgG	Immunoglobulin G
IHC	Immunohistochemistry
IMDM	Iscove's modified Dulbecco's medium
IP	Immunoprecipitation
Iscu	Iron-sulfur cluster assembly enzyme
K^+	Potasium
K48/K63	Lysine residue 48/63
KCl	Potassium chloride
kDa	Kilodalton
Kif21a	Kinesin family member 21A
LAR II	Luciferase Assay Reagent II
Limk1	LIM domain kinase 1
lncRNA	Long non-coding RNA
Lpin1	Lipin-1
Lypla2	Lysophospholipase 2
M	Months
MACS	Magnetic activated cell sorting
MAG	Myelin associated glycoprotein
MAPK	Mitogen-activated protein kinase
MAPT	Microtubule-associated protein tau
MBP	Myelin basic protein
MCI	Mild cognitive impairment
MCT	Monocarboxylate transporter
mHepa	Mouse Hepatocellular Carcinoma
min	Minute
miRNA	MicroRNA
ML	Medio-lateral

MOG	Myelin oligodendrocyte glycoprotein
MRI	Magnetic resonance imaging
mRNA	Messenger ribonucleic acid
mTOR	Mammalian Target of Rapamycin
MW	Molecular weight
MYRF	Myelin regulatory factor
MYRF-CUGS	MYRF-related Cardiac Urogenital Syndrome
N-MYRF	N-terminal fragment of MYRF
Na^+	Sodium
ncRNA	Non-coding RNA
Ndfip1	Nedd4 Family Interacting Protein 1
NEM	N-ethylmaleimide
Nfasc	Neurofascin
NG2	Neuron-glial antigen 2
NGS	Normal goat serum
Nipal4	Nipa-Like Domain-Containig 4
Nkx2.2	NK2 Homeobox 2
Nkx6.2	NK6 Homeobox 2
NPC	Neural progenitor cell
ns	Not significant
NT-3	Neurotrophin 3
O/N	Overnight
OL(s)	Oligodendrocyte(s)
Olig1 and 2	Oligodendrocyte transcription factor 1 and 2
OPC	Oligodendrocyte progenitor cell
ORA	Over-representation analysis
Otulin1	OTU deubiquitinase with linear linkage specificity
P	Phosphate / phosphorylation
P/S	Penizilin and streptomycin
p70S6K	Ribosomal protein S6 kinase beta-1
PB	Phosphate buffer
PBS	Phosphate saline buffer
PCR	Polymerase chain reaction
PDGF	Platelet-derived growth factor
PDGFR-α	Platelet-derived growth factor receptor-α
PDL	Poly-D-Lysine
Peli1	Pellino E3 Ubiquitin Protein Ligase 1
PFA	Paraformaldehyde
Pgk1	Phosphoglycerate kinase 1
PI3K	Phosphatidylinositol 3-kinase
PKA	Protein kinase A
PKC	Protein kinase C
PLA	Proximity ligation assay
PLB	Passive Lysis Buffer

PLP	Myelin proteolipid protein
PNS	Peripheral nervous system
PP1A/2A	Protein Phosphatase 1A/2A
PSEN1/2	Presenilin 1 and 2
pSer	Phosphoserine
Psma5	Proteasome 20S Subunit Alpha 5
Psmb3	Proteasome 20S Subunit Beta 3
Puro	Puromycin
Rac1	Rac Family Small GTPase 1
Rbx1	Ring-Box 1
Rffl	Ring Finger and FYVE Like Domain Containing E3 Ubiquitin Protein Ligase
RIPA	Radioimmunoprecipitation assay buffer
RNA	Ribonucleic acid
RNA-seq	RNA sequencing
RNAse	Ribonuclease
Rnf220	Ring Finger Protein 220
ROI	Region of interest
Rpm	Revolutions per minute
rRNA	Ribosomal RNA
Rsrp1	Arginine and serine rich protein 1
RT	Room temperature
RT-qPCR	Real Time Quantitative Polymerase Chain Reaction
RTA	Real Time Analysis
RTK	Receptor tyrosine kinase
S.E.M.	Standard error of the mean
SCF	Skp-Cullin-F-box containing complex
SDS	Sodium dodecyl sulfate
SDS-PAGE	SDS polyacrylamide gel electrophoresis
Ser	Serine
siRNA	Small interfering RNA
SIRT2	Deacetylase sirtuin 2
Skp1	S-phase kinase-associated protein 1
Slc45a3	Solute carrier family 45 member 3
SOX2/3/10	Sex determining Region Y-Box 2/3/10
Srebf1/2	Sterol regulatory element-binding transcription factor ½
Surf1	Surfeit locus protein 1
SV40	Simian virus 40
T3	Triiodotironine / Thyroid hormone 3
T4	L-Thyroxine
TBS	Tris-buffered saline
TBST	Tris-buffered saline/0.1% Tween-20
TM	Transmembrane
TMEM98	Transmembrane protein 98

Tppp	Tubulin Polymerization Promoting Protein
TSA	Tyramide Signal Amplification
Tyr	Tyrosine
Ub	Ubiquitin
Ubb	Ubiquitin B
Ugt8	UDP Glycosyltransferase 8
UPS	Ubiquitin-proteasome system
Uqcrq	Ubiquinol-cytochrome c reductase complex III subunit VII
WB	Western blot
WM	White matter
WMH	White matter hyperintensities
WT	Wild type

Introduction

1. OLIGODENDROCYTES

Glial cells, constituting approximately half of the cells within the central nervous system (CNS), have historically been perceived as passive bystanders in CNS function. However, emerging evidence increasingly underscores their indispensable role in regulating various aspects of CNS physiology (Allen & Lyons, 2018). Oligodendrocytes (OLs) represent one of the major glial cell types in the CNS, along with microglia and astroglia. OLs were first described by Spanish neuroscientist Pío del Río Hortega in 1921, whose study unveiled their intricate cellular morphology, characterized by a small cell body containing nuclei rich in chromatin and a highly complex network of cytoplasmic extensions filled with granules. OLs stand out as specialized cells responsible for myelinating axons, and thus facilitating efficient axonal conduction while supporting neuronal health and function.

1.1. Oligodendrocyte functions

Oligodendrocytes play multifaceted roles crucial for CNS homeostasis and neuronal function. They are pivotal in regulating efficient conduction velocity, maintaining ionic balance, and supporting axonal trophic and metabolic demands with energy-rich substrates (**Figure 1**). Moreover, apart from maintaining long-term axonal integrity and neuronal homeostasis, OLs and their precursor cells, oligodendrocyte precursor cells (OPCs), also interact with other cell types in the CNS. And they have also been involved in different stages of memory, such as memory consolidation and recall in associative learning (Munyeshyaka & Fields, 2022). Consequently, the disruption or loss of OLs function can have profound implications, contributing to the pathogenesis of various neurodegenerative and neuropsychiatric disorders, including multiple sclerosis, leukodystrophies (Stadelmann et al., 2019), and Alzheimer's disease (S. Han et al., 2022). Thus, a comprehensive understanding of OLs biology is essential for elucidating the underlying mechanisms of these disorders and developing targeted therapeutic interventions aimed at preserving or restoring OL function.

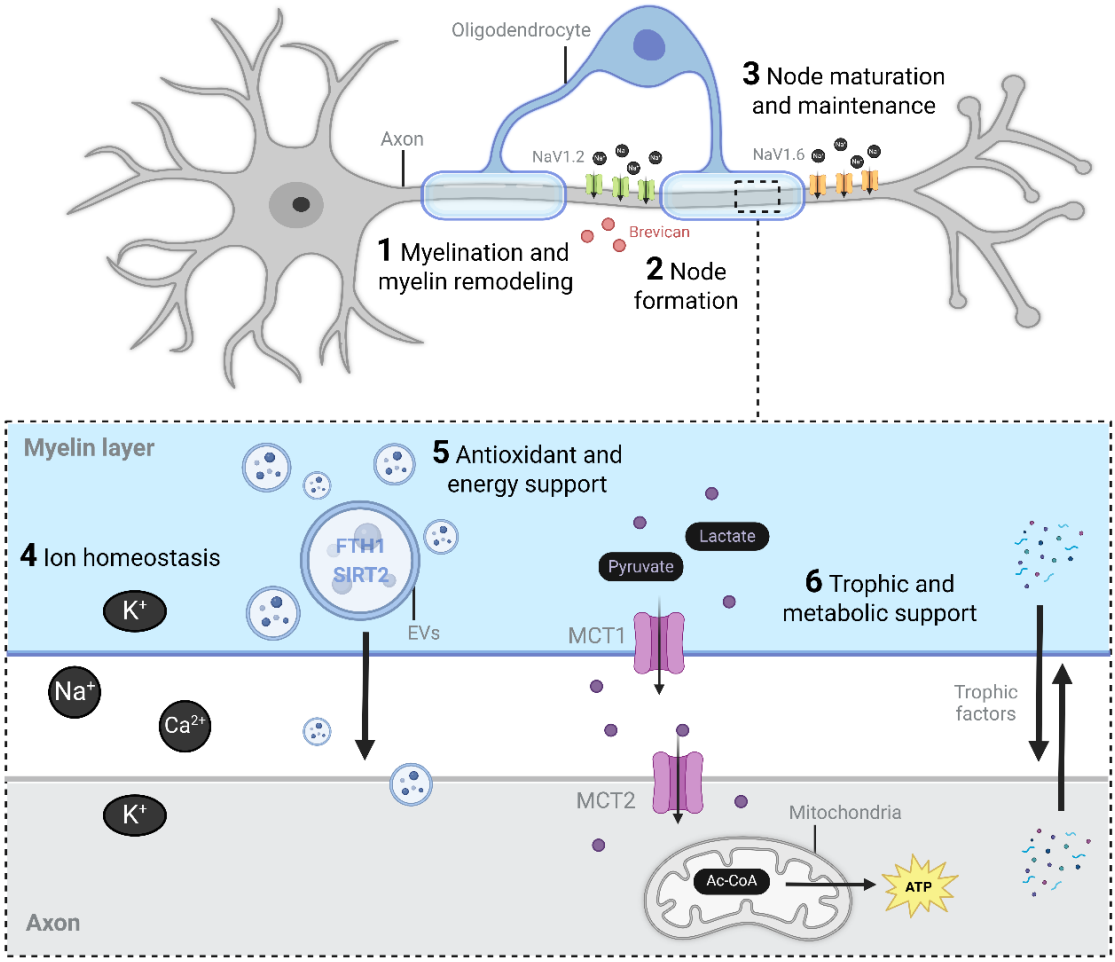

Figure 1. Oligodendrocyte functions in the developing and adult CNS. (**1**) OLs elaborate and remodel myelin sheaths. (**2**) OLs secrete extracellular matrix molecules, such as brevican, which trigger the clustering of NaV1.2 into pre-nodes. (**3**) OLs participate in nodal maturation by exchanging NaV1.2 for NaV1.6 and contribute to nodal maintenance. (**4**) OLs maintain ion homeostasis. (**5**) OLs secrete extracellular vesicles (EVs) containing molecules like FTH1 and SIRT2 to provide axons with energy and antioxidant support. (**6**) OLs provide axons with trophic factors and metabolites. They generate lactate or pyruvate and transfer them to axons via the periaxonal space through monocarboxylate transporter 1 (MCT1) and 2 (MCT2). Neurons then catabolize these molecules in the mitochondria to generate ATP. Adapted from Pepper et al., 2018, and Krämer-Albers & Werner, 2023. Created with BioRender.com

1.1.1. Myelination

The primary function of OLs is to generate and maintain myelin (**Figure 1.1**), a highly specialized multilamellar lipid-rich structure that gives the white matter (WM) its color. This specialized membrane provides the structural basis for the rapid impulse propagation required to develop motor, sensory and cognitive functions in the CNS. Functionally, myelin enables maximum conduction velocity (20-100-fold faster than non-myelinated axons) and reduces axonal energy consumption (Crotty et al., 2006; Waxman, 1997).

The precise and coordinated production of myelin is essential for the correct development and functioning of the CNS; therefore, myelination is a tightly regulated process. *In vivo*, myelin is selectively targeted to certain axons based on their biophysical properties, such as axon size, with various extracellular signals serving as permissive or repulsive cues (Rafael Góis Almeida, 2018; Snaidero et al., 2014). OLs must effectively integrate these complex regulatory signals to control their responses and ensure proper myelin formation. Upon OL stimulation by extracellular mediators, multiple intracellular signaling pathways are activated to promote myelination. Key pathways include the PI3K/Akt/mTOR and ERK1/2-MAPK pathways, as well as Ca^{2+}/CaMKII signalling, as myelin formation mediators (Gaesser & Fyffe-Maricich, 2016; White & Krämer-Albers, 2014). Additionally, myelination is also regulated by a complex interplay of OL transcription factors such as Olig1, Sox10, and MYRF. These transcription factors collectively govern the sequential events of OL development and myelination, ensuring the proper formation and maintenance of myelin sheaths. Therefore, maintaining appropriate expression levels and function of these transcription factors is crucial. Importantly, *in vivo* studies have demonstrated that ablation or blocking of these factors leads to myelin loss (Dai et al., 2015; Hornig et al., 2013; Koenning et al., 2012), highlighting their significant contribution to the myelin synthesis process.

During myelination, mature OLs extend several elongated membrane processes to make contact with axons and wrap around them, forming discrete segments of myelin sheaths along their length. The most accepted model that explains the underlying mechanism of myelination describes OLs initially forming a triangular membrane that simultaneously expands around and along the axon, in a coordinated bi-directional way. The axon is then wrapped in progressive membrane layers, where the outermost layer is closer to OL cell body, and the innermost is in direct contact with the axon (Nawaz et al., 2015; Samanta & Salzer, 2015; Zuchero et al., 2015). This process involves rapid cytoskeletal reorganization in OLs, driven by the axon-oligodendrocyte recognition (Bauer et al., 2009; Simons & Trotter, 2007; Snaidero et al., 2014).

Structurally, electron microscopy studies have revealed that myelin exhibits a high degree of conservation across species, showing fundamental similarities between zebrafish and mammalian models (Preston & Macklin, 2015). The spiraling pattern of myelin around axons gives rise to two distinct periodic morphological features: alternating electron-dense and -light layers. The dense layers consist of tightly compacted lipid

bilayers, whereas the light layers, also known as the interperiod line, contain cytoplasmic channels that allow for metabolic exchange between the OL cell body and the myelin sheath (**Figure 2**) (Hartline, 2008). This structural arrangement provides high electrical resistance and low capacitance, essential for efficient axon potential propagation. Myelinated segments along axons are separated by nodes of Ranvier, small periodic unmyelinated regions where the excitable axonal membrane is exposed to the extracellular space. Consequently, action potential generation is restricted to these nodes, characterized by a high density (>1200 / μm^2) of voltage-dependent sodium channels (**Figure 1.2, 1.3**). Action potentials jump from one node of Ranvier to the next along the axon, enabling rapid saltatory conduction (Moore et al., 2020; Nave, 2010; Waxman & Ritchie, 1993). Adjacent to the nodes, myelin lateral edges form the paranode, a non-compacted structure where myelin is firmly attached to the axon. This specialized contact area is maintained by the adhesion of contactin-1 and Caspr proteins on the axonal surface and Neurofascin-155 on the glial side (**Figure 2**) (Stadelmann et al., 2019).

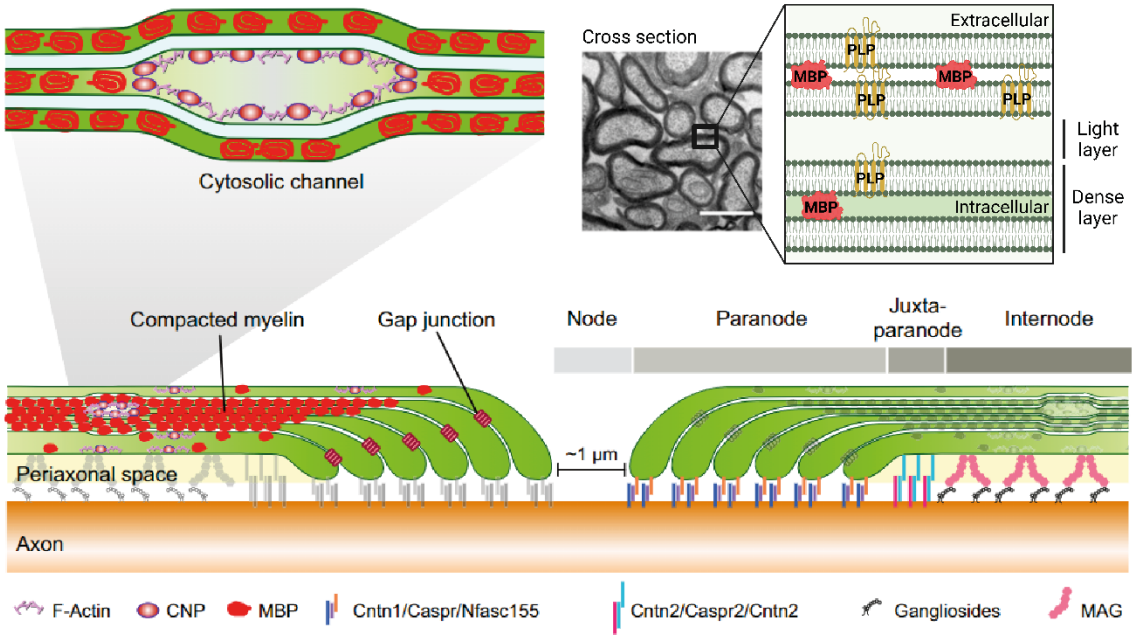

Figure 2. Schematic representation of the central nervous system myelin structure. Myelin is composed of tightly stacked layers of oligodendrocyte cell membranes, exhibiting two alternating distinct types of layers that are observable under electron microscopy: electron-dense and –light layers. The compaction of these membranes is primarily obtained by Myelin basic protein (MBP), which tightly zippers the cytoplasmic surfaces together. 2',3'-Cyclic nucleotide 3'-phosphodiesterase (CNPase) interacts with the actin cytoskeleton, counteracting the polymerizing forces exerted by MBP, and thereby forming cytoplasmic channels within the myelin sheath. Gap junctions establish connections between the paranodal loops of myelin located at the lateral edges of the myelin sheath. MAG: myelin-associated glycoprotein. Adapted from Stadelmann et al., 2019.

In addition to its membrane ultrastructure, the specialized composition of myelin makes it a unique membrane in the CNS. While most plasma membranes consist of approximately equal proportion of protein and lipids (50% proteins and 50% lipids, by dry weight), the myelin sheath is characterized by a high proportion of lipids (70%–85%) and a low proportion of small proteins (15%–30%), with Myelin basic protein (MBP) and Proteolipid protein (PLP) being the most abundant (**Figure 2**). This high lipid / protein ratio in myelin creates a hydrophobic environment that exerts a repulsive force towards the extracellular fluid, thereby contributing to the compaction and tight organization of the myelin sheath (Min et al., 2009). Furthermore, the components of the myelin membrane have half-lives ranging from several weeks to months, making it a remarkably stable structure (Fornasiero et al., 2018).

Despite its stability, myelination is a dynamic and plastic process that occurs over extended periods throughout life (Miller et al., 2012). In humans, myelination mainly occurs within the first 2 years of life, but WM volume continues to increase until around mid-life, driven by the myelination of new axonal projections. In contrast, myelin formation in rodents is typically completed in around 2 months, while robust myelination occurs within the first week of zebrafish life. Moreover, the maintenance and turnover of myelin driven by OLs enable the adaptation of myelin sheaths in response to changes in environmental stimuli, experience and neural activity, even in adulthood (Forbes & Gallo, 2017). Remarkably, neurotransmitters can modulate OPCs and OLs behavior: in response to higher neural activity, OLs regulate myelin sheath production (Fields, 2015). Furthermore, myelin plasticity also plays a critical role in the regeneration of myelin following demyelinating injuries.

1.1.2. Metabolic and trophic support of axons

In addition to electrical insulation of axons, oligodendrocytes also play essential roles in ion homeostasis (**Figure 1.4**) and trophic and metabolic support for neurons. In this line, OLs can generate lactate or pyruvate in an activity-dependent manner (Saab et al., 2016), and transfer them to neurons through monocarboxylate transporter 1 (MCT1) located at the uncompact inner tongue of the myelin sheath. Then, lactate is taken up from the extracellular space by neurons, where it is catabolized to generate ATP (**Figure 1.6**) (Y. Lee et al., 2012; Rinholm et al., 2011).

Moreover, it has been recently described that OLs also provide axonal support via transcellular delivery of extracellular vesicles (EVs), usually with neuroprotective aims. For instance, OLs provide neurons with ferritin heavy chain (FTH1) through exosomes, which is thought to be a protective mechanism against oxidative stress in aging (Mukherjee et al., 2020). Additionally, they also deliver NAD-dependent deacetylase sirtuin 2 (SIRT2), which enhances neuronal ATP production by deacetylating mitochondrial proteins boosting axonal bioenergetics under pathological conditions (**Figure 1.5**) (Chamberlain et al., 2021).

Other metabolites, nutrients and signaling molecules are also transported from OL soma towards axons through the non-compacted myelin areas called cytoplasmic channels (Nave & Werner, 2014). In fact, CNPase-null mice presents loss of these cytoplasmic channels, which results in a progressive axonal degeneration. In contrast, while MBP-null or *shiverer* mice develop a severe demyelination, they preserve the axonal integrity and function, likely by maintaining the glial metabolic support through the thin, uncompacted myelin process (Snaidero et al., 2017). Indeed, these observations in knockout mice for specific myelin proteins suggest that the absence of myelin is better than defective myelin for sustaining proper axonal functions, as defective myelin is associated with oligodendrocyte-axon metabolic support disconnection (Philips & Rothstein, 2017; Simons & Nave, 2016).

1.1.3. Other functions of oligodendrocyte progenitor cells

Interestingly, OPCs have recently been described as much more than only precursor cells for generating myelinating OLs. Actually, it has been proposed that OPCs act as sensors of physiological signals, which they integrate to subsequently mediate other surrounding cells. For example, they have been reported to be involved in sensing hypoxia to stimulate angiogenesis (Yuen et al., 2014) and acting as antigen-presenting cells upon demyelination (Falcão et al., 2018; Kirby et al., 2019), among other novel functions. In addition to their roles as signal integrators and mediators of non-neuronal cells, OPCs also participate in the regulation of neuronal circuitry in the healthy CNS (Y. Xiao & Czopka, 2023).

1.2. Oligodendrocyte differentiation

The development and differentiation of OLs are tightly regulated processes that involve a series of molecular signaling events and interactions with surrounding neural cells. During late embryonic developmental stages, oligodendrocyte progenitor cells (OPCs) originate from multipotential neural progenitor cells (NPCs) in specific regions of the CNS. Under specific signals, NPCs start to express Olig2, triggering the first embryonic wave of OPC specification (**Figure 3**) (Naruse et al., 2017). Then, these OPCs migrate from the ventricular/subventricular zone of the brain to the developing WM, where they proliferate and establish an evenly spaced network of cell processes. Interestingly, unlike other undifferentiated stem and progenitor cells, OPCs are evenly distributed throughout the CNS rather than residing in specific niches (Dawson et al., 2003; Marisca et al., 2020). Upon OPC migration and establishment at a suitable region, some of them stay in a precursor state, while others undergo differentiation into post-mitotic mature OLs (Simons & Nave, 2016). Intrinsic and extrinsic factors allow segregation of OPCs into functionally different groups, which restrict their roles and propensities to differentiate (Marisca et al., 2020; Spitzer et al., 2019).

The process of creating mature OLs from OPCs is called oligodendrogenesis, and it is characterized by several stages of cell maturation defined by morphological aspects and the expression of specific marker proteins (Emery, 2010). This sequential expression of developmental markers divide the oligodendroglial lineage into distinct phenotypic stages (Baumann & Pham-Dinh, 2001). In fact, a recent single-cell RNA-sequencing analysis identified a continuum of 12 different subpopulations within the oligodendrocytic lineage ranging from OPCs to mature OLs, suggesting that oligodendrocyte differentiation represents a series of linked cellular transformations (Marques et al., 2016).

Shortly, initially early progenitor cells (early OPCs), responsible for migration and proliferation, express the platelet-derived growth factor receptor-α (PDGFR-α) and exhibit a bipolar or stellate morphology. Then, early OPCs differentiate into late progenitor cells (late OPCs), which acquire the marker O4 and the proteoglycan neuron-glial antigen 2 (NG2), and develop a more complex shape. At this stage, cells keep their ability to proliferate, but they lose their motility almost completely. Following oligodendrocyte lineage progression, late OPCs give rise to pre-myelinating or immature OLs, down-regulating PDGFR-α and NG2 expression while retaining SOX10 and OLIG2

expression. Immature OLs are characterized by the expression of the earliest myelin-related marker, 2′,3′-cyclic nucleotide 3′-phosphodiesterase (CNPase), along with OL cell surface markers O4 and O1. Moreover, they can be further distinguished from other OL lineage cells based on their aspect, as they develop a highly branched morphology of fine processes aimed at reaching axons. Finally, these immature cells differentiate into mature myelinating OLs, expressing CC1 and producing myelin-related proteins such as myelin basic protein (MBP), proteolipid protein (PLP), myelin-associated glycoprotein (MAG), and myelin oligodendrocyte glycoprotein (MOG) (**Figure 3**) (Fletcher et al., 2021). Morphologically, mature OLs form myelin sheaths, with rod-like processes oriented parallel in the WM and randomly in the grey matter (GM) (Young et al., 2013a). It has been recently shown that mature OLs persist life-long in mice and humans, actively producing and maintaining myelin throughout the CNS (Tripathi et al., 2017; Yeung et al., 2014).

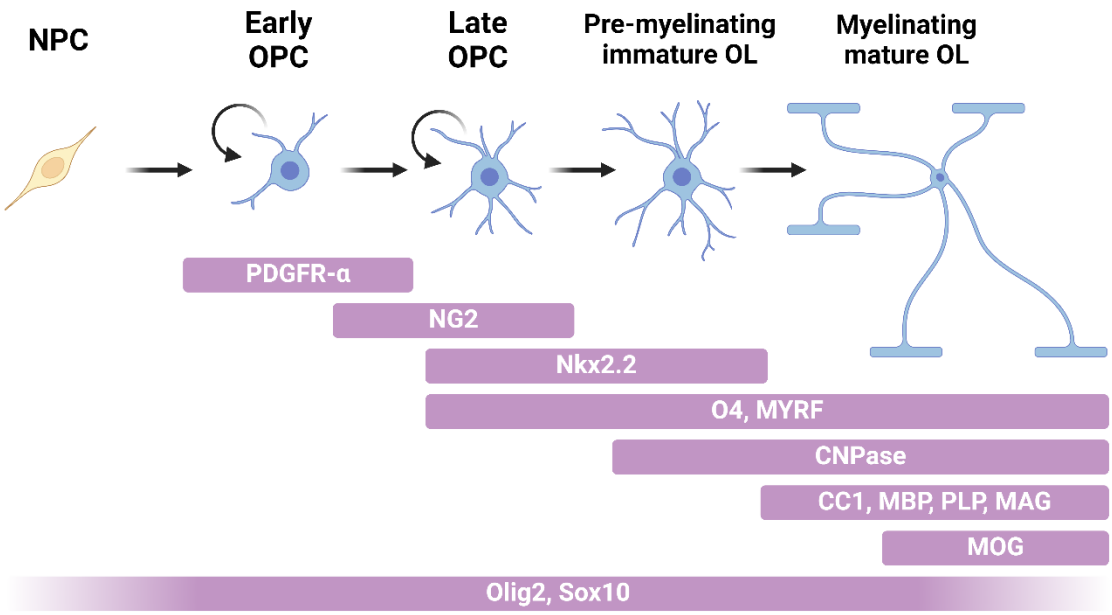

Figure 3. Oligodendrocyte differentiation stages. Cells within the oligodendroglial lineage arise from neural progenitor cells (NPCs), and undergo distinct stages of differentiation characterized by specific protein expression patterns. These stages include early oligodendrocyte progenitor cells (early OPCs), late oligodendrocyte progenitor cells (late OPCs), pre-myelinating or immature OLs, and myelinating mature OLs. OPCs express PDGFR-α and the NG2 proteoglycan. Upon differentiation, pre-myelinating OLs upregulate Nkx2.2, O4 and MYRF, and initiate expression of the first myelin-related protein, CNPase. Mature myelinating OLs express CC1 and various myelin-related proteins, including MBP, PLP and MAG, with MOG being the last to be expressed. All cells of the oligodendroglial lineage express the transcription factors Olig2 and SOX10, although their expression levels gradually decline during maturation. Adapted from Pepper et al., 2018. Created with BioRender.com

After development, a population of OPCs remains in the adult brain, preserving their ability to proliferate and generate new mature OLs, which will be needed to maintain myelin in both healthy or diseased brains (Young et al., 2013a). Notably, it has been described that new myelin formation after demyelination primarily occurs through the differentiation of specialized OPCs rather than existing mature OLs (Czopka et al., 2013).

1.2.1. Mechanisms regulating oligodendrocyte differentiation

The process of oligodendrocyte differentiation is intricately controlled by a multitude of well-coordinated events and regulatory mechanisms, spanning from the proliferation of OPCs to the regulation of myelin synthesis. This regulatory landscape is governed by a complex interplay of molecular signals, transcriptional networks, epigenetic modifications, and extracellular cues, collectively ensuring the precise orchestration of OL differentiation and myelination (Almeida et al., 2011; Samudyata et al., 2020). Therefore, a wide repertoire of both positive and negative regulators contribute to the tight control of these processes.

Extrinsic factors present in the microenvironment surrounding OPCs play a crucial role in regulating OL differentiation. For instance, in the adult brain, OPCs exhibit region-dependent differences in their ability to proliferate and differentiate: cells in GM regions have a longer cell cycle and lower differentiation properties, as compared to cells in the WM (Dimou et al., 2008; Simon et al., 2011). Among regulatory extracellular cues, growth factors such as platelet-derived growth factor (PDGF) and fibroblast growth factor (FGF) promote OPC proliferation and survival (Pukos et al., 2018; Woodruff et al., 2004), while neurotrophic factors like brain-derived neurotrophic factor (BDNF) regulate OL maturation and myelination (Fletcher et al., 2018; J. Xiao et al., 2011). Moreover, in addition to its involvement in OPC survival and proliferation, insulin-like growth factor 1 (IGF-1) signalling is also required for OL differentiation and myelin formation (Zeger et al., 2007) via PI3K/Akt/mTOR signaling pathway (Flores et al., 2008; Tyler et al., 2009). Thyroid hormone 3 (T3) also contributes to OL differentiation, with observations of reduced myelin gene expression in hypothyroidism patients and rodents (S. Mitew et al., 2014). Furthermore, cell-cell interactions mediated by signalling molecules and extracellular matrix components also influence OL differentiation and myelination capacity (Colognato & Tzvetanova, 2011).

Concerning the intracellular regulators of OL differentiation, transcription factors play a central role in regulating and shaping the progression of OPCs towards mature OLs (**Figure 4**). Positive regulators include Myelin Regulatory Factor (MYRF), Olig1/2, Sox2/3/10 and Nkx2.2 that interact synergistically to drive OL maturation (Elbaz & Popko, 2019; Hornig et al., 2013). Olig2, a key transcriptional factor expressed in OPCs and throughout the whole OL lineage, is essential for the OL fate determination during early CNS development. Olig2 promotes the expression of genes involved in OL differentiation while repressing alternative lineage pathways (Kitada & Rowitch, 2006; Küspert et al., 2011). Then, its levels progressively decrease at mature stages. In fact, ablation of Olig2 in OPCs causes a sustained decrease in OL differentiation, while ablation in mature cells have no detrimental effect, suggesting that Olig2 mediates cell differentiation but has no role on mature OL functions, as myelination (Mei et al., 2013). Similarly, Sox10, a member of the SRY-related HMG-box (Sox) family of transcription factors, is also critical for the maintenance of OPC identity and the progression of OPCs towards mature OLs (Küspert & Wegner, 2016; Wittstatt et al., 2019). Sox10, in conjunction with Olig2, regulates the expression of genes required for OL differentiation and myelination, including the transcription factor MYRF and lipid synthesis enzymes (Hornig et al., 2013). Finally, MYRF is specifically upregulated during OL differentiation, and it is essential for the induction of myelin-related genes expression (Emery, 2010; H. Huang et al., 2021). Importantly, MYRF is also required for maintaining myelin in the adult brain (Emery et al., 2009; Koenning et al., 2012).

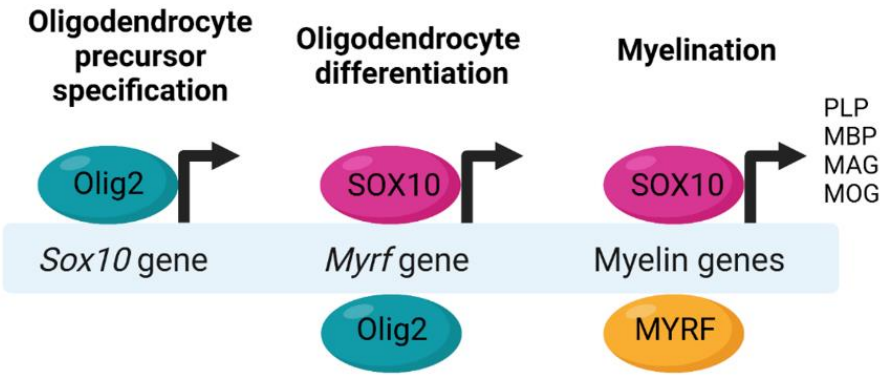

Figure 4. Transcriptional networks regulating myelination in oligodendrocytes. Olig2 acts during OPC specification stage to promote the expression of Sox10. Next, during OL differentiation, the collaborative action of Sox10 and Olig2 induces the expression of MYRF, with Sox10 binding the intron 1 enhancer/ECR9. Finally, Sox10 and MYRF act together at myelin gene promoters and enhancers to drive myelin-related genes and proteins expression. Adapted from Emery, 2013. Created with BioRender.com

Conversely, negative regulators such as Hes family basic helix-loop-helix (bHLH) transcription factors 1 and 5 (Hes1/5) and inhibitor of DNA binding 2 and 4 (Id2/4) act to inhibit OL differentiation by directly binding to pro-differentiation factors such as Olig1 and Sox10, thereby repressing their function (Liu et al., 2006; Samanta & Kessler, 2004). These negative regulators play essential roles in maintaining the proper balance between OPC proliferation and differentiation within the OL lineage.

Moreover, in the recent years several epigenetic mechanisms, such as DNA methylation, histone modifications, long non-coding RNAs (lncRNAs), and chromatin remodelling, have been described to contribute to the regulation of OL differentiation (Samudyata et al., 2020). These mechanisms modulate the accessibility of chromatin to transcription factors and other regulatory proteins, thereby influencing gene expression programs associated with OL development (Koreman et al., 2018). Ultimately, epigenetic remodelling of the genome not only regulates gene expression levels, but it can also modulate the binding affinities of transcription factors to target genes.

Finally, microRNAs (miRNAs) have also recently emerged as critical regulators of OL differentiation, exerting post-transcriptional control over gene expression. Dynamic expression patterns of miRNAs during OL development suggest their pivotal roles in modulating the differentiation process (Galloway & Moore, 2016). For instance, during the maturation of OLs, miR-219, -338, and -138 promote OL development and myelination by repressing factors that inhibit OL differentiation, including Hes5, Sox6 and PDGFR-α (X. Zhao et al., 2010).

2. MYELIN REGULATORY FACTOR

The process of myelination, whereby oligodendrocytes ensheath axons with myelin, constitutes a critical event in CNS development and function. Among the diverse array of transcription factors orchestrating this intricate process, Myelin Regulatory Factor (MYRF) stands out as a key regulator of late OL differentiation and myelin-related functions, including myelin formation, upkeep, and repair (Elbaz & Popko, 2019; H. Huang et al., 2021).

The *Myrf* gene was initially identified through gene profiling studies utilizing immunopanning to isolate astrocytes, neurons, and OLs from the postnatal mouse forebrain (Cahoy et al., 2008). This study revealed that *Myrf*, previously denoted as Gene Model 98, is expressed in pre-myelinating and myelinating OLs but not in OPCs, underscoring its specific involvement in OL maturation and myelination processes. Indeed, genetic ablation of *Myrf* within the OL lineage did not perturb OPC generation or proliferation, but notably impeded their differentiation into fully mature myelinating OLs. Furthermore, inducible conditional deletion of *Myrf* in mature cells of adult mice resulted in a marked down-regulation of myelin gene expression and severe demyelination, accompanied by neurological impairments (Emery et al., 2009; Koenning et al., 2012). Interestingly, *Myrf* is not expressed in the peripheral nervous system (PNS), including Schwann cells responsible for PNS myelination (Emery et al., 2009). Collectively, these findings firmly establish MYRF as a pivotal regulator of OL maturation, primary myelin formation, and the life-long maintenance and repair of myelin in the CNS.

2.1. Molecular structure and mechanism of action of MYRF

MYRF exhibits atypical molecular characteristics as a transcriptional factor. Structurally, the protein contains at least four distinct functional and structural domains that demonstrate remarkable homology across species. These domains include a DNA-binding domain (DBD) at the N-terminal, which shares homology with the one in the yeast transcription factor *Ndt80*, and an Intramolecular Chaperone Auto-cleavage domain (ICA), a transmembrane domain, and a functionally uncharacterized MYRF conserved domain (MYRF_C2) at the C-terminal (**Figure 5**) (Bujalka et al., 2013; Li et al., 2013). Notably, the ICA domain demonstrates homology to a domain found in the bacteriophage endosialidase tailspike protein, establishing MYRF as the first eukaryotic protein identified with this homology (Li et al., 2013; Senoo et al., 2013). Typically, such domains contribute to quaternary structure assembly.

Initially synthesized as a type-II transmembrane protein anchored in the endoplasmic reticulum (ER), MYRF follows a unique activation process. First, it must undergo a homo-trimerization process facilitated by the ICA domain, which acts as an intramolecular chaperone to assist MYRF in forming a triple β helix (D. Kim et al., 2017; Schulz et al., 2010; Schwarzer et al., 2007). Following homo-trimerization, the ICA

domain catalyzes an auto-processing reaction, cleaving the full-length MYRF (FL-MYRF) at three P586-S587 peptide bonds that connect the ICA homo-trimer to the N-terminal region of MYRF (N-MYRF) (**Figure 5**). Given its evident participation in MYRF's processing, the integrity of the ICA domain is crucial for MYRF activation. In fact, mutations in critical residues of this domain have been demonstrated to significantly impair not only the trimerization, but also the auto-cleavage, and the subsequent transcriptional activity of MYRF (An et al., 2020).

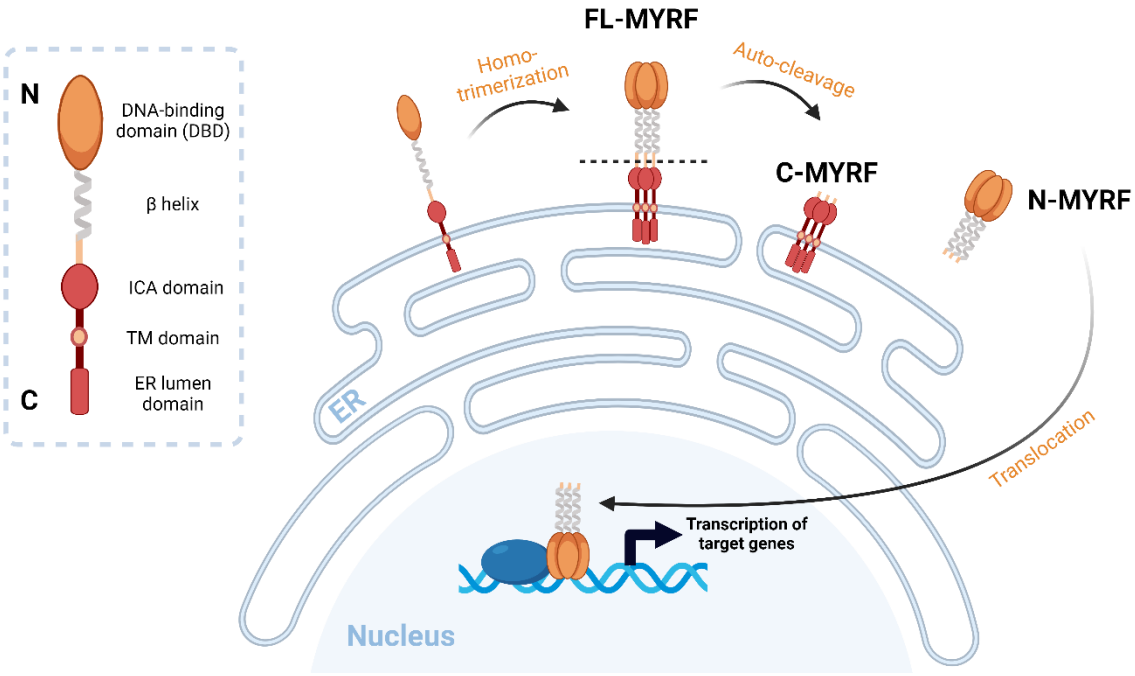

Figure 5. MYRF protein structure and mechanism of action. MYRF is generated as a transmembrane (TM) protein in the endoplasmic reticulum (ER), and needs to undergo a homo-trimerization process to perform its activity. Once trimerized, the full-length protein (FL-MYRF) is auto-cleaved from the ICA domain, and its N-terminal fragment (N-MYRF) is released from the ER to enter the nucleus, where it acts as a transcriptional factor thanks to its DNA-binding domain (DBD). Adapted from An et al., 2020. Created in BioRender.com

Upon auto-processing, the cleaved C-terminal fragment (C-MYRF) remains in the ER with yet unclear biological functions, while the N-MYRF containing the DBD is released from the ER and translocated to the nucleus, where it functions as a homo-trimeric transcription factor, inducing the expression of numerous genes (**Figure 5**) (B. Chen et al., 2018; D. Kim et al., 2017; Zhen et al., 2017). Chromatin immunoprecipitation-sequencing (ChIP-seq) analysis of MYRF in rat OLs revealed enrichment primarily in myelin-related genes, such as *Mbp*, *Plp1*, *Mag*, and *Mog*, conferring upon MYRF the

nowadays well-established identity as a key myelin regulator. However, results demonstrated that MYRF also targets other genes with diverse important biological functions for OL. These included genes encoding for cytoskeletal proteins (*Tppp, Kif21a*), receptors (*Fgfr2, Gpr37*), oligodendrocyte-neuron junctional proteins (*Cntn2, Hapln2, Nfasc*), lipid metabolism protein (*Aspa, Ugt8, Slc45a3*), transcription factors (*Sox10, Nkx6.2*), and others whose roles in myelination remain to be elucidated (*Rffl, Nipal4, Rnf220*) (Bujalka et al., 2013). This broad range of targets underscores the multifaceted functions of MYRF beyond OL differentiation and myelination processes.

Despite the necessity for exquisite regulation of MYRF's expression and activity, the mechanisms governing its regulation are not yet fully understood. Unlike other known membrane-associated transcription factors, MYRF's cleavage does not appear to be regulated in response to any known biological signal; instead, it seems to occur constitutively (Bujalka et al., 2013). However, importantly, the recent discovery of repressive interactions with the ER transmembrane protein TMEM98 suggests that MYRF's processing is subject to regulation *in vivo* (Choi et al., 2018). MYRF and TMEM98 show a similar expression pattern in pre-myelinating OLs, indicating their coexistence during OL differentiation. TMEM98 has been shown to bind to the C-terminal end of MYRF in the ER, thereby inhibiting its self-cleavage and activity. Indeed, overexpression of *Tmem98* suppressed MYRF cleavage in transfected HEK cells (Garnai et al., 2019) and inhibited OL maturation in electroporated embryonic chick spinal cords (H. Huang et al., 2018). Thus, this likely represents a crucial cellular mechanism for preventing premature OL differentiation and myelination. Nonetheless, additional regulatory mechanisms governing MYRF activity remain unclear.

2.2. Molecular mechanisms involved in MYRF degradation

Maintaining appropriate levels of transcription factors is essential for precise gene expression control and cellular function. Key to this regulation is the efficient clearance of transcription factors from the nucleus once their activity is no longer required. Thus, an effective degradation program is crucial to prevent prolonged or inappropriate gene activation, which can disrupt cellular homeostasis and contribute to diseases like cancer and neurodegenerative disorders (Chu et al., 2007; Desterro et al., 2000). However, the mechanisms governing nuclear N-MYRF degradation are incompletely understood.

According to a study conducted in mouse hepatocellular carcinoma (mHepa) cells, the stability of nuclear MYRF is regulated through the ubiquitin-proteasome system (UPS). Initially, to undergo degradation, the N-terminal of MYRF must be phosphorylated at Ser138 and Ser142 residues by glycogen synthase kinase 3 (GSK3). Then, this phosphorylation is recognized by the F-box protein Fbxw7, leading to its subsequent ubiquitination and proteasomal degradation (**Figure 6**) (Nakayama et al., 2018). Nevertheless, no studies have been conducted in oligodendrocytes to date.

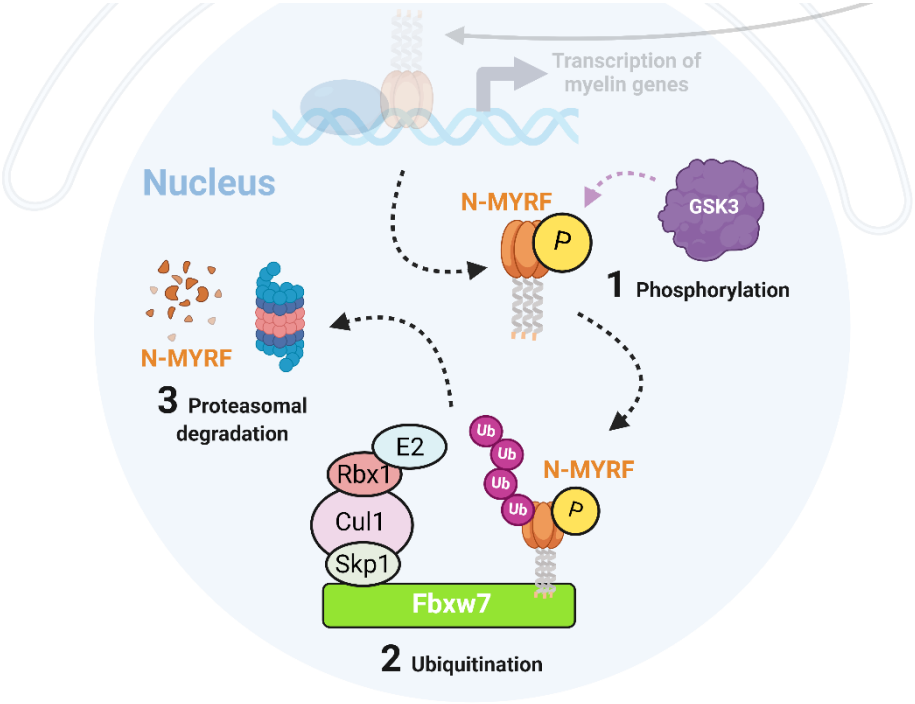

Figure 6. Model for MYRF degradation pathway. The nuclear form of N-MYRF is (**1**) phorphorylated by glycogen synthase kinase 3 (GSK3), (**2**) ubiquitinated by SCF^{Fbxw7}, and thereby targeted for (**3**) degradation by the proteasome. (Ub, ubiquitin. P, phosphorylation.) Adapted from Nakayama et al., 2018. Created with BioRender.com

2.2.1. GSK3-mediated phosphorylation

The first described step in the MYRF degradation pathway involves GSK3-mediated serine phosphorylation of N-MYRF (Nakayama et al., 2018). Glycogen synthase kinase 3 (GSK3) is a proline-directed serine/threonine kinase that stands out among kinases due to its unconventional characteristics, including constitutive activity and inhibition through phosphorylation at specific residues, diverging from typical kinase activation paradigms (Beurel et al., 2015).

This kinase exists in cells as two distinct gene products, GSK3α and GSK3β, which exhibit high homology in the catalytic domain while differing in N- and C-terminal sequences (Woodgett, 1990). GSK3 is ubiquitously expressed across the animal kingdom and in all tissues, being particularly abundant in the brain (Salcedo-Tello et al., 2011). Both GSK3α and β are collectively implicated in various physiological and pathological processes such as cancer, diabetes, neurodegeneration, and psychiatric disorders (Beurel et al., 2015). In fact, GSK3β was predicted to have more substrates than any other known kinase (Linding et al., 2007). As a result, GSK3 employs multiple regulatory mechanisms to effectively modulate its substrate-specific actions. These mechanisms include changing the subcellular localization of GSK3 and its substrates, the pre-phosphorylation of substrates by other kinases, the incorporation of GSK3 into protein complexes, and the regulatory phosphorylation of GSK3 itself (Doble & Woodgett, 2003; Jope & Johnson, 2004), with the latter being the most extensively studied.

Thus, GSK3 activity depends on its phosphorylation state (**Figure 7**). Activation requires phosphorylation at Tyr216-GSK3β and Tyr279-GSK3α residues (Hughes et al., 1993). Notably, GSK3 itself autophosphorylates these residues during translation, enabling its synthesis as an active kinase (Cole et al., 2004). Conversely, inhibition primarily occurs through phosphorylation at Ser9-GSK3β and Ser21-GSK3α. This inhibitory serine phosphorylation can be mediated by a large number of different kinases, including Akt, protein kinases A (PKA) and C (PKC), and p70S6K, all of which play crucial roles in cellular signalling pathways and pathologies (Beurel et al., 2015). In contrast, protein phosphatases 1A (PP1A) and 2A (PP2A) dephosphorylate the inhibitory serine sites of GSK3, leading to its activation (Salcedo-Tello et al., 2011).

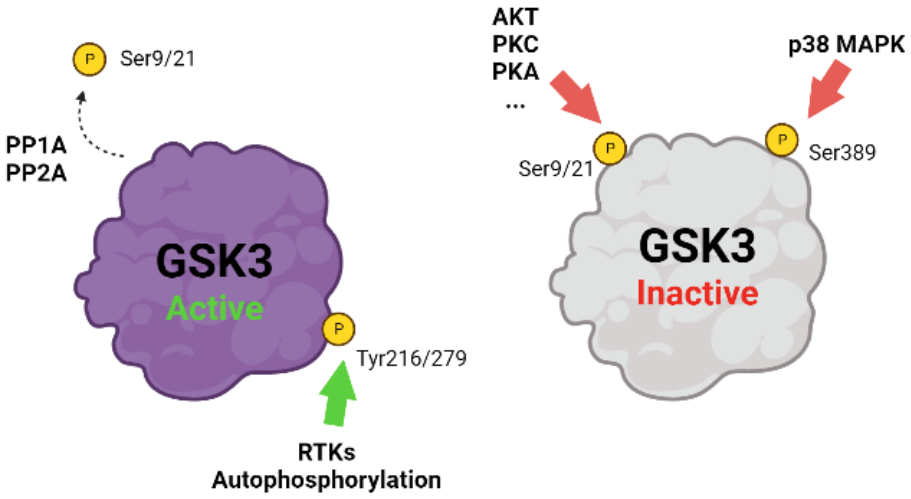

Figure 7. Modulation of GSK3 activity by phosphorylation. GSK3 can be active or inactive depending on its phosphorylation state. GSK3 is synthesized as a constitutively active kinase, through autophosphorylation in tyrosine (Tyr216/279). Members of the receptor tyrosine kinase family of cell surface receptors (RTKs) can also mediate the phosphorylation in tyrosine to activate GSK3. Protein phosphatases 1 (PP1A) and 2A (PP2A) activate GSK3 by removing the inhibitory serine (Ser9/21) phosphorylation. On the other hand, serine-phosphorylation mediated by kinases such as Akt, protein kinase C (PKC) , protein kinase A (PKA) or p38 mitogen-activated protein kinase (MAPK) inhibit GSK3 activity. Adapted from Salcedo-Tello et al., 2011. Created with BioRender.com

Therefore, the activation of PKC serves as a key upstream mechanism for inhibiting GSK3 activity, thereby blocking GSK3-mediated downstream signalling cascades. Protein kinase C (PKC) encompasses a family of phospholipid-dependent serine-threonine kinases consisting of around fifteen isozymes, categorized into three subgroups: classical, novel, and atypical PKCs. Initially catalytically inert, PKC needs to undergo phosphorylation for catalytic activation and translocation for conformational activation, relieving its autoinhibition to become a fully-active kinase (Seki et al., 2005). This activation occurs in a subtype-specific manner, stimulated by different second messengers: classical PKCs can be stimulated by both diacylglicerol (DAG) or calcium ions (Ca^{2+}), novel PKCs are DAG-dependent but calcium-independent; and, lastly, atypical PKCs are not regulated by either of these second messengers (Nakamura & Nishizuka, 1994; Ohno & Nishizuka, 2002).

PKC plays pivotal roles in multiple signal transduction cascades through the phosphorylation of its target proteins, including GSK3. In particular, PKC is implicated in a wide range of disorders such as cancer (Garg et al., 2014) and neurodegenerative diseases like multiple sclerosis, Parkinson's, and Alzheimer's disease (Garrido et al., 2002). Additionally, it also contributes to various physiological processes including neuroprotection, cell cycle regulation (Nelson & Alkon, 2009), and the differentiation of various cell types (Damato et al., 2021). Indeed, several studies have implicated PKCs in oligodendrocyte differentiation and myelination processes (Cavaliere et al., 2013; Swire et al., 2019). However, further detailed investigation is needed to elucidate the underlying molecular mechanisms governing the interaction between PKC and OL differentiation.

Therefore, although the interplay between PKC and GSK3 seems vital for relevant signalling pathways, their role in the MYRF degradation pathway in OLs remains unexplored.

2.2.2. Fbxw7-mediated ubiquitination and proteasomal degradation

Upon GSK3-mediated phosphorylation, phosphorylated N-MYRF is recognized by Fbxw7 to its subsequent ubiquitination and proteasomal degradation (Nakayama et al., 2018). The ubiquitin-proteasome system (UPS) stands as one of the most relevant protein degradation systems in eukaryotes, meticulously mediating the degradation of numerous cellular proteins with remarkable specificity. Central to this system is the covalent attachment of ubiquitin molecules to target proteins, marking them for recognition and subsequent degradation by the proteasome (Ciechanover & Schwartz, 1998; Hershko & Ciechanover, 1998). This finely tuned process ensures the elimination of misfolded or damaged proteins. Hence, dysfunctions in the UPS are associated with a variety of pathological conditions, with particular significance observed in neurodegenerative diseases characterized by pathogenic protein aggregation, such as Alzheimer's disease (Oddo, 2008). Interestingly, ubiquitin also mediates alternative non-degradative cellular signalling functions, depending on the type of ubiquitin chain and substrate involved (O'Neill, 2009), what makes it an even more complex regulatory mechanism.

In essence, the ubiquitination cascade involves three enzymes: an ubiquitin-activating enzyme (E1), an ubiquitin-conjugating enzyme (E2), and an ubiquitin ligase (E3), with the latter determining substrate specificity. Among E3 ligases, the Skp1–Cul1–F-box protein (SCF) complex is one of the most well-characterized, and it is composed of four subunits: Skp1, Cul1, Rbx1, and an F-box protein. F-box proteins are responsible for substrate recognition within each complex (Frescas & Pagano, 2008; Nakayama et al., 2018). Among these, F-box and WD repeat domain-containing 7 (Fbxw7) plays a critical role in regulating cell proliferation, differentiation and development, through the ubiquitination of key target proteins such as cyclin E, c-Myc, Notch, and c-Jun (Hoeck et al., 2010; Koepp et al., 2001; Welcker et al., 2004; Welcker & Clurman, 2008). Interestingly, a study in zebrafish identified a mutation disrupting Fbxw7, resulting in the formation of excess oligodendrocyte lineage cells (Snyder et al., 2012) and ectopic and excessive myelin gene expression. Given Fbxw7's role in targeting mTOR for degradation in cancer cells, it has been proposed that Fbxw7 modulates myelination by negatively regulating mTOR signalling activity both in OLs (Kearns et al., 2015) and in Schwann cells (Harty et al., 2018).

A considerable proportion of Fbxw7 targets are ER-anchored transcription factors, whose N-terminal domains undergo translocation into the nucleus to initiate the transactivation of target genes; this is also the case of MYRF, at least in mHepa cells (Nakayama et al., 2018). However, the biological significance of the relationship between Fbxw7 and MYRF in OLs and in myelin-related pathologies remain to be elucidated.

2.3. Myelin-independent implications of MYRF

MYRF's critical role extends beyond oligodendrocyte-generated myelination. In fact, *Myrf* orthologues have been found in organisms lacking myelin (Russel et al., 2011; Senoo et al., 2012). For instance, it plays an essential role in larval development and promotes neuronal rewiring in the nematode *C. elegans* (Meng et al., 2017). Continuing with myelin-independent functions, recent studies in pancreatic cancer cells have suggested a role for MYRF in maintaining ER homeostasis (Milan et al., 2020).

Indeed, it is worth mentioning that *Myrf* expression is not limited to the CNS: genomic-level RNA profiling studies indicated that it is also present in various tissues such as the stomach, lung, heart, eye, and developing gonads in both humans and mice (Hamanaka et al., 2019; Pinz et al., 2018). Notably, *Myrf* coding variants have been implicated in both myelin-related and non-myelin-related diseases (Rossetti et al., 2019).

Pathogenic variants of human *MYRF* have been linked to nanophthalmos and high hyperopia, highlighting MYRF's role in eye development (Garnai et al., 2019; Guo et al., 2019; Siggs et al., 2019). Moreover, *MYRF* haploinsufficiency leads to human development disorders recently classified as MYRF-related Cardiac Urogenital Syndrome (MYRF-CUGS) (Kaplan et al., 1993). This rare syndrome primarily manifests anomalies in internal and external genitalia, congenital heart defects, and ocular conditions, along with a broad spectrum of developmental delay and intellectual disability (Garnai et al., 2019; Pinz et al., 2018; Qi et al., 2018; Qiao et al., 2020). These disorders encompassing deficiencies in the development of vital organs underscore the critical role of *MYRF* in regulating human development. In line with this, whole-body *Myrf* knockout resulted in embryonic lethality in mice, emphasizing its significance in murine embryonic development (Emery et al., 2009)

Despite the extensive pathological implications of MYRF and its crucial roles in both myelin and non-myelin related functions, its potential association with neurodegenerative disorders such as Alzheimer's disease has not yet been investigated.

3. ALZHEIMER'S DISEASE

Alzheimer's disease (AD) is the most common cause of dementia and a devastating chronic neurodegenerative disorder characterized by cognitive decline, memory impairment, and behavioral changes, consequence of a progressive and irreversible neuronal loss. The incidence rate of AD is continuously increasing, and effective therapeutic drugs or intervention strategies are still lacking due to the incomplete understanding of its pathogenesis.

AD was first reported by the German psychiatrist Aloysius (Alois) Alzheimer, who described for the first time a peculiar symptomatology in a patient exhibiting hallucinations and the loss of several mental functions, such as memory and language. Post-mortem analyses of the patient's brain revealed the presence of abnormal intra- and extracellular aggregates, which years later were identified as extracellular insoluble aggregates of amyloid β peptide (Aβ), called senile plaques (**Figure 8A**), and intracellular neurofibrillary tangles composed of hyperphosphorylated tau protein (**Figure 8B**). These two features are still considered the main histopathological hallmarks of the disease.

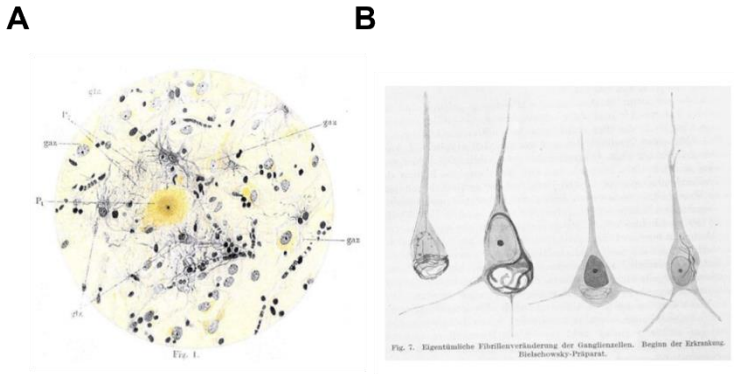

Figure 8. Histopathological features of Alzheimer's disease. Pictures of original drawings of Alois Alzheimer showing (**A**) senile plaques composed by amyloid β peptide aggregates and (**B**) neurons with intracellular tangles present in tissue samples from AD patients.

There are two types of AD: late-onset or sporadic AD, which constitutes the majority of cases (95%) and typically affects individuals over 65 years of age; and early-onset or familial AD, occurring before 65 years of age. Although it represents a smaller percentage of cases, familial AD is characterized by its more aggressive nature. The majority of familial AD cases are associated with genetic mutations in genes encoding amyloid precursor protein (APP), or γ-secretase complex proteins presenilin-1 (PSEN1) and -2 (PSEN2). Furthermore, the apolipoprotein E (APOE) gene is a risk factor for developing the disease (J. Kim et al., 2009). However, both types of AD are multifactorial, and non-genetic environmental factors such as age (the major risk factor), sex, lifestyle, exposures to toxic substances, and cardiovascular- and cerebrovascular-diseases also contribute to the development and progression of the disease (George & Hemachandra Reddy, 2019).

Anatomically, the development of the pathology follows a well-established pattern, with the entorhinal cortex and the hippocampus being the first affected brain structures (Braak & Braak, 1995). Aβ deposits spread from the neocortex to allocortical regions and then to the brainstem, eventually reaching the cerebellum (Thal et al., 2002). Conversely, the spreading of neurofibrillary tangles begins in the transenthortinal region and progresses into the neocortex (Braak & Braak, 1995). The neuronal degeneration in these specific areas is associated with deficits in cognitive functions like learning and the formation of new memories. Notably, important biological changes such as neuroinflammation, oxidative stress, mitochondrial dysfunction and impaired proteostasis also contribute to neuronal death during the neurodegenerative process of AD (Jellinger, 2010).

3.1. Amyloid beta hypothesis

Although AD is a multifactorial disorder with a still unclear etiology, the identification of Aβ as the main constituent of the senile plaques and the discovery of gene mutations associated with Aβ formation in familial AD, led to formulate the amyloid beta cascade hypothesis. This theory postulates that the abnormal deposition of Aβ peptides in the brain, resulting from an imbalance between production and elimination, is the triggering event for the neurodegeneration and subsequent dementia (Hardy & Higgins, 1992; Selkoe, 1991). Consistent with this, several studies have shown that tau tangles fail to spread into the neocortex in the absence of Aβ, suggesting that Aβ may be a prerequisite

for tau pathology development (Long & Holtzman, 2019). However, despite the widespread acceptance of this hypothesis, the precise mechanisms underlying Aβ-induced neuro toxicity and its role in AD pathology remain subjects of ongoing research and debate.

The Aβ peptide is a 4.5 kDa monomer originated from the proteolytic processing of the amyloid precursor protein (APP), a transmembrane glycoprotein with a large extracellular domain that performs various biological functions in the CNS (Zheng & Koo, 2011). These functions include regulating neurite growth during development (Herms et al., 2004), as well as cell adhesion, synapse formation, and transcription modulation in the adult brain (Raychaudhuri & Mukhopadhyay, 2007).

The proteolytic processing of APP can occur through two main pathways: the non-amyloidogenic and amyloidogenic cascades (**Figure 9**). The non-amyloidogenic pathway involves cleavage of APP by the α-secretase protease, generating the soluble fragment APPsα and CTFα, the latter staying anchored to the cell membrane. CTFα is subsequently cleaved by γ-secretase, producing two soluble peptides called p3 and APP intracytoplasmic domain (AICD). AICD can act as a transcriptional regulator of several genes such as GSK3β or p53 (Kimberly et al., 2001; von Rotz et al., 2004). In contrast, the amyloidogenic pathway involves initial cleavage of APP by the β-secretase protease, generating APPsβ and CTFβ fragments. Further processing of CTFβ by γ-secretase produces AICD and Aβ peptide, which is released into the extracellular medium. Remarkably, while the non-amyloidogenic pathway predominates in physiological conditions, the balance between the two pathways appears to be altered in AD patients. Additionally, there are several non-canonical pathways through which APP can be processed, some of which also contribute to Aβ peptide generation (Müller et al., 2017).

Due to the lack of specificity of γ-secretases in the proteolytic cleavage of APP, the length of resulting Aβ peptides can vary (Weidemann et al., 2002). While most circulating Aβ peptides consist of 40-amino-acid-long peptides ($A\beta_{1-40}$), species formed of 42 ($A\beta_{1-42}$) or 43 ($A\beta_{1-43}$) amino acids can also be found, although to a lesser extent (Takami et al., 2009). Following APP processing, Aβ monomers, particularly $A\beta_{1-42}$, tend to aggregate into various species, including dimers, trimers, high-n oligomers, protofibrils, or fibrils, which deposit in the brain and eventually form senile plaques (Recuero et al., 2004). Both *in vitro* and *in vivo* experiments have demonstrated that the aggregation of Aβ into high

molecular weight species makes them toxic (Pike et al., 1991; Walsh et al., 1997), with Aβ oligomers representing the most neurotoxic species (Glabe, 2005). Interestingly, the density of plaques is lower in clinically relevant regions of the brain such as the hippocampus (Braak & Braak, 1995), suggesting that oligomers, rather than plaques, are the most toxic species

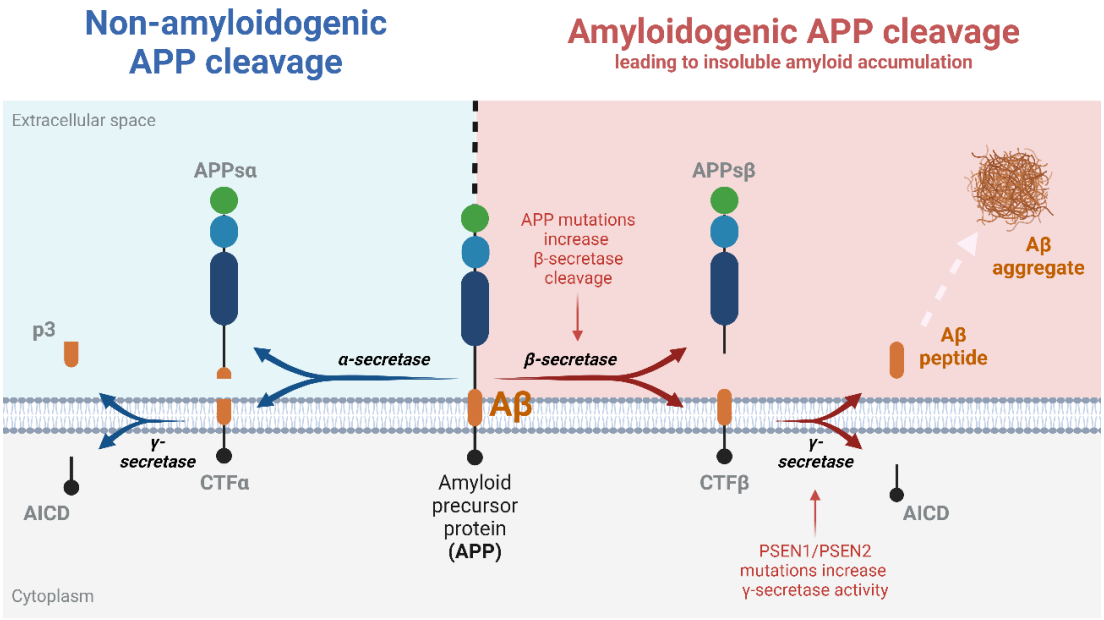

Figure 9. Schematic representation of canonical amyloid precursor protein (APP) processing. The non-amyloidogenic (blue) and amyloidogenic (red) pathways are depicted. The proteolytic cleavage of APP by α- or β-secretase, and subsequently by γ-secretase, generates AICD, and p3 or amyloid β (Aβ) peptides, respectively. Aβ tends to aggregate in the extracellular space, first forming oligomers and ultimately amyloid plaques. Mutations in the APP gene inhibit cleavage by α-secretase and consequently enable preferential cleavage by β-secretase. Mutations in the presenilin-1 (PSEN1) and presenilin-2 (PSEN2) genes increase cleavage by γ-secretase at this site. Both mutations result in excessive Aβ peptide production. Adapted from Patterson et al., 2008 and Müller et al., 2017. Created in BioRender.com

3.2. Animal models of Alzheimer's disease

Extensive research efforts are underway to gain a deeper understanding of the molecular and cellular mechanisms implicated in AD. In this line, the identification of mutations associated with AD onset and progression facilitated the generation of animal models that serve as indispensable tools for advancing our knowledge on the pathobiology of the disease. These models, designed to recapitulate key aspects of AD pathology, have enabled the independent investigations into each pathological event occurring in the disease.

On one hand, it was successfully generated an animal model exhibiting increased synthesis and/or deposition of Aβ peptide leading to senile plaque formation, through APP overexpression or mutations in PSN1 (Games et al., 1995). Besides, after the identification of mutations in the protein tau gene, transgenic mice developing tauopathies were also generated (Higuchi et al., 2002; Lewis et al., 2000). However, although most of the models develop either tangles or senile plaques, the emergence of one histopathology does not necessarily induce the other. Consequently, the triple transgenic mouse model (3xTg-AD) was created to address the need for more complex models to fully comprehend AD pathology (Oddo et al., 2003).

The 3xTg-AD model represents one of the most complete mouse models of AD, carrying three transgenes associated with AD development: the Swedish mutation of APP (APP^{Swe}; K670N/M671L), a mutation in PSEN1 (M146V), and a mutation in the protein tau gene (P301L). This model was a pioneer as it manifests both senile plaques and neurofibrillary tangles in AD-relevant brain regions, exhibiting age-related cognitive impairments that highly resemble those found in AD patients. The first histopathological feature observed in 3xTg-AD mice is intraneuronal Aβ peptide, detectable from 3-4 months in the cortex and from 6 months in the hippocampus. From this point onward, extracellular Aβ peptide deposits start to appear mainly in the cortex at 6 months and in the hippocampus at 12 months. Soluble Aβ peptide oligomers are detectable intracellularly from the second month of life, with levels declining at 12 months likely due to increased fiber formation, and in 15- month-old mice these levels rise again. In contrast, neurofibrillary tangles begin to form at 12 months in the hippocampus before spreading to the cortex (Oddo et al., 2003). This observation further supports the Aβ cascade hypothesis, as the initial event in these mice is the accumulation of Aβ peptide.

Indeed, both clinical and experimental evidence suggests that acute elevation of Aβ levels in the brain leads to the development of Alzheimer-like phenotypes (H. Y. Kim et al., 2016). Hence, as an alternative to transgenic mice, intracerebral infusions of Aβ peptide have been extensively used in rodents, and more recently, in zebrafish (Nery et al., 2014b), as a strategy to investigate the pathology. Zebrafish has emerged as a valuable complementary model organism for numerous molecular studies and high-throughput pharmacological screenings, in part due to its genetic similarity to humans, sharing 84% of genes associated with human diseases (Howe et al., 2013), including those linked to AD (Xia, 2010).

3.3. White matter and Alzheimer's disease

AD has traditionally been considered a grey matter (GM) disease, characterized by neuronal loss and synaptic dysfunctions (Deture & Dickson, 2019). However, emerging evidence suggests that white matter (WM) degeneration and demyelination are also key pathophysiological features in AD.

More than half of the human brain volume is made up of WM, which consists of areas of the CNS primarily composed of myelinated axons. The integrity of the WM is essential for efficient nerve conduction, required for numerous high-order cognitive processes such as attention, memory, executive functioning, and processing speed, all of which are impaired in AD. Therefore, it is plausible to consider that myelin loss and the inability of OLs to repair myelin damage may be central features of AD.

Actually, studies have observed WM atrophy occurring at early stages of AD, even before GM degeneration and plaque formation, indicating that myelin abnormalities may precede neuronal loss (Nasrabady et al., 2018; Sachdev et al., 2013). Moreover, an alternative hypothesis suggests that Aβ and tau pathologies are secondary (rather than primary) outcomes of the brain's attempt to maintain myelin homeostasis through a cycle of damage, repair, and maintenance (Bartzokis, 2011). Recent research supports this idea, where they propose that structural defects in myelin promote Aβ deposition, thereby serving as an upstream risk factor for AD. Consequently, enhancing OL health and myelin integrity emerges as a promising therapeutic target to delay disease onset and slow its progression (Depp et al., 2023). In line with this, it was recently proposed that the efficacy of the only FDA-approved amyloid-targeting drug, Aducanumab, could be enhanced by combining it with drugs targeting OLs to promote remyelination (Fessel, 2022).

3.3.1. WM pathologies in AD patients

WM progressively deteriorates with normal aging (Damoiseaux et al., 2009; Inano et al., 2011), and whole brain imaging studies suggest that this natural tendency is exacerbated and accelerated in AD (Bartzokis et al., 2003; de la Monte, 1989). *Post-mortem* and *in vivo* magnetic resonance imaging (MRI) studies have demonstrated significant WM impairment in AD, characterized by reduced WM volume, alterations in WM microstructure (Bartzokis, 2011), and differences in the physical organization of the myelin lipid bilayer (Chia et al., 1984).

In a recent study combining various imaging measurements of myelin status and psychological tests, they demonstrated that age-related demyelination is associated with memory impairment (Kavroulakis et al., 2018). Similarly, an MRI study comparing Aβ-positive AD patients to Aβ-negative controls revealed larger white matter hyperintensities (WMH) in the corpus callosum of Aβ-positive AD patients, which were associated with worse cognitive performance (Garnier-Crussard et al., 2022). Accordingly, AD patients exhibit myelin loss in specific brain regions, such as cortical GM and WM (Roher et al., 2002), along with a significant decrease in the number of $Olig2^{+}$ cells in the WM and GM of the superior temporal gyrus and the sensory motor cortex (Behrendt et al., 2013).

Notably, several studies have reported WM disruption in asymptomatic individuals with genetic risk factors for AD and in patients with mild cognitive impairment (MCI) (Bartzokis et al., 2006; Parente et al., 2008). Interestingly, asymptomatic individuals presented reduced myelin content, which correlated with soluble Aβ concentration in the cerebrospinal fluid (CSF). These results suggest that myelin alterations may precede cognitive decline in AD.

The underlying mechanisms of OL and myelin dysfunctions in AD have not been fully elucidated. However, accumulating evidence propose Aβ as the main candidate in promoting WM dysfunction. In fact, the complexity of Aβ biochemistry makes it a promiscuous molecule able to signal through a repertoire of receptors, promoting a wide range of effects in neurons, but also in OLs (Viola & Klein, 2015).

In AD patients, increased levels of Aβ peptide correlate with brain regions exhibiting myelin abnormalities (Roher et al., 2002). Moreover, focal demyelination is observed in plaque-associated myelinated axons from AD temporal cortex, whereas plaque-free cortical GM of AD patients have no significant loss of myelin or OL density (S. Mitew et al., 2014). Consistent with those findings, biochemical analysis of myelin in AD patients has revealed increased $A\beta_{1\text{-}42}$ levels, accompanied by a significant decrease in the levels of MBP, PLP and CNPase (Roher et al., 2002). While MBP levels are significantly lower in the frontal WM of AD brains compared to those with MCI, increased levels of MBP are observed in cortical GM of AD patients (Selkoe et al., 1981; Zhan et al., 2015). However, the mechanisms by which MBP levels are higher in AD patients and mouse models compared to healthy individuals remain unclear.

3.3.2. WM impairments in AD mouse models

The generation of animal models of AD has facilitated the detailed study of the progression of WM pathologies in the disease. In this sense, Aβ has been implicated in WM abnormalities in mouse models such as Tg2576, 3xTg-AD, APP/PS1 and 5XFAD, which overproduce Aβ peptide. In these models, focal demyelination areas associated with Aβ plaques have been observed, resembling those found in human patient samples (Behrendt et al., 2013; Mitew et al., 2010). Interestingly, plaque-free tissues of transgenic mice show no significant loss of myelin or $Olig2^+$ cell numbers (Mitew et al., 2010).

Regarding APP/PS1 transgenic mice, it exhibits an increased density of proliferating OPCs and newly generated mature OLs at 6 and 11 months compared to wild-type (WT) mice (Behrendt et al., 2013). Interestingly, these mice also show alterations in myelin integrity in the hippocampus at early stages of the disease: they present increased MBP expression, thicker myelin sheaths, and shorter internodal distance (Y. Wu et al., 2017a). However, in another study decreased OPC density was noted in the hippocampus of 9-month-old APP/PS1 mice, but not at 14 months (Chacon-De-La-Rocha et al., 2020). Curiously, OPCs exhibit a senescent phenotype in the Aβ plaque environment, suggesting a role for cell senescence in the cascade of events by which Aβ causes cognitive impairment in AD (P. Zhang et al., 2019). Another study showed that APP/PS1 mice have increased rates of new myelin formation (J. F. Chen et al., 2021).

Furthermore, 3xTg-AD mice also display myelin impairments in hippocampal CA1 and the entorhinal cortex (Desai et al., 2009), as well as in the fimbria (Nie et al., 2019). Conversely, recent studies suggest that Aβ oligomers correlate with higher MBP levels in the hippocampus of 3xTg-AD mice (Quintela-López et al., 2019), in addition to thicker myelin and increased oligodendrogenesis (Ferreira et al., 2020). Altered OPC densities, replication ratios, and morphology have been also reported in the hippocampus of 3xTg-AD mice, with more hypertrophic progenitor cells (Vanzulli et al., 2020).

The numerous discrepancies in OL responses to pathology in AD models remain unexplained, but they may be associated with the timing and progression of the pathology in each animal model. These highlights the need for a more extensive study of the role of OLs in the pathogenesis of AD.

3.3.3. Amyloid β-induced oligodendrocyte impairments

Despite the relevance that WM and myelin seem to have in AD pathology, little is known about the direct effect of Aβ peptide in OLs. In fact, OLs show high expression levels of APP as well as β-secretase 1 (BACE1), the secretase involved in the amyloidogenic pathway. BACE1 and APP play important and distinct roles in CNS myelination, demyelination, and remyelination processes. While BACE1 regulates myelin sheath thickness (Hu et al., 2006), APP ensures normal myelination and remyelination in adult nerves (Truong et al., 2019). Interestingly, OLs themselves can produce Aβ, that may potentially exacerbate AD progression (Skaper et al., 2009).

According to *in vitro* studies, Aβ becomes toxic upon oligomerization (L. N. Zhao et al., 2012) and can directly damage OLs. In fact, both $A\beta_{1-40}$ and $A\beta_{25-35}$ have been shown to induce dose-dependent OL death, characterized by nuclear and cytoskeletal disintegration, DNA fragmentation, and mitochondrial dysfunction (Xu et al., 2001). In addition, injection of high concentrations of $A\beta_{1-42}$ into the rat corpus callosum results in considerable axonal damage and OL loss (Jantaratnotai et al., 2003).

On the other hand, conflicting results have been reported regarding the susceptibility of OLs at different differentiation stages to Aβ toxicity. It has been observed that after $A\beta_{1-42}$ treatment (0.5, 1, 2, 4 µM for 4 h) both immature and mature OLs present an increased abundance of cells with pyknotic nuclei (Desai et al., 2010). In contrast, others describe that soluble $A\beta_{1-42}$ (10 µM for 48 h) inhibits the survival of mature OLs but not of OPCs (Horiuchi et al., 2012). In the same line, another study has shown decreased numbers of MBP^+ cells upon $A\beta_{1-42}$-treatement (10 µM for 96 h) (M. Zhang et al., 2018). Conversely, low doses of $A\beta_{1-42}$ (200 nM for 24 h) have been found to increase OL viability, promote OL differentiation, and induce MBP expression via integrin β1 and Fyn kinase signalling (Quintela-López et al., 2019).

Overall, OLs and myelin, away from being secondary characters in AD pathology, they actively respond to injury and play critical roles in disease onset and progression. Thus, understanding the mechanisms underlying OL failure and myelin impairments may offer valuable insight for the development of innovative therapeutic strategies to prevent or treat AD.

Hypothesis & Objectives

HYPOTHESIS AND OBJECTIVES

Alzheimer's disease is characterized by the accumulation of extracellular aggregates of amyloid β peptide, and its oligomeric forms have been proposed to trigger early events in AD pathogenesis, including dysfunctions in oligodendrocytes and myelin. While amyloidosis has been associated with increased oligodendrogenesis, elevated MBP levels, and altered myelin structure, the precise underlying molecular mechanisms remain unclear. The transcription factor MYRF is essential for OL differentiation and CNS myelination processes; however, its connection with Aβo and the specific molecular mechanism through which MYRF operates in the context of AD have not been elucidated.

We hypothesize that Aβo induce OLs disruptions by dysregulating MYRF. These alterations may impair myelin formation and function, ultimately contributing to cognitive decline in AD. Thus, our main objective is to investigate the potential role of MYRF as a key molecular mechanism governing OL pathology in AD.

To test our hypothesis, the following specific objectives were set:

Aim 1. To characterize alterations in oligodendroglial lineage cells in Alzheimer's disease mouse models, both at the population and gene expression levels.

Aim 2. To investigate the impact of Aβ oligomers on myelin regulatory factor, and its underlying molecular mechanisms, *in vitro*.

Aim 3. To evaluate the therapeutic potential of pharmacological PKC inhibition as a strategy to mitigate Aβo-induced disruptions in MYRF, oligodendrocytes, and myelin, using both *in vitro* and *in vivo* AD models.

Material & Methods

1. Animals

All experimental procedures with mice and rats were approved by the Animal Ethic Committees of the University of the Basque Country (UPV/EHU) and followed the European Communities Council Directive 2010/63/EU. Specifically, all protocols were approved by the Ethics Committee on Animal Experimentation (CEEA), which is a collegiate authority within the operational structure of the Ethics Commission for Research and Teaching (CEID) of the UPV/EHU.

For procedures involving zebrafish, the Institutional Animal Care and Use Committee (IACUC) at the University of Colorado Anschutz Medical Campus approved all protocols, which were in compliance with the US National Research Council's Guide for the Care and Use of Laboratory Animals and the US Public Health Service's Policy on Humane Care and Use of Laboratory Animals.

1.1. Mice

Animals were housed in standard conditions, with a 12-hour light cycle and ad libitum access to food and water. Rigorous efforts were undertaken to minimize animal suffering and to reduce the number of animals used in the study. Experiments were performed in Sprague Dawley rat pups, C57BL6/J strain mice, and the triple transgenic mouse model of Alzheimer´s disease (3xTg-AD), which harbors the Swedish mutation in the human amyloid precursor protein (APP^{Swe}), the presenilin 1 knock-in mutation ($PSEN1^{M146V}$), and the tau P301L mutant transgene ($MAPT^{P301L}$) (Oddo et al., 2003).

1.2. Zebrafish

Nontransgenic embryos were obtained through crosses of male and female zebrafish from the AB strain. Embryos were raised at 28.5°C in E3 media (5 mM NaCl, 0.17 mM KCl, 0.33 mM CaCl, 0.33 mM $MgSO_4$ (pH 7.4), supplemented with sodium bicarbonate). Larvae were staged according to hours or days post-fertilization (hpf/dpf), and selected based on criteria ensuring good health and normal developmental patterns. We used the previously established zebrafish lines *Tg(olig2:EGFP)*^{vu12}, *Tg(myrf:mScarlet)*^{co66}, and *Tg(mbpa:tagRFPT)*^{co25}.

2. Cell cultures

2.1. Primary cortical oligodendrocyte culture

Highly enriched OPCs were derived from mixed glial cultures obtained from the forebrain cortices of newborn (P_0-P_2) Sprague-Dawley rats, following previously described protocol (McCarthy & De Vellis, 1980) with modifications (Sánchez-Gómez et al., 2018). Briefly, forebrains were dissected from the skulls, meninges were removed, and cortices were isolated and enzymatically digested by incubation in Hank's balanced salt solution (without Ca^{2+} and Mg^{2+}; HBSS-/-) containing 0.25% trypsin and 0.004% deoxyribonuclease (DNAse) (both from Sigma-Aldrich) at 37 °C for 15 minutes. Then, the enzymatic reaction was stopped by adding Iscove's modified Dulbecco's medium (IMDM; Gibco) supplemented with 10% fetal bovine serum (FBS, Hyclone; Gibco). The resulting cell suspension was centrifuged (1,000 x g, 5 min) and resuspended in 1 ml of the same solution, and, subsequently, cells were mechanically dissociated using needles (21G and 23G). After centrifugation (1,000 x g, 5 min), cells were resuspended again in IMDM supplemented with 10% FBS Hyclone.

Mixed glial cells were cultured in 75 cm^2 (T75) flasks coated with poly-D-lysine (PDL; 1 μg/ml; Sigma-Aldrich) and maintained at 37 °C with 5% CO_2 until they were confluent (8-10 days). Flasks with confluent mixed glia were shaken (400 rpm, 1 h, 37 ºC, 5% CO_2) on a rotary shaker to remove adherent microglia. Further shaking for 18 h at 200 rpm isolated the OPCs, which were filtered through a 10 μm pore size nylon mesh and pre-plated in 100 mm coated Petri dishes (ThermoFisher Scientific) for 45 min (37 °C, 5% CO_2) to remove remaining microglia (microglia firmly attaches to the Petri dish, while OPCs are loosely attached). The collected OPCs were filtered again, and cell number was determined using trypan blue staining (Sigma-Aldrich). The resulting cell suspension was centrifuged (1,000 x g, 10 min), and the pellet was resuspended to a final concentration of 1,000 cell/μl in chemically defined SATO medium consisting of a supplemented (4.5 g/l glucose and 0.11 g/l sodium piruvate) DMEM base with several factors that favor oligodendrocyte (OL) proliferation (SATO-) or differentiation (SATO+) (**Table 1**). Cells were seeded onto PDL-coated plates, with or without coverslips depending on experimental requirements, at densities ranging from $1x10^4$ to $1x10^6$ cells per well. Cultures were maintained at 37 °C with 5% CO_2.

Table 1. SATO medium components. Both SATO– (proliferation media) and SATO+ (differentiation media) contain several shared reagents (black), but T3 and T4 are only present in SATO+ (orange). Moreover, SATO+ (orange) contains CNTF and NT-3 neurotrophic factors that promote OL differentiation, while SATO– (blue) contains PDGF-AA and FGFb growth factors.

Reagent	Concentration	Company
Dulbecco's Modified Eagle Medium (DMEM)	Base medium	Gibco
Insulin	5 µg/ml	Sigma-Aldrich
Penicillin/Streptomycin (P/S)	100 U/ml	Gibco
Bovine serum albumin (BSA)	1 mg/ml	Sigma-Aldrich
L-Glutamine	2 mM	Sigma-Aldrich
N-Acetyl L-Cystein	63 µg/ml	Sigma-Aldrich
Transferrin	1 µg/ml	Sigma-Aldrich
Putrescin	160 ng/ml	Sigma-Aldrich
Progesterone	0.6 ng/ml	Sigma-Aldrich
Sodium selenite	0.4 ng/ml	Sigma-Aldrich
Triiodothyronine (T3)	30 ng/ml	Sigma-Aldrich
L-Thyroxine (T4)	40 g/ml	Sigma-Aldrich
Cilliary neurotrophic factor (CNTF)	10 ng/ml	PrepoTech
Neurotrophin 3 (NT-3)	1 ng/ml	PrepoTech
Platelet-derived growth factor-AA (PDGF-AA)	5 ng/ml	PrepoTech
Fibroblast growth factor basic (FGF-b)	5 ng/ml	PrepoTech

The purity of oligodendroglial cultures was confirmed through immunostaining with cell type-specific antibodies. After 1 day in vitro (DIV), PDGFR-α+ OPCs constituted 97 ± 5% of the total cell population, and by 3 DIV in SATO+ differentiation medium, at least 98% of cells were MBP^+ (Sánchez-Gómez et al., 2018).

All experiments were conducted under SATO+ conditions, except for those in which OLs were transfected with MYRF expression plasmids. In these cases, SATO- was used in order to ensure that the only factor inducing OL differentiation was MYRF itself, rather than the differentiating factors present in SATO+ medium. Hence, this approach allowed us to assess MYRF's impact on OL differentiation *in vitro*.

2.2. HEK293T cells

Human embryonic kidney 293T cells (HEK293T) were thawed in pre-warmed (37 ºC) cell medium composed of DMEM supplemented with 10% FBS and 1% P/S (all from Gibco). Then, cells were centrifuged (1,000 x g, 5 min), and the resulting cell pellet was resuspended in fresh cell medium for seeding in T75 flasks. The cells were cultured in the incubator at 37 °C and 5% CO_2, with cell passaging occurring every 3-4 days to maintain appropriate cell confluence (80-90%).

For seeding, HEK293T cells were rinsed with HBSS-/- and detached from de flask by incubation with 0.25% Trypsin-EDTA (Sigma-Aldrich) at 37 ºC for 2 min. Trypsinization was stopped by adding fresh medium. The resulting cell suspension was centrifuged (1,000 x g, 5 min), the pellet was resuspended in fresh medium, and cell number was determined by trypan blue staining (Sigma-Aldrich). Then, cells were seeded onto appropriate plates at densities ranging from $1x10^4$ to $1x10^6$ cells per well, depending on experimental requirements. Cultures were maintained at 37 °C with 5% CO_2.

3. DNA plasmids and siRNAs

3.1. Gene expression via DNA plasmids

The following plasmids were used for exogenous MYRF expression: double-tagged MYRF (pcDNA3-Myc-Myrf-Flag) (kindly provided by Dr. B. Emery from Jungers Center for Neurosciences Research, OHSU, Portland, Oregon, USA) (Bujalka et al., 2013), and MYRF with GFP attached to the N-terminus (GFP-C11orf9; C11orf9 is the old name for MYRF) (provided by Dr. Y. Park from Jacobs School of Medicine & Biomedical Sciences, UB, Buffalo, New York, USA) (Li et al., 2013).

Luciferase assays were conducted using plasmids containing luciferase reporters under control of *Mbp* (pGL3-MBP), *Mag* (pGL3-MAG), *Rffl* (pGL3-Rffl) (provided by Dr.B. Emery) (Bujalka et al., 2013), and *Myrf* (pGL4.10_myrfprom_ECR9) (provided by Dr. M. Wegner from Institut für Biochemie, FAU, Erlangen, Germany) (Hornig et al., 2013).

Plasmids employed for ubiquitin studies included FLAG-tagged ubiquitin (pCDNA3.1-FLAG-Ub) (Ramirez et al., 2018), HA-tagged ubiquitin plasmids (WT, pRK5-HA-Ubiquitin-K48 (#17605, Addgene), and pRK5-HA-Ubiquitin-K48 (#17606,

Addgene)), and untagged human Parkin (Martinez et al., 2017) (all provided by Dr. J. M. Ramirez and Dr. U. Mayor from the Department of Biochemistry and Molecular Biology, Faculty of Science and Technology, UPV/EHU, Leioa, Spain). Additionally, Myc-tagged human Fbxw7 plasmid (pCMV3-Myc-FBXW7-t2) (#HG29625-NM, Sino Biological) was also used.

All constructs were purified following either the QIAGEN Plasmid Maxi Kit (Qiagen) or NZYMaxiprep (NZYtech) protocols, and the DNA concentration was measured using the spectrophotometer Nanodrop 2000 (ThermoFisher Scientific). Primary OLs were transfected by electroporation using the Amaxa™ Basic Nucleofector™ Kit (Lonza) for Primary Mammalian Glial cells, while HEK293T cells were transfected by lipofection using the Lipofectamine 3000™ reagent (Invitrogen), following manufacturers' instructions. A GFP expression construct was often co-transfected into cells as a positive control for transfection efficiency. GFP expression was monitored using an Invitrogen™ EVOS™ FL Digital Inverted Fluorescence Microscope (EVOS; Invitrogen).

3.2. Gene silencing via siRNAs

For *Myrf* gene silencing, primary OLs were transfected with 100 pmol of either scrambled control siRNA (ON-TARGETplus Non-targeting Pool, #D-001810-10-05) or *Myrf* targeted siRNA (ON-TARGETplus Rat Myrf siRNA, #L-085053-02-05) (Dharmacon, HorizonDiscovery) using electroporation. Transfected OLs were seeded onto PDL-coated 24-well plates with coverslips, at densities of $1x10^5$ cells per well for western blot experiments and $2x10^4$ cells per well for immunofluorescence. Cells were cultured in differentiation SATO+ medium for 3 DIV, during which transfection efficacy and cell morphology were monitored by the expression of co-transfected GFP and a EVOS Fluorescent Microscope (Invitrogen).

4. Preparation of amyloid β oligomers (Aβo)

Oligomeric amyloid-β ($A\beta_{1-42}$) was prepared as previously described (Dahlgren et al., 2002). Briefly, $A\beta_{1-42}$ (Bachem, Germany) was initially dissolved to a concentration of 1 mM in hexafluoroisopropanol (Sigma), which was next totally removed under vacuum using a speed vac system. The resulting peptide film was stored desiccated at -80°C.

For the aggregation protocol, the peptide was resuspended in dry dimethylsulfoxide (DMSO; Sigma) to achieve a concentration of 5 mM, and Hams F-12 (PromoCell) was then added to adjust the peptide to a final concentration of 100 µM. Control cells were treated with the vehicle consisting of DMSO + Hams F-12.

Oligomer formation was induced by incubating the peptide solution for 24 h at 4 °C, and confirmed by polyacrylamide gel electrophoresis (SDS-PAGE) followed by Coomassie Brilliant Blue R-250 (Bio-Rad) staining.

5. Drugs and inhibitors

The following drugs and inhibitors were used: AR-A014418 (1 µM; Sigma-Aldrich), Gö6983 (100 nM for *in vitro* and osmotic pump experiments, and 500 nM for zebrafish treatments through bath immersion; Tocris), MG132 (1 µM; Sigma-Aldrich), Anisomycin (40 µM; Sigma Aldrich), Puromycin dyhidrocloride (2 µM; Santa Cruz Biotechnology), and Cycloheximide (CHX; 100 µg/ml; Sigma-Aldrich).

5.1. Cycloheximide chase assay

To assess the degradation kinetics and half-life of N-terminal of MYRF following Aβo treatments, cycloheximide (CHX) chase assays were conducted in primary cultured OLs. For this purpose, $1x10^5$ cells per well were seeded onto PDL-coated 24-well plates, in duplicates, and maintained in SATO+ medium for 3 DIV. Cells were then treated with cycloheximide (100 µg/ml), a ribosome inhibitor that restricts the translation elongation of eukaryotic protein synthesis (Miao et al., 2023), by direct addition to the cell medium. Cells were harvested at indicated times thereafter: 0 (without CHX), 30 min (0.5 h), 1 h, 2 h and 3 h post-CHX treatment. Aβo (1 µM) was added 1 h prior to CHX treatments. As a positive control for MYRF degradation inhibition, cells were cultured in the presence of AR-A014418 (1 µM, 24 h), a pharmacological GSK-3 inhibitor. Cells were lysed for subsequent detection by western blot.

For data analysis, the degradation kinetics of MYRF were expressed as the percentage of N-MYRF remaining after the various CHX chase times, with 100% representing the initial expression level for each condition. Additionally, the half-life of N-MYRF was calculated using GraphPad Prism 8.2.1 software.

6. Protein extract preparation and detection by western blot

6.1. Oligodendrocyte protein preparation

After treatments, cultured cortical OLs were washed twice in cold phosphate-buffered saline (PBS; 142 mM NaCl, 2.5 mM NaH_2PO_4, 75 mM Na_2HPO_4), and cells were scraped in sample buffer (62.5 mM Tris pH 6.8, 10% glycerol, 2% SDS, 0.002% bromophenol blue, and 5.7% β-mercaptoethanol in dH_2O). At least 2 wells per treatment and $8x10^4$ - $1x10^5$ cells per well were used. The protein extraction was performed on ice to enhance cell lysis process and avoid protein degradation. Subsequently, the samples were boiled at 95 ºC for 5 min.

6.2. HEK293T protein preparation

48 hours post-transfection, and after treatments, HEK293T cells (initially seeded at densities between $5x10^4$ and $1x10^5$ cells per well) were gently scraped in their culture medium and transferred into clean tubes. The samples were then centrifuged (500 x g, 6 min, at 4 °C), pellets were rinsed with PBS, and centrifuged again under the same conditions, to remove any residual serum from the medium. The resulting pellets were resuspended in commercial RIPA lysis buffer (ThermoFisher) supplemented with protease and phosphatase inhibitor cocktails (ThermoFisher), and incubated on ice for 30 min. Next, cell lysates were centrifuged (12,000 x g, 10 min, at 4°C), pellets discarded, and the supernatants were carefully transferred to new tubes to which 4x sample buffer was added. Finally, samples were boiled at 95 °C for 5 min.

6.3. Protein preparation from mice hippocampi

Mice were anesthetized by an intraperitoneal injection of pentobarbital and perfused with saline solution (0.9% NaCl in H_2O). The hippocampi were dissected, placed on dry ice, and stored at -80 °C until further processing.

Mice tissue samples were resuspended in 50 µl of commercial RIPA lysis buffer supplemented with protease and phosphatase inhibitor cocktails (ThermoFisher), and homogenized using a douncer. Afterwards, an additional 150 µl of supplemented RIPA lysis buffer was added to reach a final volume of 200 µl, and the tissue homogenate was sonicated (25 pulses, 80% amplitude, 0.6 cycle) (Labsonic M, Sartorius). The

homogenate was then centrifuged (2,000 x g, 10 min at 4°C), and the supernatants were collected. The total protein content was quantified using the Bradford method (Bio-Rad).

6.4. Western Blot

Protein samples were size-separated by electrophoresis using 4-20% (Any KD) polyacrylamide-SDS Criterion TGX Precast gels (Bio-Rad) in a Tris-Glycine buffer (25 mM Tris, 192 mM glycine, 0.1% SDS in dH_2O, pH 8.3), and transferred using Trans-Blot® Turbo™ Midi Nitrocellulose Transfer Packs (Bio-Rad). Following transfer, membranes were blocked in a solution containing 5% BSA in Tris-buffered saline/0.1% Tween-20 (TBST; 20 mM Tris, 137 mM NaCl, 0.1% Tween-20 in dH_2O, pH 7.4) for 1 h at room temperature (RT). Proteins were detected by specific primary antibodies (**Table 2**), incubated in the same blocking solution overnight (O/N) at 4°C with gentle shaking. Subsequently, membranes were washed three times with TBST, and incubated with either horseradish peroxidase-conjugated (HRP) or fluorescence-labeled secondary antibodies (1:5,000), in blocking solution for 1 h at RT. Then, membranes were again washed twice with TBST and once with TBS.

Immunoreactive protein bands were visualized using enhanced electrochemical luminescence (NZY standard ECL or NZY advanced ECL; NZYtech) and images were obtained using a ChemiDoc XRS Imaging System (Bio-Rad). Signal intensities were quantified using Image Lab® 6.0.1 (Bio-Rad) software, and values were normalized to GAPDH, α-Tubulin or Ponceau S signals, depending on the experiment.

When needed, membranes were stripped of antibodies using Restore Western Blot Stripping Buffer (ThermoFisher Scientific) following the manufacturer's instructions. Next, membranes were washed in TBST three times, blocked in 5% BSA in TBST, and incubated with other primary antibodies of interest.

Table 2. Antibodies used for western blot analysis. MW = Molecular weight

Antibody	Host	MW (kDa)	Dilution	Reference
Anti-MYRF	Rabbit	160 – 75	1:1,000	#ABN45, Millipore
Anti-MAG	Mouse	100	1:500	#sc-166849, Santa Cruz
Anti-MOG	Mouse	28	1:1,000	#MAB5680, Millipore
Anti-MBP	Mouse	21.5 - 14	1:1,000	#SMI-99, BioLegend
Anti-p-GSK3α/β (Ser21/9)	Rabbit	51 (α) – 46 (β)	1:1,000	#9331, Cell Signaling
Anti-GSK3α/β	Mouse	51 (α) – 47 (β)	1:500	#sc-7291, Santa Cruz
Anti-β-catenin	Rabbit	90	1:1,000	#9562, Cell Signaling
Anti-p-PKC	Rabbit	85 - 78	1:1,000	#9371, Cell Signaling
Anti-PKC	Rabbit	80	1:1,000	#ab179521, abcam
Anti-Fbxw7	Mouse	75	1:2,000	#TA802869S, OriGene
Anti-Parkin	Mouse	58 - 50	1:1,000	#sc-32282, Santa Cruz
Anti-Myc tag	Mouse	-	1:2,000	#05-724-25UG, Millipore
Anti-FLAG tag	Rabbit	-	1:1,000	#2368, Cell Signaling
Anti-HA	Mouse	-	1:1,000	#3663, Sigma
Anti-GFP	Mouse	-	1:1,000	#11814460001, Millipore
Anti-α-Tubulin	Mouse	50	1:5,000	#ab7291, abcam
Anti-GAPDH	Mouse	36	1:5,000	#MAB374, Millipore

7. Immunoprecipitation assays in HEK293T cells

7.1 Phosphoserine immunoprecipitation

To assess changes in MYRF phosphorylation levels following Aβo treatments, immunoprecipitation (IP) assays were conducted for phosphoserine (pSer) in HEK293T cells. Cells were seeded into 6-well plates at a density of $7.5x10^5$ cells per well for each condition. The following day, after confirming adequate cell confluence (70-90%), cells were transfected with 2.5 µg of GFP-MYRF plasmid per well using Lipofectamine 3000™ reagent (Invitrogen). Cells were incubated for 48 h at 37 ºC with 5% CO_2, and transfection efficiency was verified through GFP visualization using an EVOS Fluorescence Microscope (Invitrogen). Cells were then subjected to treatments with either vehicle, Aβo (1 µM; 15 min, 30 min, or 1 h), or the GSK3 inhibitor AR-A014418 (1 µM) as a positive control for GSK3-mediated phosphorylation inhibition.

For the IP assay, 1 µg of agarose-conjugated mouse anti-pSer antibody (#A8076, Sigma-Aldrich) and mouse anti-IgG (#sc-2342 AC, Santa Cruz Biotechnology) were used. Cells were washed twice with cold PBS, scraped with 100 µl of supplemented RIPA lysis buffer (ThermoFisher Scientific), incubated on ice for 10 min, and centrifuged for 5 min at 12,000 x g and 4 ºC. A 1/10 fraction of the supernatant was saved for input samples, and the remaining supernatant was added to 50 µl of the agarose-conjugated anti-pSer or anti-IgG beads, which had been previously washed twice with RIPA. After a 2 h incubation at 4°C (to prevent nonspecific interactions), the lysate-antibody-beads complex was centrifuged at 2,000 x g for 2 min to separate beads from the unbound material. Then, beads were subjected to three washing steps in rotation: they were washed twice with RIPA lysis buffer and once with PBS, followed by centrifugation (2,000 x g, 2 min) to obtain the immunocomplex. Finally, protein elution was carried out in 50 µl/sample of 2x sample buffer by boiling the samples at 95°C for 5 min, followed by centrifugation at 14,000 x g for 1 min. Proteins were analyzed by western blot using an anti-MYRF antibody.

7.2 GFP pull-down

To investigate MYRF ubiquitination in the presence of Aβo, we employed the GFP pull-down method. For that, HEK293T cells were seeded in 6-well plates at a density of $1x10^6$ cells per well. For MYRF ubiquitination levels experiment, each well was co-transfected with 1 µg of GFP-MYRF, 1 µg of FLAG-Ub, and 1 µg of either an empty plasmid (ø), Myc-Fbxw7, or untagged Parkin. For the experiment aimed to assess the type of ubiquitination used, HEK293T cells were co-transfected with 1 µg of GFP-MYRF and 1 µg of Myc-Fbxw7 plasmids, along with 1 µg of WT, K48, or K63 HA-tagged ubiquitin plasmids. 48 h post-transfection, cells were treated with Aβo (1 µM) or its vehicle for 3 h, followed by a GFP pull-down to isolate GFP-tagged MYRF.

The GFP pull-down was performed as previously described (Elu et al., 2019). Briefly, transfected HEK293T cells were washed twice with PBS and lysed with 300 µl of lysis buffer (50 mM Tris–HCl pH 7.5, 150 mM NaCl, 1 mM EDTA, 0.5% Triton, 1× protease inhibitor cocktail (Roche Applied Science), and 50 mM N-ethylmaleimide (NEM; Sigma)), followed by centrifugation (16,000 x g, 10 min, 4 ºC). A 1/10 fraction of each supernatant was saved for input samples, and the remaining supernatants were mixed with

20 µl/condition of GFPTrap-A agarose beads suspension (GFP-beads; Chromotek GmbH), which had been previously washed twice with a dilution buffer (10 mM Tris-HCl pH 7.5, 150 mM NaCl, 0.5 mM EDTA, 1× protease inhibitor cocktail, 50 mM NEM). After incubation for 2.5 h at room temperature with gentle rolling, samples were centrifuged at 2,700 x g for 2 min to separate the beads from the unbound material. GFP beads were then subjected to several washing steps: once with the dilution buffer, thrice with washing buffer (8 M urea, 1% SDS in PBS), and once with 1% SDS in PBS. GFP-tagged proteins bound to the beads were eluted by incubating at 95◦C for 10 min with 25 µl elution buffer (250 mM Tris–HCl pH 7.5, 40% glycerol, 4% SDS, 0.2% bromophenol blue, 100 mM DTT), followed by a final centrifugation step (16,000 x g, 2 min). MYRF-linked ubiquitin was then detected and analyzed via western blotting, using anti-FLAG or anti-HA antibodies, depending on the experiment.

8. Immunofluorescence

8.1. Immunocytochemistry of primary oligodendrocytes and HEK293T cells

Primary cultured OLs and HEK293T cells were seeded onto PDL-coated 24-well plates containing 12- or 14-mm-diameter coverslips, respectively. OLs were seeded in densities of $1x10^4$ - $2x10^4$ cells per well, and HEK23T cells at $5x10^4$ cells per well. After the corresponding treatments, OLs were fixed in 4% paraformaldehyde (PFA) with 4% sucrose for 15 min and HEK293T cells in 4% PFA for 10 min, followed by 3 washes with PBS. Cells were stored at 4 ºC or processed immediately.

Fixed cells were permeabilized and blocked for 1 h in a blocking solution consisting of 4% normal goat serum (NGS; Palex) and 0.1% Triton X-100 (Sigma-Aldrich) in PBS. Afterward, cells were incubated with specific primary antibodies (**Table 3**) in the blocking solution O/N at 4 °C. Samples were washed thrice in PBS and incubated with fluorochrome-conjugated secondary antibodies (1:500) in the blocking solution for 1 h at RT. Subsequently, cells were washed twice and incubated with DAPI (4 µg/ml; Sigma-Aldrich) for 10 min for nuclei detection. Cells were again washed with PBS, and coverslips were mounted on glass slides using Fluoromount-G® mounting medium (SouthernBiotech). Prepations were stored at 4 °C until examination.

Table 3. Antibodies used in immunocytochemistry (ICC) and immunohistochemistry (IHC).

Antibody	Host	Dilution	Reference
Anti-MYRF	Rabbit	ICC 1:100	#ABN45, Millipore
Anti-MYRF	Rabbit	IHC 1:500	#A16355, ABclonal
Anti-MBP	Chicken	ICC 1:200	#AB9348, Millipore
Anti-Olig2	Mouse (IgG_{2A})	ICC 1:1,000 / IHC 1:500	#MABN50, Millipore
Anti-GSK3α/β	Mouse (IgG_{2A})	ICC 1:500	#sc-7291, Santa Cruz
Anti-Fbxw7	Mouse (IgG_{2A})	ICC 1:300	#TA802869S, OriGene
Anti-Myc tag	Mouse (IgG_1)	ICC 1:500	#05-724-25UG, Millipore
Anti-FLAG tag	Rabbit	ICC 1:1,000	#2368, Cell Signaling
Anti- PDGFR-α	Goat	IHC 1:500	#AF1062, Biotechne
Anti-NG2	Rabbit	IHC 1:200	#AB5320, Millipore
Anti-Nkx2.2	Mouse (IgG_{2B})	IHC 1:20	#74.5A5, DSHB
Anti-APC (CC1)	Mouse (IgG_{2B})	IHC 1:200	#OP80, Millipore
Anti-Iba1	Guinea pig	IHC 1:500	#234308, Synaptic Systems

8.2. Floating mouse tissue immunohistochemistry

For oligodendroglial population studies in AD mouse models, immunohistochemical analysis of specific OL lineage markers was performed. For that, mice were anesthetized by an intraperitoneal injection of pentobarbital and perfused with 4% paraformaldehyde (PFA; Electron Microscopy Sciences) in PBS. Subsequently, brains were carefully extracted and post-fixed with the same solution for 4 h at RT. Brains were then washed with PBS and sectioned using a Leica VT 1200S vibratome (Leica microsystems) to obtain 40 μm-thick coronal sections.

Free-floating slices were washed in 0.1 M PB, and incubated in R-Universal Epitope Recovery Buffer (Aptum) for heat-induced antigen unmasking for 5 min at 95 ºC, followed by 5 min at RT. The sections were then washed 3 times in PBS (pH 7.4), and permeabilized in ice-cold 100% ethanol (EtOH) for 10 min at -20 ºC. Afterwards, brain slices were washed three times with PBS, and permeabilized and blocked with 10% NGS, 0.1% Triton X-100 in PBS for 30 min at RT. Slices were washed three times, and incubated with the blocking solution containing specific primary antibodies (**Table 3**) O/N at 4 ºC. After incubation, slices were washed thrice and incubated with

fluorochrome-conjugated secondary antibodies (1:500) in the blocking solution for 1 h at RT. Then, slices were washed twice, incubated with DAPI for 10 min, and washed again twice in PBS. Finally, slices were mounted on glass slides with Fluoromount-G® mounting medium (Southern Biotech).

For PDGFR-α labeling antigen retrieval protocol was not utilized, and Triton X-100 was only used during permeabilization. On the other hand, EtOH permeabilization step was not followed for MYRF labeling.

8.2.1. EdU labeling and detection by immunohistochemistry

For oligodendroglial population dynamics analysis in 3xTg-AD mice, cumulative EdU labeling was performed. For that, 11 month-old WT and 3xTg-AD mice (n = 4 for each group) were exposed to 5'-ethynyl-2'-deoxyuridine (EdU; Invitrogen) during 30 days. EdU was dissolved in the drinking water at 0.2 mg/ml, which has previously been determined to be nontoxic (Young et al., 2013). The water was exchanged every 48 h, and adequate drinking was monitored. After the treatment, mice were perfused and brains sectioned as previously described.

For EdU visualization, the Click-iT™ EdU Alexa Fluor 647 Imaging Kit (Invitrogen) was used according to the manufacturer's instructions. Briefly, before starting with the immunohistochemistry protocol, brain slices were incubated in 0.5% Triton X-100 in PBS for 20 min at RT, washed twice in 3% BSA in PBS, and incubated in the dark with Click-iT™ EdU reaction cocktail (Invitrogen) for 40 min. Afterwards, slices were washed once in 3% BSA in PBS, and 3 times in PBS. Then, previously described immunohistochemistry protocol was followed.

8.3. Acquisition and analysis of immunofluorescence images

Images were acquired using a Leica TCS STED CW SP8X confocal microscope (Leica), with a 63X oil-immersion objective for cultured cells and a 40X oil-immersion objective (with a zoom factor of 0.75) for mouse tissue imaging. In immunostainings with multiple fluorophores, channels were scanned sequentially to minimize crosstalk. The same settings were applied to all the images within the same experiment. Image analysis was performed using ImageJ/Fiji software (NIH).

8.3.1. Primary oligodendrocyte and HEK293T cell cultures

For cultured cells, a minimum of 10 cells per condition were captured in each experiment. In nuclear expression experiments (Myc-tag and Fbxw7), nuclei were determined using Olig2 or DAPI staining, and the integrated density of the protein of interest was quantified within the nuclear region of interest (ROI). For analysis of GSK3 localization, the cytosol was manually delineated based on GSK3 labeling, while the nucleus was outlined using DAPI staining. Subsequently, the mean intensity of GSK3 within each cellular compartment was measured, and the ratio between nuclear and cytosolic mean intensities was calculated.

8.3.2. Mouse tissue

For tissue imaging, z-stacks were captured, from 1-3 sections per animal. When assessing densities of oligodendroglial lineage cells, the entire image was analyzed for the corpus callosum, while in the dentate gyrus only the hilus was quantified. For morphological analysis of $NG2^+$ OLs, the area occupied by each OL was measured as an indicator of cell size and hypertrophy. This involved manually defining the area occupied by the cell body and the main cellular processes of each OL. 14 OLs were analyzed per animal, 7 per hemisphere. Finally, for the analysis of nuclear MYRF fluorescence intensity, cell nuclei were determined by Olig2 labeling, and the mean intensity within the nucleus of the OLs was quantified.

9. Cell viability assays

To assess the potential toxic effect of prolonged MYRF overexpression in OLs, cell viability assays were conducted. For that, primary OLs were transfected via electroporation with either an empty plasmid or the double-tagged MYRF expression construct, and then were seeded onto 48-well plates at a density of $2x10^4$ cells per well, in triplicates. Cells were cultured in proliferation SATO- medium, and at 3, 6, and 10 DIV they were loaded with Calcein-AM (1 μM; Invitrogen) and NucBlue™ Live ReadyProbes™ Reagent (2 drops/ml; Invitrogen) for 30 min at 37°C. Afterward, cells were washed twice with sterile PBS, images were captured using EVOS fluorescent microscope (Invitrogen), and fluorescence was measured using a CLARIOstar® Plus microplate reader (BMG Labtech) with excitation at 485 nm and emission at 528 nm for

Calcein-AM and excitation at 360 nm and emission at 460 nm for NucBlue. The results were expressed as the ratio of Calcein-AM (indicative of living cells) to NucBlue (total cells), and represented as percentages relative to OLs transfected with an empty control plasmid at each time point.

10. Dual-luciferase assays

To assess the transcriptional activity of MYRF following Aβo-treatments, luciferase assays were conducted in primary cultured OLs. In brief, OLs were co-transfected with the respective test luciferase construct (pGL3-Basic, pGL3-Control, pGL3-MBP, pGL3-MAG, pGL3-Rffl, or pGL4.10_myrfprom_ECR9) and a constitutive *Renilla* construct (1:10), as an internal experimental luminescence control. In experiments aimed at evaluating the role of MYRF in Aβo-induced alterations in myelin-related genes, cells were also co-transfected with control or *Myrf* siRNAs, as previously described. Transfected cells were seeded into PDL-treated 24-wells plates, in triplicates, at a density of $7.5x10^4$ cells per well.

At 72 h post-transfection (3 DIV), cells were harvested in Passive Lysis Buffer (1X PLB; Promega), and luciferase assays were performed using the Dual-Luciferase® Reporter Assay System (Promega), according to the manufacturer's instructions. For each triplicate of each condition, 10 µl of cell lysate was transferred into a white opaque-bottomed 96-well plate, and after the addition of 50 µl per well of Luciferase Assay Reagent II (LAR II; Promega), luciferase activity was measured by luminescence in a Synergy H4 Hybrid Reader (BioTek Instruments). Upon completion of the luciferase measurement, 50 µl of Stop&Glo Reagent (Promega) was added per well, and luminescence readings were repeated, this time for *Renilla* activity.

All data were normalized to the luminescence control established by *Renilla* activity, as well as to the protein concentration measured using a Lowry assay (Bio-Rad).

11. Chymotrypsin-like proteasome activity assay

In order to investigate the impact of Aβo treatments on proteasomal activity, we measured the chymotrypsin-like activity of the proteasome in both HEK293T cells and 3 DIV primary cultured OLs. With this aim, cells were seeded in 96-well plates at a density of $1x10^4$ cells per well and treated with either vehicle or Aβo (1 μM) for 3 or 24 h, with or without MG132 (1 μM, 1 h), a well-established proteasome inhibitor used as a control.

Following treatments, we conducted Proteasome-Glo™ Cell-Based Assay (Promega) following the manufacturer's instructions. This assay employs a specific proteasome substrate, SucLLVY-aminoluciferin, which is cleaved by the proteasome, resulting in the release of aminoluciferin. Aminoluciferin is then used by luciferase to produce luminescence, with luminescent signal intensity being directly proportional to intracellular proteasome activity. In brief, Proteasome-Glo™ Cell-Based Reagent (Promega), previously equilibrated to RT, was added to each well at a 1:1 ratio (100 μl of reagent to each 100 μl of sample). The plate was then incubated at RT on a plate shaker at 700 rpm for 2 min, followed by an additional 10-min incubation at RT. Subsequently, luminescence was measured using the CLARIOstar® Plus microplate reader (BMG Labtech). Results are expressed as percentages relative to vehicle-treated cells (100%).

12. Puromycin-proximity ligation assay (Puro-PLA)

To quantify the levels of actively synthesizing MYRF protein, control and Aβo-treated 3 DIV OLs ($2x10^4$ cells/well) were exposed to puromycin (2 μM; Sigma-Aldrich) for 10 min in the absence or presence of the protein synthesis inhibitor anisomycin (40 μM) for 25 min. After incubations, cells were washed with ice-cold PBS containing digitonin, and fixed in 4% PFA + 4% sucrose in PBS for 15 min.

Proximity Ligation Assay (PLA) was conducted following the Duolink® PLA Protocol (Sigma-Aldrich), and according to the manufacturer's recommendations. Briefly, permeabilized and blocked cells were incubated O/N at 4 ºC with rabbit anti-MYRF (1:100; #ABN45, Millipore) and mouse anti-puromycin (1:500; #MABE343, Millipore) primary antibodies. Coverslips containing cells were washed with an appropriate wash buffer and then incubated with rabbit PLA plus and mouse PLA minus probes (Sigma-Aldrich) for 1 h. The ligation solution from the kit was applied and cells were

incubated for 30 min. Subsequently, signal amplification was achieved by incubating cells with a polymerase for 100 min, protected from light. All incubation steps were conducted in a humidity chamber at 37 ºC and alternated with subsequent washing steps. Finally, cells were washed and treated with Alexa Fluor™ 488-conjugated phalloidin (#A12379, ThermoFisher) in 1% BSA for 20 min, in order to make the cytoskeleton visible. Coverslips were mounted on glass slides with Duolink® *In situ* Mounting Media with DAPI.

Images were captured with a Zeiss Apoteome 2 (Carl Zeiss Microscopy) epifluorescence microscope, using the 63X oil-immersion objective. Image analysis was performed using ImageJ/Fiji software. The phalloidin signal was processed with a Gaussian Blur plugin to create a mask, and mean values of fluorescence intensity of the PLA signal were obtained.

13. Magnetic activated cell sorting (MACS)

With the objective of conducting a transcriptomic analysis of OLs in early stages of Alzheimer's disease, $O4^+$ OLs were isolated from 6-month-old WT and 3xTg-AD mice. To ensure an adequate yield of OLs, two animals were used per sample (n^{WT} = 4 (8 animals) and $n^{3xTg\text{-}AD}$ = 3 (6 animals)). Mice were anesthetized with isoflurane and euthanized by decapitation. Then, OL isolation was carried out following previously established protocols (de la Fuente et al., 2020).

Briefly, the brains were extracted from the skull, placed in Hibernate A medium (Gibco), and sectioned into small pieces (approximately 1 mm^3). The brain tissue was then enzymatically digested using a papain solution containing papain (33 U/ml) and DNase (0.04 mg/ml) in Hibernate A for 30 min at 37 °C. After tissue digestion, the papain solution was washed out with HBSS-/- (Gibco) via centrifugation, and the tissue was mechanically dissociated in Hibernate A supplemented with B27 (Gibco) and 2 mM sodium pyruvate (Gibco), using a polished glass Pasteur pipette. The resulting single-cell suspension was passed through a 70 μm strainer (VWR) and centrifuged at 800 × g for 20 min in a 22.5% Percoll (GE Healthcare) solution with DMEM Glutamax (Gibco). Following centrifugation, the Percoll solution was aspirated, and the cells were washed with HBSS-/- (Gibco). Subsequently, cells were incubated with an anti-O4 antibody (Milteny Biotech) for 15 min on ice, followed by a washing step with

HBSS-/- to remove excess antibody. Finally, cells were magnetically sorted using a column, according to the manufacturer's instructions (Milteny Biotech). The sorted $O4^+$ cells were eluted in SATO+ medium for subsequent RNA extraction and RNA sequencing analysis.

14. Quantitative Real time-Polymerase Chain Reaction (RT-qPCR)

For cultured primary OLs and OLs isolated via MACS, total RNA extraction was performed using the RNA Mini Kit (Quiagen) and RNA Micro Kit (Quiagen), respectively, following the manufacturer's instructions. RNA concentration and integrity were assessed using the NanoDrop™ 2000 spectrophotometer (ThermoFisher Scientific).

Complementary DNA (cDNA) synthesis was conducted using the Superscript™ III reverse transcriptase (Invitrogen) with random primers in a Verity Thermal Cycler (Applied Biosystems), according to the manufacturer's protocol. The resulting cDNA samples were diluted in sterile Mili-Q H_2O. Subsequently, RT-qPCR was carried out in triplicate reactions containing 3.5 µl RNAse-free water, 5 µl Sybr Green Master Mix, 1 µl properly diluted primers, and 0.5 µl cDNA sample. Specific primers for *Myrf, Sox10*, and *Fbxw7* (**Table 4**) were newly designed using Primer3 software and synthesized by Integrated DNA Technologies (IDT). The reactions were performed using the CFX96 Touch Real-Time PCR Detection System (Bio-Rad), and the following protocol was applied: 3 min at 95 °C, 40 cycles of 10 s at 95 °C, and 30 s at 60 °C. PCR product specificity was confirmed by melting curves.

Data was normalized to a normalization factor obtained using geNorm Software through the analysis of the expression of three different housekeeping genes: *Gapdh*, *Bm2* and *Pgk1* (**Table 4**).

Table 4. Sequences of primers used in the transcriptional analysis. Both genes of interest and the housekeeping genes (grey) used for normalization are displayed.

Gene	Sequence	Company
Myrf	Fwd GTGGGCGACCCTATATGATG Rev TCCACACGATAGGTGAGCAT	IDT
Sox10	Fwd ATGTCAGATGGGAACCCAGA Rev GTCTTTGGGGTGGTTGGAG	IDT
Fbxw7	Fwd AAAGAGTTGTTAGCGGTTCTCG Rev CCACATGGATACCATCAAACTG	IDT
Gapdh	Fwd GAAGGTCGGTGTCAACGGATTT Rev CAATGTCCACTTTGTTCACAAGAGAA	Eurofins
Bm2	Fwd CACCGAGACCGATGTATATGCTT Rev TTACATGTTCTCGGTCCCAGG	Eurofins
Pgk1	Fwd ATGCAAAGACTGGCCAAGCTAC Rev AGCCACAGCCTCAGCATATTTC	IDT

15. Bulk RNA sequencing

With the aim of elucidating gene expression alterations in OLs from an early AD model, bulk RNA sequencing (RNA-seq) was conducted on the $O4^+$ OLs isolated via MACS. Therefore, the MACS-isolated samples were sent to the Genomic Platform at CICbioGUNE (Derio, Spain). RNA quantity and quality was assessed using the Qubit RNA assay Kit (Invitrogen) and Agilent 2100 Bioanalyzer (Agilent RNA 6000 Pico Chips); all samples exhibited sufficient concentration and integrity to perform the experiments.

Sequencing libraries were prepared using the "NEB Next® Single Cell/Low Input RNA Library Prep Kit for Illumina®" (#E6420S, New England Biolabs) and "NEB Next Multiplex Oligos for Illumina (Index Primers 1-12)" (#E7335S, New England Biolabs), following the corresponding instruction manual (Version5.0_5/20). The protocol started with 10 ng of total RNA when possible; otherwise, the entire sample was utilized. Briefly, full-length cDNA was generated using a template-switching method. Subsequently, cDNA amplification (number of amplification cycles depending on input RNA amount) and cleanup were performed, and 1 µl of amplified cDNA was run on a DNA High

Sensitivity Chip (#5067-4626, Agilent Technologies) to assess cDNA quantity and quality. In the next step, fragmentation, end repair, and tailing were conducted, and adapters for Illumina were ligated to the amplified cDNA. Finally, library barcoding and amplification (number of amplification cycles depending on cDNA amount) were achieved by PCR.

Libraries were visualized on an Agilent 2100 Bioanalyzer using Agilent High Sensitivity DNA Kit (#5067-4626, Agilent Technologies) and quantified using the Qubit dsDNA HS DNA Kit (#Q32854, Thermo Fisher Scientific). The Illumina sequencer generates raw images utilizing sequencing control software for system control and base calling through an integrated primary analysis software called Real Time Analysis (RTA). The base calls (BCL) were converted into FASTQ files utilizing Illumina Inc.'s package bcl2fastq, and quality control analysis was performed (FastQC) (Andrews, 2020).

The subsequent bioinformatics analysis was conducted in collaboration with R. Senovilla-Ganzo (predoctoral researcher at Dr. F. García-Moreno's lab, Achucarro Basque Center for Neuroscience, Leioa, Spain). Alignment was performed with STAR v2.7.1 (Dobin et al., 2013) against the Ensembl genome of *Mus musculus* (GRCm39.dna.primary_assembly.fa and GRCm39.104.gtf), and expression counts were obtained using htseq-count (-s no) (Anders et al., 2015). The count matrix was imported to R v4.2.2, where expression levels were normalized and further analyzed with DESeq2 (Love et al., 2014).

DESeq2 provides methods for differential expression tests based on negative binomial generalized linear models. Therefore, factors involved in the analysis must be modeled beforehand in a sample table entry (**Table 5**). This metadata allows DESeq2 to group samples by factors of interest (e.g., Genotype) to detect differentially expressed genes based on the biological question (contrast selection), but also to correct batch effect (e.g., Day).

Table 5. Sample table. Each sample (row name) is assigned a level of a factor (column names).

Sample name	Genotype	Day
S_08	AD	D3
S_09	AD	D4
S_10	AD	D5
S_01	WT	D1
S_02	WT	D2
S_03	WT	D3
S_04	WT	D4

The initial step of the DESeq2 pipeline involves filtering low-expressed genes: genes with < 2 (fewer than 2) counts in more than one sample per group were discarded. These differences in the threshold for each analysis were attributed to variations in the amount of RNA obtained in each sample. For the different analyses, the linear model design utilized was: ~ Day + Genotype and contrast: list ("Genotype_AD_vs_WT"). Those genes with a p-adjusted value < 0.05 were identified as significantly deregulated. For data visualization and functional enrichment, *ggplot2* (Wickham, 2016), clusterProfiler (Wu et al., 2021; Yu et al., 2012), and *ggVennDiagram* (Gao et al., 2021) were employed.

The code used can be found at https://github.com/rodrisenovilla/AlberdiLab. Analyzed data will be uploaded to the GEO repository (https://www.ncbi.nlm.nih.gov/geo/) once they are published.

16. Continuous intracerebroventricular (ICV) Gö6983 infusion

For experiments aimed at investigating the pharmacological inhibition of PKC in 3xTg-AD mice, 12-14-month-old animals were utilized (n = 5 animals per treatment group). Osmotic minipumps (Model 1004, Alzet) were subcutaneously implanted into the mice, connected to an infusion headstage attached to their skulls (Brain infusion kit II, Alzet), and continuously delivering either vehicle (0.01% DMSO in saline solution) or Gö6983 (100 nM) at a rate of 0.11 µl/h for a period of 28 days. Initially, the minipumps were filled with the respective solutions, and the surgical procedure was performed the following day, adhered to the manufacturer's recommendations.

On the day of surgery, mice were anesthetized with isoflurane administered via a precision vaporizer, and the scalp and the minipump implantation site were shaved and washed. Subsequently, the mice were secured in a stereotaxic apparatus. A midline sagittal incision was made to expose the skull, and a subcutaneous pocket was prepared for the minipumps in the midscapular area of the animal's backs. Using stereotaxic coordinates (AP: -0.5 mm; ML: 1 mm, DV: 2 mm), a hole was drilled in the skull to place the cannula connected to the osmotic pump, allowing continuous drug infusion into the right brain ventricle. A filled pump was inserted into the pocked, with the delivery portal positioned first, while the infusion headstage was secured in the skull hole. Dental cement was applied to cover the area, and the scalp wound was closed with sutures.

Following surgery, all animals received a subcutaneous injection of buprenorphine (3 µl/g of animal) for pain management. The overall well-being of the mice was monitored throughout the experiment, and body weight was measured before, during, and after treatment.

After 28 days, mice were anesthetized by intraperitoneal injection of pentobarbital and perfused with saline solution. The brains were dissected, with the right hemispheres (ipsilateral) post-fixed in 4% PFA in PBS O/N at 4 ºC for subsequent IHC analysis, and the left hippocampi (contralateral) were frozen for protein preparation for western blot analysis.

17. Intracerebral amyloid β injections

17.1. Intrahippocampal amyloid β injection in adult mice

Adult male mice (C57BL6/J), aged 3-4 months, were randomly assigned to treatment groups (n = 5 animals per group) and anesthetized with ketamine hydrochloride (80 mg/kg) and xylazine (10 mg/kg). Next, they were secured in a stereotaxic apparatus for intrahippocampal injections into the right dentate gyrus (coordinates AP: -2.2 mm, ML: 1.5 mm, DV: 2 mm). A total volume of 3 µL containing either vehicle (17% DMSO + 83% Ham's F12) or Aβo (10 µM) was injected. Following injection, the needle was kept in place for 5 min to prevent reflux.

After 7 days, mice were anesthetized using ketamine/xylacine and perfused with 30 mL of phosphate buffer followed by 30 mL of 4% PFA in 0.4 M PB (pH 7.5). The brains were then extracted and post-fixed in the same fixative solution for 4 h at RT. Subsequently, the brains were transferred to 30% sucrose in 0.1 M PBS (pH 7.5) at 4 ºC and kept in cryoprotectant solution (30% ethylene glycol, 30% glycerol, and 0.1 M PBS in dH_2O) at -20 ºC for subsequent sectioning using a vibratome and analysis via IHC.

17.2. Intracerebroventricular amyloid β injection in zebrafish larvae

At 24 hpf, all zebrafish embryos had their chorions removed for the brain ventricle injection procedure, following previously established protocols (Gutzman & Sive, 2009; Nery et al., 2014). Embryos were anesthetized with Tricaine (Sigma-Aldrich) and immobilized in wells on 2%-agar coated dishes under the stereomicroscope so that the brain ventricle was exposed. An injection needle was carefully positioned on the roof plate of the hindbrain, and 5–10 nl of a fresh injection buffer containing 10% either Aβo (10 µM) or vehicle, and 10% Phenol Red in 0.4 M KCl in nuclease-free water was microinjected. Subsequently, each treatment group was separated into clean plates, and the zebrafish were returned to the incubator and allowed to grow until the days of the experiments.

18. RNA *in situ* hybridization

To identify potential Aβo-induced alterations in OL differentiation- and myelination-related gene expression *in vivo*, we conducted fluorescent RNA *in situ* hybridization assays (FISH) in the spinal cord of zebrafish larvae injected with either vehicle or Aβo (10 µM). FISH was performed using the RNAScope Multiplex Fluorescent V2 Assay Kit (Advanced Cell Diagnostics; ACD).

Zebrafish larvae at 48 hpf, 72 hpf, and 5 dpf were fixed in 4% PFA in PBS, gently rocking O/N at 4 ºC. Subsequently, samples were embedded in 1.5% agar with 30% sucrose, followed by immersion in 30% sucrose O/N. The blocks were frozen on dry ice, and 15 µm-thick transverse sections were obtained using a cryostat microtome and collected on polarized slides.

FISH was performed according to the manufacturer's instructions, with the following modification: slides were covered with Parafilm for all 40°C incubations to maintain moisture and disperse reagents across the sections. The zebrafish *mbpa*, *myrf*, and *sox10* transcript probes were designed and synthesized by the manufacturer, and used at 1:50 dilutions, except for *mbpa,* which was used undiluted. The transcripts were fluorescently labelled by TSA-based Opal fluorophores Opal520 (1:1500), Opal570 (1:500) and Opal650 (1:1500) using the Opal 7 Kit (PerkinElmer).

Images were acquired on a Zeiss Cell Observer 2D 25 Spinning Disk confocal system (Carl Zeiss Microscopy) with a 40X oil-immersion objective. 15 z-stack tiles (z-step = 0.5 µm) of 5 sections of the spinal cord were acquired from each animal. The total area occupied by each probe was determined using ImageJ/Fiji.

19. *In vivo* myelin sheath visualization in zebrafish larvae

To visualize myelin sheaths *in vivo*, the *mbpa*:EGFP-CAAX construct was transiently expressed by microinjection into 1-cell stage WT zebrafish embryos. Next, zebrafish larvae were ICV injected with either vehicle or Aβo (10 µM) at 24 hpf, and treated by bath immersion with or without Gö6983 (500 nM) at 72 hpf. At 5 dpf, zebrafish larvae were anesthetized with Tricaine (Sigma-Aldrich) and embedded laterally in 1% low-melt agarose containing 0.4% Tricaine for immobilization on a glass bottom dish.

Images were acquired using a Zeiss Cell Observer 2D 25 Spinning Disk confocal system (Carl Zeiss Microscopy) with a 40X water-immersion objective. Images were collected from 1-3 field of view from each animal in 40 z-stack tiles (z-step = 0.28 µm). Subsequent analysis of sheath length and total number of sheaths per OLs was performed using Imaris software v9.9.1 (Oxford Instruments), in a blind mode.

20. Electron microscopy (EM)

At 8 dpf, vehicle- or Aβo-injected zebrafish larvae were anesthesized with Tricaine and fixed in a solution consisting of 2% glutaraldehyde and 4% PFA in 0.1 M sodium cacodylate (pH 7.4), for at least 5 days at 4°C. The tissue was then sagittally sectioned using a Leica VT 1200S vibrating blade microtome (Leica) to obtain 200 µm-thick

sections. These tissue sections were post-fixed in 2% OsO_4, dehydrated in ethanol and propylene oxide, and embedded in EPON (Serva) for 24 h at 60 °C. Ultrathin sections (50 nm thickness) were obtained using a Leica Ultracut S ultramicrotome (Leica) and contrasted for 30 min with 4% uranyl acetate and 6 min with lead citrate. Electron micrographs were captured using a Zeiss EM900 electron microscope (Carl Zeiss Microscopy), and the number of dorsal myelinated axons were quantified.

21. Statistical analysis

All data are presented as mean ± S.E.M (standard error of the mean), with sample size indicated in the figures by dots. Statistical analyses were performed using absolute values. GraphPad Prism 8.2.1 software was utilized, applying unpaired or paired two-tailed Student's t-test for comparing two experimental groups, and one-way or two-way analysis of variance (ANOVA) followed by Dunnett's, Tukey's, and Sidak's *post-hoc* tests for multiple comparisons. Results from independent animals or separate experiments were considered as biological replicates ($n \geq 3$). Statistical significance was represented as $p<0.05$ (* or #), $p<0.01$ (** or # #), $p<0.001$ (*** or # # #), and $p<0.0001$ (****or # # # #).

Results

PART I. Characterization of oligodendroglial lineage cells in Alzheimer's disease models 3xTg-AD and Aβo-injected mice

The correct structure of the WM and the functional efficiency of oligodendrocytes are indispensable factors for preserving the integrity of the CNS. In AD, although it has traditionally been considered a GM disease, accumulating evidence from both human *post-mortem* brain samples and AD mouse models indicates alterations in WM microstructure (Bartzokis et al., 2003; Han et al., 2002; Wu et al., 2017). Given that myelin in the CNS is derived from and maintained by OLs, it is reasonable to infer that OL changes may underlie, at least in part, the WM damage observed in AD.

In this line, previous studies have identified OL abnormalities that substantially contribute to the pathophysiology of AD, including disrupted oligodendrogenesis (Behrendt et al., 2013; Dong et al., 2018) and OL maturation (Desai et al., 2010), as well as impaired density and morphology of OPCs (Chacon-De-La-Rocha et al., 2020; Vanzulli et al., 2020). However, these alterations appear to be dependent on factors such as the animal model, age, analyzed brain region, and even the methodological approach used, leading to discrepancies in the literature. Thus, further investigations are needed to elucidate the pathological events involving OLs in AD.

1.1. Oligodendrocyte lineage cells are altered in 3xTg-AD mice

During development, OPCs undergo a tightly regulated complex differentiation program, transitioning through an immature premyelinating state and ultimately becoming mature myelinating OLs. Each phenotypic stages is characterized by the sequential expression of specific molecular markers and morphological changes (Baumann & Pham-Dinh, 2001), facilitating the analysis of distinct OL subpopulations by immunohistochemistry (IHC).

To investigate the oligodendroglial population and its dynamics in AD, we performed an IHC analysis of the oligodendrocytic cells in the 3xTg-AD mouse model. This model, carrying three human transgenes associated with AD development –APP^{Swe}, $MAPT^{P301L}$, and $PSEN1^{M146V}$-, is considered one of the most complete animal models of the disease, as it exhibits both senile plaques and neurofibrillary tangles, along with cognitive impairments resembling those observed in AD patients. Therefore, 12-month-old WT and 3xTg-AD mice were administered 5-ethynyl-20-deoxyuridine (EdU) via their drinking

water for 30 days (**Figure 10A, 11A**). EdU is a thymidine analog that incorporates into the chromatin of dividing cells, allowing the detection of actively proliferating and newly generated cells during the treatment period. Following the treatment, IHC analysis of oligodendroglial linage cells was conducted in the corpus callosum (CC), the brain's major white matter tract, and the dentate gyrus (DG) of the hippocampus, a key grey matter region responsible for the formation of episodic memories. These brain regions are relevant to AD pathology, as indicated by previous studies.

1.1.1. Oligodendrocyte maturation is promoted in the 3xTg-AD mice corpus callosum

Analysis in the CC (**Figure 10B, C**) revealed no changes in the density of $Olig2^+$ oligodendroglial lineage cells (**Image 10D**), nor in the total counts of PDGFR-α^+ OPCs (**Figure 10G**) or $CC1^+Olig2^+$ mature OLs (**Figure 10E**). However, a significant reduction was found in the PDGFR-$\alpha^-CC1^-Olig2^+$ cells, considered immature OLs, in the 3xTg-AD mice compared to WT mice ($2.39 \pm 1.34x10^3$ cells/mm^3 vs $9.38 \pm 2.15x10^3$ cells/mm^3, respectively) (**Figure 10F**). Next, we divided the whole $Olig2^+$ population into the three previously mentioned subpopulations, OPCs (PDGFR-α^+), immature OLs (PDGFR-α^- $CC1^-$ $Olig2^+$), and mature OLs ($CC1^+Olig2^+$), and we compared the percentage each subpopulation occupies within the total OLs between mice groups. We observed that although there were no significant changes in the percentage of OPCs (WT 9.54 ± 1.42% vs 3xTg-AD 8.55 ± 1.88%), a substantial portion of the immature OL subpopulation was lost in the 3xTg-AD mice (WT 7.96 ± 1.45% vs 3xTg-AD 1.51 ± 0.91%), leading to an increased percentage of mature OLs (WT 82.5 ± 2.04% vs 3xTg-AD 89.93 ± 1.55%) (**Figure 10H**). Further analysis according to sexes did not reveal any relevant sexual dimorphism.

To gain deeper insight into the alterations in the dynamics of those oligodendroglial cells, we analyzed EdU incorporation. No changes were observed in dividing OL ($Olig2^+EdU^+$) (**Figure 10I**) or OPC (PDGFR-α^+EdU^+) numbers between the groups (**Figure 10K**); however, surprisingly, among the OLs generated *de novo* during the EdU treatment, there were more newly generated mature OLs (%$CC1^+Olig2^+EdU^+$/$Olig2^+EdU^+$) in the 3xTg-AD mice (WT 47.03 ± 2.16% vs 3xTg-AD 68.23 ± 3.65%) (**Figure 10J**).

These findings together suggested aberrant OL differentiation in the corpus callosum of 3xTg-AD mice, which resulted in a near depletion of the immature OL population, as they mature.

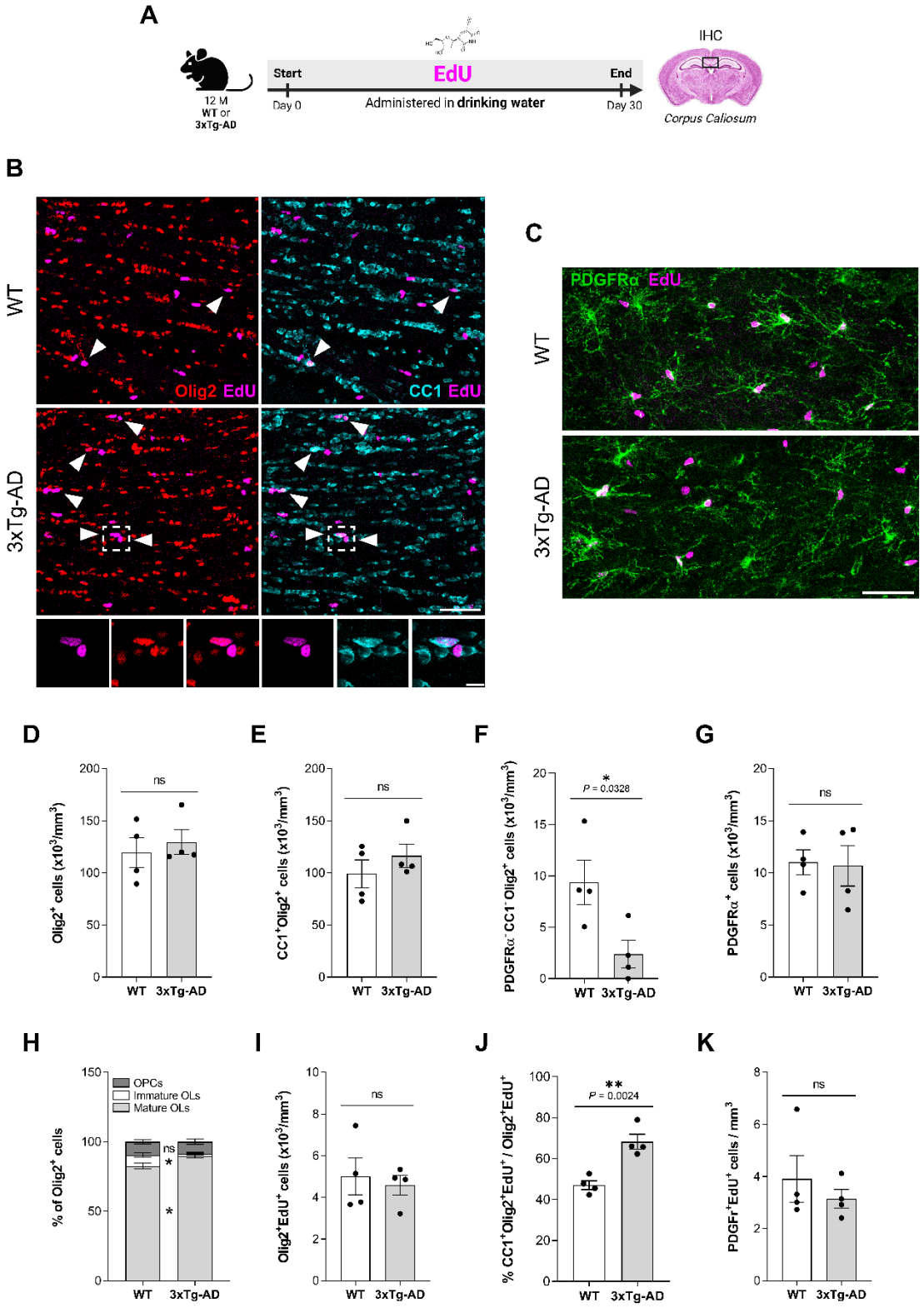

Figure 10. Oligodendroglial lineage dynamics is altered in 3xTg-AD mice corpus callosum, with increased density of newly generated mature oligodendrocytes. (**A**) Schematic representation of the experimental timeline. 12-month-old WT and 3xTg-AD mice received 5-ethynyl-20-deoxyuridine (EdU; 0.2 mg/ml) in their drinking water for up to 30 days, followed by brain dissection for IHC analysis of the CC. (**B**) Representative micrographs depicting triple-immunostaining for actively dividing cell marker EdU (magenta), the oligodendroglial lineage marker Olig2 (red), and the mature OL marker CC1 (cyan). Arrowheads indicate $CC1^+Olig2^+EdU^+$ cells. Scale bars = 50 µm / 10 µm. (**C**) Representative fluorescence images showing double-immunostaining for EdU (magenta) and OPC marker PDGFR-α (green). Scale bar = 50 µm. Histograms showing the numbers of (**D**) $Olig2^+$ (total OLs), (**E**) $CC1^+Olig2^+$ (mature OLs), (**F**) PDGFR-$\alpha^-CC1^-Olig2^+$ (immature OLs), and (**G**) PDGFR-α^+ (OPCs) cells. (**H**) Graph showing the percentage corresponding to each oligodendrogial subpopulation among the entire OL lineage in each animal group. Quantification of (**I**) $Olig2^+EdU^+$ (dividing OLs), (**J**) $\%CC1^+Olig2^+EdU^+/Olig2^+EdU^+$ (newly generated mature OLs), and (**K**) PDGFR-α^+EdU^+ (dividing OPCs) cells. Data are presented as means ± S.E.M, with dots representing individual animals. *p<0.05, **p<0.01; Statistical significance was determined by two-tailed unpaired t-test and two-way ANOVA followed by Sidak's *post-hoc* test.

1.1.2. 3xTg-AD mice present mature and immature oligodendrocyte loss in the dentate gyrus

When moving on into the oligodendroglial population analysis in the DG, changes were more notable (**Figure 11B, C**). First of all, the AD mouse model exhibited a significant loss of approximately 21% in the total density of $Olig2^+$ cells (WT 74.92 ± 4.25x10^3 cells/mm^3 vs 3xTg-AD 59.23 ± 1.68x10^3 cells/mm^3) (**Figure 11D**). More specifically, oligodendroglial loss was evident among both $CC1^+Olig2^+$ mature (WT 49.84 ± 3.02x10^3 cells/mm^3 vs 3xTg-AD 41.38 ± 2.83x10^3 cells/mm^3) (**Figure 11E**) and PDGFR-$\alpha^-CC1^-Olig2^+$ immature OLs (WT 9.51 ± 2.21x10^3 cells/mm^3 vs 3xTg-AD 2.80 ± 1.621x10^3 cells/mm^3) (**Figure 11F**). Interestingly, the number of PDGFR-α^+ OPCs remained stable across animal groups (**Figure 11G**). Regarding the proportions of each oligodendroglial subpopulation within the total $Olig2^+$ population, both OPC and mature OL percentages remained relatively constant across mice groups, but, similar to the CC, a significant reduction in the percentage of immature OLs was observed in the DG of 3xTg-AD mice compared to WT mice (12.46 ± 2.75% and 2.50 ± 4.31%, respectively) (**Figure 11H**).

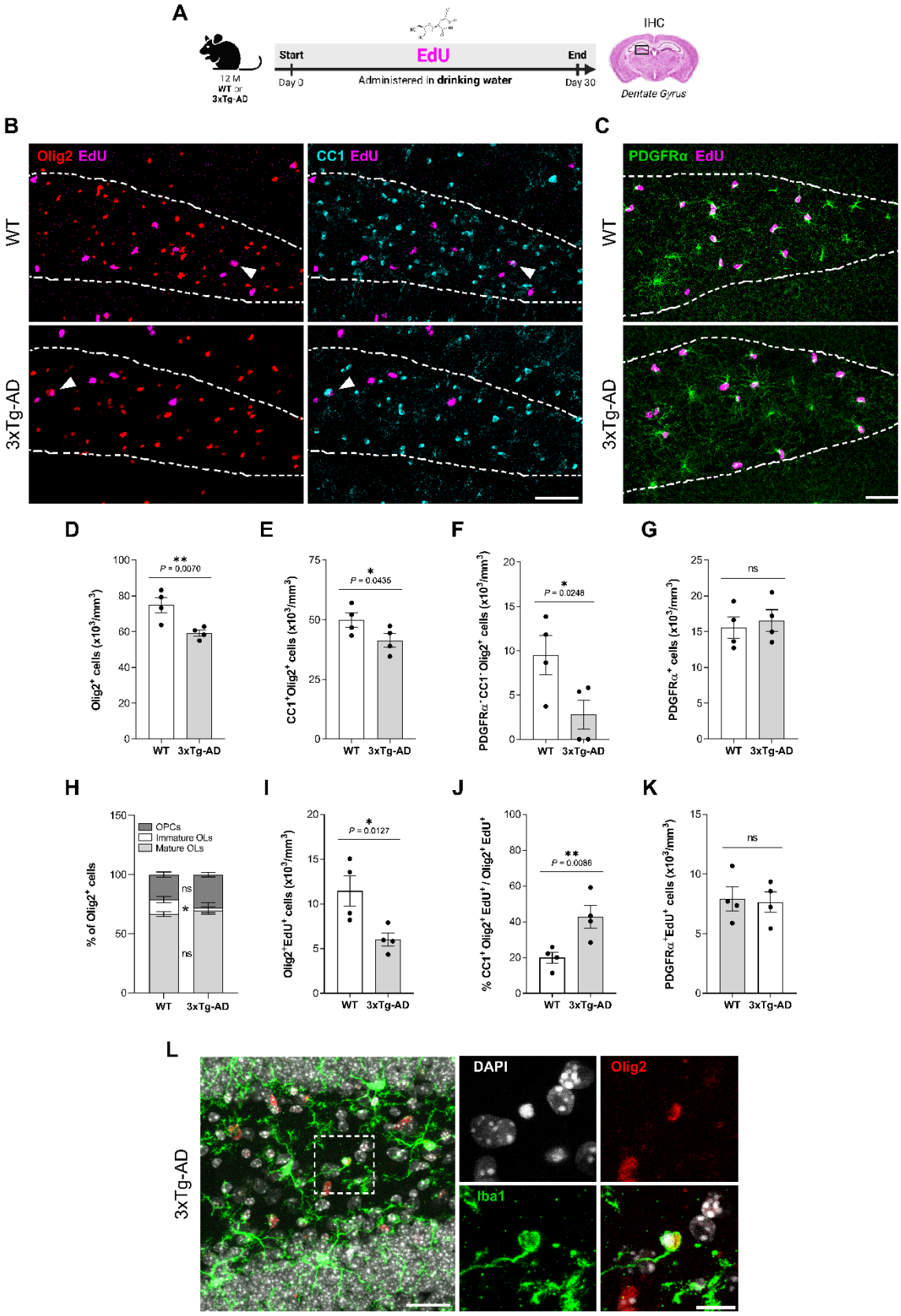

Figure 11. 3xTg-AD mice dentate gyrus exhibit loss of both mature and immature oligodendrocytes, along with aberrant oligodendrocyte maturation. (**A**) Schematic representation of the experimental approach. (**B**) Representative images depicting triple-immunostaining for the proliferating cells marker EdU (magenta), the oligodendroglial lineage marker Olig2 (red), and the

mature OL marker CC1 (cyan) in the DG of WT and 3xTg-AD mice. The dotted white line delineates the analyzed area, and arrowheads indicate $CC1^+Olig2^+EdU^+$ cells. Scale bar = 50 µm. (**C**) Representative micrographs of double-immunostaining for EdU (magenta) and OPC marker PDGFR-α (green). Scale bar = 50 µm. Histograms showing the numbers of (**D**) $Olig2^+$ (total OLs), (**E**) $CC1^+Olig2^+$ (mature OLs), (**F**) PDGFR-$\alpha^-CC1^-Olig2^+$ (immature OLs), and (**G**) PDGFR-α^+ (OPCs) cells. (**H**) Graph indicating the percentages of the oligodendrogial subpopulations in each animal group. Quantification of (**I**) $Olig2^+EdU^+$ (dividing OLs), (**J**) $\%CC1^+Olig2^+EdU^+ / Olig2^+EdU^+$ (newly generated mature OLs), and (**K**) PDGFR-α^+EdU^+ (dividing OPCs). (**L**) Representative confocal image showing microglia (Iba1; green) engulfing an OL (Olig2; red) with a pyknotic nucleus (DAPI; white) in the DG of 3xTg-AD. Scale bars = 25 µm / 10 µm. Data are presented as means ± S.E.M, with dots representing individual animals. *p<0.05; Statistical significance was determined by two-tailed unpaired t-test and two-way ANOVA followed by Sidak's *post-hoc* test.

Next, to further investigate the dynamics of the oligodendroglial population in the DG of 3xTg-AD mice, EdU incorporation was assessed. The findings revealed that while OPC proliferation appeared unchanged across groups (**Figure 11K**), 3xTg-AD mice exhibited a decreased density of $Olig2^+EdU^+$ cells compared to WT counterparts ($6.00 \pm 0.73x10^3$ cells/mm^3 and $11.43 \pm 1.69x10^3$ cells/mm^3, respectively), suggesting either altered OL proliferation or, more likely, that those newly generated OLs that have incorporated EdU were undergoing cell death (**Figure 11I**). Interestingly, here again, there was a notable increase –more than double– in newly generated mature OLs in 3xTg-AD mice relative to WT mice ($42.79 \pm 6.32\%$ and $19.84 \pm 3.07\%$, respectively) (**Figure 11J**). This finding suggested that, in line with the CC, OL differentiation is also enhanced in the DG. Nonetheless, our hypothesis is that these aberrantly differentiating mature OLs undergo cell death, as there is no discernable increase in the density or percentage of mature OLs; instead, a clear decline of this OL subpopulation was observed. Moreover, these effects, while exhibiting similar trends in both sexes, were more pronounced among males.

Given the loss of mature OLs in the DG of this AD mouse model, we subsequently sought to determine the mechanism by which those OLs may be dying. No caspase-3 or senescence markers were detected in the DG of 3xTg-AD mice; however, we did observe some $Olig2^+$ cells with pyknotic nuclei and, very occasionally, localized within phagocytic pouches while being engulfed by microglia (**Figure 11L**). Nevertheless, a more extensive and quantitative investigation of this phenomenon is required, as it is not technically easy to capture dying cells in real-time.

1.1.3. 3xTg-AD mice dentate gyrus show impaired NG2$^+$ oligodendrocyte progenitor cell density and morphology

So far, we have observed alterations in both immature and mature OLs in the DG of our AD model; however, intriguingly, no changes were noted in PDGFR-α$^+$ OPCs. Thus, with the aim of conducting a more comprehensive investigation of the oligodendroglial population in AD, we next sought to study another subset of the oligodendroglial lineage: NG2$^+$ OLs (**Figure 12A**). Often referred to as late OPCs, these cells represent a more mature subset of OPCs than early-stage PDGFR-α$^+$ OPCs; and, apart from functioning as precursor cells, they also serve critical functions including communication with neighboring cells and modulation of neuronal networks (Butt et al., 2005; Nielsen et al., 2013). Here, a significantly reduced density of NG2$^+$ OPCs was observed in the DG of 12-month-old 3xTg-AD mice compared to WT (17.01 ± 1.21x10^3 cells/mm^3 and 20.35 ± 0.78x10^3 cells/mm^3, respectively) (**Figure 12B**), aligning with the previously identified OL loss in this brain region.

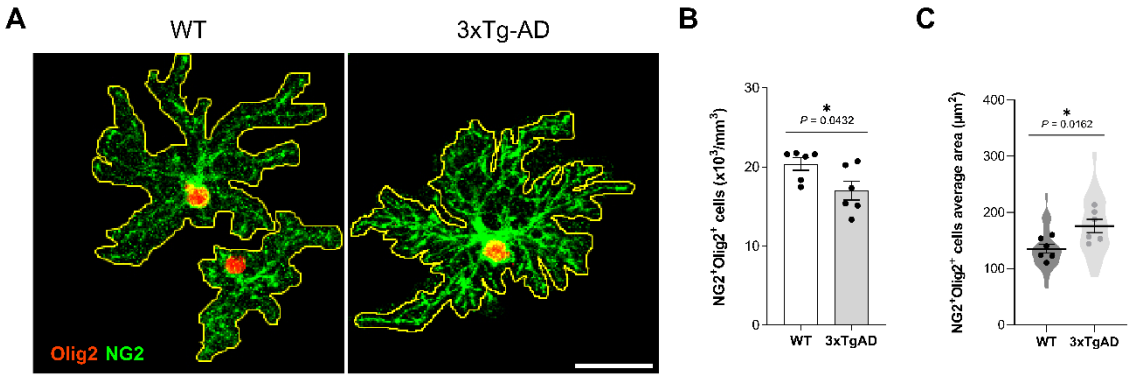

Figure 12. NG2$^+$ oligodendrocyte progenitor cells from 3xTg-AD mice dentate gyrus show reduced density and hypertrophy. (**A**) Representative micrographs of NG2$^+$Olig2$^+$ OPCs in the DG of WT and 3xTg-AD mice (NG2, green; Olig2, red). Yellow line represents the area occupied by each cell. Scale bar = 20 µm. (**B**) Histogram depicting the density of NG2$^+$Olig2$^+$ cells. (**C**) Average area quantification of NG2$^+$Olig2$^+$ cells measured in µm^2. Data are presented as means ± S.E.M; dots represent individual animals and violin plot represents quantification of individual cells. *p<0.05; Statistical significance was determined by two-tailed unpaired t-test.

Moreover, several studies conducted in AD animal models and patient samples have suggested alterations not only in the density but also in the morphology of $NG2^+$ OPCs in pathology (Rodríguez et al., 2016; Vanzulli et al., 2020). Therefore, we sought to determine if this phenomenon was also present in our 12-month-old 3xTg-AD mice. To assess a potential atrophic state of the cells, we measured the area occupied by $NG2^+$ OPCs. Our results revealed that $NG2^+$ late OPCs in the DG of 3xTg-AD mice are approximately 30% larger in size than those in WT mice (175.9 ± 11.68 μm2 and 135.1 ± 7.95 μm^2, respectively) (**Figure 12A, C**). This observed hypertrophic nature of the cells may be attributed to the need to cover a larger area to compensate for the $NG2^+$ OPC loss in this brain region. Additionally, these findings also indicated that the $NG2^+Olig2^+$ subpopulation is susceptible to AD pathophysiology, unlike the early-stage PDGFR-α^+ OPCs.

1.1.4. MYRF expression is upregulated in 3xTg-AD mice dentate gyrus

In light of the oligodendroglial-stage-specific alterations observed in the 3xTg-AD mice, and the aberrant promotion of OL maturation, our attention turned to MYRF. Initially identified as a transcriptional factor essential for myelin sheath formation and CNS myelination (Emery et al., 2009), MYRF has more recently emerged as a key regulator of OL differentiation and maturation, with its expression specifically upregulated during these processes (Aprato et al., 2020). Therefore, we next wandered what would happen with MYRF in this AD mouse model.

To conclude the IHC analysis of OLs in the DG of 12-month-old 3xTg-AD mice, we found that the percentage of $MYRF^+$ OLs was significantly increased compared to WT mice (83.6 ± 0.92% and 72.1 ± 4.1%, respectively) (**Figure 13A, B**). This finding aligns with the enhanced differentiation observed in 3xTg-AD OLs, and highlights MYRF as a promising molecular candidate underlying those alterations.

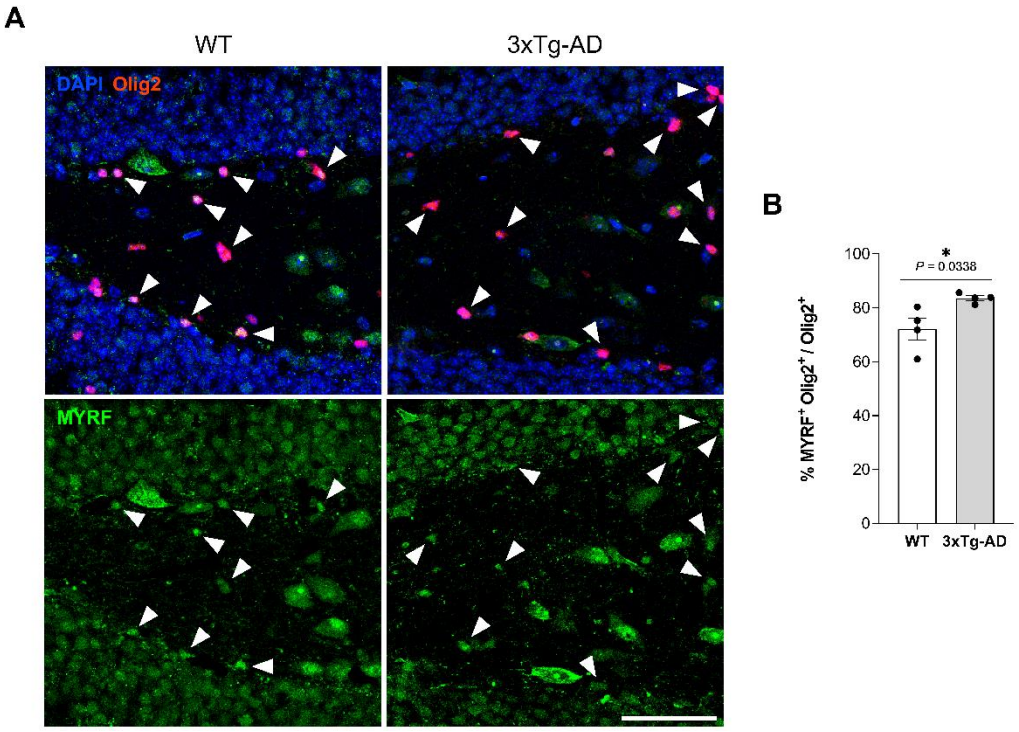

Figure 13. 3xTg-AD mice dentate gyrus show more MYRF$^+$ oligodendrocytes. (**A**) Representative fluorescent micrographs depicting triple staining for DAPI (blue), Olig2 (red) and MYRF (green). Scale bar = 50 μm. (**B**) Quantification of the percentage of MYRF$^+$ OLs within the total Olig2$^+$ population in the DG of WT and 3xTg-AD mice. Data are presented as means ±S.E.M, with dots representing individual animals. *p<0.05; Statistical significance was determined by two-tailed unpaired t-test.

1.2. Oligodendrocytes isolated from 3xTg-AD mice brains present altered transcriptome

After identifying alterations in the oligodendroglial population of our 12-month-old AD mice, particularly the OL loss found in the DG, we aimed to uncover the underlying genetic disparities preceding these changes. To this end, with the focus on earlier stages of the disease, we selectively isolated O4$^+$ immature and mature OLs from the brains of 6-month-old WT and 3xTg-AD mice using magnetic-activated cell sorting (MACS). Subsequently, bulk RNA sequencing (RNA-seq) was carried out to elucidate gene expression alterations potentially contributing to the observed OL pathology in the 3xTg-AD mice (**Figure 14A**).

A comprehensive analysis revealed 5537 differentially expressed genes (DEGs), comprising 2392 significantly upregulated and 3145 significantly downregulated genes in 3xTg-AD OLs (DeSeq2, adjusted P value<0.05) (**Figure 14B**). Interestingly, many of the highly expressed genes were directly linked to AD or were implicated in critical functions for OLs, such as those involved in iron homeostasis (*Iscu*), lipid metabolism or transport (*Lypla2* and *Apoe*), ubiquitination (*Ndfip1* and *Otulin1*), extracellular matrix remodeling (*Adamts4*), and APP processing (*Apbb1*), among others.

To gain insight into gene expression differences, we performed Gene Ontology (GO) term enrichment analyses (Cluster profiler software), and we clustered all deregulated GO terms into biological processes (BP) (**Figure 14C**). This analysis revealed a group of strongly downregulated BPs essential for OL functional integrity and survival, with known implications in AD pathology. These included DEGs associated with autophagy (e.g., *Atg4d*, *Atg7*, *Atg14*, and *Atg13*), crucial for cellular homeostasis and protein aggregate clearance; actin cytoskeleton organization (e.g., *Rac1*, *Cdc42 Arf1*, *Flna* and *Limk1*), vital for OL morphology and process extension; and lipid metabolism (e.g., *Apoe*, *Srebf1* and *Srebf2*, *Gpd1*, and *Lpin1*), particularly relevant for myelin synthesis and maintenance. Additionally, several genes associated with endocytosis, phagocytosis, and regulation of small GTPases were also significantly downregulated in 3xTg-AD OLs (**Figure 14D**).

Conversely, top upregulated genes in AD OLs were primarily linked to mitochondrial function and ATP synthesis (multiple *Nduf*s, *Uqcrq*, *Cox20*, and *Surf1*), RNA metabolism and translation (*Rsrp1*, *Hnrnpu*, *App*, *Eri1*; and *Eif4e*), and the ubiquitin proteasome system (UPS) (*Ubb*, *Ndfip1*, *Fbxw7*, *Peli1*, *Psma5* and *Psmb3*) (**Figure 14E, F**). The UPS, in particular, is highly relevant for maintaining cell homeostasis, as it governs protein quality control by targeting misfolded or damaged proteins for degradation, preventing their accumulation within the cell. Therefore, its dysregulation has extensively been studied and described in neurodegenerative diseases like AD (Gong et al., 2016; Oddo, 2008). Moreover, interestingly, substantial genes associated with apoptosis, endoplasmic reticulum (ER) stress, oxidative stress, and DNA damage response were also upregulated, indicating OL dysfunction, and potential cell death.

All these findings shed light on the intricate transcriptional landscape underlying OL dysfunction in the context of early AD.

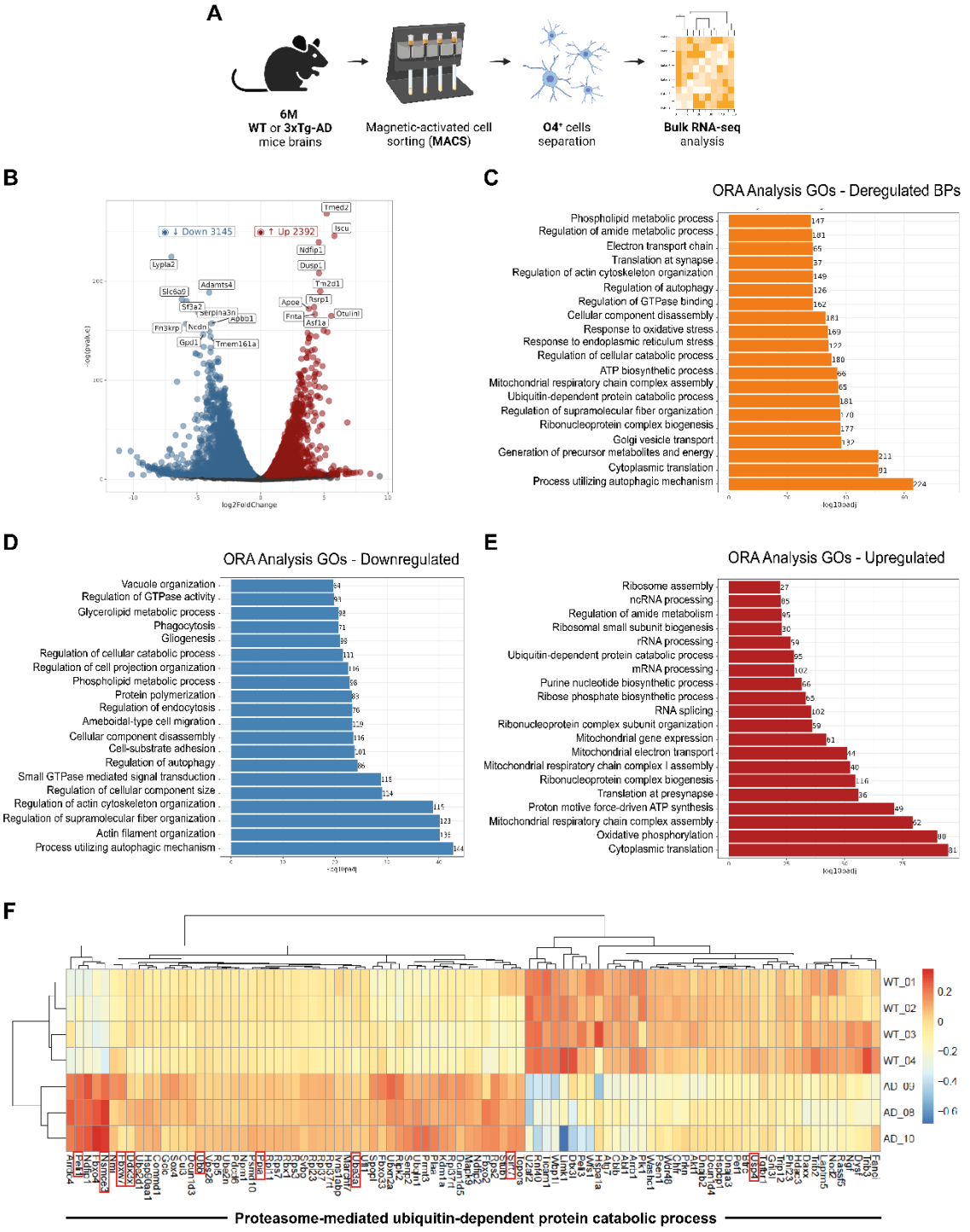

Figure 14. Transcriptomic analysis of MACS-isolated oligodendrocytes from 3xTg-AD mice. (**A**) Brains from 6-month-old WT and 3xTg-AD mice were dissected, and O4^{+} OLs were isolated using MACS for subsequent transcriptional analysis via bulk RNA-sequencing (RNA-seq). (**B**) Volcano plot of transcriptome profiles of WT (n = 4) and 3xTg-AD (n = 3) OLs. Dots represent distribution of significantly upregulated (red) and downregulated (blue) genes in 3xTg-AD OLs. (**C**) Gene Ontology (GO) analysis of the top 20 biological processes (BP) of differentially expressed genes (DEGs), along with the number of genes associated with each GO term. Graph depicting (**D**) downregulated and (**E**) upregulated BPs from the GO analysis. (**F**) Heat map displaying the relative expression levels (high, red; low, blue) of each DEG (column) in each sample (row) within the "Proteasome-mediated ubiquitin-dependent protein catabolic process" GO category. Red boxes highlight some relevant genes.

1.3. Intracerebral Aβo-injection promotes aberrant oligodendrocyte differentiation and maturation

Amyloid β oligomers (Aβo) have been proposed to play a role in promoting OL and myelin dysfunctions in the early stages of neurodegeneration in AD. Indeed, previous studies from our lab and others have demonstrated that amyloidosis is associated with increased oligodendrogenesis, elevated levels of MBP, and thicker myelin in the adult mouse brain (Ferreira et al., 2020; Quintela-López et al., 2019). Motivated with these findings, and with the objective of further investigating the effect of Aβo in the oligodendroglial lineage, we moved on into our next AD mouse model. For that, 3- or 4-months-old WT mice were intracerebrally injected with either Aβo or its vehicle, specifically targeting the DG. Subsequently, one week post-injection, we performed an IHC analysis of oligodendroglial lineage cells in both the CC and the DG of the injected mice (**Figure 15A, B, C**).

Firstly, DAPI labeling confirmed the absence of alterations in the total cell count in both brain regions, thereby excluding potential injection-induced toxicity or damage (**Figure 15D**). Next, through the IHC analysis, no changes were evident in the density of $Olig2^+$ oligodendroglial lineage cells (**Image 15E**), nor in the number of PDGFR-α^+ OPCs (**Figure 15F**) or $CC1^+Olig2^+$ mature OLs (**Figure 15G**) between brains injected with or without Aβo. However, upon closer examination, considering the entire $Olig2^+$ OL lineage and dividing it into the 3 subpopulations -OPCs (PDGFR-α^+), immature OLs (PDGFR-$\alpha^-CC1^-Olig2^+$), and mature OLs ($CC1^+Olig2^+$)-, notable differences emerged. While the percentage of OPCs remained unchanged between groups (CC: mice injected with vehicle 21.85 ± 2.16% vs Aβo-injected mice 22.51 ± 1.31% / DG: vehicle 25.1 ± 3.77% vs Aβo 22.08 ± 1.94%), a significant reduction in immature OLs was observed in Aβo-injected mice (CC: vehicle 34.34 ± 3.38% vs Aβo 16.62 ± 5.94% / DG: vehicle 30.4 ± 4.94% vs Aβo 16.73 ± 3.8%), accompanied by a significant increase in mature OLs (CC: vehicle 42.79 ± 2.79% vs Aβo 60.89 ± 5.58% / DG: vehicle 44.51 ± 3.64% vs Aβo 61.17 ± 2.01%) (**Figure 15H**). These trends were consistent across both brain regions, and the results mirrored those observed in the CC of 3xTg-AD mice. The observed data imply that Aβo promote the maturation of immature into mature OLs.

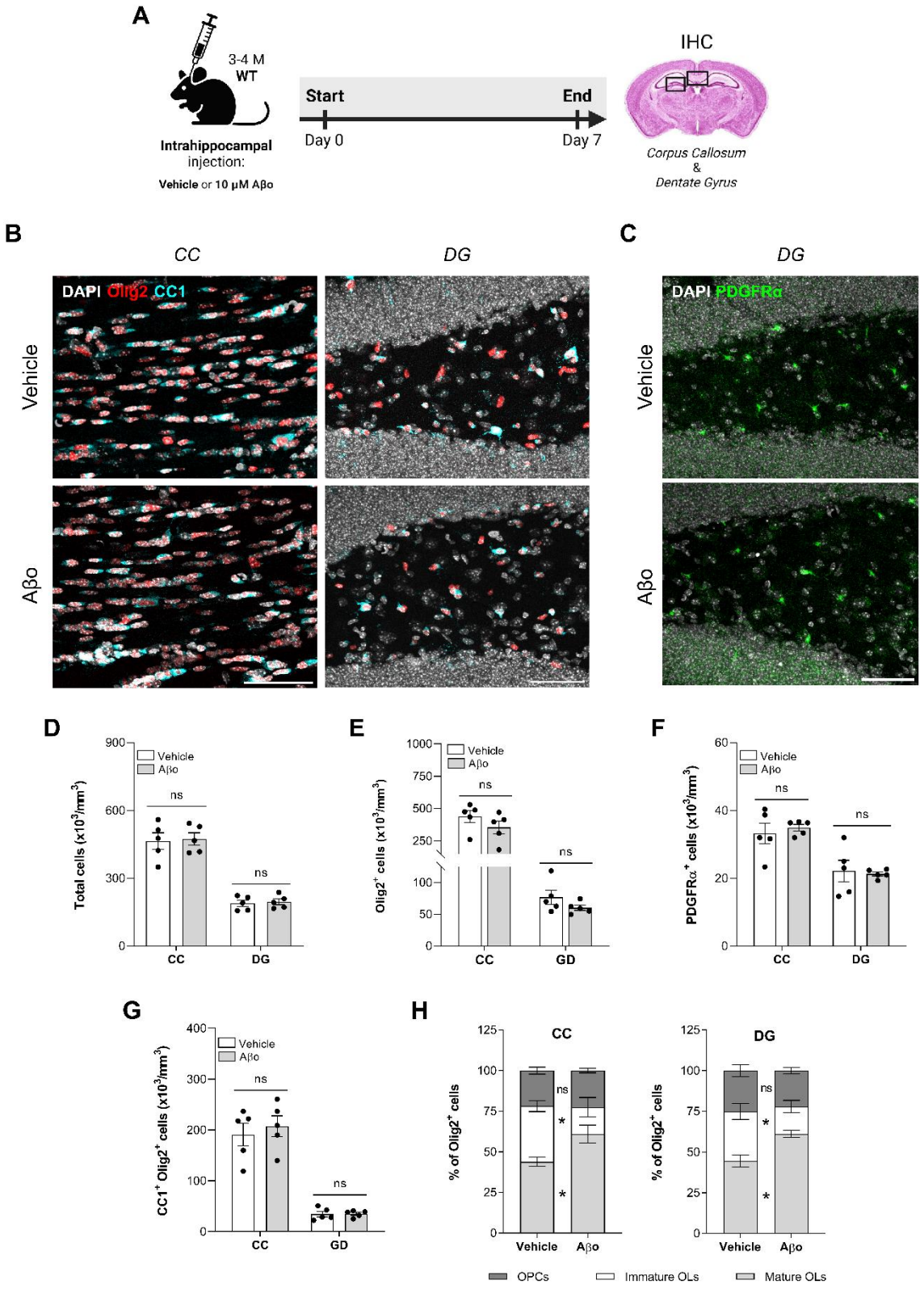

Figure 15. Intrahippocampal injection of Aβo promotes oligodendrocyte maturation, with no effect on total cell numbers. (**A**) Experimental approach scheme: 3- or 4-month-old WT mice received intrahippocampal injections of Aβo (10 µM) or its vehicle, and, one week later, brains were dissected for oligodendroglial linage cell analysis via IHC in the CC and the DG (injection site). Representative fluorescent micrographs depicting immunostainings for (**B**) CC1 (cyan) and Olig2 (red), and (**C**) PDGFR-α

(green). Nuclei were detected with DAPI (white). Scale bars = 50 µm. Histograms showing the numbers of (**D**) total cells (counted using DAPI), (**E**) total Olig2$^+$ oligodendroglial cells, (**F**) PDGFR-α$^+$ OPCs, and (**G**) CC1$^+$Olig2$^+$ mature OLs in vehicle- or Aβo-injected mice. (**G**) Proportions of each oligodendrogial subpopulation within the entire OL linage in each animal group. Data are presented as means ± S.E.M, with dots representing individual animals. *p<0.05; Statistical significance was determined by multiple t-test and two-way ANOVA followed by Sidak's *post-hoc* test.

To gain a broader understanding of the effect of Aβo on the oligodendroglial population, we examined the expression of Nkx2.2. This transcriptional factor is expressed by OPCs that are about to differentiate or committed OLs (**Figure 16A**). Remarkably, in presence of Aβo, the number of Nkx2.2$^+$Olig2$^+$ OLs significantly increased, both in the CC (vehicle 5.87 ± 1.61x10^3 cells/mm^3 vs Aβo 16.28 ± 2.44x10^3 cells/mm^3) and the DG (vehicle 3.6 ± 0.54x10^3 cells/mm^3 vs Aβo 5.8 ± 0.54x10^3 cells/mm^3) (**Figure 16B**), confirming that Aβo induce the differentiation of oligodendroglial cells.

Furthermore, to conclude the investigation of mice with intracerebral injections of Aβo, and given its crucial role in OL differentiation, we also examined the expression of MYRF in the injected mouse brains. As anticipated, we observed that the MYRF$^+$Olig2$^+$/Olig2$^+$ ratio was increased in the CC (vehicle 38.83 ± 2.24% vs Aβo 52.92 ± 1.68%) and DG (vehicle 40.31 ± 3.43% vs Aβo 54.07 ± 1.33%) of Aβo-injected mice compared to vehicle-injected mice (**Figure 16C**). Althoug MYRF is synthesized in the endoplasmic reticulum, it is translocated to the nucleus to perform its transcriptional function; so, here, we also measured the nuclear MYRF intensity (**Figure 16E**). Surprisingly, we found that those MYRF$^+$ OLs exhibited a slight yet significant increase in the mean intensity of nuclear MYRF in the CC in the presence of Aβo (vehicle 63.9 ± 1.94 a.u. vs Aβo 75.8 ± 4.85 a.u.) (**Figure 16D**). These results suggest that MYRF could be a valid candidate to, at least partially, mediate some of the alterations observed in OL populations.

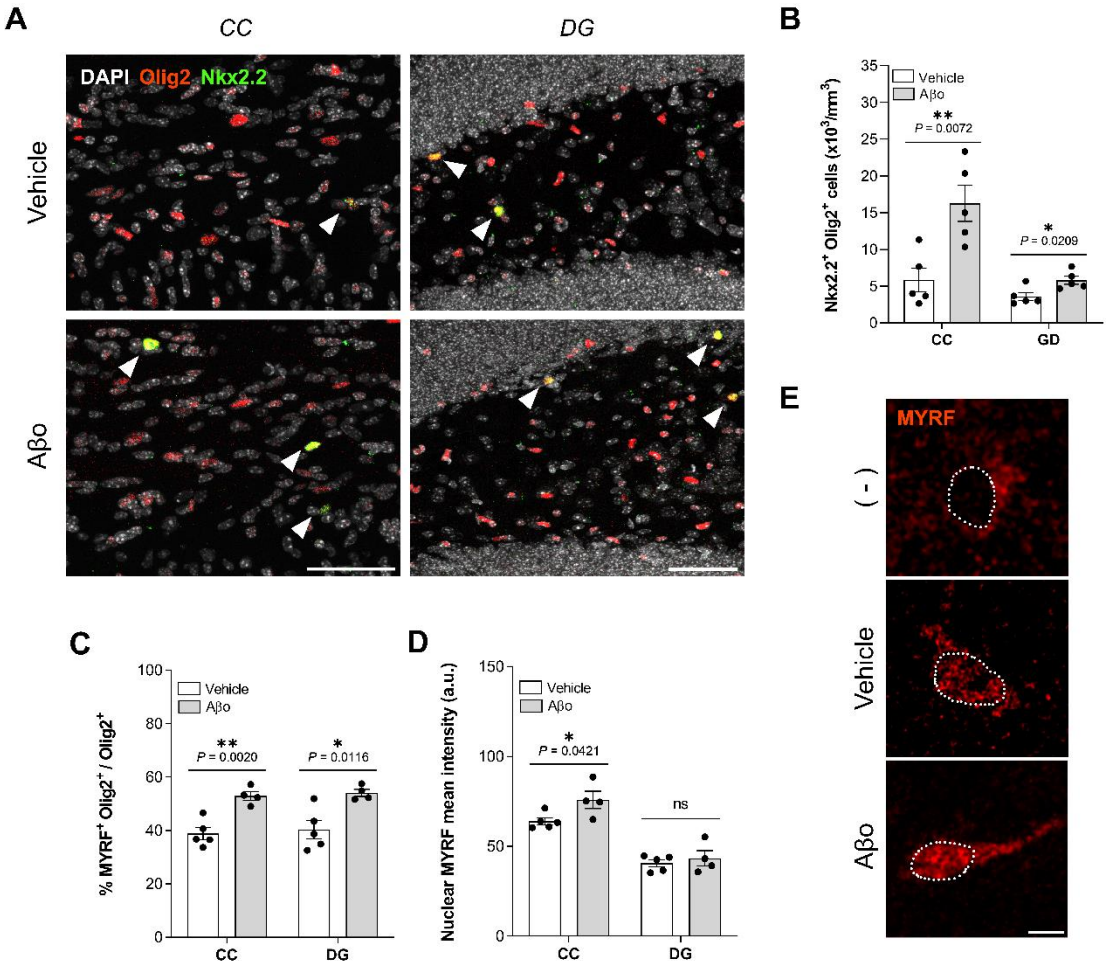

Figure 16. Oligodendrocyte differentiation and MYRF expression are increased in Aβo-injected mice. (**A**) Representative images and (**B**) quantification of the number of differentiating committed OLs (Nkx2.2, green; Olig2, red) in the CC and the DG of vehicle- or Aβo-injected mice. Scale bars = 50 µm. Histograms depicting (**C**) the $MYRF^{+}Olig2^{+}/Olig2^{+}$ ratio (%) and (**D**) the quantification of the mean intensity of nuclear MYRF. (E) Representative cropped micrographs of OLs stained against MYRF (red). The nucleus is outlined by the dotted white line. (-): Nuclear-MYRF-negative OL. Scale bar = 5 µm. Data are presented as means ± S.E.M, with dots representing individual animals. *p<0.05, **p<0.01; Statistical significance was determined by multiple t-test.

Therefore, these findings collectively suggest that Aβo induce alterations in the oligodendroglial population by promoting OL maturation and differentiation, resembling those observed in 3xTg-AD mice. Consequently, we propose that Aβo contribute, at least in part, to the observed OL alterations in AD mice. Furthermore, it is hypothesized that these changes may be mediated by the impact of Aβo on the transcripcional regulation of OLs, particularly targeting MYRF.

<u>PART II.</u> Study of the impact of Aβo on MYRF and its underlying molecular mechanisms

MYRF is known for being a crucial transcriptional factor in regulating terminal OL differentiation and CNS myelination, processes that are disrupted in AD, but yet not fully understood. Previous findings from this study revealed enhanced OL maturation in both 3xTg-AD and Aβo-injected mice, along with increased $MYRF^{+}$ OLs or MYRF levels. These results highlighted the potential role MYRF may play in these AD models. Nevertheless, despite the relevance of MYRF in OLs and myelin, the impact of Aβ on this transcription factor and its implication in AD pathology remain largely unknown. Understanding MYRF's role in AD could provide valuable insight into OL dysfunction and myelin alterations observed in the disease, making it a promising avenue for further investigation.

2.1. Functional characterization of MYRF in oligodendrocytes *in vitro*

Prior to delving into investigating MYRF's involvement in AD, our first objective was to thoroughly characterize and confirm its functions in OLs. Hence, we conducted functional studies using primary cultured cortical rat OLs to further understand MYRF's role in OL differentiation and myelination processes.

2.1.1 MYRF silencing prevents myelin gene expression and morphological maturation in oligodendrocytes

Myrf gene expression knockdown was performed in primary OLs using small interfering RNA (siRNA), and cells were cultured for 3 days in differentiating media. Both western blot (**Figure 17A, B**) and IHC analysis (**Figure 17C**) confirmed that MYRF expression was significantly reduced in cells transfected with *Myrf*-targeted siRNA (*Myrf* siRNA) compared to control cells transfected with scrambled siRNA (control siRNA).

MYRF is a transmembrane protein initially synthesized in the ER, where it undergoes a homo-trimerization process. This full-length MYRF (fl-MYRF) is then auto-processed and cleaved, and its N-terminal fragment (N-MYRF) is translocated into the nucleus to exert its function as a transcriptional factor. (Kim et al., 2017). Consequently, western blot analysis of OLs with reduced MYRF expression enabled the identification of distinct

specific MYRF bands: a smaller band corresponding to the cleaved N-MYRF (~75 kDa) and a larger band representing fl-MYRF (~160 kDa) (**Figure 17A**).

Furthermore, in line with existing literature, RNA interference-mediated knockdown of MYRF resulted in a significant reduction in the expression levels of key CNS myelin proteins: MBP, MAG and MOG were downregulated by 75-80% compared to cells transfected with control siRNA (16.75 ± 6.63%, 26.01 ± 12.6%, and 27.41 ± 3.35%, respectively, relative to 100% in control siRNA-transfected cells) (**Figure 17A, B**). IHC also revealed minimal MBP levels in MYRF knockdown cells at 3 DIV (**Figure 17C**).

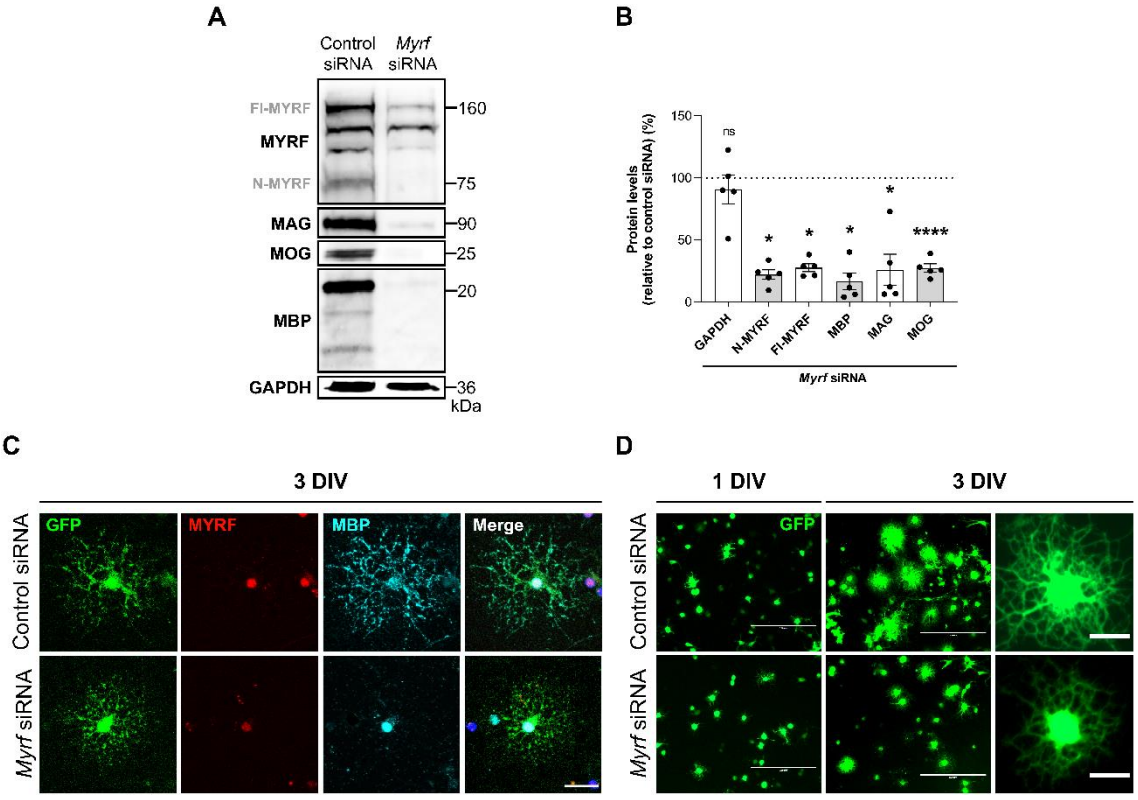

Figure 17. Knockdown of MYRF prevents myelin-related gene expression and morphological maturation in oligodendrocytes *in vitro*. Primary OL cultures were co-transfected with EGFP and either scramble siRNA (control siRNA) or *Myrf*-targeted siRNA, and differentiated for 3 days. (**A**) Western blot analysis of MYRF, MAG, MOG and MBP protein expression in 3 DIV OLs. Full-length MYRF (fl-MYRF) and cleaved N-terminal fragment of MYRF (N-MYRF) were identified. (**B**) Quantification of protein levels in OLs transfected with *Myrf* siRNA, normalized to GAPDH, and presented as a percentage relative to control siRNA levels. (**C**) Representative images of 3 DIV OLs immunostained with GFP (green), MYRF (red) and MBP (cyan). Scale bar = 20 µm (**D**) Representative fluorescent micrographs of GFP^+ cells at 1 and 3 DIV. Scale bars = 200 µm / 10 µm. Data are presented as means ± S.E.M, with dots representing individual experiments. *p<0.05, ****p<0.0001; Statistical significance was determined by two-tailed paired t-test.

During OL lineage progression, OPCs differentiate into premyelinating OLs, which develop a highly branched morphology to, effectively reach and myelinate multiple axons. Therefore, increased arborization is typically associated with the maturation and functional competence of OLs in myelination. Compared to control cells, MYRF knockdown cells displayed less mature morphology with reduced process complexity. Although morphology was similar between cultures at 1 DIV, controls exhibited more extensive and complex arborization than MYRF-silenced OLs by 3 DIV (**Figure 17D**).

These findings conclusively demonstrated that MYRF is not only important but also essential for proper OL maturation and myelin gene induction, corroborating previous literature.

2.1.2. Forced MYRF expression promotes OL morphological maturation and MBP expression in oligodendrocytes

To further characterize this transcription factor, we performed gain-of-function studies using a double-tagged MYRF expression construct, Myc-MYRF-FLAG (**Figure 18A**). Initially, the plasmid was transfected into HEK293T cells and characterized using IHC and western blot. Given that this MYRF expression construct features distinct tags at each terminal of the protein, it enabled the visualization of specific terminals: N-MYRF was detected in the nucleus using an anti-Myc tag antibody, while C-MYRF was identified in the ER employing an anti-FLAG tag antibody (**Figure 18B**).

Consistent with previous findings, western blot analysis revealed distinct fragments of MYRF: a cleaved N-terminal fragment (bound to the Myc tag) of approximately 90 kDa in size, a cleaved C-terminal fragment (FLAG tag) of around 75 kDa, and a notably fainter band representing the full-length protein at approximately 160 kDa (**Figure 18C**). The faintness of the fl-MYRF band suggests its high instability when MYRF is overexpressed in HEK293T cells, undergoing immediate auto-processing and cleavage.

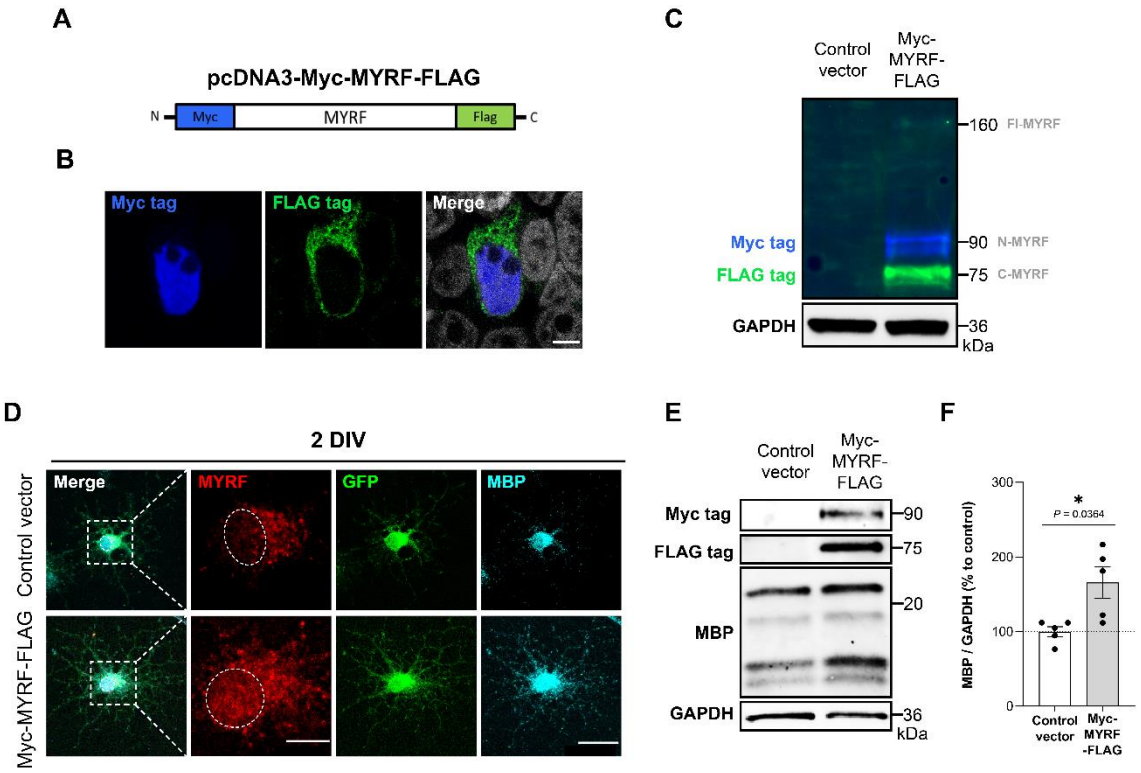

Figure 18. Overexpression of MYRF induces morphological maturation and MBP expression in oligodendrocytes *in vitro*. (**A**) Ilustration depicting the double-tagged MYRF expression vector pcDNA3 Myc-MYRF-FLAG. (**B**) Characterization of MYRF expression vector in HEK293T cells by IHC. N-MYRF was detected using an anti-Myc tag antibody (blue) and C-MYRF by anti-FLAG tag (green). Scale bar = 5 µm (**C**) Representative fluorescent western blot bands for fl-MYRF and its cleavage products N-MYRF (Myc tag, blue) and C-MYRF (FLAG tag, green), in HEK293T cells overexpressing MYRF. (**D**) Immunofluorescent images showing primary OLs cotransfected with EGFP and either a control empty vector or the double-tagged MYRF expression vector at 2 DIV. MYRF (red), GFP (green) and MBP (cyan). A dotted white line outlines the nucleus. Scale bars = 5 µm / 20 µm (**E**) Western blot analysis and (**F**) quantification of MBP protein expression in 2 DIV OLs transfected with control plasmid or the plasmid encoding for MYRF, normalized to GAPDH and presented as a percentage relative to control. Data are presented as means ± S.E.M, with dots representing individual experiments. *p<0.05; Statistical significance was determined by two-tailed paired t-test.

Next, primary OLs were transfected with either the MYRF expression construct or an empty control vector, alongside an EGFP expression plasmid, and were cultured in proliferative SATO- media for 2 DIV. We used SATO- medium to exclude differentiation factors found in SATO+, allowing for a more accurate assessment of MYRF's impact on OL differentiation and the expression of myelin-related genes. IHC analysis confirmed MYRF overexpression, particularly within the nucleus (**Figure 18D**), while western blot validated the presence of the Myc and FLAG tags (**Figure 18E**).

Moreover, as anticipated, both IHC (**Figure 18D**) and western blot analysis (**Figure 18E, F**) demonstrated that MYRF overexpression in cultured OLs led to increased MBP expression levels (165.8 ± 20.79%, relative to 100% in control cells). Furthermore, OLs overexpressing MYRF exhibited a more mature morphology, characterized by more complex arborizations compared to control cells (**Figure XD**).

2.1.3. Prolonged MYRF overexpression reduces cell viability in oligodendrocytes

MYRF is selectively upregulated in differentiating OLs, and its forced expression is known to induce myelin gene expression both *in vitro* (**Figure 18**) and *in vivo* (Emery et al., 2009). However, little is known about the potential consequences of prolonged MYRF overexpression on OLs viability.

To address this question, we conducted cell viability studies using Calcein-AM in primary OLs cultured for 3, 6, and 10 DIV, with and without MYRF overexpression. Intriguingly, our findings suggested that while initial MYRF overexpression appears benign and may even exhibit a tendency to enhance cell viability (121.91 ± 16.73% vs 100% of control at 3 DIV), prolonged overexpression leads to a gradual decline in viability compared to OLs transfected with a control plasmid (84.99 ± 4.29% at 6 DIV and 71.9 ± 7.05% at 10 DIV) (**Figure 19A**). Corresponding fluorescent images of OLs with forced MYRF expression that were subjected to viability assays clearly demonstrate the decrease in Calcein^{+} cells over time (**Figure 19B**).

These results imply a potentially detrimental or toxic effect of sustained aberrant MYRF expression on OLs viability, highlighting the importance of tightly regulating MYRF levels to ensure proper OL function and survival.

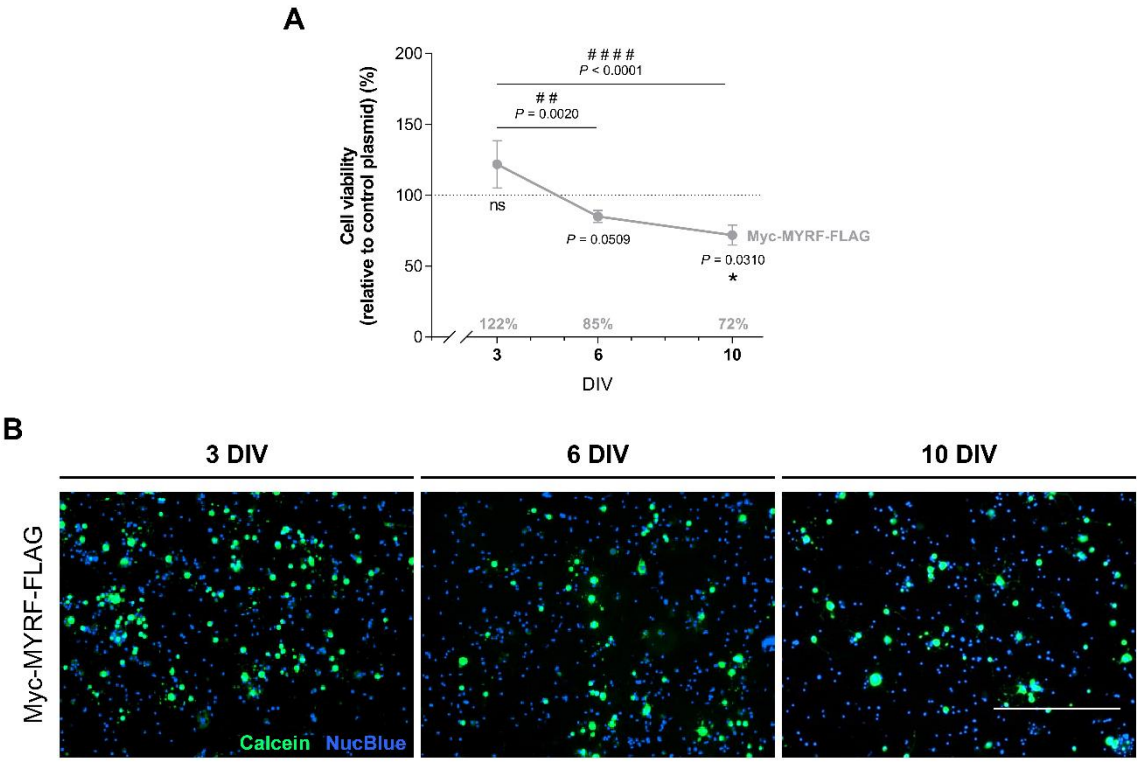

Figure 19. Prolonged MYRF overexpression reduces cell viability in oligodendrocytes *in vitro*. (**A**) Cell viability quantification in OLs overexpressing MYRF for 3, 6 or 10 DIV by Calcein-AM assay. Viability was calculated as the ratio of Calcein (living cells) to NucBlue (total cells), and it is presented as percentages relative to OLs transfected with an empty control plasmid. (**B**) Representative fluorescent images of OLs expressing Myc-MYRF-FLAG at 3, 6 and 10 DIV, showing Calcein (green) and NucBlue (blue) staining. Scale bar = 200 µm. Data indicate means ± S.E.M over time. *p<0.05 between plasmids; # #p<0.01, # # # #p<0.0001 over time. Statistical significance was determined by two-way ANOVA followed by Sidak's *post-hoc* test. $n^{3\ DIV}$ = 9 independent experiments; $n^{6\ DIV}$ and $n^{10\ DIV}$ = 6 independent experiments.

2.2. Study of Aβ-induced effects on MYRF

Next, to investigate the role of MYRF in Alzheimer's disease, we sought to explore the impact of Aβo on this transcriptional factor. Particularly, considering that intracerebral injections of Aβo elevated MYRF levels *in vivo* (**Figure 16C, D, E**), our objective was to determine whether Aβo exerts a similar effect on primary rat OLs *in vitro*.

2.2.1. Aβo increase MYRF and MBP protein levels in oligodendrocytes *in vitro*

With that aim in mind, we again transfected primary cultured OLs with the double-tagged MYRF expression vector Myc-MYRF-FLAG, followed by a 3 h treatment with either Aβo or its vehicle at 3 DIV. On one hand, a double-immunostaining was conducted for Olig2 and Myc tag, and both nuclear and total MYRF levels were quantified (**Figure 20A**). We observed a significant increase not only in the nuclear MYRF expression (54.53 ± 2.72 a.u. vehicle-treated vs 76.18 ± 6.77 a.u. Aβo-treated OLs) (**Figure 20B**), but also in total MYRF protein levels (249.1 ± 25.15 a.u. vehicle vs 403.7 ± 35.29 a.u. Aβo) (**Figure 20C**). Furthermore, western blot analysis revealed that a 3 h treatment with Aβo significantly increased the expression levels of both cleaved N- and C-terminal fragments of MYRF, detected using Myc and FLAG tags, respectively (N-MYRF 174.6 ± 31.87% and C-MYRF 153.6 ± 18.16%, relative to 100% of control) (**Figure 20D, E**). Collectively, these results suggested that Aβo do not selectively target a specific MYRF fragment, but rather increase overall MYRF protein levels.

The subsequent step was to analyze whether the effect of Aβo persisted on endogenous MYRF. To accomplish this, OPCs isolated from mixed glial cultures were differentiated for 3 DIV and treated with vehicle or 1 μM Aβo for 3 or 24 h. Next, MYRF and MBP levels were measured through western blot (**Figure 20F**). The results were consistent with previous findings: Aβo treatment significantly elevated both cleaved N-MYRF (165.4 ± 15.69% at 3 h and 155.8 ± 15.89% at 24 h of Aβo treatment, compared to 100% of control cells) and fl-MYRF protein levels (164 ± 16.48% at 3 h and 158.1 ± 23.5% at 24 h of Aβo vs 100% of control) (**Figure 20G, H**). Moreover, the proportion of cleaved N-MYRF to total MYRF levels was calculated as an indicator of MYRF cleavage ratio, and no differences were observed between conditions (**Figure 20I**). This suggested that Aβo may not modulate the processing of this transcription factor but rather its expression levels.

Interestingly, MBP protein levels were also significantly increased at 24 h of Aβo treatment (123.5 ± 7.42% Aβo vs 100% of control), indicating that Aβo do not only impact MYRF levels but also affect myelin protein expression (**Figure 20J**).

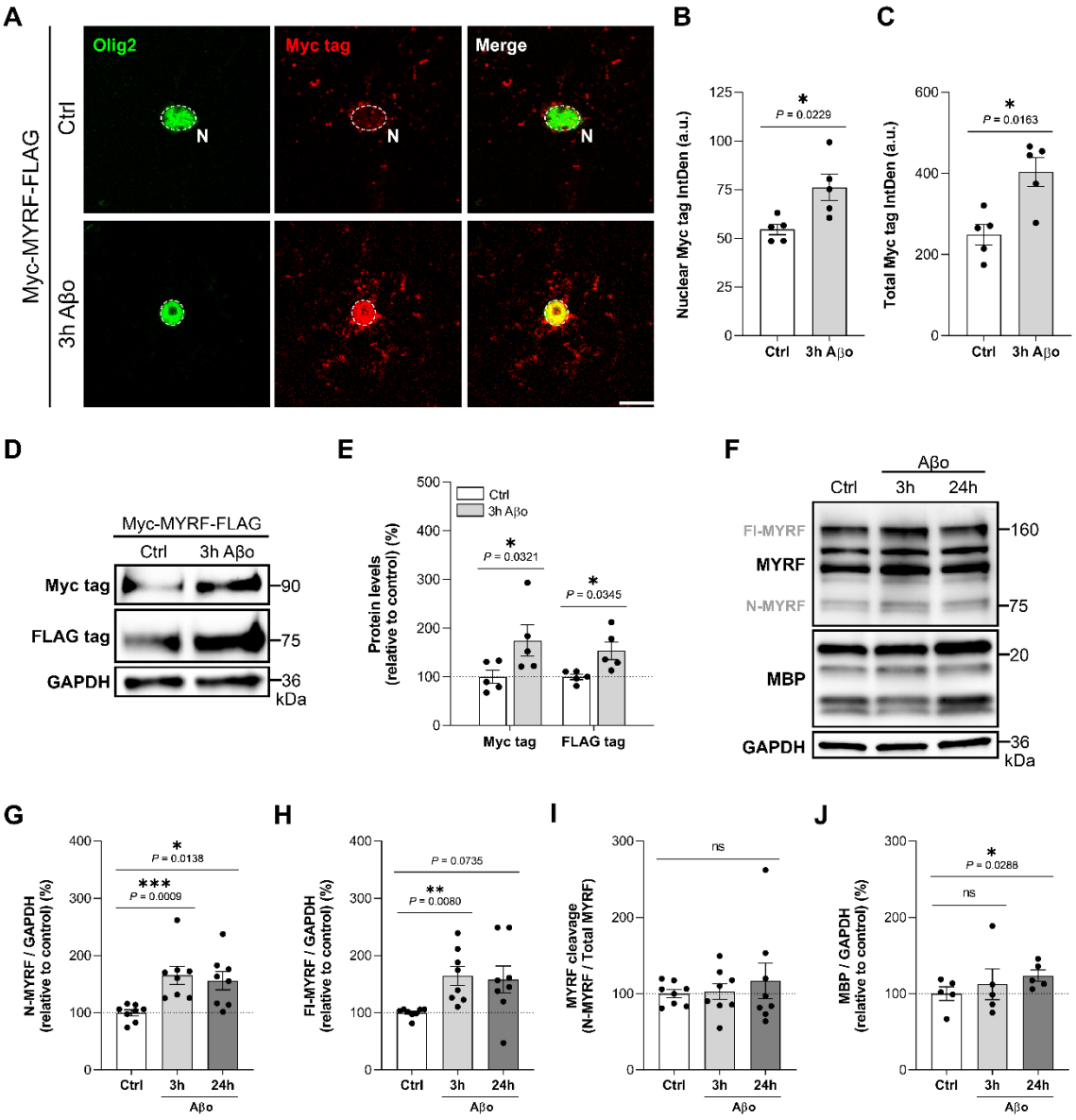

Figure 20. MYRF and MBP protein levels are upregulated by Aβo in oligodendrocytes *in vitro*. (**A**) Primary culture OLs were transfected with Myc-MYRF-Flag and treated with vehicle or Aβo (1 µM) for 3 h at 2 DIV. Representative images of double-immunostaining for the nuclear OL marker Olig2 (green) and the N-terminal MYRF marker MYC tag (red). A white dotted line outlines the nucleus (N). Scale bar = 10 µm. Graphs depicting (**B**) nuclear and (**C**) total MYRF integrated densities detected using the MYC tag antibody. (**D**) Western blot of 2 DIV rat OLs overexpressing MYRF and treated with or without Aβo. (**E**) Histogram presenting cleaved N- and C-MYRF levels detected by MYC and FLAG tag antibodies, respectively. (**F**) Western blot of primary OPCs cultured in differentiating media for 3 DIV, and treated with vehicle or 1 µM Aβo during 3 or 24 h. Quantification of endogenous (**G**) cleaved N-MYRF and (**H**) fl-MYRF levels. (**I**) Graph showing MYRF cleavage ratio, measured as cleaved N-MYRF/total MYRF. (**J**) Quantification of MBP levels. GAPDH was used to normalize protein expressions, and data are shown as percentages relative to vehicle-treated cells. Data are presented as means ± S.E.M, and dots represent independent experiments. *p<0.05, **p<0.01, ***p<0.001; Statistical significance was determined by two-tailed paired t-test and repeated measures one-way ANOVA followed by Dunnett's *post-hoc* test.

2.2.2. Aβo enhance MYRF's transcriptional activity in oligodendrocytes *in vitro*

Since Aβo treatments led to increased levels of MYRF and MBP proteins, we hypothesized that Aβo may induce an overactivation of MYRF's transcriptional activity, which could in turn promote myelin gene expression, and, ultimately, OL maturation.

To investigate this hypothesis, we conducted dual-luciferase reporter assays using primary cultured OLs. Specifically, we used three highly specific and sensitive *Myrf* luciferase reporters, generated by cloning *Myrf* ChIP-seq peaks for *Mbp, Mag* or *Rffl* into pGL3-Promoter, a luciferase reporter containing a SV40 promoter (Bujalka et al., 2013) (**Figure 21A**). These luciferase constructs were co-transfected into primary OLs along with either scrambled or *Myrf*-targeting siRNAs, followed by treatments with vehicle or 3 or 24 h of Aβo. As control reporters, we used pGL3 (a luciferase reporter construct without any promoter) as a negative control, and pGL3-Control (luciferase reporter construct containing the SV40 promoter, but lacking *Myrf*-regulated enhancers) as a reference reporter, with its activity arbitrarily set to 1.

The results revealed that de *Mbp, Mag* and *Rffl* enhancers induced luciferase activity approximately 18-, 3- and 21-fold, respectively, compared to pGL3-Control. These fold-inductions were significantly reduced to approximately 6-, 1.6- and 4-fold, respectively, upon *Myrf* silencing, confirming that the enhancers really were *Myrf*-dependent. Interestingly, while Aβo had no significant effect on luciferase expression from the pGL3-Control reporter, the luciferase activity of *Mbp* (17.74 ± 5.07 fold-induction in vehicle-treated cells, 24.12 ± 6.03 fold-induction at 3 h of Aβo treatment, and 22.58 ± 4.49 fold-induction at 24 h of Aβo), *Mag* (vehicle 3.2 ± 0.49 fold-induction vs 3 h Aβo 4.79 ± 0.78 fold-induction), and *Rffl* (vehicle 20.85 ± 0.71 fold-induction vs 3 h Aβo 26.08 ± 1.48 fold-induction) luciferase reporters was significantly enhanced in the presence of Aβo. This Aβo-induced increase in luciferase activity was prevented when cells were co-transfected with *Myrf*-targeting siRNA (**Figure 21B**).

With all these results together, we concluded that MYRF's transcriptional activity is overactivated in presence of Aβo, and that the Aβo-induced alterations in myelin gene expression are MYRF-dependent.

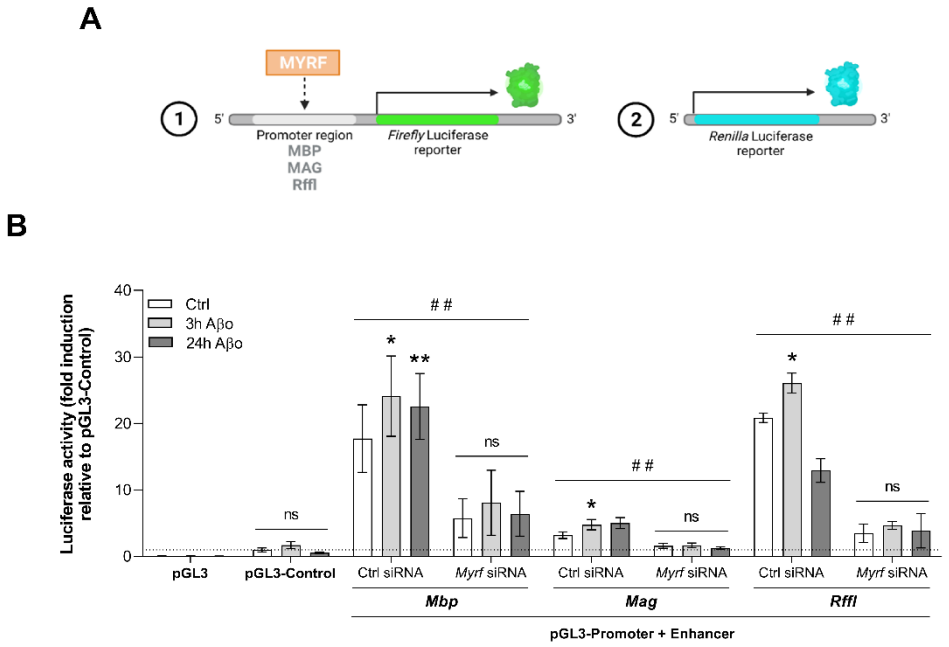

Figure 21. Transcriptional activity of MYRF is upregulated in Aβo-treated oligodendrocytes. (**A**) Schematic representation of dual-luciferase reporter assays using luciferase constructs with regulatory regions from *Mbp, Mag* or *Rffl*. *Renilla* luciferase was used as an internal control. (**B**) Luciferase assays performed in 3 DIV primary cultured OLs co-transfected with luciferase constructs and either scrambled or *Myrf*-targeted siRNAs, and treated with Aβo (1 µM) for 3 or 24 h. Luciferase activity for each condition is presented as fold induction relative to the pGL3-Control plasmid (reporter under the SV40 promoter, lacking a *Myrf*-regulated enhancer). Data indicate means ± S.E.M. *p<0.05; **p<0.01 between treatments; # #p<0.01 between siRNAs. Statistical significance was determined by two-way ANOVA followed by Sidak's and Dunnett's *post-hoc* tests. n = 3 - 6 individual experiments.

2.3. Molecular mechanisms underlying Aβo-induced MYRF upregulation

For the first time, we established that Aβo aberrantly increase MYRF levels both *in vitro* and *in vivo*, potentially disrupting the canonical differentiation and maturation of OLs. Therefore, our next objective was to unravel the molecular mechanisms responsible for these Aβo-induced effects. By doing so, we aimed to gain a deeper insight and ultimately identify potential molecular targets involved in the dysregulation of OL function and maturation in AD.

2.3.1. Aβo do not increase the transcriptional or translational levels of MYRF

To explore the impact of Aβo on MYRF expression at the transcriptional level, we initially conducted RT-qPCR analysis in OLs exposed to various Aβo treatments. Given that MYRF is genetically downstream of SOX10 (Hornig et al., 2013), we analyzed the mRNA expression of both *Myrf* and its inducer *Sox10*. Interestingly, we found no significant changes in *Myrf* or *Sox10* mRNA levels following Aβo treatments (**Figure 22A**), indicating that Aβo do not modify MYRF expression transcriptionally nor by influencing its inducer's transcription.

As an additional approach to assess MYRF at transcriptional levels, we next conducted a luciferase assay using the pGL4-myrfluc_ECR9 construct. This construct integrates ECR9 (a *Myrf* gene enhancer regulated by SOX10) along with the minimal promoter of the *Myrf* gene, both cloned upstream of the luciferase reporter gene within the pGL4 vector (Hornig et al., 2013). Hence, it enables the evaluation of the transcriptional activity of the *Myrf* promoter. Primary OLs were transfected with the luciferase construct, and were treated with or without Aβo at 3 DIV, before the luciferase assay. The results revealed that a 3 h exposure to Aβo do not alter the activity of the *Myrf* promoter, as demonstrated by the absence of significant changes in luciferase activity across treatments (**Figure 22B**). This further suggests that there is no alteration in the SOX10-mediated transcriptional regulation of *Myrf* in the presence of Aβo.

Next, in order to determine whether Aβo alter MYRF at translational levels, we performed a proximity ligation assay (PLA) using puromycin and MYRF antibodies (puro-PLA MYRF). This molecular method is based on the ability of the antibiotic puromycin to incorporate into nascent polypeptide chains, causing premature termination of protein synthesis, and thereby allowing the labeling of actively synthesizing proteins (tom Dieck et al., 2015); in this case MYRF. Thus, this approach also enables the *in situ* visualization of protein synthesis within the cell, with puromycin-labeled peptides serving as markers for translation rate.

To perform this experiment, primary OLs were differentiated for 3 DIV and treated with vehicle or Aβo for 1, 3 or 24 h. Puromycin was added during the last 10 minutes of the assay. Moreover, anisomycin, a translation initiation inhibitor, served as a technical negative control and was added to the cells 15 minutes before puromycin.

Analysis of puro-PLA images revealed minimal PLA$^+$ puncta in cells preincubated with anisomycin (**Figure 22C, D**), confirming that the puncta observed in the absence of this inhibitor were reliable and translation-dependent. Using nuclear DAPI and the cytoskeleton marker phalloidin, which binds to F-actin, we observed that the PLA signal primarily localized to the soma (**Figure 22D**), indicating that MYRF synthesis predominantly occurs in this cellular compartment, consistent with its ER location.

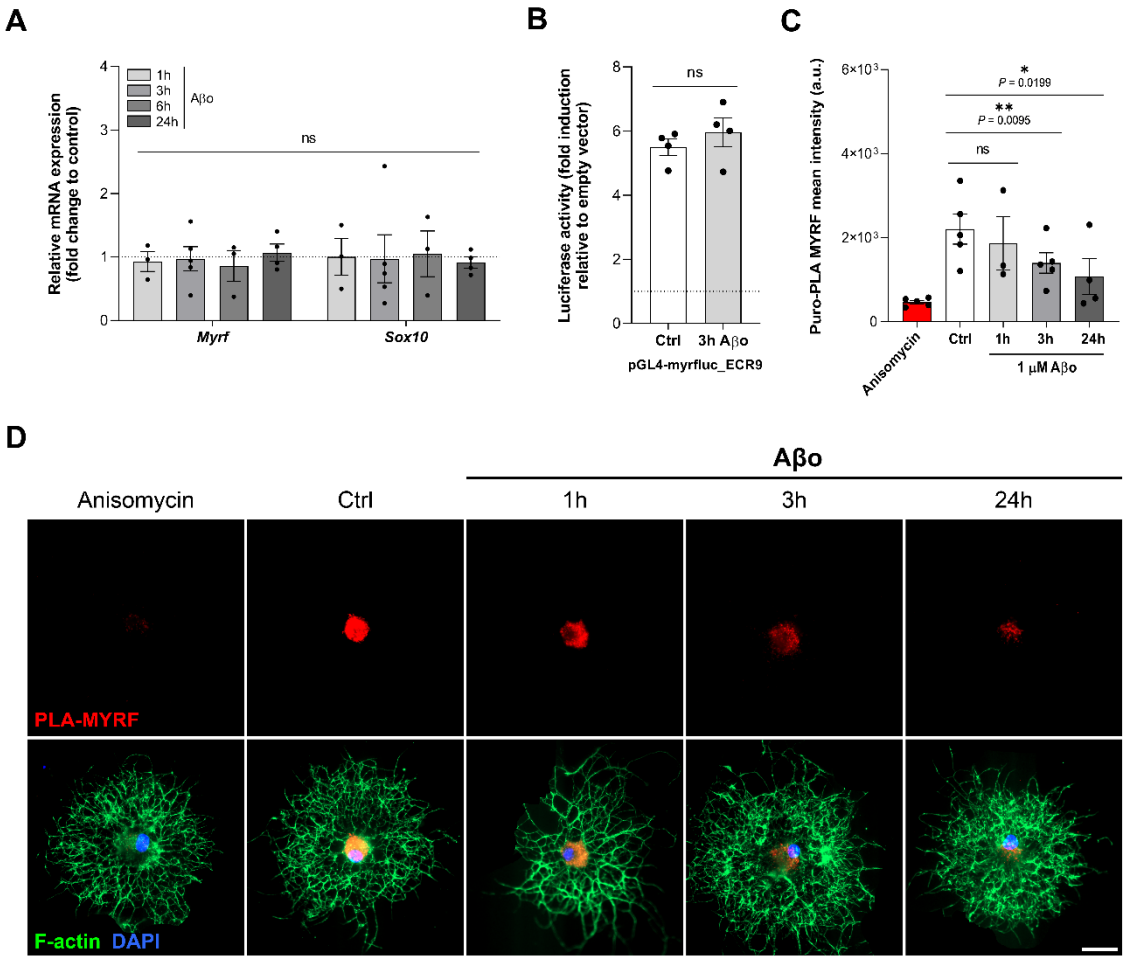

Figure 22. Aβo do not increase MYRF at transcriptional or translational levels. (**A**) RT-qPCR analysis of *Myrf* and *Sox10* mRNA levels in primary cultured OLs at 3 DIV treated with either vehicle or 1, 3, 6, and 24 h of Aβo (1 μM). (**B**) Luciferase assay using myrfluc_ECR9, a luciferase reporter under the control of a minimal promoter for *Myrf*, in 3 DIV OLs treated with or without Aβo. The luciferase activity is presented as fold induction relative to an empty vector. (**C**) Proximity ligation assay for puromycin and MYRF (puro-PLA MYRF) conducted in 3 DIV OLs treated with vehicle or Aβo. (**D**) Representative fluorescent images showing immunostaining for F-actin (green) and the MYRF puro-PLA signal (red). The translation inhibitor anisomycin (40 μM) served as a technical negative control. At least 10 cells were analyzed per condition per experiment. Scale bar = 20 μm. Data indicate means ± S.E.M, and dots represent independent experiments. *p<0.05, **p<0.01. Statistical significance was determined by two-tailed paired t-test and one-way ANOVA followed by Dunnett's *post-hoc* test.

Surprisingly, while no statistically significant changes were observed after 1 h of Aβo treatment (2.21 ± 0.36x10^3 a.u. in control cells vs 1.87 ± 0.63x10^3 a.u. after 1 h of Aβo), the mean intensity of MYRF puro-PLA signal was significantly decreased after 3 h (1.4 ± 0.24x10^3 a.u.) and 24 h of Aβo exposure (1.08 ± 0.43x10^3 a.u.), suggesting decreased newly synthesizing MYRF levels (**Figure 22C, D**). In fact, the longer the Aβo treatment, the lower the MYRF protein synthesis was. This initially unexpected finding led to the hypothesis of a negative feedback loop suppressing MYRF synthesis in response to Aβo-induced aberrantly increased protein levels, consistent with the necessity of tightly regulating MYRF levels.

All these results together suggested that Aβo-triggered MYRF increase likely involve posttranslational mechanisms rather than transcriptional and translational regulation.

2.3.2. Aβo increase N-MYRF stability by interfering with its degradation pathway

The increased protein levels of MYRF with no changes in RNA levels suggested that Aβo may be affecting its degradation process. Notably, dysregulation of proteostasis and protein degradation pathways, has been described in AD. Several studies have reported decreased proteasomal activity in the hippocampus of AD patients, along with altered expression and activity of enzymes involved in ubiquitination and deubiquitination processes (Hegde et al., 2019; Morawe et al., 2012). Consistently, our RNA-seq analysis also identified altered pathways related to protein degradation in OLs from 3xTg-AD mice (**Figure 14F**), suggesting that Aβo could be altering MYRF degradation.

In order to explore this possibility, we performed a cyclohexamide (CHX) chase assay in primary cultured rat OLs (**Figure 23A**). This assay consists on treating cells with various durations of CHX, an antibiotic that inhibits protein synthesis, and observing the stability of the protein of interest during time via western blot. Here, we assessed three different conditions: cells treated with vehicle, Aβo or AR-A014419 (1 μM). GSK3 is described to phosphorylate N-MYRF for initiating its degradation (Nakayama et al., 2018); therefore, AR-A014418, a GSK3 inhibitor, was used as a control to inhibit N-MYRF degradation.

Western blot analysis of MYRF levels revealed that AR-A014418 effectively prolonged the half-life of N-MYRF from 44.12 ± 10.55 minutes to 110.1 ± 13.08 minutes, confirming that GSK3 is a key player in N-MYRF degradation process in OLs.

Remarkably, treatment with Aβo also increased the stability of N-MYRF, as evidenced by a significant prolongation of its half-life to 71 ± 9.8 minutes (**Figure 23B, C**).

These findings revealed that Aβo interfere with N-MYRF protein degradation, potentially resulting in prolonged nuclear retention and enhanced transcriptional activity.

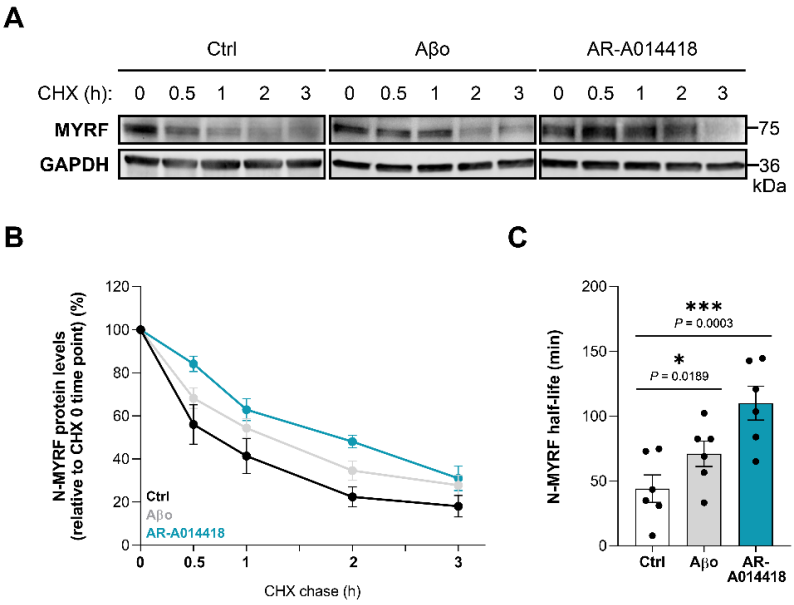

Figures 23. Aβo slow down N-MYRF degradation. Cycloheximide chase analysis of N-MYRF in primary cultured OLs treated with vehicle, Aβo (1 µM) or AR-A014418 (1 µM), a GSK3 inhibitor used as a positive control. (**A**) Cells incubated with cyclohexamide (CHX) (100 µg / ml) for the indicated times were subjected to immunoblot analysis with antibodies against MYRF and GAPDH (to normalize protein levels). Graphs showing (**B**) the percentage of N-MYRF remaining after the various CHX chase times and (**C**) the half-life of N-MYRF in each condition. Data are represented as means ± S.E.M, and dots represent independent experiments. *p<0.05, ***p<0.001. Statistical significance was determined by one-way ANOVA followed by Tukey's *post-hoc* test.

However, the knowledge on MYRF degradation pathways remains limited. Existing studies conducted in mHepa mouse hepatocellular carcinoma cells, suggest a process wherein GSK3 phosphorylates N-MYRF at serine residues, facilitating its recognition by the E3 ligase Fbxw7 for ubiquitination and subsequent degradation via the proteasome (Nakayama et al., 2018). Nevertheless, no studies have explored this process in OLs or within the context of neurodegenerative disorders. Thus, our next aim was to thoroughly investigate this degradation mechanism to determine the specific stage at which Aβo may exert its influence.

2.3.2.1. Aβo reduce GSK3-mediated phosphorylation of N-MYRF by activating its upstream inhibitor PKC

The first step described in the MYRF degradation pathway involves a GSK3-mediated phosphorylation. Therefore, we conducted a phosphoserine (pSer) immunoprecipitation (IP) assay in HEK293T cells overexpressing MYRF and treated with Aβo at different times. All proteins phosphorylated at serine were immunoprecipitated, followed by the detection of phosphorylated MYRF (p-MYRF) via western blot using an anti-MYRF antibody. Once again, AR-A014418 was used as a positive control for GSK3 inhibition (**Figure 24A**).

As expected, pharmacological inhibition of GSK3 resulted in a significant decrease in p-MYRF levels (47.51 ± 7.09% in AR-A014418-treated cell, in contrast to 100% of control cells). Moreover, results indicated that the longer the Aβo treatment time, the lower the phosphorylation levels of N-MYRF were (15 min of Aβo 85.46 ± 24.79%, 30 min 60.13 ± 16% and 1 h 26.3 ± 8.67%, in contrast to 100% in control cells) (**Figure 24A, B**), which suggests a potential reduction in GSK3 activity induced by Aβo.

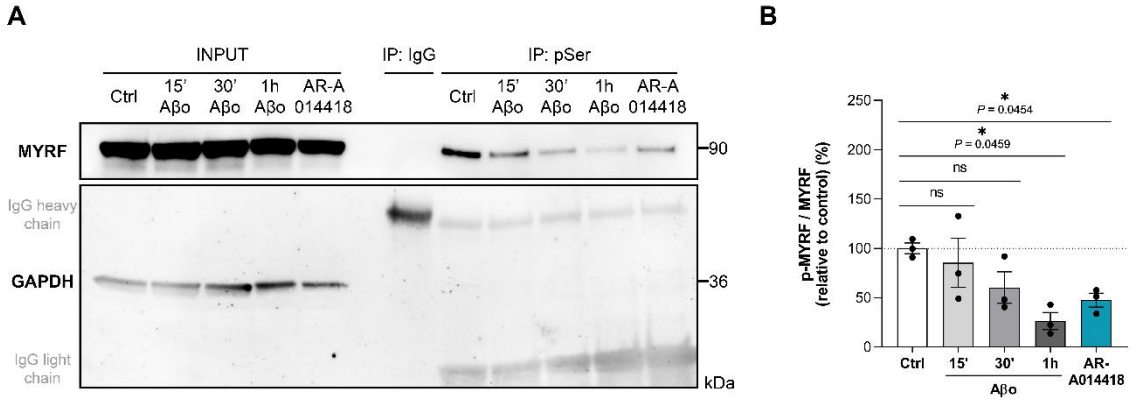

Figures 24. Reduction of N-MYRF phosphorylation levels in response to Aβo treatment. A phosphoserine (pSer) immunoprecipitation (IP) assay was conducted in MYRF-overexpressing HEK293T cells subjected to treatments with either vehicle or 15 minutes, 30 minutes or 1 h of Aβo (1 µM). The GSK3 inhibitor AR-A014418 (1 µM) was used as a positive control. (**A**) Corresponding western blot analysis for MYRF and GAPDH (technical control for the IP). (**B**) Quantification of p-MYRF levels, expressed as a percentage relative to control cells. Data are presented as means ± S.E.M, and dots represent independent experiments. *p<0.05; Statistical significance was determined by one-way ANOVA followed by Dunnett's *post-hoc* test.

The activity of GSK3 has been extensively investigated *in vitro* (Doble & Woodgett, 2003; Jope & Johnson, 2004). Although it is regulated by various mechanisms, GSK3 activity is primarily controlled by its phosphorylation state: activation requires phosphorylation at tyrosine residue in the activation loop (Hughes et al., 1993; Lochhead et al., 2006), while inactivation occurs through phosphorylation at the N-terminal serine residues Ser21/9 (Beurel et al., 2015). Therefore, to confirm whether GSK3 was indeed more inhibited in OLs in the presence of Aβo, we analyzed its phosphorylation state via western blotting (**Figure 25A**). While no significant changes were observed at the activating tyrosine residue (data not shown), results revealed increased phosphorylation levels of the inhibitory Ser21/9 residues of GSK3 in Aβo-treated OLs (after 3 h of Aβo treatment 113.6 ± 3.34% and after 24 h 110.9 ± 2.43%, compared to 100% in control cells) (**Figure 25C**). Moreover, particularly the phosphorylation of the residue Ser9, corresponding to the GSK3β isoform, was increased following 3 h of Aβo treatment (120.4 ± 3.58%, compared to 100% in control cells) (**Figure 25D**). These results suggested that Aβo inhibit GSK3 activity in OLs, mainly affecting GSK3β.

Another method of indirectly assessing GSK3 activity is to examine the expression levels of its substrates, such as β-catenin. Similar to MYRF, GSK3 phosphorylates β-catenin targeting it for proteasome degradation. Consequently, increased GSK3 activity results in diminished β-catenin levels, while low GSK3 activity leads to reduced β-catenin phosphorylation, facilitating its accumulation (Huang et al., 2017; McCubrey et al., 2014). Western blot analysis of β-catenin levels was performed in 3 DIV primary OLs treated with or without Aβo (**Figure 25B**). Interestingly, treatment with Aβo for 3 h significantly increased β-catenin levels (130.1 ± 8.77% compared to 100% in control) (**Figure 25E**), consistent with prior findings indicating GSK3β inhibition.

Furthermore, we also explored the subcellular localization of GSK3. Although traditionally has been considered primarily a cytosolic protein, GSK3 is also found within the mitochondria, nucleus, and other subcellular compartments. Thus, its activity is influenced not only by its phosphorylation state but also by the physical proximity or availability of its substrates (Beurel et al., 2015). Given that GSK3 is implicated in phosphorylating N-MYRF for its degradation, its translocation into the nucleus is necessary for interaction with MYRF. Consequently, we quantified the localization of GSK3 in presence of Aβo using IHC (**Figure 25F**). Results indicated a predominance of GSK3 in the nucleus under control conditions, whereas a notable shift toward cytosolic

localization was observed in Aβo-treated OLs (1.07 ± 0.04 a.u. in vehicle-treated cells compared to 0.81 ± 0.02 a.u. in Aβo-treated) (**Figure 25G**). This suggested a reduced availability of GSK3 for phosphorylating nuclear N-MYRF.

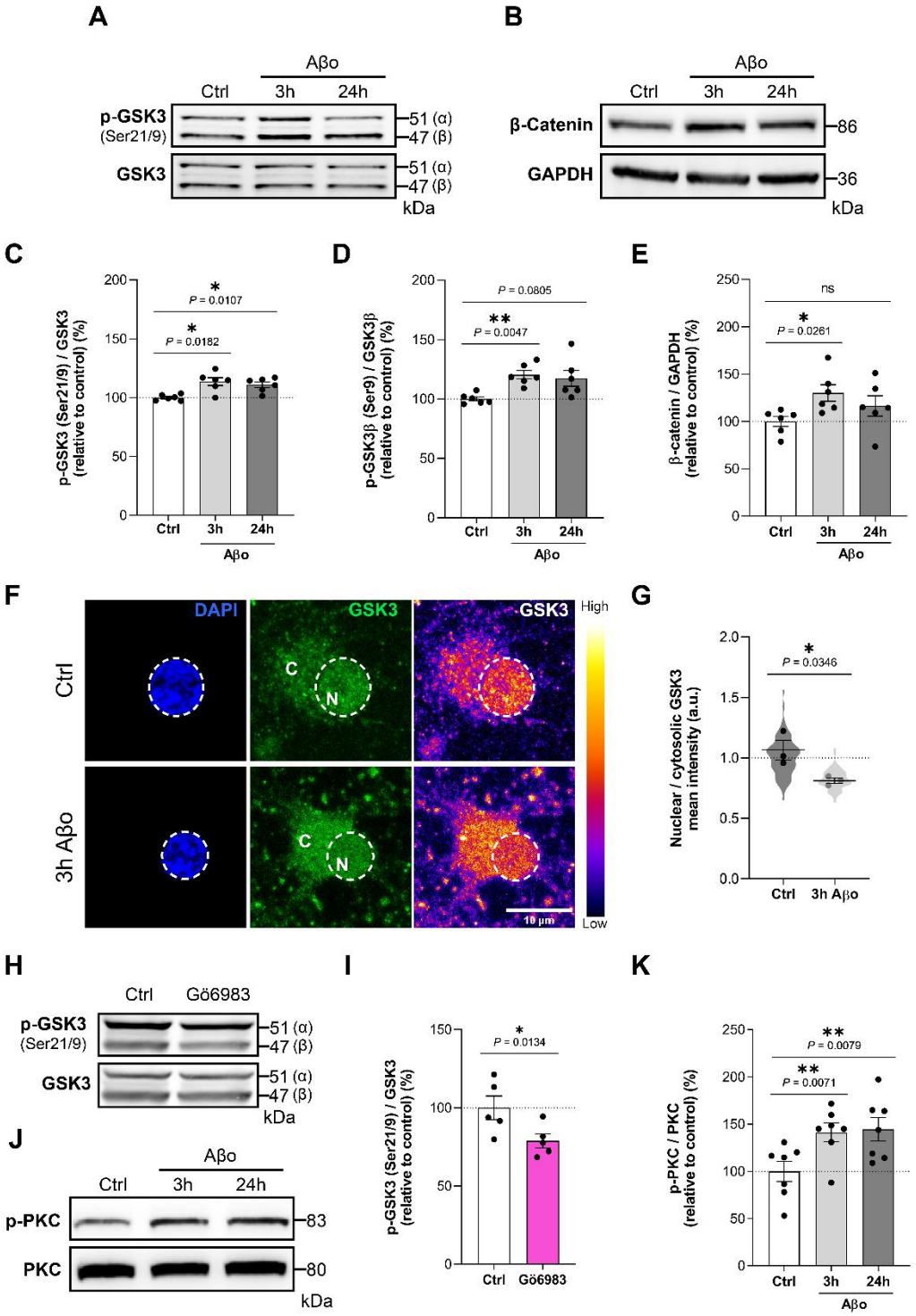

Figure 25. Aβo inhibit GSK3 by activating its upstream inhibitor PKC. Primary cultured OLs were differentiated for 3 DIV and subjected to treatments with vehicle or 3 or 24 h of Aβo. (**A**) Western blot analysis and (**C**) quantification of the phosphorylation state of inhibitory serine residues of GSK3

(Ser21-GSK3α and (**D**) Ser9-GSK3β). (**B**, **E**) Measurements of β-catenin protein levels via western blot. (**F**) Representative fluorescent micrographs of OLs immunostained against GSK3 (green and fire). A white dotted line outlines the nucleus (N), and C represents the cytosol. The color scale bar represents expression intensities for the fire LUT of GSK3. Scale bar = 10 µm. (**G**) Graph illustrating the ratio between nuclear and cytosolic GSK3 levels in control or Aβo-treated cells. (**H**) Western blot analysis and (**I**) quantification of GSK3 activity in OLs treated with the PKC pan-inhibitor Gö6983 (100 nM), measured by inhibitory serine phosphorylation levels of GSK3. (**J**, **K**) Western blot analysis of PKC phosphorylation levels in control and Aβo-treated OLs. All histograms represent protein expression levels as percentages relative to control cells. Data are presented as means ± S.E.M; dots represent individual experiments and violin plot represents quantification of individual cells. *p<0.05, **p<0.01; Statistical significance was determined by one-way ANOVA followed by Dunnett's *post-hoc* test and two-tailed nested or paired t-test.

To conclude with the study about the effect of Aβo on GSK3, we aimed to investigate upstream regulatory factors. The aforementioned inhibitory phosphorylation of GSK3 at Ser21/9 is mediated by a complex interplay of various kinases and phosphatases, including the kinase PKC (**Figure 25H, I**) (Beurel et al., 2015). Considering previous studies indicating increased PKC activity in response to Aβ in both astrocytes (Abramov & Duchen, 2005; Wyssenbach et al., 2016) and neurons (Manterola et al., 2013; Ortiz-Sanz et al., 2022), we next sought to determine if a similar phenomenon occurs in OLs. Thus, the phosphorylation status of PKC in primary OLs treated with Aβo for 3 or 24 h was assessed via western blot analysis (**Figure 25J**). The results revealed significantly higher phosphorylation levels following Aβo treatments (141.3 ± 10.09% after 3 h of Aβo treatment and 144.5 ± 12.38% after 24 h of Aβo treatment compared to 100% in control cells), indicative of increased PKC activation in the presence of Aβo (**Figure 25K**).

All these consistent findings suggest that the hyperactive state of PKC induced by Aβo may lead to GSK3 inhibition, thereby reducing MYRF phosphorylation and promoting its stability in the nucleus.

2.3.2.2. Aβo promote Fbxw7-dependent non-proteolytic ubiquitination of N-MYRF

Following with the investigation about the effects of Aβo on MYRF degradation mechanisms, our next objective was to check the ubiquitination status of MYRF in the presence of Aβo. Notably, ubiquitination emerged as one of the most dysregulated pathways, particularly upregulated, in the RNA-seq study conducted in OLs from 6-month-old 3xTg-AD mice (**Figure 14F**).

To study the role of Aβo in MYRF ubiquitination, HEK293T cells were transfected with GFP-tagged MYRF, FLAG-tagged ubiquitin (Ub), and various E3 ligases, including Fbxw7 –known to detect the phosphorylation state of MYRF for subsequent degradation (Nakayama et al., 2018)–, and Parkin as a negative control. Subsequently, cells were treated with or without Aβo for 3 h, followed by a GFP-pulldown assay to isolate MYRF. Myrf-linked Ub levels were then detected via western blot using an anti-FLAG antibody (**Figure 26A**).

First of all, the results confirmed the essential role of Fbxw7 in MYRF ubiquitination and degradation: the ubiquitination levels in elution samples were significantly lower or almost undetectable when Fbxw7 was absent (mock 0.27 ± 0.12 a.u.; Fbxw7 1.42 ± 0.09 a.u.; Parkin 0.48 ± 0.23 a.u.), and total lysate samples (input) demonstrated clear MYRF (GFP) degradation in Fbxw7-expressing cells (**Figure 26B, C**). Surprisingly, cells transfected with Fbxw7 also exhibited a significant increase of approximately 54% in MYRF ubiquitination levels in the presence of Aβo compared to vehicle-treated cells (1.42 ± 0.09 a.u. vs 2.19 ± 0.15 a.u., respectively) (**Figure 26B, C**). Nevertheless, this heightened ubiquitination appeared to be non-proteolytic or ineffective, as MYRF levels detected in the Fbxw7-transfected cells elution samples showed no reduction in the presence of Aβo; on the contrary, MYRF levels were slightly yet significantly increased (116 ± 4.32% compared to 100% of control) (**Figure 2D**). Importantly, this Aβo-induced ubiquitination increase was not observed in input samples, suggesting a MYRF-specific phenomenon.

The elongation of Ub chains can occur at any of its seven lysines, which results in different polyubiquitin chains in length, composition and cellular function. According to the literature, chains formed exclusively through the addition of Ub at lysine 48 (K48) serve as signals for the well-established proteasome protein degradation (Glickman & Ciechanover, 2002; Ihara et al., 2012). In contrast, K63-linked Ub chains are implicated in diverse regulatory functions beyond protein degradation, which may vary depending on the cellular context and specific proteins involved (Tramutola et al., 2018). In light of this, our next aim was to investigate whether the presence of Aβo alters the type of ubiquitination utilized to label MYRF.

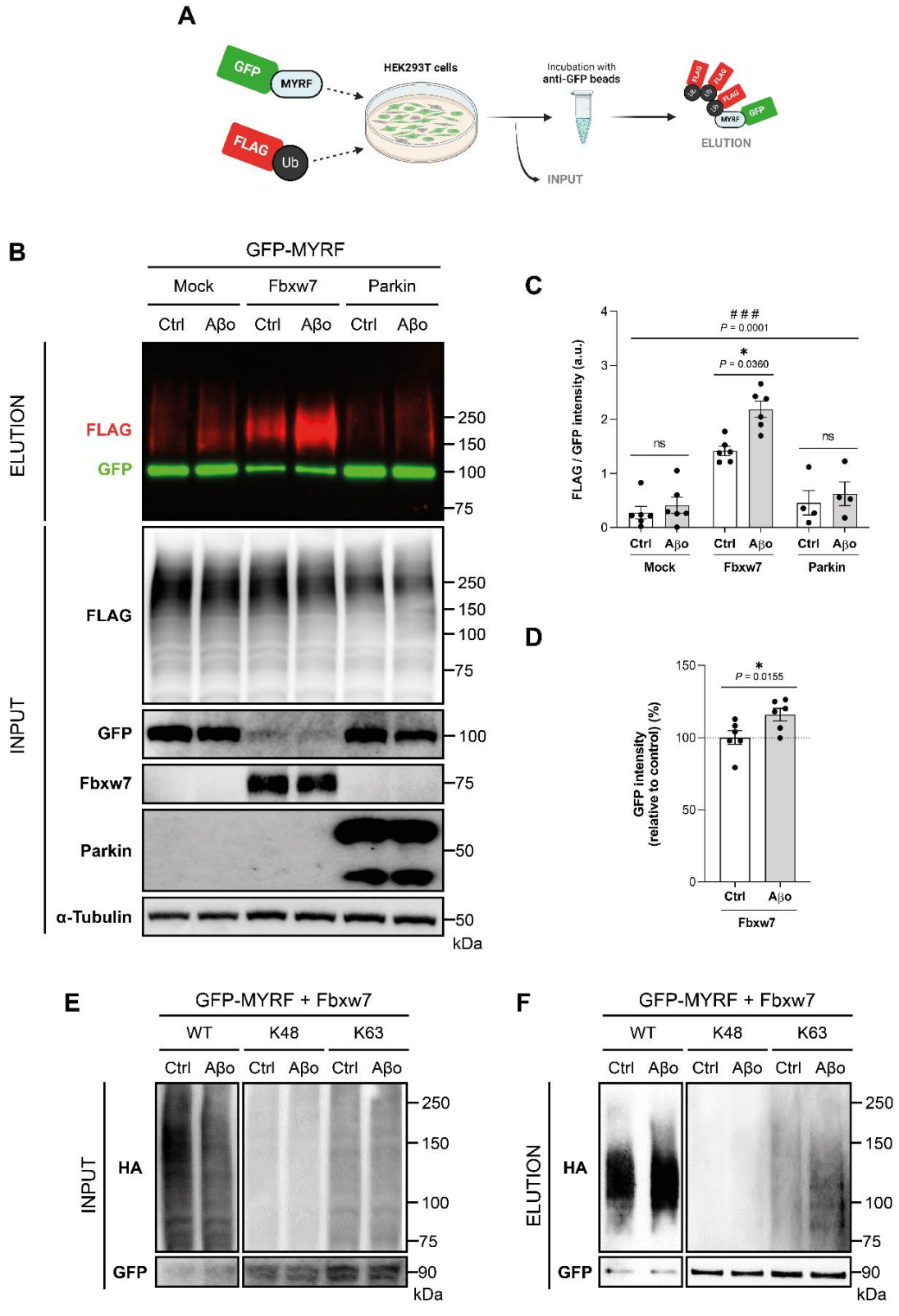

Figures 26. Aβo increase non-proteolytic ubiquitin levels of MYRF in an Fbxw7-dependent manner in HEK293T cells. (**A**) Schematic representation of the experimental procedure for the GFP-pulldown in HEK293T cells. (**B**) GFP-tagged MYRF isolation via GFP-pulldown and subsequent detection of MYRF-linked ubiquitin (FLAG) levels through western blot analysis. Cells were transfected with no E3 ligase (ø), Fbxw7, or Parkin, and treated with or without Aβo for 3 h. MYRF-ubiquitin is depicted in red and the unmodified GFP-MYRF in green. Total cell lysates (input) samples showing

ubiquitin (FLAG), MYRF (GFP), Fbxw7, Parkin, and Tubulin expression by western blotting. (**C**) Quantification of MYRF ubiquitination by normalizing FLAG intensities to GFP levels. (**D**) MYRF protein levels in the elution fraction of Fbxw7-expressing cells treated with or without Aβo, detected by GFP intensities. Protein expression levels are presented as percentages relative to control cells. (**E**, **F**) Analysis of Fbxw7-dependent ubiquitination in the presence or absence of Aβo, using three distinct ubiquitin-HA species (WT, K48 and K63), conducted by western blotting after GFP-pulldown isolation (preliminary data; n = 1). Data are presented as means ± S.E.M, and dots represent independent experiments. *p<0.05 between treatments; # # #p<0.001 between E3 ligases. Statistical significance was determined by two-way ANOVA followed by Sidak's *post-hoc* test and two-tailed paired t-test.

To address this question, we employed the same GFP-pulldown method described earlier; however, in this instance, HEK293T cells were transfected with GFP-MYRF and Fbxw7-myc plasmids, along with three different exogenous HA-tagged ubiquitins: WT Ub, a mutant Ub allowing ubiquitination only at lysine 48 (K48; degradative), and a mutant Ub allowing ubiquitination only at lysine 63 (K63; non-degradative). Subsequently, cells were treated with Aβo or vehicle, and ubiquitination levels were detected by western blot using an anti-HA antibody (**Figure 26E, F**).

The results obtained from the GFP-pulldown assay, although preliminary, again corroborated that Aβo promote aberrant MYRF ubiquitination, as evidenced by increased levels of MYRF-linked Ub in the case of WT Ub. On the other hand, regarding mutant Ub species, while the contribution of K48 to MYRF ubiquitination remained consistent across treatments, a higher level of MYRF ubiquitination was observed with K63 in the presence of Aβo compared to vehicle-treated cells (**Figure 26E, F**). This finding suggests that Aβo alter the type of ubiquitination used to label MYRF, leading to non-conventional ubiquitination that stabilizes MYRF rather than promoting its degradation.

Having verified that MYRF ubiquitination is Fbxw7-dependent, we next aimed to examine the expression of Fbxw7 in primary cultured OLs treated with or without Aβo. No significant changes were observed in either the nuclear expression of Fbxw7 protein, as measured by immunofluorescence (**Figure 27A, B**), or in the mRNA levels determined via RT-qPCR (**Figure 27C**), following treatments of 3 or 24 h with Aβo. Conversely, a longer Aβo exposure time of 72 h induced a significant increase in *Fbxw7* mRNA expression levels compared to vehicle-treated cells (3.34 ± 1.06 fold change relative to control cells) (**Figure 27C**). This result aligned with the upregulated *Fbxw7* levels found in the RNA-seq analysis of OLs isolated from 3xTg-AD mice (**Figure14F**).

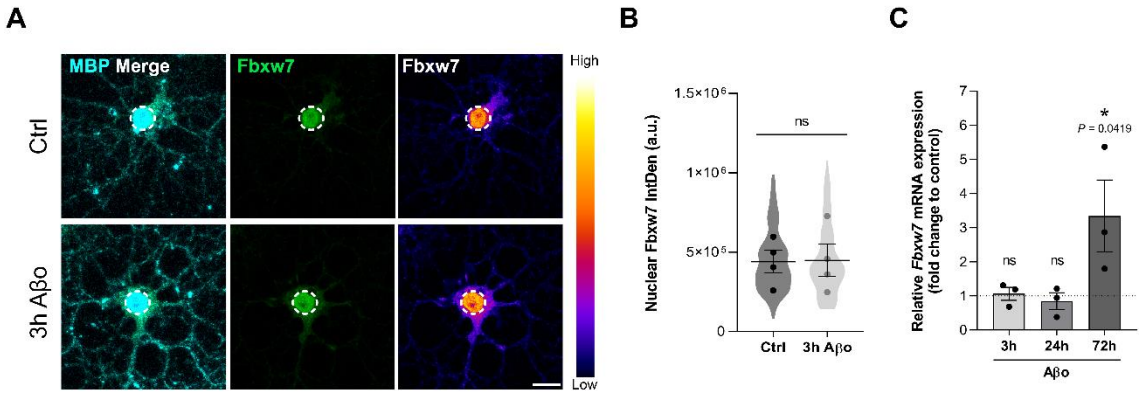

Figures 27. Long exposure times of Aβo increase *Fbxw7* mRNA levels in OLs *in vitro*. (**A**) Representative fluorescent micrographs of 3 DIV primary cultured OLs immunostained against MBP (cyan) and Fbxw7 (green and fire). The white dotted line outlines the nucleus, and the color scale bar represents expression intensities for the fire LUT of Fbxw7. Scale bar = 10 µm. (**B**) Graph illustrating the integrated density of nuclear Fbxw7 levels in control or 3 h Aβo-treated cells. (**C**) RT-qPCR analysis of *Fbxw7* mRNA expression in OLs treated with Aβo for 3, 24, and 72 h, presented as fold change compared to vehicle-treated cells. Data are presented as means ± S.E.M; dots represent individual experiments, and violin plot represents quantification of individual cells. *p<0.05; Statistical significance was determined by two-tailed paired t-test and one-way ANOVA followed by Dunnett's *post-hoc* test.

2.3.2.3. Aβo do not impact proteasome activity

Lastly, to conclude the study of the effect of Aβo on MYRF degradation, we assessed the final step in the degradation pathway: proteasome activity. While Aβo have been reported to induce proteasome dysfunction in various cell types, including neurons and astrocytes (Lopez Salon et al., 2003; Oh et al., 2005), research specifically investigating proteasome activity in OLs with Aβo treatment is limited. Here, we measured the chymotrypsin-like activity of the proteasome using luminescent Proteasome-Glo cell-based assays in both our *in vitro* models, the HEK293T cell line and 3 DIV primary cultured OLs. The well-established proteasome inhibitor MG132 was used as a control, and it effectively reduced the chymotrypsin-like activity in both cell types. Surprisingly, results conclusively demonstrated that, at least under these experimental conditions, Aβo treatments did not induce alterations in proteasome activity in either cell model (**Figure 28A, B**).

In summary, we described that the mechanisms governing MYRF degradation are dysregulated in the presence of Aβo. Particularly, this dysregulation appears to primarily occur in the initial steps of the MYRF degradation pathway, including the PKC/GSK3β signaling pathway or the Fbxw7-mediated ubiquitination, while proteasome activity does not seem to be affected by Aβo treatment.

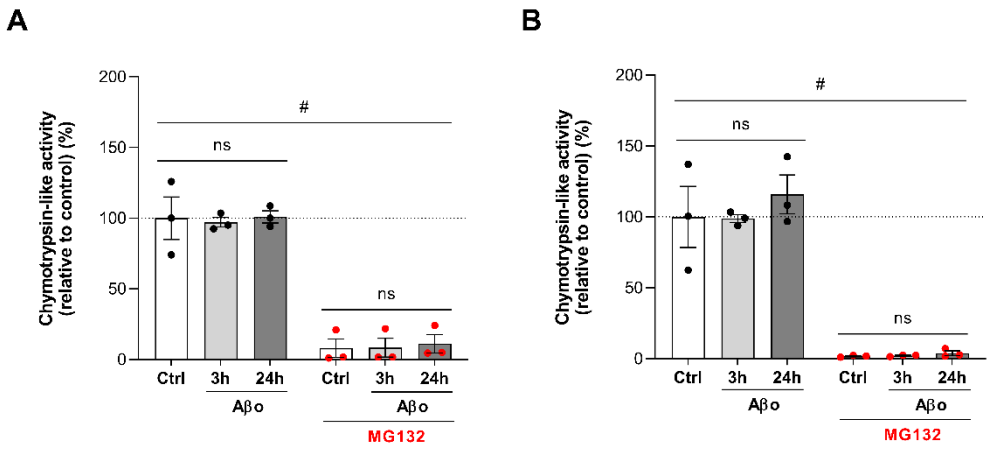

Figures 28. Aβo do not alter proteasome activity. Luminescent Proteasome-Glo cell-based assays conducted in (**A**) HEK293T cells and (**B**) primary cultured OLs treated with vehicle or 3 or 24 h of Aβo to assess chymotrypsin-like proteasome activity. The proteasome inhibitor MG132 (1 µM; 1 h) was used as a control. Data are presented as means ± S.E.M, and dots represent individual experiments. #p<0.05; Statistical significance was determined using two-way ANOVA followed by Sidak's *post-hoc* test.

<u>PART III.</u> Pharmacological modulation of Aβ-mediated effects through PKC inhibition

We have described that Aβo modulate the PKC/GSK3β signaling pathway, leading to a decrease in N-MYRF phosphorylation and consequent inhibition of its degradation. We propose that this process promotes abnormal OL maturation and myelination, and can result in brain-region specific OL death. Subsequently, our next aim was to explore the potential effectiveness of pharmacological modulation of PKC/GSK3β signaling pathway as a strategy to mitigate the effects induced by Aβo on MYRF, OLs and myelin in Alzheimer's disease models.

3.1. *In vitro* pharmacological study of GSK3 and PKC inhibitions for modulating N-MYRF levels in oligodendrocytes

Prior to moving on to *in vivo* studies, we examined GSK3 and PKC inhibitions *in vitro*. Specifically, we sought to elucidate whether the already mentioned GSK3 inhibitor AR-A014418 and the pan-PKC inhibitor Gö6983 could modulate the Aβo-induced aberrant N-MYRF increase in OLs.

With that aim, we treated primary OLs with or without Aβo, 30 min after the treatments with AR-A014418 and/or Gö6983. Cells were incubated with the respective drugs and Aβo for 24 h, and N-MYRF levels were analyzed by western blot. The results demonstrated that GSK3 inhibition did not have any significant effect over Aβo-induced alterations in N-MYRF levels. Conversely, PKC inhibition alone by the pan-PKC inhibitor Gö6983 significantly and fully prevented the Aβo-induced N-MYRF increase, as it was able to maintain control N-MYRF levels (100% of control vs Aβo 17 ± 12.58% vs Aβo + Gö6983 99.4 ± 14.73%). Surprisingly, the combination of both GSK3 and PKC inhibitors significantly reduced N-MYRF expression, albeit resulting N-MYRF levels were considerably lower compared to control levels (21.95 ± 9.83% vs 100% of control) (**Figure 29A, B**).

A Calcein-AM-based viability assay was conducted to confirm that the reductions in N-MYRF levels observed after treatments were not attributable to drug-induced cellular toxicity, and results showed no evidence of cell death (**Figure 29C**).

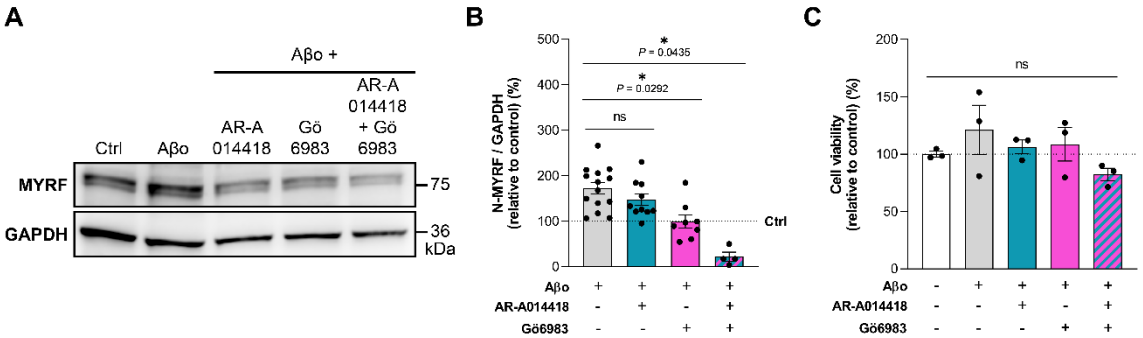

Figure 29. PKC inhibition prevents Aβo-induced aberrant MYRF levels in oligodendrocytes. Cells were treated with AR-A014418 (1 µM), Gö6983 (100 nM) or the combination of both, 30 min prior to Aβo (1 µM) exposure. Treatments were sustained for 24 h, and cells were analyzed at 3 DIV. (**A**) Western blot of N-MYRF expression and (**B**) its quantification, normalized to GAPDH. (**C**) Quantification of cell viability assessed using a Calcein-AM assay. Results are presented as the percentage of Calcein-AM / NucBlue intensities relative to control vehicle-treated cells. Data are represented as means ± S.E.M, and dots represent independent experiments. *p<0.05; Statistical significance was determined by one-way ANOVA followed by Dunnett's *post-hoc* test.

Altogether, we concluded that the use of the pan-PKC inhibitor Gö6983 could be a promising pharmacological strategy to modulate the effects of Aβo. We propose that inhibiting PKC, which is activated in presence of Aβo, we would re-establish MYRF degradation homeostasis, leading to the restoration of physiological OL populations and myelination. (**Figure 30**).

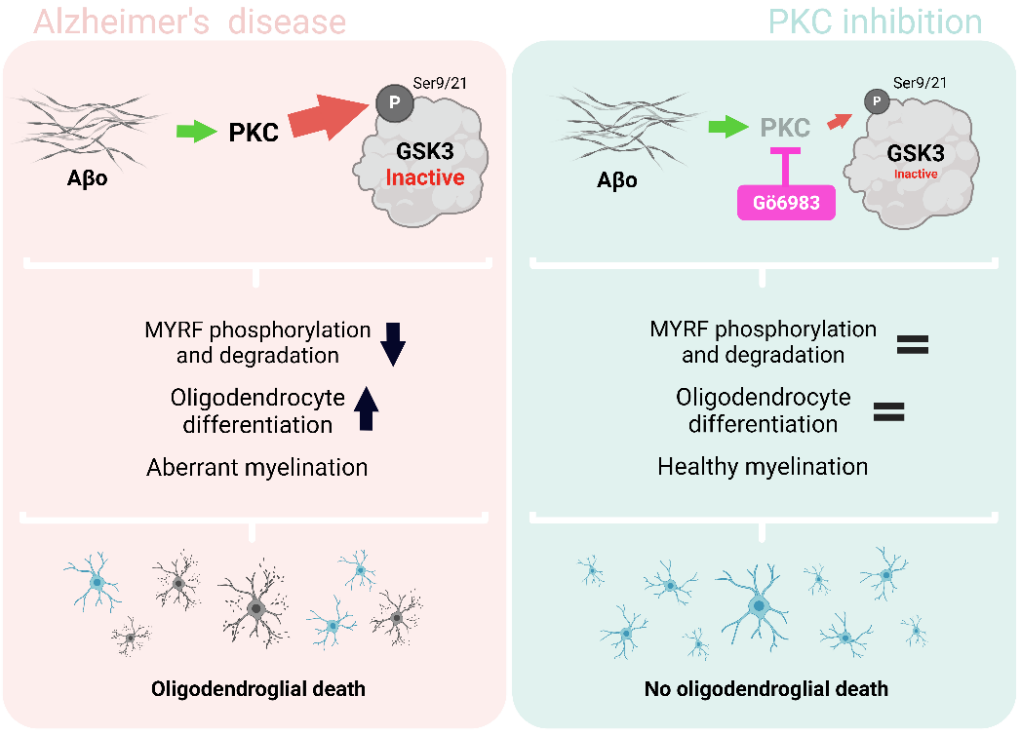

Figure 30. PKC inhibition as a novel pharmacological strategy to revert Aβo-induced alterations in MYRF, oligodendrocytes and myelin.

3.2. Study of Aβo-triggered effects and their pharmacological modulation by PKC inhibition, in zebrafish model

Emerging evidence suggests that alterations in oligodendrogenesis and disruptions in myelin integrity are key early events in AD pathology (Ferreira et al., 2020; Y. Wu et al., 2017). Given our identification of a pathway linking Aβo and MYRF, crucial transcriptional factor for promoting OL differentiation and myelin gene expression (Emery et al., 2009), we hypothesized that Aβo may significantly impact on these processes. Consequently, our next aim was to investigate the potential effects of Aβo on OL differentiation and myelination *in vivo*, and to assess the feasibility of PKC inhibition as a strategy for modulating those effects.

A simple yet ideal *in vivo* model for addressing these inquiries is the zebrafish model: with its rapid postnatal development and transparent larvae, it is an optimal platform to track OLs and myelination *in vivo* upon Aβ exposure. Furthermore, it has increasingly become a valuable tool for conducting pharmacological studies (Cassar et al., 2020). With this is mind, the following experimental approach was devised: to inject 10 μM Aβo or its vehicle into the brain ventricle of wild-type zebrafish larvae at 24 hours post-fertilization (hpf) (**Figure 31A**), and to explore the impact of Aβo on OLs and myelin in the developing spinal cord.

Initially, the efficiency of the intracerebroventricular (ICV) injections was tested by injecting fluorescein-labelled dextran into 24 hpf zebrafish larvae. We could clearly see a widespread distribution of the injection mixture throughout the brain and spinal cord of the larvae (**Figure 31B**). Next, proper Aβ oligomerization was confirmed using in-gel Coomassie blue staining (**Figure 31C**). Both ICV injection and the injection mixtures of Aβo or its vehicle were considered adequate to proceed with the proposed experimental procedures.

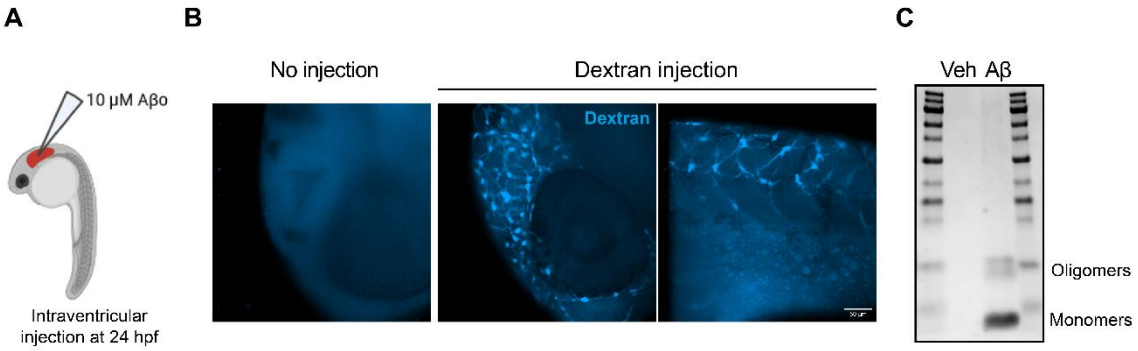

Figure 31. Aβo injection into the hindbrain ventricles of 24 hpf zebrafish larvae. (**A**) Schematic representation of the experimental approach. (**B**) Representative images of fluorescein-labelled dextran diffusion into the brain and spinal cord of 24 hpf zebrafish larvae following ICV injection. Scale bar = 50 μm (**C**) Detection of Aβ species (monomers and oligomers) in the injection mixtures of Aβ and its vehicle using Coomassie blue staining.

3.2.1. Aβo induce early oligodendrocyte differentiation and myelination in zebrafish

Next, to identify potential Aβ-induced alterations in OL differentiation and myelination, we conducted fluorescent RNA *in situ* hybridization assays (RNAscope FISH) following Aβo or vehicle ICV injections. The expression of three key genes associated with

different developmental stages of the OL lineage was assessed: *sox10*, a canonical marker of OL lineage*; myrf,* expressed in differentiating OLs (Hornig et al., 2013); and *mbpa* (*mbp*), a zebrafish orthologue of murine and human *MBP*, expressed in myelinating OLs (**Figure 32A**).

The expression of *sox10* decreased during the initial days of larvae development, particularly in Aβo-treated zebrafish ($1.18 \pm 0.1x10^5$ a.u. in vehicle-treated larvae at 5 dpf vs $0.9 \pm 0.07x10^5$ a.u. in Aβo-treated larvae) (**Figure 32B**). On the other hand, interestingly, *myrf* expression was significantly increased by ~25% at 48 hpf in the presence of Aβo ($1.54 \pm 0.19x10^5$ a.u. vehicle-treated vs $1.92 \pm 0.16x10^5$ a.u. Aβo-treated larvae). However, while *myrf* mRNA showed an expected increasing expression throughout development in control larvae, *myrf* expression levels were maintained quite constant during time in the Aβo-injected larvale, which by 5 dpf resulted in a ~21% reduced expression when compared to vehicle-injected larvae ($2.33 \pm 0.27x10^5$ a.u. vehicle vs $1.84 \pm 0.15x10^5$ a.u. Aβo) (**Figure 32C**). Regarding *mbp,* consistent with increased *myrf* levels at 48 hpf, there was a notable increase of ~147% in *mbp* expression at that same time-point in presence of Aβo ($2.33 \pm 0.33x10^4$ a.u. vehicle vs $5.77 \pm 1.08x10^4$ a.u. Aβo). However, this early boost of the myelin-related mRNA was normalized by 72 hpf, and remained at control levels throughout development (**Figure 32D**).

In zebrafish spinal cord development, not only mRNA levels but also spatial distribution is important for OL differentiation. The majority of OPCs originate from progenitor cells in the pMN domain located in the ventral spinal cord. Subsequently, they migrate towards the dorsal zone, where they undergo proliferation and differentiation into OLs (Lee et al., 2010). Therefore, we quantified where the mRNA was located, and we observed a significant shift towards the dorsal area in *mbp* in Aβo-injected larvae both at 72 hpf (only $7.2 \pm 1.82\%$ of the total area occupied by *mbp* was dorsal in vehicle-injected larvae, compared to $15.9 \pm 2.45\%$ in Aβo-injected larvae) and 5 dpf (vehicle $9.95 \pm 1.68\%$ vs Aβo $15.77 \pm 1.56\%$) (**Figure 32E**).

Overall, these results suggested that Aβo might induce a precocious OL differentiation and myelination, by altering differentiation- and myelination-related mRNA expression and regional distribution during larval development.

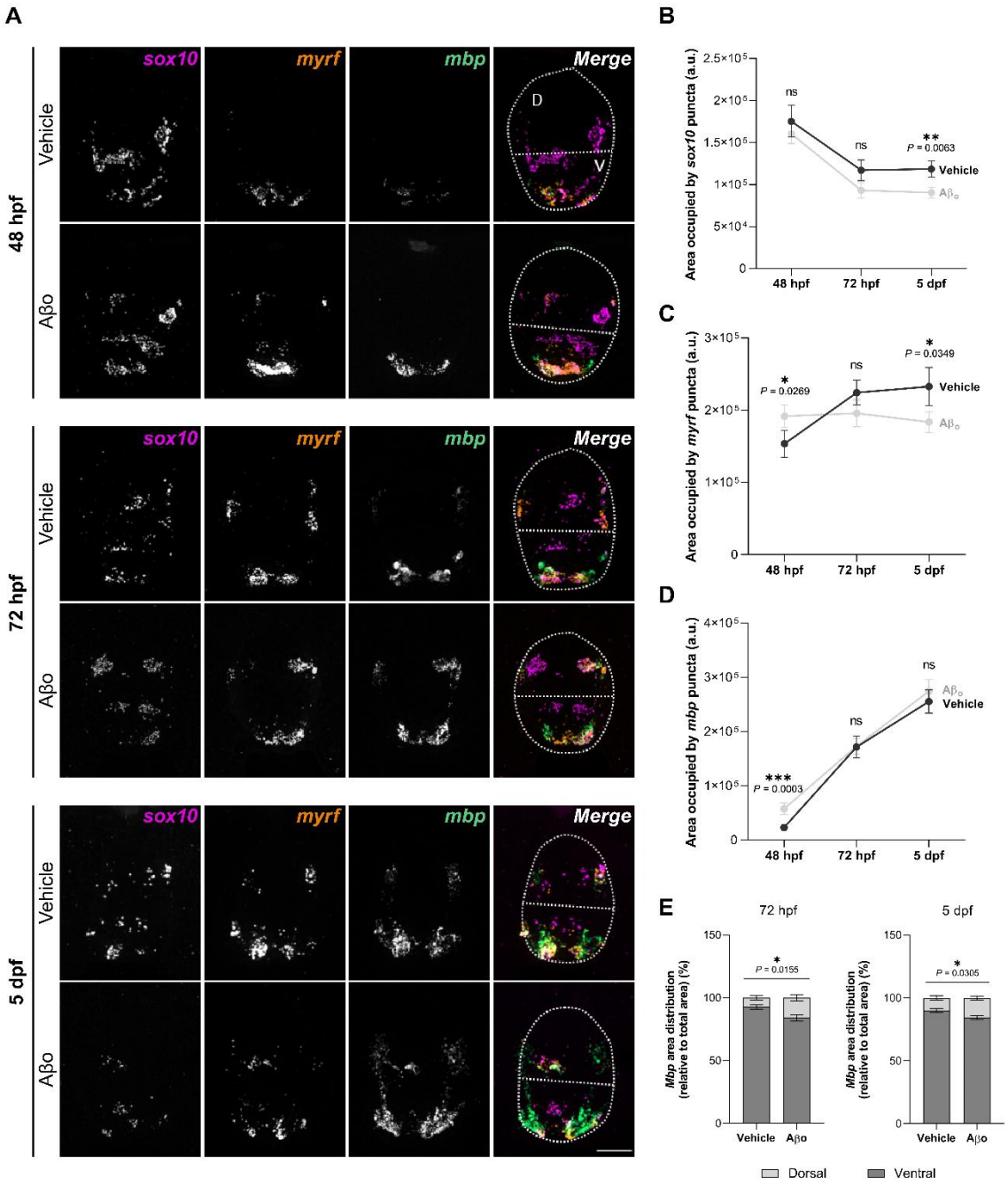

Figure 32. Aβo-injected zebrafish larvae exhibit alterations in oligodendroglial lineage mRNA levels and regional distribution in the developing spinal cord. Zebrafish larvae were injected with Aβo or its vehicle at 24 hpf, and RNAscope FISH assays were performed for *sox10*, *myrf* and *mbp* at 48 hpf, 72 hpf and 5 dpf. (**A**) Representative confocal images of spinal cord cross-sections depicting mRNA expression fluorescence. Scale bar = 20 µm (**B**, **C**, **D**) RNAscope analysis representing the area occupied by each mRNA in the developing spinal cord. (**E**) Quantification of *mbp* mRNA distribution in ventral and dorsal regions. Data are represented as means ± S.E.M, *p<0.05, **p<0.01, ***p<0.001 compared to vehicle-injected zebrafish larvae. Statistical significance was determined by two-tailed nested t-test and two-way ANOVA followed by Sidak's *post-hoc* test. n = 9 - 11 larvae per condition and time-point.

3.2.2. PKC inhibition rescues the Aβo-induced deregulation of timing of oligodendrocyte differentiation and maturation

After confirming that Aβo induce intriguing alterations in OLs in our zebrafish model, we proceeded to our next objective: to investigate the potential of PKC inhibition as a pharmacological modulation of Aβo-induced effects *in vivo*. To this end, and to explore Aβo-triggered alterations in OL differentiation more in depth, we conducted *in vivo* studies using stable transgenic zebrafish lines. Specifically, we crossed *Tg(olig2:EGFP)*^{vu12}, a reporter of pMN lineage cells, with *Tg(myrf:mScarlet)*^{co66}, a reporter of differentiating OLs. In addition to administering Aβo or vehicle into the brain ventricles of these larvae at 24 hpf, some were also treated with the pan-PKC inhibitor Gö6983 at 48 hpf (**Figure 33A**). As the combination of Aβo and the drug did not show any significant toxicity for the larvae (**Figure 33B**), we proceeded with the analysis of differentiating OLs (**Figure 33C**).

At 72 hpf, no significant differences were observed in the total number of *olig2*$^{+}$ (**Figure 33D**) or *myrf*$^{+}$ cells (**Figure 33E**) across treatments. Nevertheless, when focusing on the dorsal spinal cord, while *olig2*$^{+}$ cell counts remained consistent across all treatment groups (**Figure 33F**), we detected a notable increase in dorsal *myrf*$^{+}$ cells in larvae injected with Aβo compared to those receiving vehicle injections. Interestingly, treatment with Gö6983 effectively attenuated Aβo-induced excess of *myrf*$^{+}$ cell numbers to control values (vehicle 2.05 ± 0.44 cells vs Aβo 3.2 ± 0.39 cells vs Aβo + Gö6983 2.05 ± 0.49 cells) (**Figure 33G**). Indeed, Aβo-injected larvae exhibited an augmented proportion of differentiating OLs in the dorsal spinal cord at this larval stage: while only 14% of dorsal OLs were *myrf*$^{+}$ in vehicle-treated larvae, this ratio increased to 24% following Aβo treatment and was maintained at 15% when Aβo-injected larvae were treated with Gö6983 (**Figure 33H**).

No significant changes were observed in differentiating OL numbers at 5 dpf. Therefore, the sequential study of OL differentiation in this transgenic line suggested that Aβo induce an initial increased premature dorsal OL differentiation around 72 hpf that returns to normal levels by 5 dpf (**Figure 33I**).

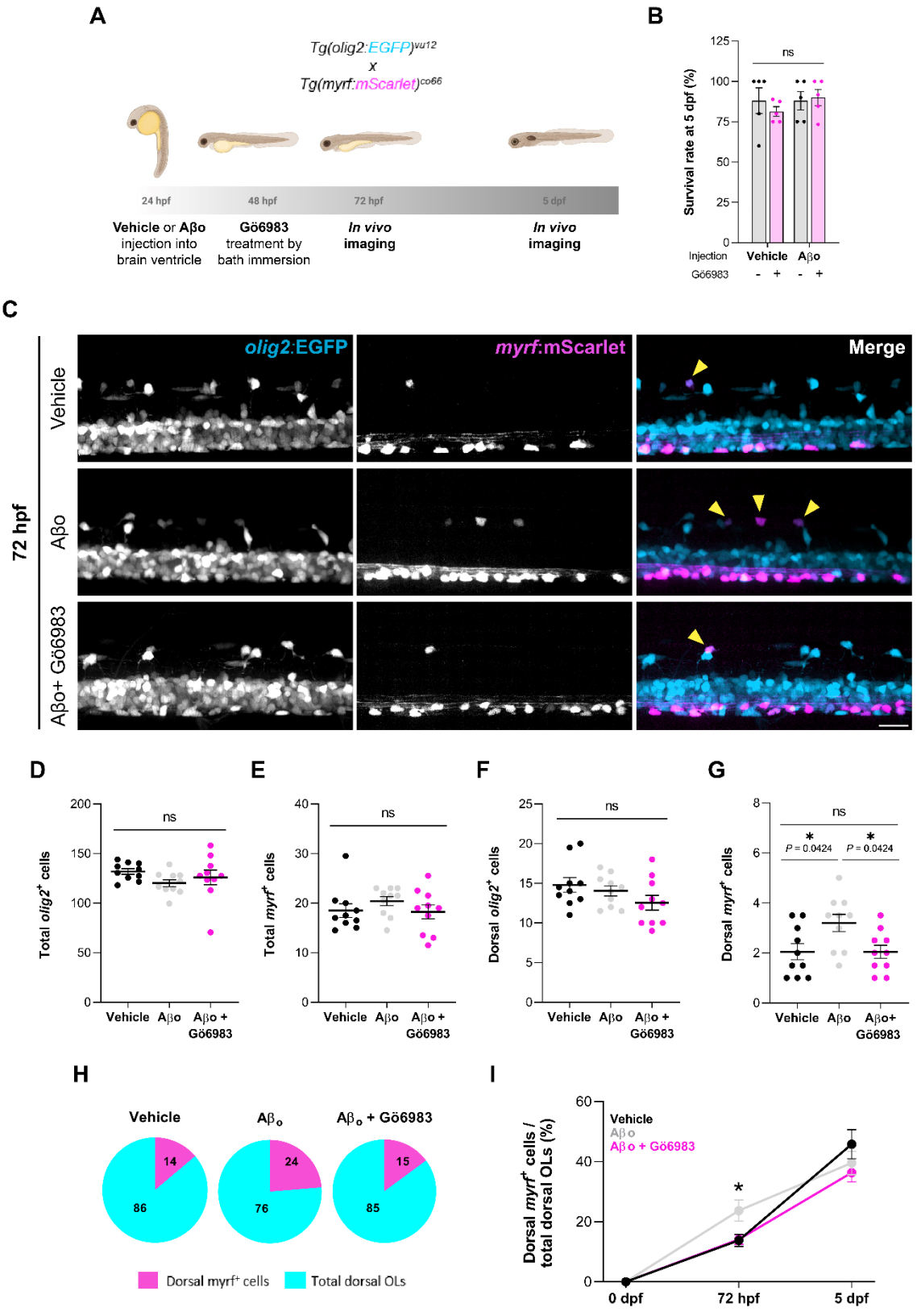

Figure 33. Aβo induce early oligodendrocyte differentiation through PKC, without affecting total cell numbers. (**A**) Transgenic zebrafish stably expressing *olig2*:EGFP and *myrf*:mScarlet were injected with Aβo or its vehicle at 24 hpf, and treated with Gö6983 (500 nM) at 48 hpf by bath immersion. Live imaging was performed at 72 hpf and 5 dpf. (**B**) Survival rate was measured at 5 dpf. (**C**) Representative lateral fluorescence images of the spinal cord in live transgenic larvae at 72 hpf. Yellow

arrowheads indicate *olig2*$^{+}$*myrf*$^{+}$ cells. Scale bar = 20 μm (**D**) Graphs comparing the number of total *olig2*$^{+}$ cells, (**E**) total *myrf*$^{+}$ cells, (**F**) dorsal *olig2*$^{+}$ cells, and (**G**) dorsal *myrf*$^{+}$ cells. (**H**) Pie charts showing the ratio of differentiating dorsal OLs (percentage of dorsal *myrf*$^{+}$ cells among dorsal *olig2*$^{+}$ cells) at 72 hpf for each condition. (**I**) Graph showing the progression of differentiating dorsal OLs during development. Data indicate means ± S.E.M, and dots represent individual larvae. *p<0.05; Statistical significance was determined by ordinary one-way ANOVA followed by Sidak's *post-hoc* and two-way ANOVA followed by Tukey's *post-hoc* test. $n^{72\ hpf}$ = 10 larvae per condition; $n^{5\ dpf}$ = 7 - 9 larvae per condition.

The above data suggest that a higher proportion of OPCs undergo differentiation into mature myelinating OLs in Aβo-injected larvae. To directly test this possibility, we employed a similar approach as previously described, now crossing *Tg(olig2:EGFP)*^{vu12} with *Tg(mbpa:tagRFPT)*^{co25}, a reporter line for myelinating OLs (**Figure 34A**). Since changes in *myrf* were observed at 72 hpf and OL maturation occurs later in time, we focused our analysis on 5 dpf to examine mature myelinating OLs.

At this developmental stage, Aβo-injected larvae exhibited an excess of *mbp*$^{+}$ cells in the dorsal spinal cord compared to vehicle-injected larvae (**Figure 34E**), with no changes in *olig2*$^{+}$ (**Figure 34B, D**) or total *mbp*$^{+}$ cells (**Figure 34C**). Once again, Gö6983 treatment effectively inhibited the effect triggered by Aβo (vehicle 9.58 ± 1.13 cells vs Aβo 14.25 ± 1.5 cells vs Aβo + Gö6983 7.4 ± 1.4 cells) (**Figure 34E**).

Regarding the proportion of myelinating OLs, consistent with our hypothesis, only 36% of dorsal OLs were *mbp*$^{+}$ in the control larvae, compared to 53% in Aβo-treated larvae and 33% when PKC was inhibited (**Figure 34F**). Although no remarkable changes were observed in the number of *mbp*$^{+}$ myelinating OLs at 72 hpf, this transgenic line enabled us to conclude that OL maturation is significantly promoted by Aβo at 5 dpf (**Figure 34G**).

Taken together, these results suggest that Aβo induce precocious differentiation, resulting in altered OL maturation. Furthermore, Gö698 effectively inhibits these effects, confirming the involvement of the PKC signaling pathway in the Aβo-induced misregulation of OL differentiation and maturation.

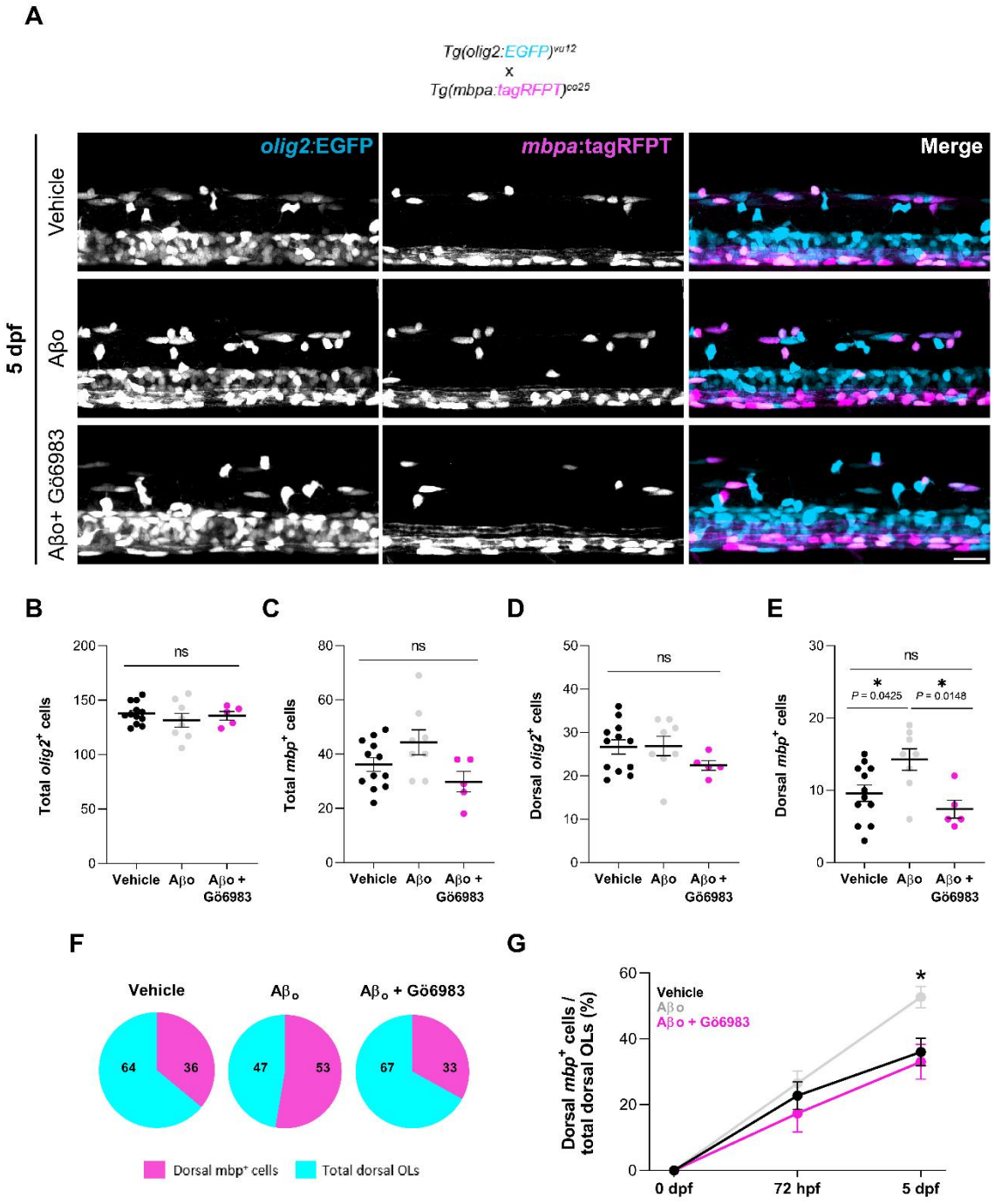

Figure 34. Aβo promote oligodendrocyte maturation via PKC, without changing total cell numbers. (**A**) Representative lateral images of the spinal cord of live transgenic larvae stably expressing *olig2*:EGFP and *mbpa*:tagRFPT, at 5 dpf. Yellow arrowheads indicate *mbp*$^{+}$*myrf*$^{+}$ cells. Scale bar = 20 µm (**B**) Graphs comparing the quantity of total *olig2*$^{+}$ cells, (**C**) total *mbp*$^{+}$ cells, (**D**) dorsal *olig2*$^{+}$ cells, and (**E**) dorsal *mbp*$^{+}$ cells. (**F**) Pie charts showing the ratio of mature myelinating dorsal OLs (percentage of dorsal *mbp*$^{+}$ cells among dorsal *olig2*$^{+}$ cells) at 5 dpf. (**G**) Graphical representation of the progression of maturing dorsal *mbp*$^{+}$ OLs thoughout development. Data indicate means ± S.E.M, and dots represent individual larvae. *p<0.05; Statistical significance was determined by ordinary one-way ANOVA followed by Sidak's *post-hoc* and two-way ANOVA followed by Tukey's *post-hoc* test. $n^{72\ hpf}$ = 6-10 larvae per condition; $n^{5\ dpf}$ = 5-12 larvae per condition.

3.2.3. Aβo-induced myelin excess in the dorsal spinal cord is reversed by PKC inhibition

Next, we sought to investigate whether the potential effects of Aβo on OL differentiation and maturation could affect myelination *in vivo*. To assess myelin sheaths in individual OLs, we transiently expressed *mbpa*:EGFP-CAAX by microinjection into 1-cell stage zebrafish embryos. This genetic construct leads to the expression of membrane-tethered EGFP in the myelin tracts of the larvae. Aβo or vehicle injections were administered followed by Gö6983 treatments, and myelin sheath number per cell and sheath length were measured in the dorsal spinal cord at 5 dpf.

Aβo significantly increased the number of myelin sheaths per cell by around 40% in the dorsal spinal cord compared to vehicle-injected animals. Interestingly, while PKC inhibition alone did not significantly alter sheath numbers, treatment of Aβ-injected zebrafish larvae with Gö6983 restored the aforementioned Aβo-induced increase to control levels (vehicle: 9.08 ± 0.9 sheaths per cell; Gö6987: 11.1 ± 0.73; Aβo: 12.7 ± 0.9; Aβo + Gö6983: 9.38 ± 0.79) (**Figure 35A, B**). This change in sheath number per cell occurred without any alteration in myelin sheath length (**Figure 35C**).

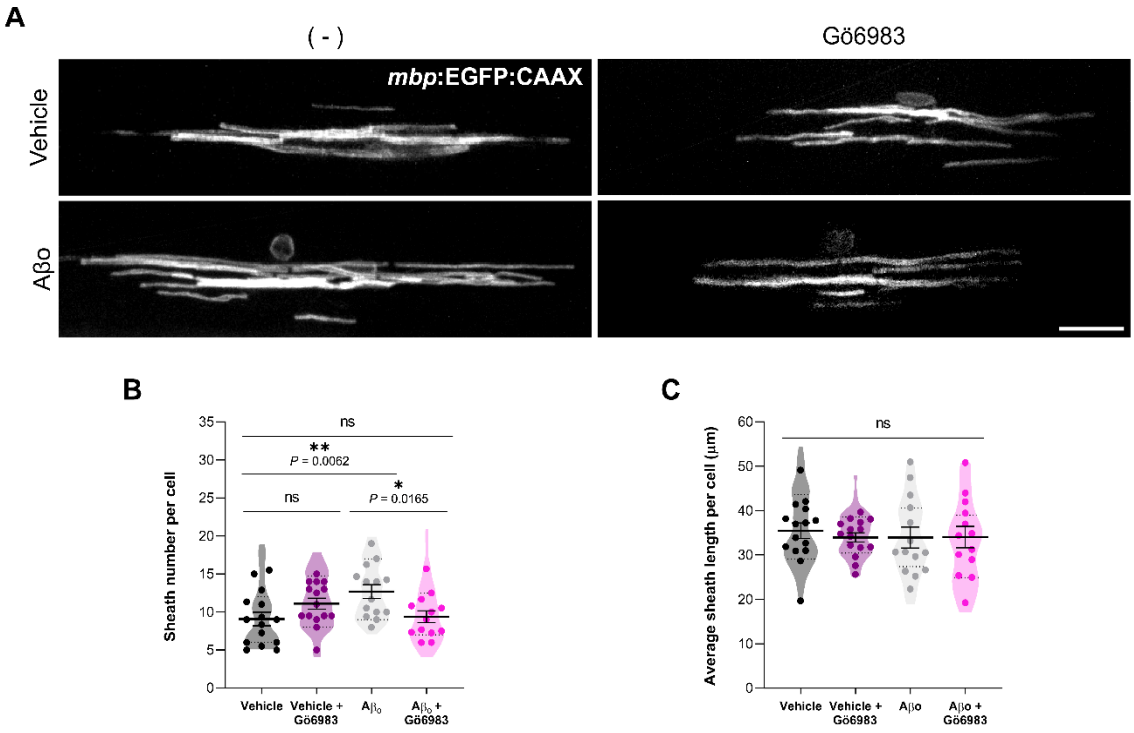

Figure 35. Aβo dysregulate dorsal myelin sheath number per oligodendrocyte via PKC. The *mbpa*:EGFP-CAAX plasmid was injected into zebrafish embryos at the 1-cell stage, followed by the administration of Aβo (10 µM) or its vehicle into the hindbrain ventricle of zebrafish larvae at 24 hpf. Gö6983 (500 nM) treatments were performed at 48 hpf, and live imaging of myelin sheaths was performed

at 5 dpf. (**A**) Representative fluorescent images of OLs in the spinal cord of live zebrafish larvae. Scale bar = 20 µm (**B**) Histograms illustrating the sheath number per cell and (**C**) the average individual sheath length. Data are presented as means ± S.E.M; dots represent individual larvae and violin plot represents quantification of individual cells. *p<0.05, **p<0.01; Statistical significance was determined by two-way ANOVA followed by Sidak's *post-hoc* test.

Next, we wandered whether the reported increase in the numbers of dorsal myelin sheaths per cell could result in notable changes in myelination. To address this question, electron microscopy was conducted on 8 dpf larvae, and the myelinated axons within the dorsal region of the spinal cord were analyzed (**Figure 36A, B**).

In line with our previous findings, a significant increase of around 66% in the number of dorsal myelinated axons was observed in Aβo-injected zebrafish larvae compared to vehicle-injected larvae (108.9 ± 2.64 and 65.65 ± 8.24 myelinated axons, respectively). Moreover, while Gö6983 alone had minimal non-significant impact on dorsal myelination (81.98 ± 12.96 myelinated axons), PKC inhibition in Aβ-injected larvae nearly completely reversed the myelin excess induced by Aβo (74.07 ± 6.44 myelinated axons) (**Figure 36C**).

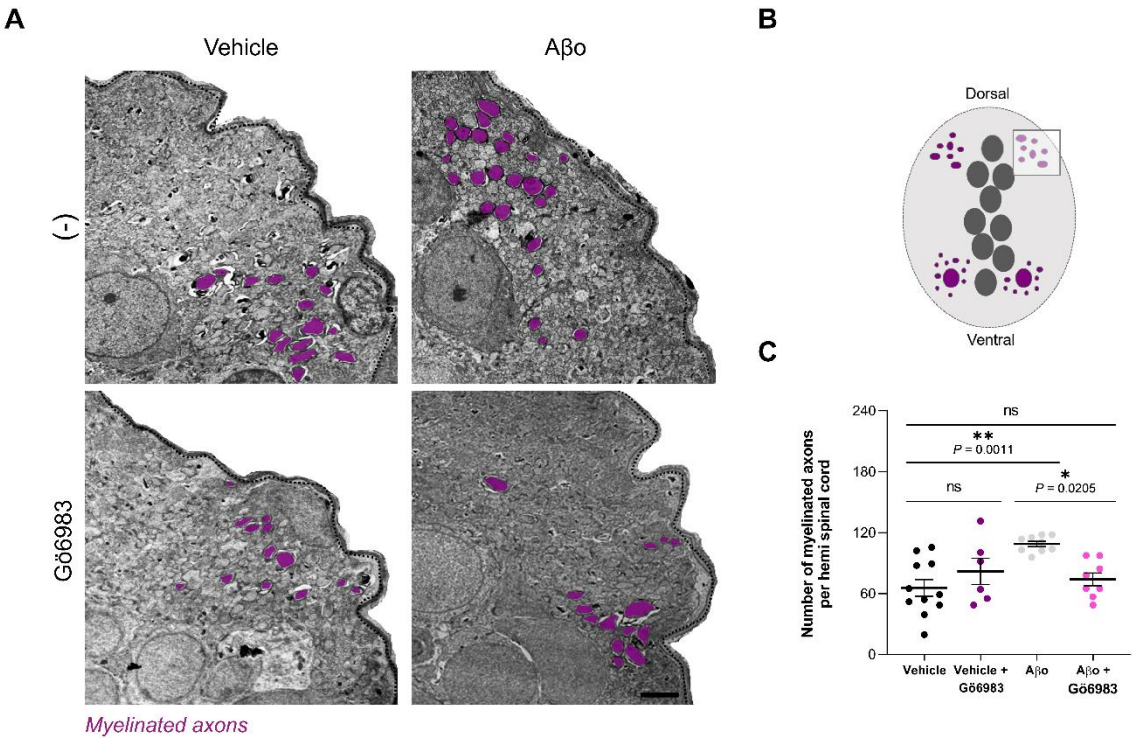

Figure 36. Aβo increase the number of dorsal myelinated axons through PKC. Zebrafish larvae were administered with Aβo (10 µM) or its vehicle by ICV injection at 24 hpf, and some were exposed to

Gö6983 (500 nM) at 48 hpf. Larvae were fixed for electron microscopy analysis at 8 dpf. (**A**) Representative electron micrographs of the dorsal spinal cord, with myelinated axons shaded in purple. (**B**) Schematic illustration of a cross-section of the spinal cord. The square represents the analysed area. (**C**) Histogram showing the number of myelinated axons in the dorsal area for each condition. Scale bar = 2 µm. Data indicate means ± S.E.M, with dots representing individual larvae. *p<0.05, **p<0.01; Statistical significance was determined by two-way ANOVA followed by Sidak's *post-hoc* test.

Overall, we not only demonstrated that Aβo induce precocious OL differentiation leading to dysregulated myelination, but we also confirmed PKC inhibition as an effective pharmacological strategy to rescue Aβo-induced dysregulation *in vivo*.

3.3. PKC inhibition as a pharmacological tool to modulate oligodendroglia alterations in 3xTg-AD mice

Once having tested the effectiveness of Gö6983 in reversing Aβo effects in OLs and myelin in zebrafish, we aimed to extend our *in vivo* investigation to a more biologically complex and clinically relevant model. The 3xTg-AD mouse model presents changes in OL population and MYRF levels, as indicated by our previous results together with others' works. Therefore, our next objective was to determine whether PKC inhibition could reverse at least some of these alterations present in 3xTg-AD mice.

To address this, 12-14 month-old 3xTg-AD mice were surgically implanted with osmotic minipumps delivering either vehicle or Gö6983 continuously for 28 days (**Figure 37A**). Throughout the experiment, we monitored the mice's overall well-being by measuring body weight before, during, and after treatment. The absence of significant changes in body weight across time and experimental groups allowed us to rule out any potential adverse effects of the surgery or drug administration (**Figure 37B**).

Additionally, we evaluated the efficacy of continuous Gö6983 ICV infusion in inhibiting PKC activity within the hippocampus of treated mice. We specifically focused in the hippocampus as it is well described as one of the most affected brain regions both in Alzheimer's disease and in this particular animal model. Western blot analysis of protein extracts from the contralateral hippocampus revealed a substantial 41% decrease in PKC

activity following Gö6983 treatment (5.38 ± 0.72 a.u. vehicle vs 3.19 ± 0.4 a.u. Gö6983) (**Figure 37C, D**). This result not only affirmed adequate PKC inhibition by Gö6983 treatment but also indicated successful drug diffusion from the ventricle to both brain hemispheres.

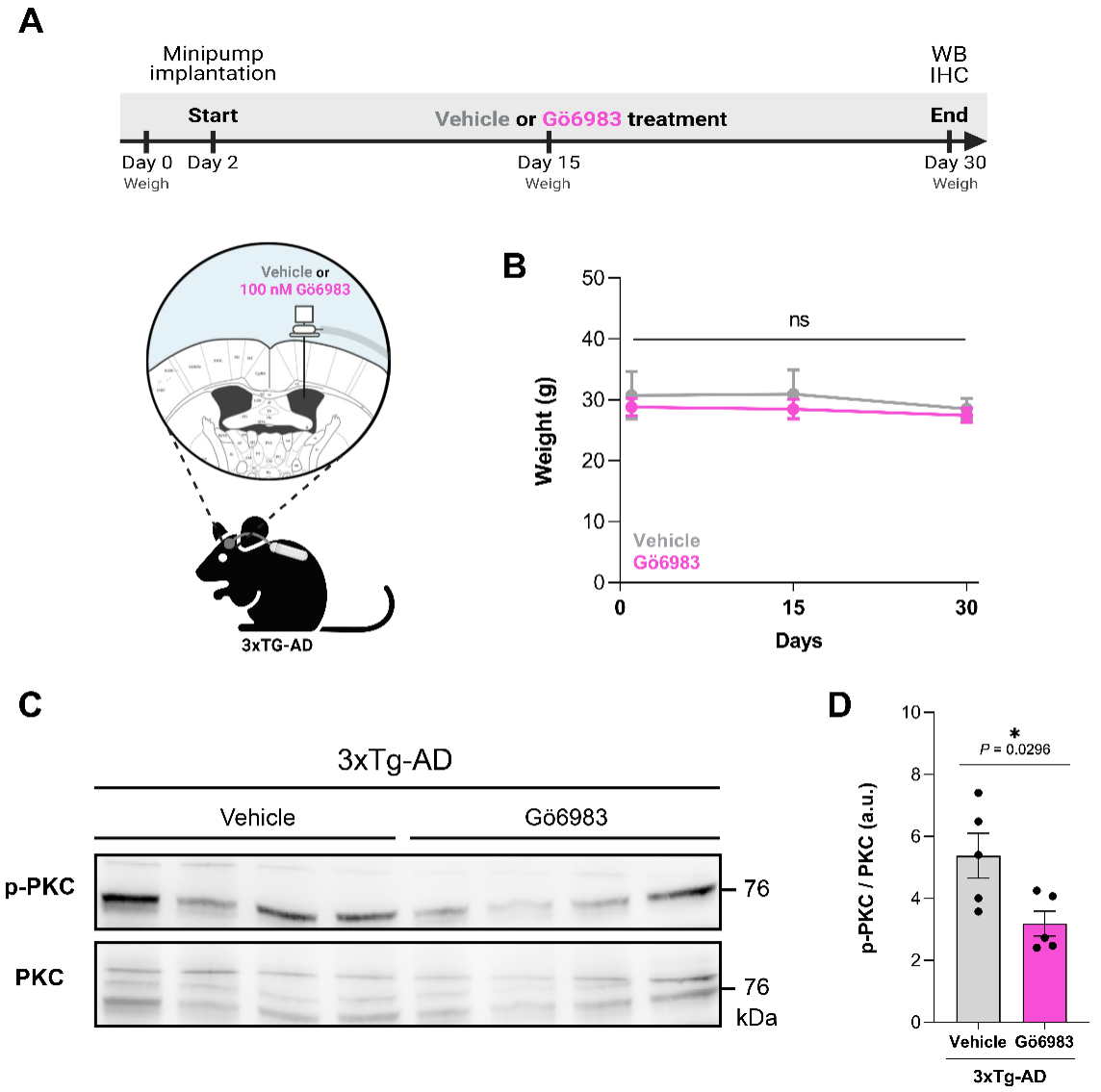

Figure 37. Pharmacological inhibition of PKC in 3xTg-AD mice hippocampus by intracerebroventricular infusion of Gö6983. (**A**) Depiction of the experimental procedure: 3xTg-AD mice underwent implantation of osmotic minipumps to deliver Gö6983 (100 nM) or its vehicle ICV during 28 days (flow rate = 0.11 µL / h). Mice were subsequently perfused, and brains were collected for western blot (WB) (contralateral) or immunohistochemistry (IHC) (ipsilateral) analysis. (**B**) Weight (g) measurements of mice throughout the experiment. (**C**) Western blot analysis of PKC expression levels in contralateral hippocampal protein extracts from 3xTg-AD mice treated with or without Gö6983. (**D**) Quantification of PKC activity state, assessed by expression levels of phosphorylated PKC (p-PKC) normalized to total PKC levels. Data are presented as means ± S.E.M, with dots representing individual animals. *p<0.05; Statistical significance was determined by two-tailed unpaired t-test.

3.3.1. PKC inhibition reduces MYRF in 3xTg-AD mice

One of the alterations that we observed in 12-month-old 3xTg-AD mice hippocampus, particularly in the DG, was an excess in $MYRF^+$ cells compared to WT animals (**Figure 13**). Moreover, we described a signaling pathway linking PKC and MYRF, which is altered in presence of Aβo *in vitro* (**Figure 25, 29**). Thus, we subsequently examined whether PKC inhibition could modulate MYRF levels *in vivo* in the hippocampus of ICV-treated 3xTg-AD mice.

On the one hand, we conducted western blot analysis on protein extracts from the contralateral hippocampus of these animals. The results revealed a significant reduction in MYRF protein levels in mice treated with Gö6983 compared to the control group (0.85 ± 0.04 a.u. and 1.1 ± 0.16 a.u., respectively) (**Figure 38A, B**). On the other hand, the ipsilateral DG was analyzed using IHC to measure the proportion of $MYRF^+$ cells among all OLs. Consistent with our hypothesis and western blot results, Gö6983 treatment resulted in a significant reduction in $MYRF^+$ cells compared to vehicle-treated mice (71.26 ± 2.4% vehicle vs 62.47 ± 2.56% Gö6983) (**Figure 38C, D**).

These findings suggest that PKC inhibition via Gö6983 ICV infusion effectively mitigates the aberrant increased MYRF levels in the hippocampus of 3xTg-AD mice.

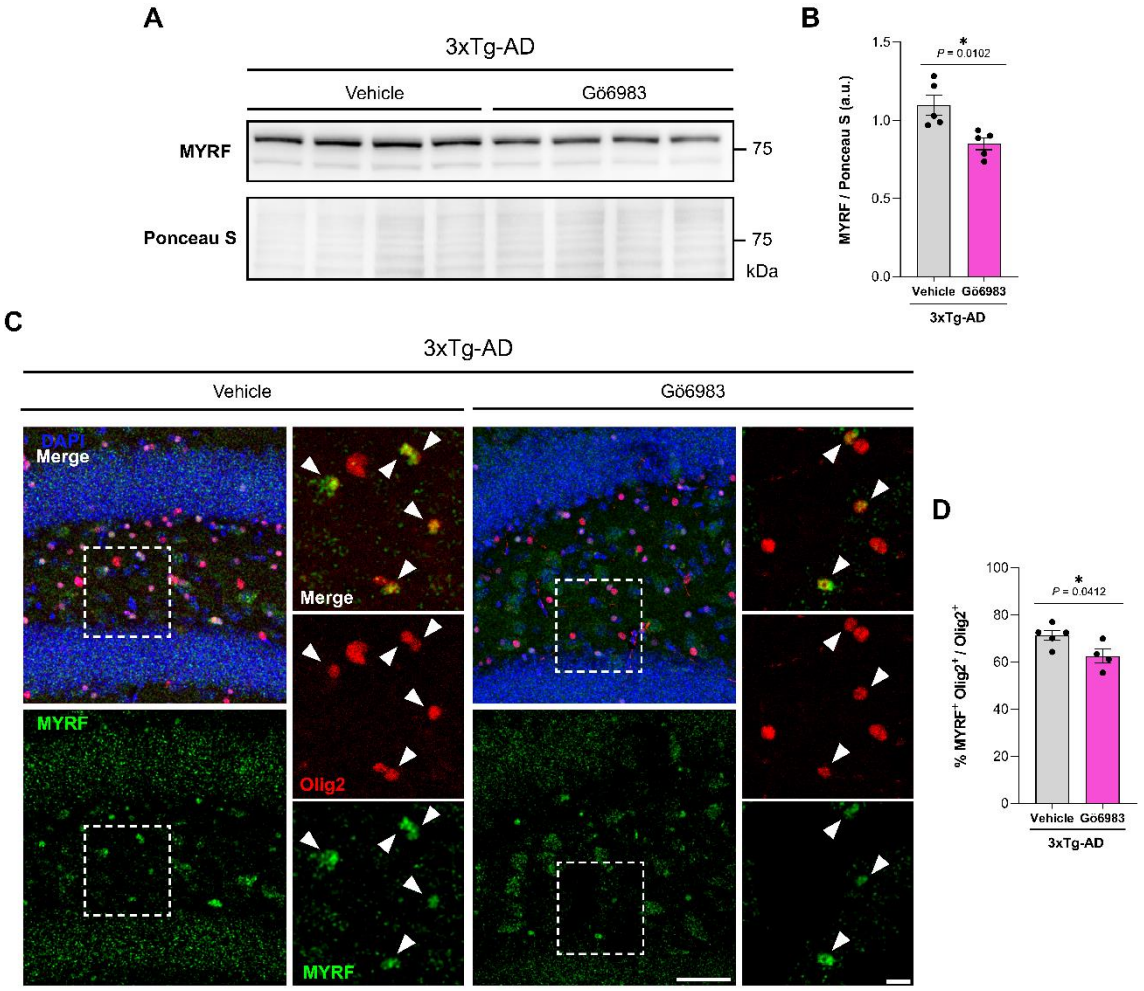

Figure 38. Gö6983 reduces MYRF protein levels in 3xTg-AD mice hippocampus. (**A**) Western blot analysis of MYRF in contralateral hippocampal protein extracts from 3xTg-AD mice ICV treated with Gö6983 (100 nM) or its vehicle. (**B**) Quantification of MYRF levels normalized to total protein levels assessed by Ponceau S staining. (**C**) Representative fluorescent images of Olig2$^+$ (red) and MYRF$^+$ (green) cells in the ipsilateral DG of 3xTg-AD mice treated with or without Gö6983. Arrowheads indicate cells positive for both Olig2 and MYRF. Scale bars = 50 µm / 10 µm (**D**) Histogram representing the percentage of MYRF$^+$ OLs among the total OL population (MYRF$^+$Olig2$^+$ / Olig2$^+$). Data are presented as means ± S.E.M, with dots representing individual animals. *p<0.05; Statistical significance was determined by two-tailed unpaired t-test.

3.3.2. PKC inhibition rescues OL population in 3xTg-AD mice

According to our previous results and other studies (Tse et al., 2018), 12-month-old 3xTg-AD mice also demonstrate brain region-specific alterations in OL populations, including a loss of OLs within the DG (**Figure 11D**), among other changes. Notably, sustained overexpression of MYRF was found to be toxic for OLs *in vitro* (**Figure 19**). Therefore, our last objective was to investigate whether inhibition of PKC, along with the

normalization of MYRF levels induced by this treatment, could have a beneficial effect on OL populations in the DG of 3xTg-AD mice.

To assess this question, we conducted an IHC study of OL populations in the ipsilateral DG of treated 3xTg-AD mice. The results showed a restoration in the number of OLs in mice treated with Gö6983 compared to control 3xTg-AD mice (58.19 ± 8.2x10^3 cells / mm^3 vehicle vs 73.19 ± 4.1x10^3 / mm^3 Gö6983), suggesting that PKC inhibition mitigates OL cell death (**Figure 39A, C**). Additionally, a significant increase in both $CC1^+$ mature (47.14 ± 6.54x10^3 / mm^3 vehicle vs 63.13 ± 2.87x10^3 / mm^3 Gö6983) (**Figure 39D**) and PDGFR-α^-CC1^- immature OLs (3.42 ± 2.98x10^3 / mm^3 vehicle vs 9.46 ± 2.76x10^3 / mm^3 Gö6983) (**Figure 39E**) was also observed in Gö6983-treated mice, OL subpopulations that were significantly reduced in 3xTg-AD mice compared to WT mice (**Figure 11E, F**). Conversely, PDGFR-α^+ OPC numbers remained consistent across treatment groups (**Figure 39B, F**), aligning with the absence of alterations in PDGFR-α^+ cells in our AD mouse model (**Figure 11G**).

To further analyze the OL population following the ICV treatment, we calculated the percentage of each OL subpopulation (OPCs, immature or mature OLs) relative to the total $Olig2^+$ cells for each experimental group. 12-months-old 3xTg-AD mice showed a reduced percentage of immature OLs, with no significant changes in OPCs or mature OLs compared to WT mice (**Figure 11H**). This finding highlighted the vulnerability of the immature OL subpopulation to AD-related alterations. Here again, consistent with those results, while no significant changes were observed in the percentages of OPCs or mature OLs, a notable recovery of the immature subpopulation was observed in 3xTg-AD mice treated with Gö6983 (**Figure 39G**).

In summary, we concluded that the PKC inhibitor Gö6983 was able to revert at least part of the alterations observed in the 3xTg-AD mouse model: continuous treatment with this drug inhibited OL loss, restored the balance of OL subpopulations, and rescued excessive MYRF levels in the hippocampus of the animals.

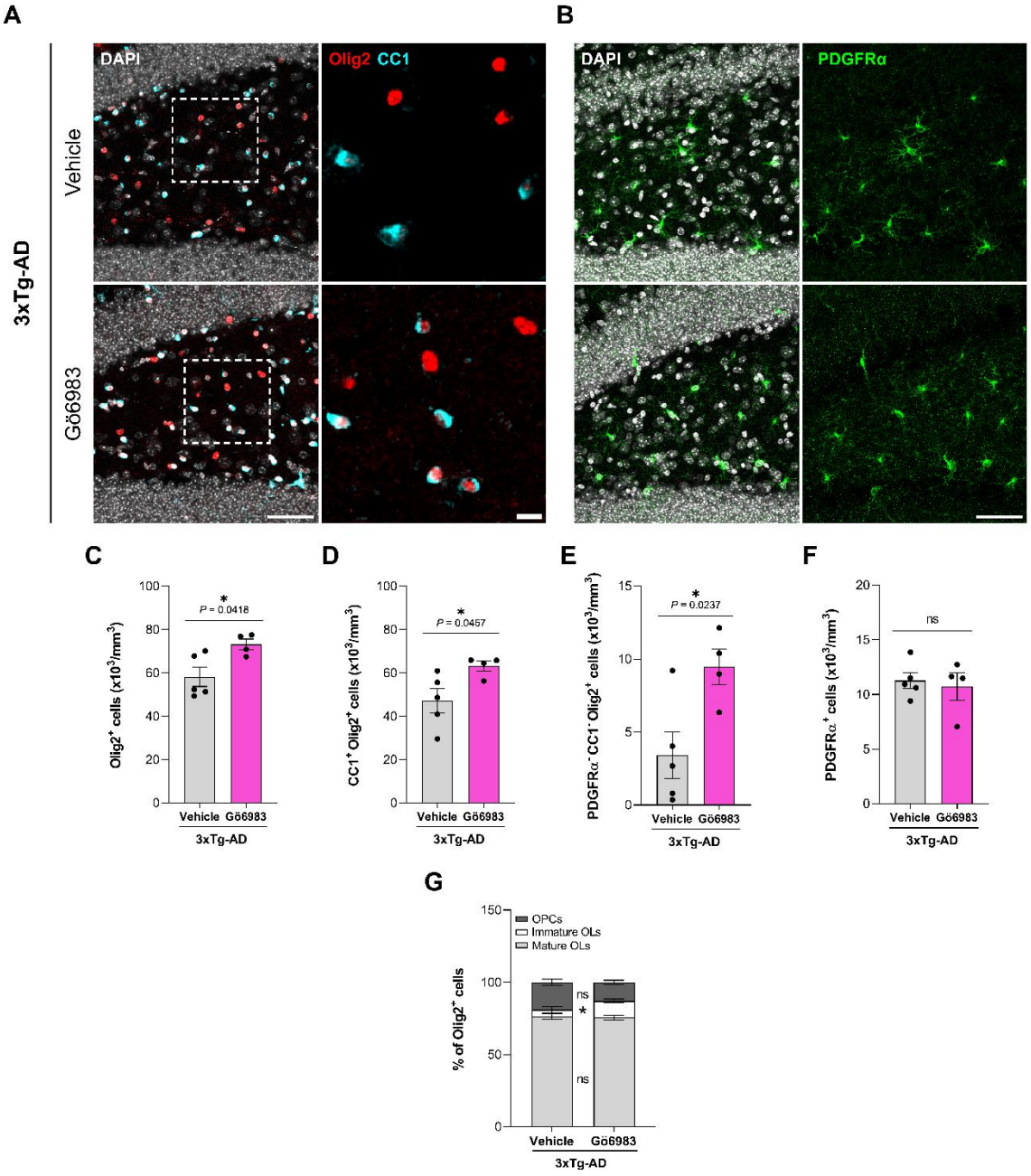

Figure 39. Pharmacological inhibition of PKC restores oligodendroglial population in 3xTg-AD mice dentate gyrus. IHC analysis of the ipsilateral dentate gyrus of 12-14 months-old 3xTg-AD mice subject to ICV treatment with Gö6983 (100 nM) or its vehicle. Representative fluorescent micrographs of (**A**) Olig2 (red) and CC1 (cyan), and (**B**) PDGFR-α (green); DAPI staining is showed in white. Scale bars = 50 µm and 10 µm. Histograms showing numbers of (**C**) Olig2^{+} (total OLs), (**D**) CC1^{+}Olig2^{+} (mature OLs), (**E**) PDGFR-α^{-}CC1^{-}Olig2^{+} (immature OLs), and (**F**) PDGFR-α^{+} (OPC) cells. (**G**) Graph showing the percentages of oligodendroglial subpopulations (OPCs, immature OLs and mature OLs) in each experimental group. Data are presented as means ± S.E.M, with dots representing individual animals. *p<0.05; Statistical significance was determined by two-tailed unpaired t-test and two-way ANOVA followed by Sidak's *post-hoc* test.

Discussion

DISCUSSION

Given the indispensable role of OLs in supporting neuronal function and cognitive processes, it is reasonable to speculate that alterations in oligodendroglial cells may contribute to various age-related neurodegenerative diseases. While Alzheimer's disease has traditionally been perceived primarily as a disorder associated with neuronal damage, evidence of diverse structural, histopathological, and biochemical abnormalities in the WM preceding neuronal damage has been documented in the disease. Consequently, investigating changes in oligodendroglial lineage cells is of paramount importance, not only for shedding light on AD pathogenesis but also for identifying potential therapeutic targets aimed at preserving WM integrity and OL function.

In this context, two central questions have emerged: 1) what happens to OLs in AD? and 2) what mechanisms underlie these alterations? Throughout this thesis, we have revealed altered dynamics of oligodendroglial populations in AD mouse models, characterized by enhanced maturation in both the corpus callosum and the dentate gyrus, accompanied by a loss of $Olig2^+$ cells in the dentate gyrus. Additionally, we observed that these effects were at least partially induced by the presence of Aβo, as similar pathology was evident in WT mice injected with Aβo. Furthermore, we propose that Aβo-induced dysregulation of MYRF may underlie these OL alterations. Our findings indicate that Aβo disturb the signaling pathway responsible for MYRF degradation, specifically by interfering with the PKC/GSK3 pathway and Fbxw7-mediated ubiquitination, resulting in increased MYRF protein levels and likely a prolonged transcriptional activity. This dysregulation could potentially contribute to the aberrant upregulation of OL differentiation and myelination programs within the context of AD. Finally, we validated the inhibition of PKC as a promising strategy to reverse these alterations *in vivo*.

1. Oligodendrocyte differentiation and maturation are promoted in the corpus callosum and the dentate gyrus of AD mouse models

Changes in OPCs or OLs can profoundly affect myelin integrity, which potentially implicates them in AD pathogenesis. Thus, numerous human and animal studies have investigated WM and OL changes in AD, revealing abnormal alterations in OL-lineage cells and myelin damage in *post-mortem* AD brain tissues (Behrendt et al., 2013; Mitew et al., 2010; Tse et al., 2018) and AD mouse models (Chacon-De-La-Rocha et al., 2020;

Desai et al., 2009; Tse et al., 2018; Vanzulli et al., 2020). However, there are many discrepancies in the literature, as results reveal differences depending on factor such as the animal model, age, sex, and brain region studied.

To further investigate alterations in oligodendroglial population and dynamics, we focused our IHC analysis on two distinct AD mouse models: 3xTg-AD, considered one of the most complex animal models of the disease exhibiting both senile plaques and neurofibrillary tangles, and Aβo-injected WT mice. Specifically, we analyzed the corpus callosum and the dentate gyrus, which are WM and GM regions affected in AD, respectively, with their impairment correlating with the progression and severity of the disease (Teipel et al., 2002). Using an EdU incorporation assay, we demonstrated significant changes in oligodendroglial population dynamics in both the CC and the DG of 12-month-old 3xTg-AD mice. These alterations were characterized by a decreased density of immature OLs (PDGFR-α^-CC1$^-$Olig2$^+$) and an increased proportion of newly generated mature OLs, with no changes in PDGFR-α^+ OPCs. These findings suggest that OL differentiation is promoted in this AD model, with a heightened propensity for immature OLs to transition into mature ones. Nevertheless, although the differentiation from OPCs to immature OLs may be unaffected, it seems decompensated or not effective enough to counteract the increased OL maturation ratio, with potential further implications in more advanced stages of the disease.

In contrast, numerous previous studies have described that the differentiation of OPCs is susceptible to the deterioration of the microenvironment in AD pathology, resulting in a reduction of OPC differentiation capability or oligodendrogenesis (Vanzulli et al., 2020; Zhang et al., 2019; Zou et al., 2023). Nevertheless, our findings suggest that the focus should be switched to studying alterations in differentiating and/or mature OLs, rather than OPCs, as the most substantial changes were observed in OL differentiation and maturation dynamics. Interestingly, another previous work reported increased expression of CC1$^+$ mature OLs in the hippocampal CA1 region of 6-month-old 3xTg-AD mice (Desai et al., 2010). Although authors also described unchanged immature OL numbers, this finding could indicate that between 6 and 12 months, OL differentiation has already been promoted, and by 12 month, almost a complete depletion of the immature subpopulation has occurred. Therefore, it would be plausible to hypothesize that in more advanced ages, the pathology could completely disturb the oligodendroglial population,

with potential implications in the maintenance of the OL lineage homeostasis, and consequently, myelin. This could be a key event in the development of AD pathology.

Another AD mouse model is the APP/PS1 mice. Previous studies have revealed enhanced OPC proliferation followed by differentiation into mature OLs in the corpus callosum of mice aged 6 and 11 months (Behrendt et al., 2013). Similarly, Ferreira and colleagues also found increased oligodendrogenesis with more newly generated OLs in the same mouse model (Ferreira et al., 2020). Collectively, these findings, along with ours, suggest that the generation of mature OLs is promoted in AD mouse models. Furthermore, increased rates of new myelin formation have also been observed in APP/PS1 mice (Chen et al., 2021), likely resulting from this promoted OL differentiation into mature myelinating cells.

Conversely, numerous studies have reported demyelination in AD animal models (Behrendt et al., 2013; Desai et al., 2009; Mitew et al., 2010), and as occurs in other demyelinating lesions such as multiple sclerosis, adult OPCs are able to differentiate into mature OLs to remyelinate damaged axons (Zawadzka et al., 2010). Therefore, it is challenging to determine whether the alterations observed in oligodendroglial population dynamics are led directly by AD-related pathophysiological mechanisms or are a compensatory response to already occurring brain and myelin damage. Nevertheless, although we cannot completely rule out that possibility, strong evidence points toward Aβo as a candidate to directly mediate OL changes. In fact, our results from the IHC analysis of the oligodendroglial population in mice with intrahippocampal Aβo injections correlated with those observed in the 3xTg-AD mice: a reduced proportion of immature OLs, an increased proportion of mature OLs, and no changes in OPCs were found. Therefore, we concluded that the OL alterations in 3xTg-AD mice were at least partially triggered by the presence of Aβo. This idea is also supported by previous studies, where they demonstrated that Aβo increase morphological differentiation and maturation in cultured OLs and cerebellar slices (Quintela-López et al., 2019). More interestingly, Desai and coworkers demonstrated that the elevated density of mature OLs in 3xTg-AD mice was effectively reduced by the injection of an anti-$A\beta_{1-42}$ engineered intrabody, further indicating a direct effect of Aβ on OL differentiation (Desai et al., 2010).

However, the underlying mechanisms remain elusive. An important event to consider is the increase in neuronal activity observed in AD. Clinical studies have consistently reported heightened cortical and hippocampal neuronal activity in patients during the early stages of the disease (Targa Dias Anastacio et al., 2022), and the administration of Aβ to neurons has been shown to increase action potential firing (Yamamoto et al., 2015). What is more, researchers have unveiled a bidirectional relationship between AD and neuronal hyperactivity, where Aβ induces neuronal activity, and, in turn, neuronal hyperactivity exacerbates Aβ deposition. Indeed, recent studies in mouse models have revealed that restoring abnormal neuronal excitability in brain regions affected early by Aβ not only reduces Aβ accumulation in those areas but also prevents its spread to other brain regions (Gail Canter et al., 2019). Intriguingly, increased neuronal activity has also been found to promote proliferation, differentiation, and myelination in oligodendroglial lineage cells, to support the formation and function of neural circuits (Gibson et al., 2014; Hines et al., 2015; Thornton & Hughes, 2020). Given the crucial role of the transcription factor MYRF in OL terminal differentiation and myelination processes (Koenning et al., 2012), it is plausible to hypothesize its involved in Aβ-induced OL differentiation; however, whether neuronal signals can regulate MYRF activity remains to be studied.

2. 3xTg-AD mouse model exhibit brain-region-specific oligodendrocyte loss in the dentate gyrus

Changes in the number of oligodendrocytic lineage cells is a common feature observed in both physiological aging and neurodegenerative disorders such as AD. For instance, post-mortem analysis of AD patients' tissues revealed a decrease in $Olig2^{+}$ cells (Behrendt et al., 2013). However, our examination of the corpus callosum in 12-month-old 3xTg-AD mice revealed that although there was an increased formation of mature OLs from immature OLs altering the proportions of these OL subpopulations, the total number of oligodendroglial cells remained unchanged. Similar findings were reported by Ferreira and colleagues, who described that despite the increased addition of new mature OLs in the brain of *APP* transgenic mice, total OL density was equivalent between *APP* transgenic mice and WT mice. With these results, they concluded that new OLs may be produced to replace lost mature OLs (Ferreira et al., 2020), indicating a promoted recycling of mature cells. Nevertheless, the significant reduction we observed in the proportion of the immature subpopulation suggests that the replacement of

immature cells from OPCs may not be effective enough. Consequently, while this phenomenon did not result in alterations in total OL numbers, it may be exacerbated in more advanced disease stages.

Interestingly, the OL population disruption was more pronounced in the dentate gyrus of 3xTg-AD mice. In this brain region, alongside increased newly generated mature OLs, we observed a marked loss of total Olig2$^+$ cells of approximately 20% in contrast to WT mice. Specifically, significantly reduced densities of NG2$^+$ late OPCs, immature OLs, and mature OLs were found, with unchanged PDGFR-α$^+$ OPC numbers. This finding again suggested that the initial stage of the oligodendroglial lineage is not directly affected by the pathology. Instead, we hypothesize that mature OLs may be undergoing cell death, and the sustained effort of the oligodendroglial lineage to replace lost mature OLs through differentiation and maturation may induce exhaustion of other subpopulations. Thus, despite the apparently intact potential of OPCs to proliferate and differentiate into mature OLs, oligodendrogenesis may not be sufficient to restore normal OL density in the dentate gyrus of 3xTg-AD mice.

In addition to reduced cell densities, morphology of NG2$^+$ OPCs was also altered: cells in the dentate gyrus of the 3xTg-AD mice occupied a significantly larger area compared to WT mice cells, indicating hypertrophy. This could signify that cells were trying to compensate for cell loss by increasing their covered area. This finding is consistent with previous studies reporting subtle changes in density and morphology in both patients (Nielsen et al., 2013; Zhang et al., 2019) and mouse models of AD (Chacon-De-La-Rocha et al., 2020; Vanzulli et al., 2020). Interestingly, previous research has also described hypertrophic NG2$^+$ OPCs in response to brain lesions, characterized by increased cell volume and surface area, with more complex processes and swollen cell bodies (Ong & Levine, 1999). This suggests that NG2$^+$ cell morphology might serve as a marker for brain and OL damage. Nevertheless, while morphological changes and atrophy in OPCs may indicate altered or decreased physiological activity, further investigations are needed to understand their functional consequences for the cell, myelin, and ultimately, the brain.

The observed OL loss in the dentate gyrus, but not in the corpus callosum, indicated a greater vulnerability of GM to AD pathology compared to WM, suggesting that alterations in the oligodendroglial population are region-specific, with variations across distinct brain areas. This aligns with previous studies that described a particular

susceptibility for OL and myelin damage in areas that are myelinated at older ages, such as the entorhinal cortex and the hippocampus (Desai et al., 2009) –a phenomenon known as "neuropathologic retrogenesis" (Bartzokis et al., 2004; Braak & Braak, 1996; Nasrabady et al., 2018). Importantly, this results in initial impairments affecting brain regions crucial for cognitive functions like memory. More interestingly, even within the hippocampus, OL changes exhibit subregion specificity. In our study, although alterations were evident in the dentate gyrus, no significant changes were observed in the oligodendroglial population in the CA1 and CA3 hippocampal subregions (data not shown). On the other hand, recent research has demonstrated that OL loss was most pronounced in the CA3 and CA4 regions of APP/PS1 mice compared to the CA1 (DeFlitch et al., 2022). These results, combined with ours, highlight the diversity and region-specific nature of oligodendroglial alterations related to AD.

Notably, contradictory findings have emerged regarding whether the stage of OL differentiation influences cell susceptibility to AD damage or Aβ toxicity. Some studies suggested that $A\beta_{1-42}$ treatments impact the viability of both immature and mature OLs, resulting in an increased abundance of cells with pyknotic nuclei (Desai et al., 2010), while others indicated that higher concentrations of soluble $A\beta_{1-42}$ inhibit the survival of mature OLs but not OPCs (Horiuchi et al., 2012). Consistent with the latter study, we hypothesized that mature OLs are the primary targets of cell death in the dentate gyrus of 3xTg-AD mice. Although the most prominent and consistent alteration we observed in 3xTg-AD OLs was the loss of the immature subpopulation, we propose that immature OLs have undergone differentiation to compensate for the lost mature subpopulation. This idea is further supported by a recent study where authors describe distinct cell death mechanisms depending on the maturation stage of OLs. Specifically, they demonstrate that immature or differentiating OLs undergo caspase-3-dependent cell death, whereas mature OLs experience caspase-3-independent cell death characterized by DNA damage and disruption in poly-ADP-ribose subcellular localization (Chapman et al., 2024). In an attempt to elucidate the mechanism underlying OL death in 3xTg-AD mice, no evidence of caspase-3 activation was observed across the brains, ruling out immature OL death.

In recent years, single-cell genomics has highlighted common signaling pathways perturbed across multiple cell types in AD, such as inflammation, metabolic stress, protein folding, lipid metabolism, DNA damage, and cellular senescence, among others (Murdock & Tsai, 2023). Similarly, we performed RNA-seq in OLs isolated from

6-month-old 3xTg-AD mice to uncover genetic disparities preceding the observed OL pathology in the animal. The overall altered genes suggested that OLs already show significant disruptions in early stages of the disease, underscoring the relevance of this glial cell in the disease. Intriguingly, in addition to alterations in genes involved in crucial biological processes for OL homeostasis, myelin formation, and AD development such as autophagy, lipid and iron metabolism, and APP processing, several genes related to pathways indicating OL dysfunction and cell death were found to be upregulated. Among them, we found DNA damage. Considering our transcriptomic analysis together with the findings of Chapman and colleagues, who described DNA damage-dependent cell death for mature OLs (Chapman et al., 2024), it is possible that mature OLs in 3xTg-AD mice are undergoing cell death due to DNA damage. Indeed, DNA damage has been widely linked to aging and degenerative illness such as multiple sclerosis or AD (Tse & Herrup, 2017), where cumulative damage overwhelms the DNA repair mechanisms in OLs, ultimately leading to cell apoptosis.

Another significant mechanism that could contribute to mature OL cell death is oxidative stress, which our RNA sequencing analysis also found to be upregulated and has been extensively studied in the context of AD. For example, studies in rat OLs revealed that Aβ-induced oxidative stress drives OL death and dysfunction (Xu et al., 2001). Notably, myelinating OLs are highly sensitive to oxidative stress due to their elevated metabolic demand, and high iron and lipid content. During myelination, OLs require 2–3 fold higher energy levels than other CNS cell types to produce such a vast amount of membrane, making them susceptible to excitotoxicity, heavy metals, and free radicals that induce oxidative stress. Additionally, OLs have the highest iron content of all cell types, which further increases with age and even more in AD (Bartzokis, 2011), and, compared with other glial cells, they contain smaller amounts of antioxidant agents (Juurlink et al., 1998). Together, these characteristics make OLs particularly vulnerable to oxidative stress (Nasrabady et al., 2018).

Overall, the evidence suggests that mature myelinating OLs are undergoing cell death in the dentate gyrus of the 3xTg-AD mice. However, further studies are required to elucidate the precise mechanism underlying mature OLs' cell death.

3. Amyloid β oligomers dysregulate oligodendrocyte differentiation and myelination *in vivo* in zebrafish larvae

Growing evidence suggests that OL and myelin damage play significant roles in AD, with myelin impairment potentially leading to neuronal dysfunction and cognitive decline. However, the potential effects of Aβo on OL differentiation and myelination *in vivo* remain poorly understood. In recent years, zebrafish have emerged as a well-established model organism for studying OL and myelin biology *in vivo*, offering several advantages over traditional mammalian models. Notably, their optical transparency during embryonic and larval stages enables real-time observation of OL development, myelin formation, and myelin dynamics. Additionally, the rapid external development of zebrafish embryos and their genetic tractability facilitate genetic manipulation and screening approaches, which allows for the study of specific genes and signaling pathways involved in myelination. Importantly, many aspects of OL biology and myelin formation are highly conserved between zebrafish and mammals, which makes zebrafish an attractive model for investigating fundamental principles relevant to human health and disease (Choi et al., 2021; Preston & Macklin, 2015).

In this study, we investigated the effects of intracerebroventricular injection of Aβo on OLs and myelin in the developing spinal cord of zebrafish larvae. For that, we focused on the expression of two well-established genes known to play pivotal roles in OL differentiation and myelination: *myrf*, primarily expressed in differentiating OLs, and *mbp*, expressed in mature myelinating OLs. Our analysis revealed that Aβo administration led to alterations in the expression levels of both *myrf* and *mbp* mRNAs during larval development. Initially, *myrf* expression was significantly elevated in Aβo-injected larvae but decreased by 5 dpf. Similarly, consistent with *myrf*, *mbp* expression showed a notable increase in the presence of Aβo at early developmental stages, which was then normalized to control levels as development progressed. This finding was surprising, considering that myelination typically commences around 72 hpf (Buckley et al., 2010) and *mbp* expression is usually barely detectable at 48 hpf, as confirmed by the vehicle-injected zebrafish. The early induction of *mbp* mRNA observed in Aβo-injected larvae at 48 hpf suggested an accelerated myelination process in presence of Aβo. Furthermore, we also identified *mbp* transcript to be accumulated in the dorsal region of the spinal cord, indicating enhanced OL differentiation and migration. Consistently, using live imaging of transgenic reporter lines for *olig2*, *myrf*, and *mbp*

transcripts, we found that Aβo exposure increased the number of *myrf*$^{+}$ and *mbp*$^{+}$ OLs in the dorsal spinal cord at 72 hpf and 5 dpf, respectively, without altering the total cell count. These results collectively suggest a precocious differentiation and maturation of OLs in the presence of Aβo, without affecting cell proliferation or viability.

Accordingly, we also demonstrated that Aβo increase the number of myelin sheaths per OL in the dorsal spinal cord of zebrafish larvae, with no changes in sheath length. Interestingly, this observation is consistent with findings from a previous study where they used a transgenic zebrafish line with constitutively active Fyn kinase in all myelinating OLs. In this study, authors reported an increase in sheath number per cell, without alterations in OL number or myelin sheath length (Czopka et al., 2013), which is comparable to what we observed in Aβo-injected zebrafish larvae. This suggests a potential involvement of Fyn kinase in mediating the effects of Aβo on myelination *in vivo*. Interestingly, Fyn has previously been described to be a downstream target of Aβ both *in vitro* and in animal models (Boehm, 2013; Quintela-López et al., 2019). Furthermore, we observed elevated numbers of myelinated axons in the dorsal spinal cord of the zebrafish larvae exposed to Aβo. Previous zebrafish studies have shown that Aβo-injected zebrafish exhibit reduced avoidance of aversive stimuli compared to animals injected with vehicle alone (Nery et al., 2014). Consequently, we speculate that the hypermyelination resulting from precociously differentiated OLs in Aβo-injected zebrafish larvae may be aberrant or dysfunctional; however, further investigations are needed to confirm this hypothesis.

In summary, our findings strongly indicate that Aβo disrupt OL differentiation and myelination processes *in vivo*.

4. Amyloid β oligomers increase MYRF levels both *in vitro* and *in vivo*

Once demonstrated significant alterations in OL differentiation, maturation, and myelination in both 3xTg-AD mice and Aβo-injected murine and zebrafish models, our attention turned to MYRF, a transcription factor essential for those biological processes (Emery et al., 2009; Koenning et al., 2012). We hypothesized, for the first time, that MYRF might be involved in all the previously mentioned alterations and, consequently, in AD pathology.

Through our investigation, we discovered that Aβo exposure led to an increase in MYRF protein levels, both *in vitro* in HEK293T cells expressing exogenous MYRF and in cultured primary OLs, as well as *in vivo* in the corpus callosum and dentate gyrus of Aβo-injected mice. Consistently, 12-months-old 3xTg-AD mice also exhibited a higher number of $MYRF^+$ OLs compared to WT mice in the dentate gyrus. Maintaining proper levels of transcription factors is vital for precise control of gene expression and ensuring cellular function. Therefore, finding out that MYRF levels were dysregulated in the context of AD was intriguing, strongly suggesting a potential implication of MYRF in AD-related OL and myelin pathology.

Interestingly, Aβo treatment increased levels of both full-length and nuclear N-terminal fragment of MYRF *in vitro*. Moreover, MBP protein levels were also augmented, suggesting that the Aβo-induced MYRF protein was transcriptionally active. This was further confirmed by luciferase assays. Specifically, the luciferase reporter activities of *Mbp*, *Mag*, and *Rffl* luciferase reporters (three target genes of MYRF), were significantly increased in the presence of Aβo. Furthermore, silencing *Myrf* expression through siRNAs prevented this Aβo-induced enhanced activity, underscoring that Aβo-mediated alterations in myelin-related gene expression are MYRF-dependent.

During demyelinating lesions like those observed in multiple sclerosis, $MYRF^+$ OLs are initially lost but then recuperated during the remyelination process (Duncan et al., 2017). Therefore, considering MYRF as a pro-myelinating factor, its upregulation could potentially serve as a strategy to combat demyelinating pathologies by promoting remyelination. However, while an upregulation in MYRF expression may initially seem advantageous for the cell, we propose that Aβo-mediated dysregulation of MYRF is implicated in early OL and myelin dysfunctions observed in the disease. Elevated levels of MYRF protein and transcriptional activity might lead to enhanced expression of myelin-related genes, inducing uncontrolled or aberrant OL differentiation and maturation. This, in turn, could result in significant consequences for CNS function, such as improper myelination patterns and exhaustion of OPCs, potentially leading to neurological deficits and impairments. Indeed, negative regulation of OL differentiation is crucial to ensure adequate homeostasis of oligodendroglial subpopulations. Thus, we propose that Aβo-mediated increased MYRF may be inducing the OL maturation that contributes to the depletion of immature OLs observed in AD mouse models, as well as promoting the precocious OL differentiation and maturation observed in zebrafish larvae.

Interestingly, our findings also revealed that although initially MYRF overexpression appears benign and may even exhibit a tendency to enhance cell viability, sustained overexpression of MYRF is cytotoxic to OLs *in vitro*. This intriguing observation suggests that the heightened levels of MYRF induced by Aβo, if prolonged, may contribute not only to the dysregulation of OL differentiation but also to the observed OL loss in the dentate gyrus of 3xTg-AD mice. This notion is further supported by the specific expression of MYRF during the differentiation and myelination stages of OLs, that is, in immature and mature subpopulations, which were found to be more vulnerable to AD-related disruptions compared to early OPCs that do not typically express MYRF. It is conceivable that this toxicity arises from a potential shift in MYRF's transcriptional activity towards non-physiological or nonspecific target genes, possibly leading to the activation of signaling pathways that directly or indirectly culminate in cell death. Nevertheless, this hypothesis remains unexplored and needs further investigation.

The precise and coordinated production of myelin is essential for the correct development and functioning of the CNS. Premature OL differentiation can disrupt this process, leading to improper myelin synthesis and potentially impaired neuronal function. Therefore, the induction of MYRF expression by Aβo may lead to hypermyelination, as observed in our zebrafish experiments, but this synthesized myelin may not be physiological or functionally normal. Multiple studies have reported myelin abnormalities in AD mouse models, including 3xTg-AD and APP/PS1 (Behrendt et al., 2013; Desai et al., 2009, 2010). Moreover, slower axonal conduction velocity has been observed in 3xTg-AD mice. For instance, a significant reduction in conduction velocity was noted in myelinated axons of the corpus callosum in 3xTg-AD mice, whereas no differences were observed in unmyelinated axons. As exclusively myelinated axons displayed AD-related functional deficits, these findings suggested that 3xTg-AD mice develop axonal conduction defects due to myelin abnormalities (Quintela-López et al., in preparation). In this context, evidences from various myelin models suggests that the presence of defective myelin sheaths is more detrimental to proper axonal function than their absence, as aberrant myelin is associated with the uncoupling of OL support for axons (Schäffner et al., 2023; Simons & Nave, 2016). Indeed, myelin deficits have been proposed to promote Aβo deposition, exacerbating AD pathology. (Depp et al., 2023).

Altogether, we describe for the first time that Aβo aberrantly increase MYRF protein levels, potentially disrupting OLs and myelin in the context of AD. This underscores the involvement of MYRF in AD pathology.

5. Amyloid β oligomers increase MYRF levels by disrupting its degradation pathway

Our next objective was to elucidate the molecular mechanisms underlying the Aβo-induced upregulation of MYRF, aiming for the identification of potential molecular targets implicated in the dysregulation of OL function and maturation in AD. First, we observed that Aβo elevated MYRF protein levels without altering the mRNA levels of *Myrf* and its genetic inducer, *Sox10*. In addition, using Puro-PLA (tom Dieck et al., 2015) to directly visualize newly synthesized MYRF levels, we discovered that the longer the Aβo treatment, the lower MYRF protein synthesis was. This intriguing result suggested the presence of a negative feedback loop that inhibits MYRF synthesis in response to Aβo-induced aberrantly increased protein levels, consistent with the critical necessity for tightly regulating MYRF levels. However, prolonged exposure to Aβo may ultimately result in MYRF depletion, affecting OL population homeostasis and long-term myelin maintenance. This could correlate with advanced stages of AD.

These results collectively indicate that the Aβo-triggered MYRF increase likely involves posttranslational mechanisms rather than regulation at the transcriptional and translational levels. Specifically, using a CHX chase assay we revealed that Aβo inhibits the degradation of nuclear MYRF fragment, thereby prolonging its half-life. The pathway responsible for MYRF degradation remains poorly understood. To date, the only investigation has been conducted in mHepa cells, where researchers propose that GSK3 phosphorylates N-MYRF at serine residues, enabling its recognition by the E3 ligase Fbxw7 for ubiquitination and subsequent degradation via the proteasome (Nakayama et al., 2018). Nonetheless, this process has not been explored in OLs or in the context of neurodegenerative disorders like AD. Hence, our subsequent objective was to determine the specific stage at which Aβo exert its effect.

First, we focused on investigating GSK3 and GSK3-induced phosphorylation of MYRF. Glycogen synthase 3β is recognized as a pivotal kinase involved in the aberrant phosphorylation of the microtubule-binding protein tau in the process thought to form

neurofibrillary tangles, characteristic of AD pathology (Hanger et al., 1992; Mandelkow et al., 1992). Additionally, GSK3 serves as a crucial mediator of various proliferation and differentiation signals governing cell fate. Its inhibition has been extensively explored in the past years as a potential therapeutic avenue for AD (Avila & Hernández, 2007), but the results are contradictory regarding whether GSK3 inhibition positively or negatively regulates OL differentiation (Azim & Butt, 2011; Zhou et al., 2014). Remarkably, our findings revealed a decrease in GSK3-mediated phosphoserine levels in MYRF, together with elevated levels of inhibitory Ser21/9 phosphorylation of the kinase following Aβo treatments. This suggested that under our experimental conditions (3 and 24 h of 1 µM Aβo), Aβo inhibit GSK3-mediated phosphorylation of MYRF and its subsequent degradation, resulting in the nuclear accumulation of MYRF and a potential induction of OL differentiation. This finding goes against the majority of investigations claiming GSK3 activation, but aligns with a study reporting that GSK3β inhibition promotes OL differentiation via the canonical Wnt/β-catenin pathway (Azim & Butt, 2011). Accordingly, we also noted a modest increase in β-catenin levels in the presence of Aβo, which serves as an indirect indicator of GSK3 activity. β-catenin, another substrate of GSK3, functions as a transcriptional co-activator, modulating the expression of genes involved in various cellular processes including proliferation and differentiation. Its nuclear accumulation is controlled by GSK3-mediated phosphorylation, which targets it for degradation. Hence, elevated β-catenin levels correlate with diminished GSK3 activity. Moreover, β-catenin may also be acting together with MYRF to induce OL differentiation in response to Aβo.

Next, we aimed to explore upstream regulatory factors involved in the inhibition of GSK3. The inhibitory phosphorylation of GSK3 is mediated by a complex interplay of various kinases and phosphatases, including PKC. Previous investigations have reported increased PKC activity in response to Aβ both in astrocytes (Abramov & Duchen, 2005; Wyssenbach et al., 2016) and neurons (Manterola et al., 2013; Ortiz-Sanz et al., 2022). In our study, we found a similar increase in PKC activation in OLs upon exposure to Aβo. Interestingly, recent research conducted using the human oligodendrocytic cell line MO3.13 demonstrated that PKC activation promotes oligodendroglial maturation (Damato et al., 2021). This finding aligns with our proposed signaling pathway, wherein Aβo-induced PKC activation leads to the inhibition of GSK3, resulting in sustained nuclear MYRF stability and the subsequent induction of OL differentiation.

Following the degradation pathway, GSK3-mediated MYRF phosphorylation is subsequently recognized by Fbxw7, leading to MYRF ubiquitination (Nakayama et al., 2018). While Nakayama and colleagues were the first researchers to identify MYRF as a target of Fbxw7, the involvement of this E3 ligase in OLs and myelin is not new. Mutations in Fbxw7 have been associated with the excessive formation of OL lineage cells (Snyder et al., 2012) and ectopic and excessive myelination in both OLs (Kearns et al., 2015) and Schwann cells (Harty et al., 2019). Authors proposed that Fbxw7 modulates myelination by negatively regulating mTOR; however, further investigation to explore the implication of MYRF in this context would be of interest, as would align with our proposed signaling pathway.

When examining MYRF ubiquitination, we observed an intriguing significant increase in Fbxw7-dependent N-MYRF ubiquitin levels in the presence of Aβo. Moreover, this ubiquitination was found to be non-proteolytic, as MYRF levels were slightly yet significantly increased. Although we did not detect changes in Fbxw7 expression levels in Aβo-treated primary cultured OLs, it is possible that Fbxw7 exhibits enhanced E3 ligase activity or induces a non-physiological ubiquitination of MYRF due to its altered serine phosphorylation status. With seven internal lysine residues in the ubiquitin protein, different types of polyubiquitin chains can be formed, each with distinct functions (Glickman & Ciechanover, 2002; Kulathu & Komander, 2012; Tramutola et al., 2018). Our preliminary results suggest that Aβo alter the type of ubiquitination that Fbxw7 uses to label MYRF, showing a higher propensity for the non-proteolytic K63 ubiquitination compared to vehicle-treated cells. If confirmed, this result would indicate that in the presence of Aβo, Fbxw7-mediated ubiquitination of MYRF promotes its protein stability rather than degradation. Interestingly, a new research reported that the E3 ubiquitin ligase RNF220 targets Olig1 and Olig2 for K63 ubiquitination and stabilization during oligodendroglial development (Li et al., 2024). This finding underscores the importance of K63 ubiquitination in oligodendroglial biological processes, and emphasizes the necessity of precisely regulating the activity of E3 ubiquitin ligases to ensure proper functioning.

This dysregulation of the ubiquitination process aligns with our RNA-seq analysis of OLs isolated from 3xTg-AD mice, wherein the Gene Ontology term “proteasome-mediated ubiquitin-dependent protein catabolic process” emerged as one of the most differentially expressed, predominantly upregulated in 3xTg-AD. In OLs, disruptions in the

ubiquitin-proteasome system can impair the clearance of misfolded proteins, culminating in their aggregation and accumulation within the brains of AD patients. This phenomenon compromises cellular function, leading to disrupted myelin integrity, synaptic loss and functional impairments, thereby exacerbating neurodegeneration (Tramutola et al., 2018). Notably, elevated levels of ubiquitin were detected in brain homogenates and CSF samples of AD patients (Kudo et al., 1994). While the upregulation of UPS-related genes may initially appear as an adaptive response to proteotoxic stress induced by AD-associated aggregation pathologies, excessive ubiquitination can overwhelm the UPS machinery, impeding proper protein degradation and subsequently disrupting essential cellular processes such as protein synthesis, signaling pathways, and energy metabolism. This could contribute to the progression of neurodegeneration and even prompt cell death. Furthermore, considering the diversity of E3 ligases and their specific targets, dysregulated ubiquitination may lead to multifaceted consequences for the cell.

Overall, we describe that Aβo disrupt nuclear MYRF degradation by interfering with the PKC/GSK3 signaling pathway and Fbxw7-mediated ubiquitination. This disruption may lead to ineffective clearance of MYRF, resulting in aberrantly increased transcriptional activity that impacts OLs and myelin.

6. PKC inhibition alleviates Amyloid β-induced oligodendrocyte and myelin alterations

Our last objective was to pharmacologically modulate the effects of Aβo on MYRF, OLs, and myelin in AD models. We postulated that the dysregulation of MYRF is responsible for the observed disruptions in OLs and myelin, prompting us to intervene in the altered MYRF degradation pathway. We hypothesized that the Aβo-induced reduced MYRF phosphorylation might be the trigger to initiate subsequent events that disturb MYRF degradation in the presence of Aβo, including the non-physiological ubiquitination of MYRF mediated by Fbxw7. However, activating GSK3 would not be an appropriate strategy due to its implication in AD pathology. Therefore, we opted to inhibit PKC to counteract its hyperactivation driven by Aβo, aiming to restore GSK3 activity to physiological levels.

The diversity of PKC isoforms and respective available inhibitors makes a complex field of study, leading to discrepancies in the literature. For instance, while some researchers

describe therapeutic effects of PKC activation in AD models (Etcheberrigaray et al., 2004), others demonstrate that specific inhibition of PKCδ reverses AD phenotypes (Du et al., 2018). Although PKC modulation has been explored in numerous studies in the context of AD, they do not usually specifically address its effects on OL and myelin dysfunctions. Thus, before progressing to *in vivo* studies, we assessed the impact of the pan-PKC inhibitor Gö6983 on the Aβo-induced aberrant increase of N-MYRF levels in OLs *in vitro*. We observed that PKC inhibition significantly and completely prevented the Aβo-induced N-MYRF increase, maintaining control N-MYRF levels; so we moved on into our *in vivo* models.

Starting with the biologically simpler model, Aβo-injected zebrafish larvae were treated with Gö6983 via bath immersion. To ensure adequate drug penetration, a higher concentration was utilized compared to *in vitro* studies, while still maintaining subtoxic levels, as evidenced by larval survival. PKC inhibition effectively reversed both Aβo-induced precocious OL differentiation and maturation, as well as the resulting hypermyelination. Interestingly, this outcome not only confirmed Gö6983's efficacy in mitigating OL and myelin alterations induced by Aβo in the developing spinal cord of zebrafish larvae, but it also highlighted PKC's involvement in these biological processes. Interestingly, regarding the previously mentioned role of Fyn kinase in myelin modulation (Czopka et al., 2013), our findings suggest that PKC inhibition counteracts the effects of Fyn on myelin, which indicates that both kinases potentially act through a common pathway. However, whether PKC acts upstream or downstream of Fyn is yet to be elucidated.

While the zebrafish model is ideal to study both OLs and myelination *in vivo*, the 3xTg-AD model represents a more clinically relevant and complex biological system. To assess whether PKC inhibition could reverse at least some of the observed alterations in 3xTg-AD mice, animals were surgically implanted with osmotic minipumps for continuous ICV infusion of vehicle or Gö6983 for 28 days. PKC inhibition effectively reduced MYRF levels in the dentate gyrus and hippocampus, restored OL population homeostasis, and, more importantly, reverted at least part of the OL loss in the dentate gyrus of 3xTg-AD mice. Although Gö6983 is a pan-PKC inhibitor, it has a preference for classic PKCs. However, the next step would be to determine the specific isoform involved in this mechanism.

Altogether, our study validates PKC inhibition as a promising pharmacological strategy for ameliorating OL and myelin disruptions resulting from Aβo-induced MYRF dysregulation, both in zebrafish and 3xTg-AD mouse models *in vivo*.

Conclusions

CONCLUSIONS

1. 3xTg-AD mice show changes in oligodendroglial population dynamics, characterized by promoted maturation and region-specific oligodendrocyte loss. Interestingly, these alterations were triggered, at least partially, by the presence of Aβo, as corroborated by intracerebral injection of Aβo in WT mice.

2. The study of gene expression patterns in oligodendrocytes from 3xTg-AD mice unveiled disturbances in critical signaling pathways governing cell homeostasis and myelin formation. These alterations, particularly affecting pathways such as ubiquitination, autophagy and lipid metabolism, could serve as indicators of early oligodendroglial dysfunction in the context of Alzheimer's disease.

3. Aβo exposure leads to an increase in MYRF levels both *in vitro* and *in vivo*, with prolonged MYRF overexpression exhibiting toxicity to primary cultured oligodendrocytes. These intriguing findings suggest that Aβo-induced MYRF excess may contribute not only to the dysregulation of oligodendrocyte differentiation, but also to the oligodendrocyte loss observed in the dentate gyrus of 3xTg-AD mice.

4. *In vivo* analysis of Aβo-injected zebrafish larvae revealed precocious differentiation and maturation of oligodendrocytes, resulting in excessive myelination in the dorsal spinal cord. This phenomenon was manifested by altered expressions of *myrf* and *mbp* mRNAs during the larval development, alongside an increase in myelin sheaths per oligodendrocyte and the number of myelinated axons.

5. Aβo disrupt nuclear MYRF degradation by interfering with the PKC/GSK3 signaling pathway and Fbxw7-mediated ubiquitination.

6. We validate PKC inhibition as a promising pharmacological strategy to ameliorate oligodendrocyte and myelin disruptions derived from Aβo-induced MYRF dysregulation, both in zebrafish and 3xTg-AD mouse models.

Altogether, the results included in this doctoral thesis unveil and describe an amyloid β-triggered aberrant signaling for MYRF degradation, with potential functional implications over oligodendrocytes and myelin. These multi effects can contribute to the disease onset and progression of Alzheimer's disease pathology.

References

REFERENCES

Abramov, A. Y., & Duchen, M. R. (2005). The role of an astrocytic NADPH oxidase in the neurotoxicity of amyloid beta peptides. *Philosophical Transactions of the Royal Society B: Biological Sciences*, *360*(1464), 2309–2314. https://doi.org/10.1098/rstb.2005.1766

Allen, N. J., & Lyons, D. A. (2018). Glia as architects of central nervous system formation and function. In *Science* (Vol. 362, Issue 6411, pp. 181–185). Science. https://doi.org/10.1126/science.aat0473

Almeida, Rafael G., Czopka, T., Ffrench-Constant, C., & Lyons, D. A. (2011). Individual axons regulate the myelinating potential of single oligodendrocytes in vivo. *Development*, *138*(20), 4443–4450. https://doi.org/10.1242/dev.071001

Almeida, Rafael Góis. (2018). The rules of attraction in central nervous system myelination. In *Frontiers in Cellular Neuroscience* (Vol. 12, p. 420225). Frontiers Media S.A. https://doi.org/10.3389/fncel.2018.00367

An, H., Fan, C., Sharif, M., Kim, D., Poitelon, Y., & Park, Y. (2020). Functional mechanism and pathogenic potential of MYRF ICA domain mutations implicated in birth defects. *Scientific Reports*, *10*(1). https://doi.org/10.1038/s41598-020-57593-8

Anders, S., Pyl, P. T., & Huber, W. (2015). HTSeq-A Python framework to work with high-throughput sequencing data. *Bioinformatics*, *31*(2), 166–169. https://doi.org/10.1093/bioinformatics/btu638

Andrews, S. (2020). Babraham Bioinformatics - FastQC A Quality Control tool for High Throughput Sequence Data. *Soil*, *5*(1), 47–81. https://www.bioinformatics.babraham.ac.uk/projects/fastqc/

Aprato, J., Sock, E., Weider, M., Elsesser, O., Fröb, F., & Wegner, M. (2020). Myrf guides target gene selection of transcription factor Sox10 during oligodendroglial development. *Nucleic Acids Research*, *48*(3), 1254–1270. https://doi.org/10.1093/nar/gkz1158

Bartzokis, G. (2011). Alzheimer's disease as homeostatic responses to age-related myelin breakdown. In *Neurobiology of Aging* (Vol. 32, Issue 8, pp. 1341–1371). Elsevier. https://doi.org/10.1016/j.neurobiolaging.2009.08.007

Bartzokis, G., Cummings, J. L., Sultzer, D., Henderson, V. W., Nuechterlein, K. H., & Mintz, J. (2003). White matter structural integrity in healthy aging adults and patients with Alzheimer disease: A magnetic resonance imaging study. *Archives of Neurology*, *60*(3), 393–398. https://doi.org/10.1001/archneur.60.3.393

Bartzokis, G., Lu, P. H., Geschwind, D. H., Edwards, N., Mintz, J., & Cummings, J. L. (2006). Apolipoprotein E genotype and age-related myelin breakdown in healthy individuals: Implications for cognitive decline and dementia. *Archives of General Psychiatry*, *63*(1), 63–72. https://doi.org/10.1001/archpsyc.63.1.63

Bauer, N. G., Richter-Landsberg, C., & Ffrench-Constant, C. (2009). Role of the oligodendroglial cytoskeleton in differentiation and myelination. In *GLIA* (Vol. 57, Issue 16, pp. 1691–1705). Glia. https://doi.org/10.1002/glia.20885

Baumann, N., & Pham-Dinh, D. (2001). *Biology of Oligodendrocyte and Myelin in the Mammalian Central Nervous System*. http://physrev.physiology.org

Behrendt, G., Baer, K., Buffo, A., Curtis, M. A., Faull, R. L., Rees, M. I., Götz, M., & Dimou, L. (2013). Dynamic changes in myelin aberrations and oligodendrocyte generation in chronic amyloidosis in mice and men. *GLIA*, *61*(2), 273–286. https://doi.org/10.1002/glia.22432

Beurel, E., Grieco, S. F., & Jope, R. S. (2015). Glycogen synthase kinase-3 (GSK3): Regulation, actions, and diseases. In *Pharmacology and Therapeutics* (Vol. 148, pp. 114–131). https://doi.org/10.1016/j.pharmthera.2014.11.016

Braak, H., & Braak, E. (1995). Staging of alzheimer's disease-related neurofibrillary changes. *Neurobiology of Aging*, *16*(3), 271–278. https://doi.org/10.1016/0197-4580(95)00021-6

Buckley, C. E., Marguerie, A., Alderton, W. K., & Franklin, R. J. M. (2010). Temporal dynamics of myelination in the zebrafish spinal cord. *GLIA*, *58*(7), 802–812. https://doi.org/10.1002/glia.20964

Bujalka, H., Koenning, M., Jackson, S., Perreau, V. M., & Pope, B. (2013). MYRF Is a Membrane-Associated Transcription Factor That Autoproteolytically Cleaves to Directly Activate Myelin Genes. *PLoS Biol*, *11*(8), 1001625. https://doi.org/10.1371/journal.pbio.1001625

Butt, A. M., Hamilton, N., Hubbard, P., Pugh, M., & Ibrahim, M. (2005). Synantocytes: The fifth element. In *Journal of Anatomy* (Vol. 207, Issue 6, pp. 695–706). https://doi.org/10.1111/j.1469-7580.2005.00458.x

Cahoy, J. D., Emery, B., Kaushal, A., Foo, L. C., Zamanian, J. L., Christopherson, K. S., Xing, Y., Lubischer, J. L., Krieg, P. A., Krupenko, S. A., Thompson, W. J., & Barres, B. A. (2008). A transcriptome database for astrocytes, neurons, and oligodendrocytes: A new resource for understanding brain development and function. *Journal of Neuroscience*, *28*(1), 264–278. https://doi.org/10.1523/JNEUROSCI.4178-07.2008

Cassar, S., Adatto, I., Freeman, J. L., Gamse, J. T., Lawrence, C., Muriana, A., Peterson, R. T., Van Cruchten, S., & Zon, L. I. (2020). Use of Zebrafish in Drug Discovery Toxicology HHS Public Access. *Chem Res Toxicol*, *33*(1), 95–118. https://doi.org/10.1021/acs.chemrestox.9b00335

Cavaliere, F., Benito-Muñoz, M., Panicker, M., & Matute, C. (2013). NMDA modulates oligodendrocyte differentiation of subventricular zone cells through PKC activation. *Frontiers in Cellular Neuroscience*, *7*(DEC). https://doi.org/10.3389/fncel.2013.00261

Chacon-De-La-Rocha, I., Fryatt, G., Rivera, A. D., Verkhratsky, A., Raineteau, O., Gomez-Nicola, D., & Butt, A. M. (2020). Accelerated Dystrophy and Decay of Oligodendrocyte Precursor Cells in the APP/PS1 Model of Alzheimer's-Like Pathology. *Frontiers in Cellular Neuroscience*, *14*. https://doi.org/10.3389/fncel.2020.575082

Chamberlain, K. A., Huang, N., Xie, Y., LiCausi, F., Li, S., Li, Y., & Sheng, Z. H. (2021). Oligodendrocytes enhance axonal energy metabolism by deacetylation of mitochondrial proteins through transcellular delivery of SIRT2. *Neuron*, *109*(21), 3456-3472.e8. https://doi.org/10.1016/j.neuron.2021.08.011

Chen, B., Zhu, Y., Ye, S., & Zhang, R. (2018). Structure of the DNA-binding domain of human myelin-gene regulatory factor reveals its potential protein-DNA recognition mode. *Journal of Structural Biology*, *203*(2), 170–178. https://doi.org/10.1016/j.jsb.2018.04.007

Chen, J. F., Liu, K., Hu, B., Li, R. R., Xin, W., Chen, H., Wang, F., Chen, L., Li, R. X., Ren, S. Y., Xiao, L., Chan, J. R., & Mei, F. (2021). Enhancing myelin renewal reverses cognitive dysfunction in a murine model of Alzheimer's disease. *Neuron*, *109*(14), 2292-2307.e5. https://doi.org/10.1016/j.neuron.2021.05.012

Chia, L. S., Thompson, J. E., & Moscarello, M. A. (1984). X-ray diffraction evidence for myelin disorder in brain from humans with alzheimer's disease. *BBA - Biomembranes*, *775*(3), 308–312. https://doi.org/10.1016/0005-2736(84)90185-8

Choi, J. ok, Fan, C., Kim, D., Sharif, M., An, H., & Park, Y. (2018). Elucidating the transactivation domain of the pleiotropic transcription factor Myrf. *Scientific Reports*, *8*(1), 1–9. https://doi.org/10.1038/s41598-018-31477-4

Chu, C. T., Plowey, E. D., Wang, Y., Patel, V., & Jordan-Sciutto, K. L. (2007). Location, location, location: Altered transcription factor trafficking in neurodegeneration. In *Journal of Neuropathology and Experimental Neurology* (Vol. 66, Issue 10, pp. 873–883). https://doi.org/10.1097/nen.0b013e318156a3d7

Ciechanover, A., & Schwartz, A. L. (1998). The ubiquitin-proteasome pathway: The complexity and myriad functions of proteins death. In *Proceedings of the National Academy of Sciences of the United States of America* (Vol. 95, Issue 6, pp. 2727–2730). National Academy of Sciences. https://doi.org/10.1073/pnas.95.6.2727

Cole, A., Frame, S., & Cohen, P. (2004). Further evidence that the tyrosine phosphorylation of glycogen synthase kinase-3 (GSK3) in mammalian cells is an autophosphorylation event. *Biochemical Journal*, *377*(1), 249–255. https://doi.org/10.1042/BJ20031259

Colognato, H., & Tzvetanova, I. D. (2011). Glia unglued: How signals from the extracellular matrix regulate the development of myelinating glia. *Developmental Neurobiology*, *71*(11), 924–955. https://doi.org/10.1002/dneu.20966

Crotty, P., Sangrey, T., & Levy, W. B. (2006). Metabolic energy cost of action potential velocity. *Journal of Neurophysiology*, *96*(3), 1237–1246. https://doi.org/10.1152/jn.01204.2005

Czopka, T., Ffrench-Constant, C., & Lyons, D. A. (2013). Individual oligodendrocytes have only a few hours in which to generate new myelin sheaths invivo. *Developmental Cell*, *25*(6), 599–609. https://doi.org/10.1016/j.devcel.2013.05.013

Dahlgren, K. N., Manelli, A. M., Blaine Stine, W., Baker, L. K., Krafft, G. A., & Ladu, M. J. (2002). Oligomeric and fibrillar species of amyloid-β peptides differentially affect neuronal viability. *Journal of Biological Chemistry*, *277*(35), 32046–32053. https://doi.org/10.1074/jbc.M201750200

Dai, J., Bercury, K. K., Ahrendsen, J. T., & Macklin, W. B. (2015). Olig1 function is required for oligodendrocyte differentiation in the mouse brain. *Journal of Neuroscience*, *35*(10), 4386–4402. https://doi.org/10.1523/JNEUROSCI.4962-14.2015

Damato, M., Cardon, T., Wisztorski, M., Fournier, I., Pieragostino, D., Cicalini, I., Salzet, M., Vergara, D., & Maffia, M. (2021). Protein kinase c activation drives a differentiation program in an oligodendroglial precursor model through the modulation of specific biological networks. *International Journal of Molecular Sciences*, *22*(10). https://doi.org/10.3390/ijms22105245

Damoiseaux, J. S., Smith, S. M., Witter, M. P., Sanz-Arigita, E. J., Barkhof, F., Scheltens, P., Stam, C. J., Zarei, M., & Rombouts, S. A. R. B. (2009). White matter tract integrity in aging and alzheimer's disease. *Human Brain Mapping*, *30*(4), 1051–1059. https://doi.org/10.1002/hbm.20563

Dawson, M. R. L., Polito, A., Levine, J. M., & Reynolds, R. (2003). NG2-expressing glial progenitor cells: An abundant and widespread population of cycling cells in the adult rat CNS. *Molecular and Cellular Neuroscience*, *24*(2), 476–488. https://doi.org/10.1016/S1044-7431(03)00210-0

de la Fuente, A. G., Queiroz, R. M. L., Ghosh, T., McMurran, C. E., Cubillos, J. F., Bergles, D. E., Fitzgerald, D. C., Jones, C. A., Lilley, K. S., Glover, C. P., & Franklin, R. J. M. (2020). Changes in the Oligodendrocyte Progenitor Cell Proteome with Ageing. *Molecular & Cellular Proteomics : MCP*, *19*(8), 1281–1302. https://doi.org/10.1074/MCP.RA120.002102

de la Monte, S. M. (1989). Quantitation of cerebral atrophy in preclinical and end-stage alzheimer's disease. *Annals of Neurology*, *25*(5), 450–459. https://doi.org/10.1002/ana.410250506

Depp, C., Sun, T., Sasmita, A. O., Spieth, L., Berghoff, S. A., Nazarenko, T., Overhoff, K., Steixner-Kumar, A. A., Subramanian, S., Arinrad, S., Ruhwedel, T., Möbius, W., Göbbels, S., Saher, G., Werner, H. B., Damkou, A., Zampar, S., Wirths, O., Thalmann, M., … Nave, K. A. (2023). Myelin dysfunction drives amyloid-β deposition in models of Alzheimer's disease. *Nature*, *618*(7964), 349–357. https://doi.org/10.1038/s41586-023-06120-6

Desai, M. K., Mastrangelo, M. A., Ryan, D. A., Sudol, K. L., Narrow, W. C., & Bowers, W. J. (2010). Early oligodendrocyte/myelin pathology in Alzheimer's disease mice constitutes a novel therapeutic target. *American Journal of Pathology*, *177*(3), 1422–1435. https://doi.org/10.2353/ajpath.2010.100087

Desai, M. K., Sudol, K. L., Janelsins, M. C., Mastrangelo, M. A., Frazer, M. E., & Bowers, W. J. (2009). Triple-transgenic Alzheimer's disease mice exhibit region-specific abnormalities in brain myelination patterns prior to appearance of amyloid and tau pathology. *GLIA*, *57*(1), 54–65. https://doi.org/10.1002/glia.20734

Desterro, J. M. P., Rodriguez, M. S., & Hay, R. T. (2000). Regulation of transcription factors by protein degradation. In *Cellular and Molecular Life Sciences* (Vol. 57, Issues 8–9, pp. 1207–1219). https://doi.org/10.1007/PL00000760

Deture, M. A., & Dickson, D. W. (2019). The neuropathological diagnosis of Alzheimer's disease. In *Molecular Neurodegeneration* (Vol. 14, Issue 1). Mol Neurodegener. https://doi.org/10.1186/s13024-019-0333-5

Dimou, L., Simon, C., Kirchhoff, F., Takebayashi, H., & Götz, M. (2008). Progeny of Olig2-expressing progenitors in the gray and white matter of the adult mouse cerebral cortex. *Journal of Neuroscience*, *28*(41), 10434–10442. https://doi.org/10.1523/JNEUROSCI.2831-08.2008

Dobin, A., Davis, C. A., Schlesinger, F., Drenkow, J., Zaleski, C., Jha, S., Batut, P., Chaisson, M., & Gingeras, T. R. (2013). STAR: Ultrafast universal RNA-seq aligner. *Bioinformatics*, *29*(1), 15–21. https://doi.org/10.1093/bioinformatics/bts635

Doble, B. W., & Woodgett, J. R. (2003). GSK-3: Tricks of the trade for a multi-tasking kinase. In *Journal of Cell Science* (Vol. 116, Issue 7, pp. 1175–1186). https://doi.org/10.1242/jcs.00384

Dong, Y. X., Zhang, H. Y., Li, H. Y., Liu, P. H., Sui, Y., & Sun, X. H. (2018). Association between Alzheimer's disease pathogenesis and early demyelination and oligodendrocyte dysfunction. *Neural Regeneration Research*, *13*(5), 908–914. https://doi.org/10.4103/1673-5374.232486

Elbaz, B., & Popko, B. (2019). Molecular Control of Oligodendrocyte Development. In *Trends in Neurosciences* (Vol. 42, Issue 4, pp. 263–277). Trends Neurosci. https://doi.org/10.1016/j.tins.2019.01.002

Elu, N., Osinalde, N., Beaskoetxea, J., Ramirez, J., Lectez, B., Aloria, K., Rodriguez, J. A., Arizmendi, J. M., & Mayor, U. (2019). Detailed dissection of UBe3A-mediated DDI1 ubiquitination. *Frontiers in Physiology*, *10*(MAY), 534. https://doi.org/10.3389/fphys.2019.00534

Emery, B. (2010). Regulation of oligodendrocyte differentiation and myelination. In *Science* (Vol. 330, Issue 6005, pp. 779–782). https://doi.org/10.1126/science.1190927

Emery, B., Agalliu, D., Cahoy, J. D., Watkins, T. A., Dugas, J. C., Mulinyawe, S. B., Ibrahim, A., Ligon, K. L., Rowitch, D. H., & Barres, B. A. (2009). Myelin Gene Regulatory Factor Is a Critical Transcriptional Regulator Required for CNS Myelination. *Cell*, *138*(1), 172–185. https://doi.org/10.1016/j.cell.2009.04.031

Falcão, A. M., van Bruggen, D., Marques, S., Meijer, M., Jäkel, S., Agirre, E., Samudyata, Floriddia, E. M., Vanichkina, D. P., Ffrench-Constant, C., Williams, A., Guerreiro-Cacais, A. O., & Castelo-Branco, G. (2018). Disease-specific oligodendrocyte lineage cells arise in multiple sclerosis. *Nature Medicine*, *24*(12), 1837–1844. https://doi.org/10.1038/s41591-018-0236-y

Ferreira, S., Pitman, K. A., Wang, S., Summers, B. S., Bye, N., Young, K. M., & Cullen, C. L. (2020). Amyloidosis is associated with thicker myelin and increased oligodendrogenesis in the adult mouse brain. *Journal of Neuroscience Research*, *98*(10), 1905–1932. https://doi.org/10.1002/jnr.24672

Fessel, J. (2022). Reversing Alzheimer's disease dementia with clemastine, fingolimod, or rolipram, plus anti-amyloid therapy. *Alzheimer's and Dementia: Translational Research and Clinical Interventions*, *8*(1). https://doi.org/10.1002/trc2.12242

Fields, R. D. (2015). A new mechanism of nervous system plasticity: Activity-dependent myelination. In *Nature Reviews Neuroscience* (Vol. 16, Issue 12, pp. 756–767). Nature Publishing Group. https://doi.org/10.1038/nrn4023

Fletcher, J. L., Makowiecki, K., Cullen, C. L., & Young, K. M. (2021). Oligodendrogenesis and myelination regulate cortical development, plasticity and circuit function. In *Seminars in Cell and Developmental Biology* (Vol. 118, pp. 14–23). Academic Press. https://doi.org/10.1016/j.semcdb.2021.03.017

Fletcher, J. L., Murray, S. S., & Xiao, J. (2018). Brain-derived neurotrophic factor in central nervous system myelination: A new mechanism to promote myelin plasticity and repair. In *International Journal of Molecular Sciences* (Vol. 19, Issue 12). Multidisciplinary Digital Publishing Institute (MDPI). https://doi.org/10.3390/ijms19124131

Flores, A. I., Narayanan, S. P., Morse, E. N., Shick, H. E., Yin, X., Kidd, G., Avila, R. L., Kirschner, D. A., & Macklin, W. B. (2008). Constitutively active Akt induces enhanced myelination in the CNS. *Journal of Neuroscience*, *28*(28), 7174–7183. https://doi.org/10.1523/JNEUROSCI.0150-08.2008

Forbes, T. A., & Gallo, V. (2017). All Wrapped Up: Environmental Effects on Myelination. In *Trends in Neurosciences* (Vol. 40, Issue 9, pp. 572–587). Trends Neurosci. https://doi.org/10.1016/j.tins.2017.06.009

Fornasiero, E. F., Mandad, S., Wildhagen, H., Alevra, M., Rammner, B., Keihani, S., Opazo, F., Urban, I., Ischebeck, T., Sakib, M. S., Fard, M. K., Kirli, K., Centeno, T. P., Vidal, R. O., Rahman, R. U., Benito, E., Fischer, A., Dennerlein, S., Rehling, P., … Rizzoli, S. O. (2018). Precisely measured protein lifetimes in the mouse brain reveal differences across tissues and subcellular fractions. *Nature Communications*, *9*(1), 1–17. https://doi.org/10.1038/s41467-018-06519-0

Frescas, D., & Pagano, M. (2008). Deregulated proteolysis by the F-box proteins SKP2 and β-TrCP: Tipping the scales of cancer. In *Nature Reviews Cancer* (Vol. 8, Issue 6, pp. 438–449). Nat Rev Cancer. https://doi.org/10.1038/nrc2396

Gaesser, J. M., & Fyffe-Maricich, S. L. (2016). Intracellular signaling pathway regulation of myelination and remyelination in the CNS. In *Experimental Neurology* (Vol. 283, Issue Pt B, pp. 501–511). Exp Neurol. https://doi.org/10.1016/j.expneurol.2016.03.008

Galloway, D. A., & Moore, C. S. (2016). MiRNAs as emerging regulators of oligodendrocyte development and differentiation. In *Frontiers in Cell and Developmental Biology* (Vol. 4, Issue JUN, p. 59). Frontiers Media SA. https://doi.org/10.3389/fcell.2016.00059

Games, D., Adams, D., Alessandrini, R., Barbour, R., Borthelette, P., Blackwell, C., Carr, T., Clemens, J., Donaldson, T., Gillespie, F., Guido, T., Hagopian, S., Johnson-Wood, K., Khan, K., Lee, M., Leibowitz, P., Lieberburg, I., Little, S., Masliah, E., … Zhao, J. (1995). Alzheimer-type neuropathology in transgenic mice overexpressing V717F β-amyloid precursor protein. *Nature*, *373*(6514), 523–527. https://doi.org/10.1038/373523a0

Gao, C. H., Yu, G., & Cai, P. (2021). ggVennDiagram: An Intuitive, Easy-to-Use, and Highly Customizable R Package to Generate Venn Diagram. *Frontiers in Genetics*, *12*. https://doi.org/10.3389/fgene.2021.706907

Garg, R., Benedetti, L. G., Abera, M. B., Wang, H., Abba, M., & Kazanietz, M. G. (2014). Protein kinase C and cancer: What we know and what we do not. In *Oncogene* (Vol. 33, Issue 45, pp. 5225–5237). Oncogene. https://doi.org/10.1038/onc.2013.524

Garnai, S. J., Brinkmeier, M. L., Emery, B., Aleman, T. S., Pyle, L. C., Veleva-Rotse, B., Sisk, R. A., Rozsa, F. W., Ozel, A. B., Li, J. Z., Moroi, S. E., Archer, S. M., Lin, C. M., Sheskey, S., Wiinikka-Buesser, L., Eadie, J., Urquhart, J. E., Black, G. C. M., Othman, M. I., … Wegener, M. (2019). Variants in myelin regulatory factor (MYRF) cause autosomal dominant and syndromic nanophthalmos in humans and retinal degeneration in mice. *PLoS Genetics*, *15*(5). https://doi.org/10.1371/journal.pgen.1008130

Garnier-Crussard, A., Bougacha, S., Wirth, M., Dautricourt, S., Sherif, S., Landeau, B., Gonneaud, J., De Flores, R., de la Sayette, V., Vivien, D., Krolak-Salmon, P., & Chételat, G. (2022). White matter hyperintensity topography in Alzheimer's disease and links to cognition. *Alzheimer's and Dementia*, *18*(3), 422–433. https://doi.org/10.1002/alz.12410

Garrido, J. L., Godoy, J. A., Alvarez, A., Bronfman, M., & Inestrosa, N. C. (2002). Protein kinase C inhibits amyloid beta peptide neurotoxicity by acting on members of the Wnt pathway. *The FASEB Journal : Official Publication of the Federation of American Societies for Experimental Biology*, *16*(14), 1982–1984. https://doi.org/10.1096/fj.02-0327fje

George, E. K., & Hemachandra Reddy, P. (2019). Can Healthy Diets, Regular Exercise, and Better Lifestyle Delay the Progression of Dementia in Elderly Individuals? In *Journal of Alzheimer's Disease* (Vol. 72, Issue s1, pp. S37–S58). J Alzheimers Dis. https://doi.org/10.3233/JAD-190232

Glabe, C. C. (2005). Amyloid accumulation and pathogensis of Alzheimer's disease: significance of monomeric, oligomeric and fibrillar Abeta. In *Sub-cellular biochemistry* (Vol. 38, pp. 167–177). Subcell Biochem. https://doi.org/10.1007/0-387-23226-5_8

Glickman, M. H., & Ciechanover, A. (2002). The ubiquitin-proteasome proteolytic pathway: Destruction for the sake of construction. In *Physiological Reviews* (Vol. 82, Issue 2, pp. 373–428). American Physiological Society. https://doi.org/10.1152/physrev.00027.2001

Gong, B., Radulovic, M., Figueiredo-Pereira, M. E., & Cardozo, C. (2016). The ubiquitin-proteasome system: Potential therapeutic targets for alzheimer's disease and spinal cord injury. In *Frontiers in Molecular Neuroscience* (Vol. 9, Issue JAN, p. 168119). Frontiers Media S.A. https://doi.org/10.3389/fnmol.2016.00004

Guo, C., Zhao, Z., Chen, D., He, S., Sun, N., Li, Z., Liu, J., Zhang, D., Zhang, J., Li, J., Zhang, M., Ge, J., Liu, X., Zhang, X., & Fan, Z. (2019). Detection of clinically relevant genetic variants in chinese patients with nanophthalmos by trio-based whole-genome sequencing study. *Investigative Ophthalmology and Visual Science*, *60*(8), 2904–2913. https://doi.org/10.1167/iovs.18-26275

Gutzman, J. H., & Sive, H. (2009). Zebrafish brain ventricle injection. *Journal of Visualized Experiments*, *26*(26). https://doi.org/10.3791/1218

Hamanaka, K., Takata, A., Uchiyama, Y., Miyatake, S., Miyake, N., Mitsuhashi, S., Iwama, K., Fujita, A., Imagawa, E., Alkanaq, A. N., Koshimizu, E., Azuma, Y., Nakashima, M., Mizuguchi, T., Saitsu, H., Wada, Y., Minami, S., Katoh-Fukui, Y., Masunaga, Y., … Matsumoto, N. (2019). MYRF haploinsufficiency causes 46,XY and 46,XX disorders of sex development: Bioinformatics consideration. *Human Molecular Genetics*, *28*(14), 2319–2329. https://doi.org/10.1093/hmg/ddz066

Han, S., Gim, Y., Jang, E. H., & Hur, E. M. (2022). Functions and dysfunctions of oligodendrocytes in neurodegenerative diseases. In *Frontiers in Cellular Neuroscience* (Vol. 16, p. 1083159). Frontiers Media S.A. https://doi.org/10.3389/fncel.2022.1083159

Han, X., Holtzman, D. M., McKeel, D. W., Kelley, J., & Morris, J. C. (2002). Substantial sulfatide deficiency and ceramide elevation in very early Alzheimer's disease: Potential role in disease pathogenesis. *Journal of Neurochemistry*, *82*(4), 809–818. https://doi.org/10.1046/j.1471-4159.2002.00997.x

Hardy, J. A., & Higgins, G. A. (1992). Alzheimer's disease: The amyloid cascade hypothesis. In *Science* (Vol. 256, Issue 5054, pp. 184–185). Science. https://doi.org/10.1126/science.1566067

Hartline, D. K. (2008). What is myelin? In *Neuron Glia Biology* (Vol. 4, Issue 2, pp. 153–163). Neuron Glia Biol. https://doi.org/10.1017/S1740925X09990263

Harty, B. L., Coelho, F., Ackerman, S. D., Herbert, A. L., Lyons, D. A., & Monk, K. R. (2018). Fbxw7 is a critical regulator of Schwann cell myelinating potential. *BioRxiv*, 342931. https://doi.org/10.1101/342931

Hegde, A. N., Smith, S. G., Duke, L. M., Pourquoi, A., & Vaz, S. (2019). Perturbations of Ubiquitin-Proteasome-Mediated Proteolysis in Aging and Alzheimer's Disease. In *Frontiers in Aging Neuroscience* (Vol. 11, p. 475441). Frontiers Media S.A. https://doi.org/10.3389/fnagi.2019.00324

Herms, J., Anliker, B., Heber, S., Ring, S., Fuhrmann, M., Kretzschmar, H., Sisodia, S., & Müller, U. (2004). Cortical dysplasia resembling human type 2 lissencephaly in mice lacking all three APP family members. *EMBO Journal*, *23*(20), 4106–4115. https://doi.org/10.1038/sj.emboj.7600390

Hershko, A., & Ciechanover, A. (1998). The ubiquitin system. In *Annual Review of Biochemistry* (Vol. 67, pp. 425–479). Annu Rev Biochem. https://doi.org/10.1146/annurev.biochem.67.1.425

Higuchi, M., Ishihara, T., Zhang, B., Hong, M., Andreadis, A., Trojanowski, J. Q., & Lee, V. M. Y. (2002). Transgenic mouse model of tauopathies with glial pathology and nervous system degeneration. *Neuron*, *35*(3), 433–446. https://doi.org/10.1016/S0896-6273(02)00789-4

Hoeck, J. D., Jandke, A., Blake, S. M., Nye, E., Spencer-Dene, B., Brandner, S., & Behrens, A. (2010). Fbw7 controls neural stem cell differentiation and progenitor apoptosis via Notch and c-Jun. *Nature Neuroscience*, *13*(11), 1365–1372. https://doi.org/10.1038/nn.2644

Horiuchi, M., Maezawa, I., Itoh, A., Wakayama, K., Jin, L. W., Itoh, T., & DeCarli, C. (2012). Amyloid β1-42 oligomer inhibits myelin sheet formation in vitro. *Neurobiology of Aging*, *33*(3), 499–509. https://doi.org/10.1016/j.neurobiolaging.2010.05.007

Hornig, J., Frö B, F., Vogl, M. R., Hermans-Borgmeyer, I., & Tamm, E. R. (2013). The Transcription Factors Sox10 and Myrf Define an Essential Regulatory Network Module in Differentiating Oligodendrocytes. *PLoS Genet*, *9*(10), 1003907. https://doi.org/10.1371/journal.pgen.1003907

Howe, K., Clark, M. D., Torroja, C. F., Torrance, J., Berthelot, C., Muffato, M., Collins, J. E., Humphray, S., McLaren, K., Matthews, L., McLaren, S., Sealy, I., Caccamo, M., Churcher, C., Scott, C., Barrett, J. C., Koch, R., Rauch, G. J., White, S., … Stemple, D. L. (2013). The zebrafish reference genome sequence and its relationship to the human genome. *Nature*, *496*(7446), 498–503. https://doi.org/10.1038/nature12111

Hu, X., Hicks, C. W., He, W., Wong, P., MacKlin, W. B., Trapp, B. D., & Yan, R. (2006). Bace1 modulates myelination in the central and peripheral nervous system. *Nature Neuroscience*, *9*(12), 1520–1525. https://doi.org/10.1038/nn1797

Huang, H., Teng, P., Du, J., Meng, J., Hu, X., Tang, T., Zhang, Z., Qi, Y. B., & Qiu, M. (2018). Interactive repression of MYRF self-cleavage and activity in oligodendrocyte differentiation by TMEM98 protein. *Journal of Neuroscience*, *38*(46), 9829–9839. https://doi.org/10.1523/JNEUROSCI.0154-18.2018

Huang, H., Zhou, F., Zhou, S., & Qiu, M. (2021). MYRF: A Mysterious Membrane-Bound Transcription Factor Involved in Myelin Development and Human Diseases. *Neuroscience Bulletin*, *37*(6), 881–884. https://doi.org/10.1007/s12264-021-00678-9

Huang, J., Guo, X., Li, W., & Zhang, H. (2017). Activation of Wnt/β-catenin signalling via GSK3 inhibitors direct differentiation of human adipose stem cells into functional hepatocytes. *Scientific Reports*, *7*. https://doi.org/10.1038/srep40716

Hughes, K., Nikolakaki, E., Plyte, S. E., Totty, N. F., & Woodgett, J. R. (1993). Modulation of the glycogen synthase kinase-3 family by tyrosine phosphorylation. *The EMBO Journal*, *12*(2), 803–808. https://doi.org/10.1002/j.1460-2075.1993.tb05715.x

Ihara, Y., Morishima-Kawashima, M., & Nixon, R. (2012). The ubiquitin-proteasome system and the autophagic-lysosomal system in Alzheimer disease. *Cold Spring Harbor Perspectives in Medicine*, *2*(8), a006361. https://doi.org/10.1101/cshperspect.a006361

Inano, S., Takao, H., Hayashi, N., Abe, O., & Ohtomo, K. (2011). Effects of age and gender on white matter integrity. *American Journal of Neuroradiology*, *32*(11), 2103–2109. https://doi.org/10.3174/ajnr.A2785

J. Rodríguez, J., M. Butt, A., Gardenal, E., Parpura, V., & Verkhratsky, A. (2016). Complex and Differential Glial Responses in Alzheimers Disease and Ageing. *Current Alzheimer Research*, *13*(4), 343–358. https://doi.org/10.2174/1567205013666160229112911

Jantaratnotai, N., Ryu, J. K., Kim, S. U., & McLarnon, J. G. (2003). Amyloid β peptide-induced corpus callosum damage and glial activation in vivo. *NeuroReport*, *14*(11), 1429–1433. https://doi.org/10.1097/00001756-200308060-00005

Jellinger, K. A. (2010). Basic mechanisms of neurodegeneration: A critical update. *Journal of Cellular and Molecular Medicine*, *14*(3), 457–487. https://doi.org/10.1111/j.1582-4934.2010.01010.x

Jope, R. S., & Johnson, G. V. W. (2004). The glamour and gloom of glycogen synthase kinase-3. In *Trends in Biochemical Sciences* (Vol. 29, Issue 2, pp. 95–102). Elsevier Ltd. https://doi.org/10.1016/j.tibs.2003.12.004

Kaplan, J. D., Stewart, B., Prasov, L., & Pyle, L. C. (1993). MYRF-Related Cardiac Urogenital Syndrome. In *GeneReviews*®. University of Washington, Seattle. https://www.ncbi.nlm.nih.gov/books/NBK586169/

Kavroulakis, E., Simos, P. G., Kalaitzakis, G., Maris, T. G., Karageorgou, D., Zaganas, I., Panagiotakis, S., Basta, M., Vgontzas, A., & Papadaki, E. (2018). Myelin content changes in probable Alzheimer's disease and mild cognitive impairment: Associations with age and severity of neuropsychiatric impairment. *Journal of Magnetic Resonance Imaging*, *47*(5), 1359–1372. https://doi.org/10.1002/jmri.25849

Kearns, C. A., Ravanelli, A. M., Cooper, K., & Appel, B. (2015). Fbxw7 limits myelination by inhibiting mtor signaling. *Journal of Neuroscience*, *35*(44), 14861–14871. https://doi.org/10.1523/JNEUROSCI.4968-14.2015

Kim, D., Choi, J. O., Fan, C., Shearer, R. S., Sharif, M., Busch, P., & Park, Y. (2017). Homo-trimerization is essential for the transcription factor function of Myrf for oligodendrocyte differentiation. *Nucleic Acids Research*, *45*(9), 5112–5125. https://doi.org/10.1093/nar/gkx080

Kim, H. Y., Lee, D. K., Chung, B. R., Kim, H. V., & Kim, Y. (2016). Intracerebroventricular injection of amyloid-beta peptides in normal mice to acutely induce alzheimer-like cognitive deficits. *Journal of Visualized Experiments*, *2016*(109), 53308. https://doi.org/10.3791/53308

Kim, J., Basak, J. M., & Holtzman, D. M. (2009). The Role of Apolipoprotein E in Alzheimer's Disease. In *Neuron* (Vol. 63, Issue 3, pp. 287–303). NIH Public Access. https://doi.org/10.1016/j.neuron.2009.06.026

Kimberly, W. T., Zheng, J. B., Guénette, S. Y., & Selkoe, D. J. (2001). The Intracellular Domain of the β-Amyloid Precursor Protein Is Stabilized by Fe65 and Translocates to the Nucleus in a Notch-like Manner. *Journal of Biological Chemistry*, *276*(43), 40288–40292. https://doi.org/10.1074/jbc.C100447200

Kirby, L., Jin, J., Cardona, J. G., Smith, M. D., Martin, K. A., Wang, J., Strasburger, H., Herbst, L., Alexis, M., Karnell, J., Davidson, T., Dutta, R., Goverman, J., Bergles, D., & Calabresi, P. A. (2019). Oligodendrocyte precursor cells present antigen and are cytotoxic targets in inflammatory demyelination. *Nature Communications*, *10*(1), 1–20. https://doi.org/10.1038/s41467-019-11638-3

Kitada, M., & Rowitch, D. H. (2006). Transcription factor co-expression patterns indicate heterogeneity of oligodendroglial subpopulations in adult spinal cord. *GLIA*, *54*(1), 35–46. https://doi.org/10.1002/glia.20354

Koenning, M., Jackson, S., Hay, C. M., Faux, C., Kilpatrick, T. J., Willingham, M., & Emery, B. (2012). Myelin gene regulatory factor is required for maintenance of myelin and mature oligodendrocyte identity in the adult CNS. *Journal of Neuroscience*, *32*(36), 12528–12542. https://doi.org/10.1523/JNEUROSCI.1069-12.2012

Koepp, D. M., Schaefer, L. K., Ye, X., Keyomarsi, K., Chu, C., Harper, J. W., & Elledge, S. J. (2001). Phosphorylation-dependent ubiquitination of cyctin E by the SCFFbw7 ubiquitin ligase. *Science*, *294*(5540), 173–177. https://doi.org/10.1126/science.1065203

Koreman, E., Sun, X., & Lu, Q. R. (2018). Chromatin remodeling and epigenetic regulation of oligodendrocyte myelination and myelin repair. In *Molecular and Cellular Neuroscience* (Vol. 87, pp. 18–26). NIH Public Access. https://doi.org/10.1016/j.mcn.2017.11.010

Kudo, T., Iqbal, K., Ravid, R., Swaab, D. F., & Grundke-Iqbal, I. (1994). Alzheimer disease: correlation of cerebro-spinal fluid and brain ubiquitin levels. *Brain Research*, *639*(1), 1–7. https://doi.org/10.1016/0006-8993(94)91757-4

Küspert, M., Hammer, A., Bösl, M. R., & Wegner, M. (2011). Olig2 regulates Sox10 expression in oligodendrocyte precursors through an evolutionary conserved distal enhancer. *Nucleic Acids Research*, *39*(4), 1280–1293. https://doi.org/10.1093/nar/gkq951

Küspert, M., & Wegner, M. (2016). SomethiNG 2 talk about—Transcriptional regulation in embryonic and adult oligodendrocyte precursors. In *Brain Research* (Vol. 1638, Issue Pt B, pp. 167–182). Brain Res. https://doi.org/10.1016/j.brainres.2015.07.024

Lee, J. S., Padmanabhan, A., Shin, J., Zhu, S., Guo, F., Kanki, J. P., Epstein, J. A., & Thomas Look, A. (2010). Oligodendrocyte progenitor cell numbers and migration are regulated by the zebrafish orthologs of the NF1 tumor suppressor gene. *Human Molecular Genetics*, *19*(23), 4643–4653. https://doi.org/10.1093/hmg/ddq395

Lee, Y., Morrison, B. M., Li, Y., Lengacher, S., Farah, M. H., Hoffman, P. N., Liu, Y., Tsingalia, A., Jin, L., Zhang, P. W., Pellerin, L., Magistretti, P. J., & Rothstein, J. D. (2012). Oligodendroglia metabolically support axons and contribute to neurodegeneration. *Nature*, *487*(7408), 443–448. https://doi.org/10.1038/nature11314

Lewis, J., McGowan, E., Rockwood, J., Melrose, H., Nacharaju, P., Van Slegtenhorst, M., Gwinn-Hardy, K., Murphy, M. P., Baker, M., Yu, X., Duff, K., Hardy, J., Corral, A., Lin, W. L., Yen, S. H., Dickson, D. W., Davies, P., & Hutton, M. (2000). Neurofibrillary tangles, amyotrophy and progressive motor disturbance in mice expressing mutant (P301L)tau protein. *Nature Genetics*, *25*(4), 402–405. https://doi.org/10.1038/78078

Li, Z., Park, Y., & Marcotte, E. M. (2013). A Bacteriophage Tailspike Domain Promotes Self-Cleavage of a Human Membrane-Bound Transcription Factor, the Myelin Regulatory Factor MYRF. *PLoS Biology*, *11*(8), e1001624. https://doi.org/10.1371/journal.pbio.1001624

Linding, R., Jensen, L. J., Ostheimer, G. J., van Vugt, M. A. T. M., Jørgensen, C., Miron, I. M., Diella, F., Colwill, K., Taylor, L., Elder, K., Metalnikov, P., Nguyen, V., Pasculescu, A., Jin, J., Park, J. G., Samson, L. D., Woodgett, J. R., Russell, R. B. B., Bork, P., … Pawson, T. (2007). Systematic Discovery of In Vivo Phosphorylation Networks. *Cell*, *129*(7), 1415–1426. https://doi.org/10.1016/j.cell.2007.05.052

Liu, A., Li, J., Marin-Husstege, M., Kageyama, R., Fan, Y., Gelinas, C., & Casaccia-Bonnefil, P. (2006). A molecular insight of Hes5-dependent inhibition of myelin gene expression: Old partners and new players. *EMBO Journal*, *25*(20), 4833–4842. https://doi.org/10.1038/sj.emboj.7601352

Lochhead, P. A., Kinstrie, R., Sibbet, G., Rawjee, T., Morrice, N., & Cleghon, V. (2006). A chaperone-dependent GSK3β transitional intermediate mediates activation-loop autophosphorylation. *Molecular Cell*, *24*(4), 627–633. https://doi.org/10.1016/j.molcel.2006.10.009

Long, J. M., & Holtzman, D. M. (2019). Alzheimer Disease: An Update on Pathobiology and Treatment Strategies. In *Cell* (Vol. 179, Issue 2, pp. 312–339). Cell. https://doi.org/10.1016/j.cell.2019.09.001

Lopez Salon, M., Pasquini, L., Besio Moreno, M., Pasquini, J. M., & Soto, E. (2003). Relationship between β-amyloid degradation and the 26S proteasome in neural cells. *Experimental Neurology*, *180*(2), 131–143. https://doi.org/10.1016/S0014-4886(02)00060-2

Love, M. I., Huber, W., & Anders, S. (2014). Moderated estimation of fold change and dispersion for RNA-seq data with DESeq2. *Genome Biology*, *15*(12), 1–21. https://doi.org/10.1186/s13059-014-0550-8

Manterola, L., Hernando-Rodríguez, M., Ruiz, A., Apraiz, A., Arrizabalaga, O., Vellón, L., Alberdi, E., Cavaliere, F., Lacerda, H. M., Jimenez, S., Parada, L. A., Matute, C., & Zugaza, J. L. (2013). 1–42 β-amyloid peptide requires PDK1/nPKC/Rac 1 pathway to induce neuronal death. *Translational Psychiatry*, *3*(1). https://doi.org/10.1038/tp.2012.147

Marisca, R., Hoche, T., Agirre, E., Hoodless, L. J., Barkey, W., Auer, F., Castelo-Branco, G., & Czopka, T. (2020). Functionally distinct subgroups of oligodendrocyte precursor cells integrate neural activity and execute myelin formation. *Nature Neuroscience*, *23*(3), 363–374. https://doi.org/10.1038/s41593-019-0581-2

Marques, S., Zeisel, A., Codeluppi, S., Van Bruggen, D., Falcão, A. M., Xiao, L., Li, H., Häring, M., Hochgerner, H., Romanov, R. A., Gyllborg, D., Muñoz-Manchado, A. B., La Manno, G., Lönnerberg, P., Floriddia, E. M., Rezayee, F., Ernfors, P., Arenas, E., Hjerling-Leffler, J., … Castelo-Branco, G. (2016). Oligodendrocyte heterogeneity in the mouse juvenile and adult central nervous system. *Science*, *352*(6291), 1326–1329. https://doi.org/10.1126/science.aaf6463

Martinez, A., Lectez, B., Ramirez, J., Popp, O., Sutherland, J. D., Urbé, S., Dittmar, G., Clague, M. J., & Mayor, U. (2017). Quantitative proteomic analysis of Parkin substrates in Drosophila neurons. *Molecular Neurodegeneration*, *12*(1), 1–19. https://doi.org/10.1186/s13024-017-0170-3

McCarthy, K. D., & De Vellis, J. (1980). Preparation of separate astroglial and oligodendroglial cell cultures from rat cerebral tissue. *Journal of Cell Biology*, *85*(3), 890–902. https://doi.org/10.1083/jcb.85.3.890

McCubrey, J. A., Steelman, L. S., Bertrand, F. E., Davis, N. M., Abrams, S. L., Montalto, G., D'Assoro, A. B., Libra, M., Nicoletti, F., Maestro, R., Basecke, J., Cocco, L., Cervello, M., & Martelli, A. M. (2014). Multifaceted roles of GSK-3 and Wnt/β-catenin in hematopoiesis and leukemogenesis: Opportunities for therapeutic intervention. In *Leukemia* (Vol. 28, Issue 1, pp. 15–33). https://doi.org/10.1038/leu.2013.184

Mei, F., Wang, H., Liu, S., Niu, J., Wang, L., He, Y., Etxeberria, A., Chan, J. R., & Xiao, L. (2013). Stage-specific deletion of olig2 conveys opposing functions on differentiation and maturation of oligodendrocytes. *Journal of Neuroscience*, *33*(19), 8454–8462. https://doi.org/10.1523/JNEUROSCI.2453-12.2013

Meng, J., Ma, X., Tao, H., Jin, X., Witvliet, D., Mitchell, J., Zhu, M., Dong, M. Q., Zhen, M., Jin, Y., & Qi, Y. B. (2017). Myrf ER-Bound Transcription Factors Drive C. elegans Synaptic Plasticity via Cleavage-Dependent Nuclear Translocation. *Developmental Cell*, *41*(2), 180-194.e7. https://doi.org/10.1016/j.devcel.2017.03.022

Miao, Y., Du, Q., Zhang, H. G., Yuan, Y., Zuo, Y., & Zheng, H. (2023). Cycloheximide (CHX) Chase Assayto Examine Protein Half-life. *Bio-Protocol*, *13*(11). https://doi.org/10.21769/BioProtoc.4690

Milan, M., Balestrieri, C., Alfarano, G., Polletti, S., Prosperini, E., Nicoli, P., Spaggiari, P., Zerbi, A., Cirulli, V., Diaferia, G. R., & Natoli, G. (2020). Pancreatic Cancer Cells Require the Transcription Factor MYRF to Maintain ER Homeostasis. *Developmental Cell*, *55*(4), 398-412.e7. https://doi.org/10.1016/j.devcel.2020.09.011

Miller, D. J., Duka, T., Stimpson, C. D., Schapiro, S. J., Baze, W. B., McArthur, M. J., Fobbs, A. J., Sousa, A. M. M., Sěstan, N., Wildman, D. E., Lipovich, L., Kuzawa, C. W., Hof, P. R., & Sherwood, C. C. (2012). Prolonged myelination in human neocortical evolution. *Proceedings of the National Academy of Sciences of the United States of America*, *109*(41), 16480–16485. https://doi.org/10.1073/pnas.1117943109

Min, Y., Kristiansen, K., Boggs, J. M., Husted, C., Zasadzinski, J. A., & Israelachvili, J. (2009). Interaction forces and adhesion of supported myelin lipid bilayers modulated by myelin basic protein. *Proceedings of the National Academy of Sciences of the United States of America*, *106*(9), 3154–3159. https://doi.org/10.1073/pnas.0813110106

Mitew, S., Hay, C. M., Peckham, H., Xiao, J., Koenning, M., & Emery, B. (2014). Mechanisms regulating the development of oligodendrocytes and central nervous system myelin. In *Neuroscience* (Vol. 276, pp. 29–47). Neuroscience. https://doi.org/10.1016/j.neuroscience.2013.11.029

Mitew, Stanislaw, Kirkcaldie, M. T. K., Halliday, G. M., Shepherd, C. E., Vickers, J. C., & Dickson, T. C. (2010). Focal demyelination in Alzheimer's disease and transgenic mouse models. *Acta Neuropathologica*, *119*(5), 567–577. https://doi.org/10.1007/s00401-010-0657-2

Moore, S., Meschkat, M., Ruhwedel, T., Trevisiol, A., Tzvetanova, I. D., Battefeld, A., Kusch, K., Kole, M. H. P., Strenzke, N., Möbius, W., de Hoz, L., & Nave, K. A. (2020). A role of oligodendrocytes in information processing. *Nature Communications*, *11*(1), 1–15. https://doi.org/10.1038/s41467-020-19152-7

Morawe, T., Hiebel, C., Kern, A., & Behl, C. (2012). Protein homeostasis, aging and Alzheimer's disease. *Molecular Neurobiology*, *46*(1), 41–54. https://doi.org/10.1007/s12035-012-8246-0

Mukherjee, C., Kling, T., Russo, B., Miebach, K., Kess, E., Schifferer, M., Pedro, L. D., Weikert, U., Fard, M. K., Kannaiyan, N., Rossner, M., Aicher, M. L., Goebbels, S., Nave, K. A., Krämer-Albers, E. M., Schneider, A., & Simons, M. (2020). Oligodendrocytes Provide Antioxidant Defense Function for Neurons by Secreting Ferritin Heavy Chain. *Cell Metabolism*, *32*(2), 259-272.e10. https://doi.org/10.1016/j.cmet.2020.05.019

Müller, U. C., Deller, T., & Korte, M. (2017). Not just amyloid: Physiological functions of the amyloid precursor protein family. In *Nature Reviews Neuroscience* (Vol. 18, Issue 5, pp. 281–298). Nature Publishing Group. https://doi.org/10.1038/nrn.2017.29

Munyeshyaka, M., & Fields, R. D. (2022). Oligodendroglia are emerging players in several forms of learning and memory. In *Communications Biology* (Vol. 5, Issue 1, pp. 1–12). Nature Publishing Group. https://doi.org/10.1038/s42003-022-04116-y

Nakamura, S., & Nishizuka, Y. (1994). Lipid mediators and protein kinase C activation for the intracellular signaling network. *Journal of Biochemistry*, *115*(6), 1029–1034. http://www.ncbi.nlm.nih.gov/pubmed/7982876

Nakayama, S., Yumimoto, K., Kawamura, A., & Nakayama, K. I. (2018). Degradation of the endoplasmic reticulum–anchored transcription factor MyRF by the ubiquitin ligase SCFFbxw7 in a manner dependent on the kinase GSK-3. *Journal of Biological Chemistry*, *293*(15), 5705–5714. https://doi.org/10.1074/jbc.RA117.000741

Naruse, M., Ishizaki, Y., Ikenaka, K., Tanaka, A., & Hitoshi, S. (2017). Origin of oligodendrocytes in mammalian forebrains: a revised perspective. In *Journal of Physiological Sciences* (Vol. 67, Issue 1, pp. 63–70). BMC. https://doi.org/10.1007/s12576-016-0479-7

Nasrabady, S. E., Rizvi, B., Goldman, J. E., & Brickman, A. M. (2018). White matter changes in Alzheimer's disease: a focus on myelin and oligodendrocytes. In *Acta neuropathologica communications* (Vol. 6, Issue 1, p. 22). BioMed Central. https://doi.org/10.1186/s40478-018-0515-3

Nave, K. A. (2010). Myelination and support of axonal integrity by glia. In *Nature* (Vol. 468, Issue 7321, pp. 244–252). Nature. https://doi.org/10.1038/nature09614

Nave, K. A., & Werner, H. B. (2014). Myelination of the nervous system: Mechanisms and functions. In *Annual Review of Cell and Developmental Biology* (Vol. 30, pp. 503–533). Annu Rev Cell Dev Biol. https://doi.org/10.1146/annurev-cellbio-100913-013101

Nawaz, S., Sánchez, P., Schmitt, S., Snaidero, N., Mitkovski, M., Velte, C., Brückner, B. R., Alexopoulos, I., Czopka, T., Jung, S. Y., Rhee, J. S., Janshoff, A., Witke, W., Schaap, I. A. T., Lyons, D. A., & Simons, M. (2015). Actin Filament Turnover Drives Leading Edge Growth during Myelin Sheath Formation in the Central Nervous System. *Developmental Cell*, *34*(2), 139–151. https://doi.org/10.1016/j.devcel.2015.05.013

Nelson, T. J., & Alkon, D. L. (2009). Neuroprotective versus tumorigenic protein kinase C activators. In *Trends in Biochemical Sciences* (Vol. 34, Issue 3, pp. 136–145). Trends Biochem Sci. https://doi.org/10.1016/j.tibs.2008.11.006

Nery, L. R., Eltz, N. S., Hackman, C., Fonseca, R., Altenhofen, S., Guerra, H. N., Freitas, V. M., Bonan, C. D., & Vianna, M. R. M. R. (2014a). Brain Intraventricular Injection of Amyloid-β in Zebrafish Embryo Impairs Cognition and Increases Tau Phosphorylation, Effects Reversed by Lithium. *PLoS ONE*, *9*(9), e105862. https://doi.org/10.1371/journal.pone.0105862

Nery, L. R., Eltz, N. S., Hackman, C., Fonseca, R., Altenhofen, S., Guerra, H. N., Freitas, V. M., Bonan, C. D., & Vianna, M. R. M. R. (2014b). Brain Intraventricular Injection of Amyloid-β in Zebrafish Embryo Impairs Cognition and Increases Tau Phosphorylation, Effects Reversed by Lithium. *PLoS ONE*, *9*(9), e105862. https://doi.org/10.1371/journal.pone.0105862

Nie, X., Falangola, M. F., Ward, R., McKinnon, E. T., Helpern, J. A., Nietert, P. J., & Jensen, J. H. (2019). Diffusion MRI detects longitudinal white matter changes in the 3xTg-AD mouse model of Alzheimer's disease. *Magnetic Resonance Imaging*, *57*, 235–242. https://doi.org/10.1016/j.mri.2018.12.003

Nielsen, H. M., Ek, D., Avdic, U., Orbjörn, C., Hansson, O., Veerhuis, R., Rozemuller, A. J., Brun, A., Minthon, L., & Wennström, M. (2014). NG2 cells, a new trail for Alzheimer's disease mechanisms? *Acta Neuropathologica Communications*, *2*(1). https://doi.org/10.1186/2051596017

O'Neill, L. A. J. (2009). Regulation of signaling by non-degradative ubiquitination. In *Journal of Biological Chemistry* (Vol. 284, Issue 13, p. 8209). American Society for Biochemistry and Molecular Biology. https://doi.org/10.1074/jbc.R800070200

Oddo, S. (2008). The ubiquitin-proteasome system in Alzheimer's disease. *Journal of Cellular and Molecular Medicine*, *12*(2), 363–373. https://doi.org/10.1111/j.1582-4934.2008.00276.x

Oddo, S., Caccamo, A., Shepherd, J. D., Murphy, M. P., Golde, T. E., Kayed, R., Metherate, R., Mattson, M. P., Akbari, Y., & LaFerla, F. M. (2003). Triple-transgenic model of Alzheimer's Disease with plaques and tangles: Intracellular Aβ and synaptic dysfunction. *Neuron*, *39*(3), 409–421. https://doi.org/10.1016/S0896-6273(03)00434-3

Oh, S., Hong, H. S., Hwang, E., Sim, H. J., Lee, W., Shin, S. J., & Mook-Jung, I. (2005). Amyloid peptide attenuates the proteasome activity in neuronal cells. *Mechanisms of Ageing and Development*, *126*(12), 1292–1299. https://doi.org/10.1016/j.mad.2005.07.006

Ohno, S., & Nishizuka, Y. (2002). Protein kinase C isotypes and their specific functions: prologue. *Journal of Biochemistry*, *132*(4), 509–511. http://www.ncbi.nlm.nih.gov/pubmed/12359062

Ortiz-Sanz, C., Balantzategi, U., Quintela-López, T., Ruiz, A., Luchena, C., Zuazo-Ibarra, J., Capetillo-Zarate, E., Matute, C., Zugaza, J. L., & Alberdi, E. (2022). Amyloid β / PKC-dependent alterations in NMDA receptor composition are detected in early stages of Alzheimer´s disease. *Cell Death and Disease*, *13*(3). https://doi.org/10.1038/s41419-022-04687-y

Parente, D. B., Gasparetto, E. L., Da Cruz, L. C. H., Domingues, R. C., Baptista, A. C., Carvalho, A. C. P., & Domingues, R. C. (2008). Potential role of diffusion tensor MRI in the differential diagnosis of mild cognitive impairment and Alzheimer's disease. *American Journal of Roentgenology*, *190*(5), 1369–1374. https://doi.org/10.2214/AJR.07.2617

Philips, T., & Rothstein, J. D. (2017). Oligodendroglia: Metabolic supporters of neurons. In *Journal of Clinical Investigation* (Vol. 127, Issue 9, pp. 3271–3280). American Society for Clinical Investigation. https://doi.org/10.1172/JCI90610

Pike, C. J., Walencewicz, A. J., Glabe, C. G., & Cotman, C. W. (1991). In vitro aging of ß-amyloid protein causes peptide aggregation and neurotoxicity. *Brain Research*, *563*(1–2), 311–314. https://doi.org/10.1016/0006-8993(91)91553-D

Pinz, H., Pyle, L. C., Li, D., Izumi, K., Skraban, C., Tarpinian, J., Braddock, S. R., Telegrafi, A., Monaghan, K. G., Zackai, E., & Bhoj, E. J. (2018). De novo variants in Myelin regulatory factor (MYRF) as candidates of a new syndrome of cardiac and urogenital anomalies. *American Journal of Medical Genetics, Part A*, *176*(4), 969–972. https://doi.org/10.1002/ajmg.a.38620

Preston, M. A., & Macklin, W. B. (2015). Zebrafish as a model to investigate CNS myelination. In *GLIA* (Vol. 63, Issue 2, pp. 177–193). https://doi.org/10.1002/glia.22755

Pukos, N., Yoseph, R., & M. McTigue, D. (2018). To Be or Not to Be: Environmental Factors that Drive Myelin Formation during Development and after CNS Trauma. *Neuroglia*, *1*(1), 63–90. https://doi.org/10.3390/neuroglia1010007

Qi, H., Yu, L., Zhou, X., Wynn, J., Zhao, H., Guo, Y., Zhu, N., Kitaygorodsky, A., Hernan, R., Aspelund, G., Lim, F. Y., Crombleholme, T., Cusick, R., Azarow, K., Danko, M. E., Chung, D., Warner, B. W., Mychaliska, G. B., Potoka, D., … Shen, Y. (2018). De novo variants in congenital diaphragmatic hernia identify MYRF as a new syndrome and reveal genetic overlaps with other developmental disorders. *PLoS Genetics*, *14*(12). https://doi.org/10.1371/journal.pgen.1007822

Qiao, L., Wynn, J., Yu, L., Hernan, R., Zhou, X., Duron, V., Aspelund, G., Farkouh-Karoleski, C., Zygumunt, A., Krishnan, U. S., Nees, S., Khlevner, J., Lim, F. Y., Crombleholme, T., Cusick, R., Azarow, K., Danko, M. E., Chung, D., Warner, B. W., … Chung, W. K. (2020). Likely damaging de novo variants in congenital diaphragmatic hernia patients are associated with worse clinical outcomes. *Genetics in Medicine*, *22*(12), 2020–2028. https://doi.org/10.1038/s41436-020-0908-0

Quintela-López, T., Ortiz-Sanz, C., Serrano-Regal, M. P., Gaminde-Blasco, A., Valero, J., Baleriola, J., Sánchez-Gómez, M. V., Matute, C., & Alberdi, E. (2019). Aβ oligomers promote oligodendrocyte differentiation and maturation via integrin β1 and Fyn kinase signaling. *Cell Death and Disease*, *10*(6). https://doi.org/10.1038/s41419-019-1636-8

Ramirez, J., Lectez, B., Osinalde, N., Sivá, M., Elu, N., Aloria, K., Procházková, M., Perez, C., Martínez-Hernández, J., Barrio, R., Šašková, K. G., Arizmendi, J. M., & Mayor, U. (2018). Quantitative proteomics reveals neuronal ubiquitination of Rngo/Ddi1 and several proteasomal subunits by Ube3a, accounting for the complexity of Angelman syndrome. *Human Molecular Genetics*, *27*(11), 1955–1971. https://doi.org/10.1093/hmg/ddy103

Raychaudhuri, M., & Mukhopadhyay, D. (2007). AICD and its adaptors - In search of new players. In *Journal of Alzheimer's Disease* (Vol. 11, Issue 3, pp. 343–358). J Alzheimers Dis. https://doi.org/10.3233/JAD-2007-11311

Recuero, M., Serrano, E., Bullido, M. J., & Valdivieso, F. (2004). Aβ production as consequence of cellular death of a human neuroblastoma overexpressing APP. *FEBS Letters*, *570*(1–3), 114–118. https://doi.org/10.1016/j.febslet.2004.06.025

Rinholm, J. E., Hamilton, N. B., Kessaris, N., Richardson, W. D., Bergersen, L. H., & Attwell, D. (2011). Regulation of oligodendrocyte development and myelination by glucose and lactate. *Journal of Neuroscience*, *31*(2), 538–548. https://doi.org/10.1523/JNEUROSCI.3516-10.2011

Roher, A. E., Weiss, N., Kokjohn, T. A., Kuo, Y. M., Kalback, W., Anthony, J., Watson, D., Luehrs, D. C., Sue, L., Walker, D., Emmerling, M., Goux, W., & Beach, T. (2002). Increased Aβ peptides and reduced cholesterol and myelin proteins characterize white matter degeneration in Alzheimer's disease. *Biochemistry*, *41*(37), 11080–11090. https://doi.org/10.1021/bi026173d

Rossetti, L. Z., Glinton, K., Yuan, B., Liu, P., Pillai, N., Mizerik, E., Magoulas, P., Rosenfeld, J. A., Karaviti, L., Sutton, V. R., Lalani, S. R., & Scott, D. A. (2019). Review of the phenotypic spectrum associated with haploinsufficiency of MYRF. *American Journal of Medical Genetics, Part A*, *179*(7), 1376–1382. https://doi.org/10.1002/ajmg.a.61182

Russel, S., Frand, A. R., & Ruvkun, G. (2011). Regulation of the C. elegans molt by pqn-47. *Developmental Biology*, *360*(2), 297–309. https://doi.org/10.1016/j.ydbio.2011.09.025

Saab, A. S., Tzvetavona, I. D., Trevisiol, A., Baltan, S., Dibaj, P., Kusch, K., Möbius, W., Goetze, B., Jahn, H. M., Huang, W., Steffens, H., Schomburg, E. D., Pérez-Samartín, A., Pérez-Cerdá, F., Bakhtiari, D., Matute, C., Löwel, S., Griesinger, C., Hirrlinger, J., … Nave, K. A. (2016). Oligodendroglial NMDA Receptors Regulate Glucose Import and Axonal Energy Metabolism. *Neuron*, *91*(1), 119–132. https://doi.org/10.1016/j.neuron.2016.05.016

Sachdev, P. S., Zhuang, L., Braidy, N., & Wen, W. (2013). Is Alzheimer's a disease of the white matter? In *Current Opinion in Psychiatry* (Vol. 26, Issue 3, pp. 244–251). Curr Opin Psychiatry. https://doi.org/10.1097/YCO.0b013e32835ed6e8

Salcedo-Tello, P., Ortiz-Matamoros, A., & Arias, C. (2011). GSK3 function in the brain during development, neuronal plasticity, and neurodegeneration. In *International Journal of Alzheimer's Disease* (Vol. 2011). Int J Alzheimers Dis. https://doi.org/10.4061/2011/189728

Samanta, J., & Kessler, J. A. (2004). Interactions between ID and OLIG proteins mediate the inhibitory effects of BMP4 on oligodendroglial differentiation. *Development*, *131*(17), 4131–4142. https://doi.org/10.1242/dev.01273

Samanta, J., & Salzer, J. L. (2015). Myelination: Actin Disassembly Leads the Way. In *Developmental Cell* (Vol. 34, Issue 2, pp. 129–130). Dev Cell. https://doi.org/10.1016/j.devcel.2015.07.006

Samudyata, Castelo-Branco, G., & Liu, J. (2020). Epigenetic regulation of oligodendrocyte differentiation: From development to demyelinating disorders. *GLIA*, *68*(8), 1619–1630. https://doi.org/10.1002/glia.23820

Sánchez-Gómez, M. V., Serrano, M. P., Alberdi, E., Pérez-Cerdá, F., & Matute, C. (2018). Isolation, expansion, and maturation of oligodendrocyte lineage cells obtained from rat neonatal brain and optic nerve. In *Methods in Molecular Biology* (Vol. 1791, pp. 95–113). Humana Press, New York, NY. https://doi.org/10.1007/978-1-4939-7862-5_8

Schulz, E. C., Dickmanns, A., Urlaub, H., Schmitt, A., Mühlenhoff, M., Stummeyer, K., Schwarzer, D., Gerardy-Schahn, R., & Ficner, R. (2010). Crystal structure of an intramolecular chaperone mediating triple-B-helix folding. *Nature Structural and Molecular Biology*, *17*(2), 210–215. https://doi.org/10.1038/nsmb.1746

Schwarzer, D., Stummeyer, K., Gerardy-Schahn, R., & Mühlenhoff, M. (2007). Characterization of a novel intramolecular chaperone domain conserved in endosialidases and other bacteriophage tail spike and fiber proteins. *Journal of Biological Chemistry*, *282*(5), 2821–2831. https://doi.org/10.1074/jbc.M609543200

Seki, T., Matsubayashi, H., Amano, T., Shirai, Y., Saito, N., & Sakai, N. (2005). Phosphorylation of PKC activation loop plays an important role in receptor-mediated translocation of PKC. *Genes to Cells*, *10*(3), 225–239. https://doi.org/10.1111/j.1365-2443.2005.00830.x

Selkoe, D. J. (1991). The molecular pathology of Alzheimer's disease. In *Neuron* (Vol. 6, Issue 4, pp. 487–498). Neuron. https://doi.org/10.1016/0896-6273(91)90052-2

Selkoe, D. J., Brown, B. A., Salazar, F. J., & Marchotta, C. A. (1981). Myelin basic protein in Alzheimer disease neuronal fractions and mammalian neurofilament preparations. *Annals of Neurology*, *10*(5), 429–436. https://doi.org/10.1002/ana.410100505

Senoo, H., Araki, T., Fukuzawa, M., & Williams, J. G. (2013). A new kind of membrane-tethered eukaryotic transcription factor that shares an auto-proteolytic processing mechanism with bacteriophage tail-spike proteins. *Journal of Cell Science*, *126*(22), 5247–5258. https://doi.org/10.1242/jcs.133231

Senoo, H., Wang, H. Y., Araki, T., Williams, J. G., & Fukuzawa, M. (2012). An orthologue of the Myelin-gene regulatory transcription factor regulates Dictyostelium prestalk differentiation. *International Journal of Developmental Biology*, *56*(5), 325–332. https://doi.org/10.1387/ijdb.120030jw

Siggs, O. M., Souzeau, E., Breen, J., Qassim, A., Zhou, T., Dubowsky, A., Ruddle, J. B., & Craig, J. E. (2019). Autosomal dominant nanophthalmos and high hyperopia associated with a C-terminal frameshift variant in MYRF. *Molecular Vision*, *25*, 527–534. /pmc/articles/PMC6817736/

Simon, C., Götz, M., & Dimou, L. (2011). Progenitors in the adult cerebral cortex: Cell cycle properties and regulation by physiological stimuli and injury. *GLIA*, *59*(6), 869–881. https://doi.org/10.1002/glia.21156

Simons, M., & Nave, K. A. (2016). Oligodendrocytes: Myelination and axonal support. In *Cold Spring Harbor Perspectives in Biology* (Vol. 8, Issue 1). Cold Spring Harb Perspect Biol. https://doi.org/10.1101/cshperspect.a020479

Simons, M., & Trotter, J. (2007). Wrapping it up: the cell biology of myelination. In *Current Opinion in Neurobiology* (Vol. 17, Issue 5, pp. 533–540). Curr Opin Neurobiol. https://doi.org/10.1016/j.conb.2007.08.003

Skaper, S. D., Evans, N. A., Soden, P. E., Rosin, C., Facci, L., & Richardson, J. C. (2009). Oligodendrocytes are a novel source of amyloid peptide generation. *Neurochemical Research*, *34*(12), 2243–2250. https://doi.org/10.1007/s11064-009-0022-9

Snaidero, N., Möbius, W., Czopka, T., Hekking, L. H. P., Mathisen, C., Verkleij, D., Goebbels, S., Edgar, J., Merkler, D., Lyons, D. A., Nave, K. A., & Simons, M. (2014). Myelin membrane wrapping of CNS axons by PI(3,4,5)P3-dependent polarized growth at the inner tongue. *Cell*, *156*(1–2), 277–290. https://doi.org/10.1016/j.cell.2013.11.044

Snaidero, N., Velte, C., Myllykoski, M., Raasakka, A., Ignatev, A., Werner, H. B., Erwig, M. S., Möbius, W., Kursula, P., Nave, K. A., & Simons, M. (2017). Antagonistic Functions of MBP and CNP Establish Cytosolic Channels in CNS Myelin. *Cell Reports*, *18*(2), 314–323. https://doi.org/10.1016/j.celrep.2016.12.053

Snyder, J. L., Kearns, C. A., & Appel, B. (2012). Fbxw7 regulates Notch to control specification of neural precursors for oligodendrocyte fate. *Neural Development*, *7*(1), 1–12. https://doi.org/10.1186/1749-8104-7-15

Spitzer, S. O., Sitnikov, S., Kamen, Y., Evans, K. A., Kronenberg-Versteeg, D., Dietmann, S., de Faria, O., Agathou, S., & Káradóttir, R. T. (2019). Oligodendrocyte Progenitor Cells Become Regionally Diverse and Heterogeneous with Age. *Neuron*, *101*(3), 459-471.e5. https://doi.org/10.1016/j.neuron.2018.12.020

Stadelmann, C., Timmler, S., Barrantes-Freer, A., & Simons, M. (2019). Myelin in the central nervous system: Structure, function, and pathology. *Physiological Reviews*, *99*(3), 1381–1431. https://doi.org/10.1152/physrev.00031.2018

Swire, M., Kotelevtsev, Y., Webb, D. J., Lyons, D. A., & Ffrench-Constant, C. (2019). Endothelin signalling mediates experience-dependent myelination in the CNS. *ELife*, *8*. https://doi.org/10.7554/eLife.49493

Takami, M., Nagashima, Y., Sano, Y., Ishihara, S., Morishima-Kawashima, M., Funamoto, S., & Ihara, Y. (2009). γ-Secretase: Successive tripeptide and tetrapeptide release from the transmembrane domain of β-carboxyl terminal fragment. *Journal of Neuroscience*, *29*(41), 13042–13052. https://doi.org/10.1523/JNEUROSCI.2362-09.2009

Thal, D. R., Rüb, U., Orantes, M., & Braak, H. (2002). Phases of Aβ-deposition in the human brain and its relevance for the development of AD. *Neurology*, *58*(12), 1791–1800. https://doi.org/10.1212/WNL.58.12.1791

Tom Dieck, S., Kochen, L., Hanus, C., Bartnik, I., Nassim-Assir, B., Merk, K., Mosler, T., Garg, S., Bunse, S., Tirrell, D. A., & Schuman, E. M. (2015). Direct visualization of identified and newly synthesized proteins in situ. *Nat Methods*, *12*(5), 411–414. https://doi.org/10.1038/nmeth.3319

Tramutola, A., Triani, F., Di Domenico, F., Barone, E., Cai, J., Klein, J. B., Perluigi, M., & Butterfield, D. A. (2018). Poly-ubiquitin profile in Alzheimer disease brain. *Neurobiology of Disease*, *118*, 129–141. https://doi.org/10.1016/j.nbd.2018.07.006

Tripathi, R. B., Jackiewicz, M., McKenzie, I. A., Kougioumtzidou, E., Grist, M., & Richardson, W. D. (2017). Remarkable Stability of Myelinating Oligodendrocytes in Mice. *Cell Reports*, *21*(2), 316–323. https://doi.org/10.1016/j.celrep.2017.09.050

Truong, P. H., Ciccotosto, G. D., Merson, T. D., Spoerri, L., Chuei, M. J., Ayers, M., Xing, Y. L., Emery, B., & Cappai, R. (2019). Amyloid precursor protein and amyloid precursor-like protein 2 have distinct roles in modulating myelination, demyelination, and remyelination of axons. *GLIA*, *67*(3), 525–538. https://doi.org/10.1002/glia.23561

Tse, K. H., Cheng, A., Ma, F., & Herrup, K. (2018). DNA damage-associated oligodendrocyte degeneration precedes amyloid pathology and contributes to Alzheimer's disease and dementia. *Alzheimer's and Dementia*, *14*(5), 664–679. https://doi.org/10.1016/j.jalz.2017.11.010

Tyler, W. A., Gangoli, N., Gokina, P., Kim, H. A., Covey, M., Levison, S. W., & Wood, T. L. (2009). Activation of the mammalian target of rapamycin (mTOR) is essential for oligodendrocyte differentiation. *Journal of Neuroscience*, *29*(19), 6367–6378. https://doi.org/10.1523/JNEUROSCI.0234-09.2009

Vanzulli, I., Papanikolaou, M., De-La-Rocha, I. C., Pieropan, F., Rivera, A. D., Gomez-Nicola, D., Verkhratsky, A., Rodríguez, J. J., & Butt, A. M. (2020). Disruption of oligodendrocyte progenitor cells is an early sign of pathology in the triple transgenic mouse model of Alzheimer's disease. *Neurobiology of Aging*, *94*, 130–139. https://doi.org/10.1016/j.neurobiolaging.2020.05.016

Viola, K. L., & Klein, W. L. (2015). Amyloid β oligomers in Alzheimer's disease pathogenesis, treatment, and diagnosis. In *Acta Neuropathologica* (Vol. 129, Issue 2, pp. 183–206). Acta Neuropathol. https://doi.org/10.1007/s00401-015-1386-3

von Rotz, R. C., Kohli, B. M., Bosset, J., Meier, M., Suzuki, T., Nitsch, R. M., & Konietzko, U. (2004). The APP intracellular domain forms nuclear multiprotein complexes and regulates the transcription of its own precursor. *Journal of Cell Science*, *117*(19), 4435–4448. https://doi.org/10.1242/jcs.01323

Walsh, D. M., Lomakin, A., Benedek, G. B., Condron, M. M., & Teplow, D. B. (1997). Amyloid β-protein fibrillogenesis: Detection of a protofibrillar intermediate. *Journal of Biological Chemistry*, *272*(35), 22364–22372. https://doi.org/10.1074/jbc.272.35.22364

Waxman, S. G. (1997). Axon-glia interactions: Building a smart nerve fiber. *Current Biology*, *7*(7). https://doi.org/10.1016/s0960-9822(06)00203-x

Waxman, S. G., & Ritchie, J. M. (1993). Molecular dissection of the myelinated axon. *Annals of Neurology*, *33*(2), 121–136. https://doi.org/10.1002/ana.410330202

Weidemann, A., Eggert, S., Reinhard, F. B. M., Vogel, M., Paliga, K., Baier, G., Masters, C. L., Beyreuther, K., & Evin, G. (2002). A novel ε-cleavage within the transmembrane domain of the Alzheimer amyloid precursor protein demonstrates homology with notch processing. *Biochemistry*, *41*(8), 2825–2835. https://doi.org/10.1021/bi015794o

Welcker, M., & Clurman, B. E. (2008). FBW7 ubiquitin ligase: A tumour suppressor at the crossroads of cell division, growth and differentiation. In *Nature Reviews Cancer* (Vol. 8, Issue 2, pp. 83–93). Nat Rev Cancer. https://doi.org/10.1038/nrc2290

Welcker, M., Orian, A., Jin, J., Grim, J. A., Harper, J. W., Eisenman, R. N., & Clurman, B. E. (2004). The Fbw7 tumor suppressor regulates glycogen synthase kinase 3 phosphorylation-dependent c-Myc protein degradation. *Proceedings of the National Academy of Sciences of the United States of America*, *101*(24), 9085–9090. https://doi.org/10.1073/pnas.0402770101

White, R., & Krämer-Albers, E. M. (2014). Axon-glia interaction and membrane traffic in myelin formation. In *Frontiers in Cellular Neuroscience* (Vol. 7, Issue JAN, p. 66637). Frontiers. https://doi.org/10.3389/fncel.2013.00284

Wickham, H. (2016). *ggplot2*. https://doi.org/10.1007/978-3-319-24277-4

Wittstatt, J., Reiprich, S., & Küspert, M. (2019). Crazy little thing called sox-new insights in oligodendroglial sox protein function. In *International Journal of Molecular Sciences* (Vol. 20, Issue 11, p. 2713). Multidisciplinary Digital Publishing Institute. https://doi.org/10.3390/ijms20112713

Woodgett, J. R. (1990). Molecular cloning and expression of glycogen synthase kinase-3/factor A. *The EMBO Journal*, *9*(8), 2431–2438. https://doi.org/10.1002/j.1460-2075.1990.tb07419.x

Woodruff, R. H., Fruttiger, M., Richardson, W. D., & Franklin, R. J. M. (2004). Platelet-derived growth factor regulates oligodendrocyte progenitor numbers in adult CNS and their response following CNS demyelination. *Molecular and Cellular Neuroscience*, *25*(2), 252–262. https://doi.org/10.1016/j.mcn.2003.10.014

Wu, T., Hu, E., Xu, S., Chen, M., Guo, P., Dai, Z., Feng, T., Zhou, L., Tang, W., Zhan, L., Fu, X., Liu, S., Bo, X., & Yu, G. (2021). clusterProfiler 4.0: A universal enrichment tool for interpreting omics data. *Innovation*, *2*(3). https://doi.org/10.1016/j.xinn.2021.100141

Wu, Y., Ma, Y., Liu, Z., Geng, Q., Chen, Z., & Zhang, Y. (2017a). Alterations of myelin morphology and oligodendrocyte development in early stage of Alzheimer's disease mouse model. *Neuroscience Letters*, *642*, 102–106. https://doi.org/10.1016/j.neulet.2017.02.007

Wu, Y., Ma, Y., Liu, Z., Geng, Q., Chen, Z., & Zhang, Y. (2017b). Alterations of myelin morphology and oligodendrocyte development in early stage of Alzheimer's disease mouse model. *Neuroscience Letters*, *642*, 102–106. https://doi.org/10.1016/j.neulet.2017.02.007

Wyssenbach, A., Quintela, T., Llavero, F., Zugaza, J. L., Matute, C., & Alberdi, E. (2016). Amyloid β-induced astrogliosis is mediated by β1-integrin via NADPH oxidase 2 in Alzheimer's disease. *Aging Cell*, *15*(6), 1140–1152. https://doi.org/10.1111/acel.12521

Xia, W. (2010). Exploring Alzheimer's disease in zebrafish. In *Journal of Alzheimer's Disease* (Vol. 20, Issue 4, pp. 981–990). IOS Press. https://doi.org/10.3233/JAD-2010-1412

Xiao, J., Wong, A. W., Willingham, M. M., Van Den Buuse, M., Kilpatrick, T. J., & Murray, S. S. (2011). Brain-derived neurotrophic factor promotes central nervous system myelination via a direct effect upon oligodendrocytes. *NeuroSignals*, *18*(3), 186–202. https://doi.org/10.1159/000323170

Xiao, Y., & Czopka, T. (2023). Myelination-independent functions of oligodendrocyte precursor cells in health and disease. *Nature Neuroscience*, *26*(10), 1663–1669. https://doi.org/10.1038/s41593-023-01423-3

Xu, J., Chen, S., Ahmed, S. H., Chen, H., Ku, G., Goldberg, M. P., & Hsu, C. Y. (2001). Amyloid-beta peptides are cytotoxic to oligodendrocytes. *The Journal of Neuroscience : The Official Journal of the Society for Neuroscience*, *21*(1). https://doi.org/10.1523/jneurosci.21-01-j0001.2001

Yeung, M. S. Y., Zdunek, S., Bergmann, O., Bernard, S., Salehpour, M., Alkass, K., Perl, S., Tisdale, J., Possnert, G., Brundin, L., Druid, H., & Frisén, J. (2014). Dynamics of oligodendrocyte generation and myelination in the human brain. *Cell*, *159*(4), 766–774. https://doi.org/10.1016/j.cell.2014.10.011

Young, K. M., Psachoulia, K., Tripathi, R. B., Dunn, S. J., Cossell, L., Attwell, D., Tohyama, K., & Richardson, W. D. (2013a). Oligodendrocyte dynamics in the healthy adult CNS: Evidence for myelin remodeling. *Neuron*, *77*(5), 873–885. https://doi.org/10.1016/j.neuron.2013.01.006

Young, K. M., Psachoulia, K., Tripathi, R. B., Dunn, S. J., Cossell, L., Attwell, D., Tohyama, K., & Richardson, W. D. (2013b). Oligodendrocyte dynamics in the healthy adult CNS: Evidence for myelin remodeling. *Neuron*, *77*(5), 873–885. https://doi.org/10.1016/j.neuron.2013.01.006

Yu, G., Wang, L. G., Han, Y., & He, Q. Y. (2012). ClusterProfiler: An R package for comparing biological themes among gene clusters. *OMICS A Journal of Integrative Biology*, *16*(5), 284–287. https://doi.org/10.1089/omi.2011.0118

Yuen, T. J., Silbereis, J. C., Griveau, A., Chang, S. M., Daneman, R., Fancy, S. P. J., Zahed, H., Maltepe, E., & Rowitch, D. H. (2014). Oligodendrocyte-encoded HIF function couples postnatal myelination and white matter angiogenesis. *Cell*, *158*(2), 383–396. https://doi.org/10.1016/j.cell.2014.04.052

Zeger, M., Popken, G., Zhang, J., Xuan, S., Lu, Q. R., Schwab, M. H., Nave, K. A., Rowitch, D., D'Ercole, A. J., & Ye, P. (2007). Insulin-like growth factor type 1 receptor signaling in the cells of oligodendrocyte lineage is required for normal in vivo oligodendrocyte development and myelination. *GLIA*, *55*(4), 400–411. https://doi.org/10.1002/glia.20469

Zhan, X., Jickling, G. C., Ander, B. P., Stamova, B., Liu, D., Kao, P. F., Zelin, M. A., Jin, L. W., Decarli, C., & Sharp, F. R. (2015). Myelin basic protein associates with AβPP, Aβ1-42, and Amyloid plaques in cortex of Alzheimer's disease brain. *Journal of Alzheimer's Disease*, *44*(4), 1213–1229. https://doi.org/10.3233/JAD-142013

Zhang, M., Zhang, J., Zhang, W., & Yao, Z. (2018). Demyelination Takes Place Prior To Neuronal Damage Following Intracerebroventricular Injection of Amyloid-Beta Oligomer. *Neuropsychiatry*, *8*(6), 1770–1785. https://doi.org/10.4172/Neuropsychiatry.1000519

Zhang, P., Kishimoto, Y., Grammatikakis, I., Gottimukkala, K., Cutler, R. G., Zhang, S., Abdelmohsen, K., Bohr, V. A., Misra Sen, J., Gorospe, M., & Mattson, M. P. (2019). Senolytic therapy alleviates Aβ-associated oligodendrocyte progenitor cell senescence and cognitive deficits in an Alzheimer's disease model. *Nature Neuroscience*, *22*(5), 719–728. https://doi.org/10.1038/s41593-019-0372-9

Zhao, L. N., Long, H., Mu, Y., & Chew, L. Y. (2012). The toxicity of amyloid β oligomers. In *International Journal of Molecular Sciences* (Vol. 13, Issue 6, pp. 7303–7327). Multidisciplinary Digital Publishing Institute (MDPI). https://doi.org/10.3390/ijms13067303

Zhao, X., He, X., Han, X., Yu, Y., Ye, F., Chen, Y., Hoang, T. N., Xu, X., Mi, Q. S., Xin, M., Wang, F., Appel, B., & Lu, Q. R. (2010). MicroRNA-Mediated Control of Oligodendrocyte Differentiation. *Neuron*, *65*(5), 612–626. https://doi.org/10.1016/j.neuron.2010.02.018

Zhen, X., Li, B., Hu, F., Yan, S., Meloni, G., Li, H., & Shi, N. (2017). Crystal structure of the DNA-binding domain of Myelin-gene Regulatory Factor. *Scientific Reports*, *7*(1), 1–9. https://doi.org/10.1038/s41598-017-03768-9

Zheng, H., & Koo, E. H. (2011). Biology and pathophysiology of the amyloid precursor protein. In *Molecular Neurodegeneration* (Vol. 6, Issue 1). Mol Neurodegener. https://doi.org/10.1186/1750-1326-6-27

Zuchero, J. B., Fu, M. meng, Sloan, S. A., Ibrahim, A., Olson, A., Zaremba, A., Dugas, J. C., Wienbar, S., Caprariello, A. V., Kantor, C., Leonoudakus, D., Lariosa-Willingham, K., Kronenberg, G., Gertz, K., Soderling, S. H., Miller, R. H., & Barres, B. A. (2015). CNS Myelin Wrapping Is Driven by Actin Disassembly. *Developmental Cell*, *34*(2), 152–167. https://doi.org/10.1016/j.devcel.2015.06.011